Aus der Klinik für Gastroenterologie, Hepatologie und Infektiologie an der Heinrich-Heine-Universität Düsseldorf

Role of Protein *O*-GlcNAcylation in the Pathogenesis of Hepatic Encephalopathy

Dissertation

zur Erlangung des Grades eines „Doctor of Philosophy“ (PhD) in Medical Sciences

der Medizinischen Fakultät der Heinrich-Heine-Universität Düsseldorf

vorgelegt von

Liang Zhao

(2025)

Als Inauguraldissertation gedruckt mit der Genehmigung der

Medizinischen Fakultät der Heinrich-Heine-Universität Düsseldorf

gez.:

Dekan:	Prof. Dr. med. Nikolaj Klöcker
Erstgutachter:	Prof. Dr. med. Dieter Häussinger
Zweitgutachter:	Prof. Dr. med. Philipp Lang

Meiner Familie gewidme

„Ein großer Genius bildet sich durch einen andern großen Genius, weniger durch Assimilierung als durch Reibung. Ein Diamant schleift den andern.“

— Heinrich Heine

Teile dieser Arbeit wurden veröffentlicht:

Zhao, L., Bonus, M., Poschmann, G., Gohlke, H., Stühler, K., Luedde, T., Häussinger, D., Görg, B. (2021). Identification of ammonia-induced changes in the astrocyte *O*-GlcNAcome. *Z Gastroenterol*. 59(01): e32-e33. 10.1055/s-011-50135.

Summary

Hepatic encephalopathy (HE) is a frequent neuropsychiatric complication in patients with acute or chronic liver dysfunction. Ammonia, a major toxin of HE, upregulates HO-1 protein levels by increasing protein *O*-GlcNAcylation and thereby induces oxidative and endoplasmatic reticulum (ER) stress and senescence in astrocytes. *O*-GlcNAcylation is a post-translational protein modification in which specific serine/ threonine residues in proteins are *O*-glycosidically linked to glucosamine (GlcN). However, protein species modified by *O*-GlcNAc and functional consequences thereof in ammonia-exposed astrocytes remained unclear so far and were investigated in the present study. Using „click-chemistry", affinity purification and mass spectrometry we identified more than 300 proteins of the rat astrocyte *O*-GlcNAcome compared to background controls. Compared to untreated astrocytes, *O*-GlcNAc level of 68 protein species were altered in astrocytes incubated with NH_4Cl (5 mM, 72 h) of which 51 and 17 were increased or decreased, respectively. Bioinformatics assigned these species to cellular processes known to be involved in the pathogenesis of HE, such as glutamine metabolism, mitochondrial functions and others. NH_4Cl upregulated protein levels of 32 kDa full-length (HO-1_{FL}) and 28 kDa truncated HO-1 (HO-1_{Tr}) and increased the *O*-GlcNAcylation of both. *In vitro O*-GlcNAcylation of rat HO-1 suggested serine 159 or 160 at the HO-1 dimerization interface as potential *O*-GlcNAc sites. Incubation of the astrocytes with NH_4Cl triggered HO-1 homo- and heteromerization in a GlcN synthesis- and protein *O*-GlcNAcylation-dependent way. NH_4Cl upregulated HO-1 in the ER and in the nucleus but not in mitochondria. In the nucleus, HO-1_{FL} and HO-1_{Tr} were upregulated but this was not paralleled by an enhanced transcription of Nrf-2-dependent genes. NH_4Cl increased the levels of HO-1_{Tr} in the supernatants of the astrocytes in a *O*-GlcNAc-dependent way. *O*-GlcNAc, HO-1 and GRP78 were also increased and OGT and GFAT1, 2 protein level were unchanged in protein lysates from the cerebellum of ammonium acetate-treated rats. The present study identified multiple ammonia-induced changes in the astrocytic *O*-GlcNAcome. The ammonia-induced *O*-GlcNAc-dependent homomerization of HO-1 and release of HO-1_{TR} may contribute to oxidative and ER stress and senescence in astrocytes which all were suggested to play an important role in the pathogenesis of HE.

Zusammenfassung

Die hepatische Enzephalopathie (HE) ist eine häufige neuropsychiatrische Komplikation bei Patienten mit beeinträchtigter Leberfunktion. Ammoniak, ein Haupttoxin der HE steigert Protein-*O*-GlcNAcylierung (*O*-GlcNAc)-vermittelt die Proteinspiegel der HO-1 und induziert hierüber oxidativen- und endoplasmatisch retikulären (ER) Stress und Seneszenz in Astrozyten. *O*-GlcNAc ist eine posttranslationale Proteinmodifikation, bei der Glucosamin enzymatisch an Serin-/ Threonin-Reste in Proteinen *O*-glykosidisch gebunden wird. Hierdurch modifizierte Proteinspezies und damit verbundene funktionale Konsequenzen in Ammoniak-behandelten Astrozyten sind unbekannt und wurden in der vorliegenden Arbeit untersucht. Nach Aufreinigung *O*-GlcNAcylierter Proteine wurden mittels Massenspektrometrie mehr als 300 Spezies gegenüber Hintergrundkontrollen identifiziert, die dem astroglialen *O*-GlcNAcome zugeordnet werden können. Verglichen mit unbehandelten Astrozyten waren nach Inkubation mit NH_4Cl (5 mM, 72 h) unter den *O*-GlcNAcylierten Proteinen die Spiegel von insgesamt 68 Spezies verändert, 51 waren erhöht und 17 erniedrigt. Bioinformatische Analysen zeigten, dass diese Spezies in für die HE-Pathogenese relevante Prozesse involviert sind, wie z.B. dem Glutaminstoffwechsel oder Mitochondrienfunktionen. NH_4Cl steigerte die Proteinspiegel des 32 kDa HO-1 Monomers und der trunkierten 28 kDa Variante (HO-1_{Tr}) sowie deren *O*-GlcNAcylierung in den Astrozyten. *In vitro* wurde Ratten-HO-1 durch OGT an Serin 159 oder 160 am HO-1 Dimerisierungsinterface *O*-GlcNAcyliert. Die Inkubation der Astrozyten mit NH_4Cl induzierte GlcN-Synthese- und *O*-GlcNAcylierungs-abhängig die Bildung von HO-1 Homo- und Heteromeren. NH_4Cl steigerte die HO-1 Proteinspiegel im ER und Zellkern, aber nicht in Mitochondrien. Im Zellkern waren die HO-1 Monomer und HO-1_{Tr} Proteinspiegel erhöht. Dies ging jedoch nicht mit einer gesteigerten Transkription Nrf-2-abhängiger Gene einher. NH_4Cl steigerte *O*-GlcNAcylierungs-abhängig die Proteinspiegel des HO-1 Monomers und von HO-1_{Tr} im Zellkulturüberstand. *O*-GlcNAcylierte Proteine, HO-1 und GRP78, aber nicht OGT und GFAT1, 2 waren in Proteinlysaten aus dem Kleinhirn NH_4Azetat-behandelter Tiere erhöht. Die Ammoniak-induzierte *O*-GlcNAc-abhängige HO-1 Homo-/ Heteromerisierung und HO-1_{Tr} Freisetzung könnten im Zusammenhang stehen mit der Bildung von oxidativem und ER-Stress und Seneszenz in Astrozyten und damit eine wichtige Rolle in die Pathogenese der HE spielen.

Table of contents

List of figures

List of tables

List of abbreviations

% [v/v]	volume/ volume percent
% [w/v]	weight/ volume percent
$\Delta\Delta C_t$	delta-delta threshold cycle
3-NT	3-nitrotyrosine
ADP	adenosine diphosphate
ANOVA	analysis of variance
AP-1	activator protein-1
APS	ammonium persulfate
ARA	arachidonic acid
ARE	antioxidant response element
ATP	adenosine triphosphate
BDL	bile duct ligated
BSA	bovine serum albumin
BVR	biliverdin reductase
BV	biliverdin
BR	bilirubin
cAMP	cyclic adenosine monophosphate
cGMP	cyclic guanylate monophosphate
Ca^{2+}	calcium ions
CatB	cathepsin B
CO	carbon monoxide
CFF	critical flicker frequency
CPS1	carbamoyl phosphate synthetase 1
$CuSO_4$	copper(II) sulfate
cDNA	complementary desoxyribonucleic acid
CPR	cytochrome P450 reductase
DMEM	dulbecco's minimal essential medium

DTT	dithiothreitol
DSP	3,3´-dithiobis(succinimidyl propionate)
dNTPs	deoxynucleotide triphosphates
DMSO	dimethyl sulfoxide
EDTA	ethylenediaminetetraacetic acid
ER	endoplasmic reticulum
ERK	extracellular signal-regulated kinase
ESI	eeyarestatin I
EVs	extracellular vesicles
FAS	fatty acid synthase
FC	fold change
FCS	fetal calf serum
FDR	false discovery rate
Fe^{2+}	free ferrous iron
FITC	fluorescein isothiocyanate
Fru-6-P	fructose-6-phosphate
G-6-P	glucose-6-phosphate
G6Pase	glucose-6-phosphatase
GADD45α	growth-arrest and DNA damage-inducible protein 45α
$GABA_A$	gamma-aminobutyric acid A
Gal-T1 (Y289L)	galactosyltransferase
GAPDH	glyceraldehyde 3-phosphate dehydrogenase
gDNA	genomic DNA
GFAT	fructose-6-phosphate amidotransferase
GLAST	glutamate/ aspartate transporter 1
GlcN	D-glucosamine
GlcNAc-6-P	*N*-acetylglucosamine-6-phosphate
GlcN-6-P	glucosamine-6-phosphate
Glud1	glutamate dehydrogenase 1

GO	gene ontology enrichment
GRP78	glucose-regulated protein 78
GS	glutamine synthetase
GS^+	glutamine synthetase-positive
H_2O_2	hydrogen peroxide
HBP	hexosamine biosynthetic pathway
HE	hepatic encephalopathy
HO-1	heme oxygenase-1
$HO\text{-}1_{FL}$	full-length heme oxygenase-1
$HO\text{-}1_{rec}$	recombinant heme oxygenase 1
$HO\text{-}1_{Tr}$	truncated heme oxygenase 1
HPRT1	hypoxanthine ribosyl transferase 1
HRMs	heme regulatory motifs
HRPOD	horseradish peroxidase
Hsp	heat shock protein
IFN-γ	interferon gamma
IgG	immunoglobulin G
IL	interleukins
lncRNAs	long noncoding RNAs
iNOS	inducible nitric oxide synthase
IR	immunoreactivity
JNK	c-Jun N-terminal kinase
kDa	kilo dalton
KEGG	Kyoto Encyclopedia of Genes and Genomes
LPS	lipopolysaccharide
L-OGA	long *O*-GlcNAcase
mAb	monoclonal antibody
MAPK	mitogen-activated protein kinase
MHE	minimal hepatic encephalopathy

miRNA	microRNA
Mg^{2+}	magnesium ions
$MnCl_2$	manganese (II) chloride
MS	mass spectrometry
ms	milliseconds
MSO	methionine sulfoximine
MT	metallothionein
m/z	mass number/ charge number
NADPH	nicotinamide adenine dinucleotide phosphate
NF-κB	nuclear factor-κB
NH_3	ammonia
NH_4^+	ammonium ion
NH_4Cl	ammonium chloride
NKCC1	sodium potassium chloride cotransporter 1
NMDA	N-methyl-D-aspartate
NO	nitric oxide
NOX	NADPH oxidase
nNOS	neuronal nitric oxide synthase
NQO1	NAD(P)H-quinone oxidoreductase 1
Nrf2	nuclear factor erythroid 2-related factor 2
$O_2^{\bullet-}$	superoxide radical
$^{\bullet}OH$	hydroxyl radical
O-GlcNAc	*O*-linked β-N-acetylglucosamine
OGA	*O*-GlcNAcase
OGT	*O*-GlcNAc transferase
$ONOO^-$	peroxynitrite
PAA	polyacrylamide
pAb	polyclonal antibody
PBR	peripheral-type benzodiazepine receptors

PBS	phosphate buffered saline
PFA	paraformaldehyde
pH	potential of hydrogen
PHES	psychometric hepatic encephalopathy score
pKa	acid dissociation constant
PLA2	phospholipase A_2
PMSF	phenylmethane sulfonyl fluoride
PNGase F	peptide *N*-glycosidase F
PPAR	peroxisome proliferator-activated receptor
PTMs	post-translational modifications
PUGNAc	*O*-(2-Acetamido-2-deoxy-D-glucopyranosylidenamino)-N-phenylcarbamat
qPCR	quantitative polymerase chain reaction
RNS	reactive nitrogen species
ROS	reactive oxygen species
rpm	revolutions per minute
RT	reverse transcription
RTase	reverse transcriptase
SASP	senescence-associated secretory phenotype
SEM	standard error of the mean
sER	smooth endoplasmic reticulum
SMIT	sodium-dependent inositol transporter
SOD	superoxide dismutase
SP1	specificity protein 1
SPP	signal peptide peptidase
TCA	trichloroacetic acid
TEMED	tetramethylethylenediamine
TMS	transmembrane segment
TNF-α	tumor necrosis factor α
TIPS	transjugular intrahepatic portosystemic shunt

TPRs	tetratricopeptide repeats
TGR5	G-protein-coupled bile acid receptor 1
UDP-GalNAz	uridine diphosphate-azido-modified galactose
UPS	ubiquitin-proteasome system
WB	Western blot
Zn^{2+}	zinc ions
ZnPP	zinc protoporphyrin IX

1. Introduction

1.1 Hepatic Encephalopathy

Hepatic Encephalopathy (HE) is a complex neuropsychiatric syndrome frequently seen in patients with either acute or chronic liver diseases [*1*]. HE is characterized by cognitive disturbances and fine motor skill impairments of varying severity, which are suggested to arise from the slowing of cerebral oscillatory networks [*1*]. Globally, liver diseases account for around 2 million deaths annually, with complications from cirrhosis contributing to half of these cases [*13*]. Subtle symptoms of HE are detectable in nearly 60% of cirrhosis patients, significantly decreasing their quality of life. Notably, overt HE is observed in approximately 30-45% of individuals with cirrhosis [*14*]. In Germany, over 5 million individuals are living with liver disease, approximately one-fifth of whom are diagnosed with cirrhosis [*15*, *16*]. Among hospitalized patients with liver cirrhosis, HE symptoms are observed in nearly 60% of cases, making it one of the most intricate complications which may occur [*17*, *18*]. In the United States, the prevalence of HE spans an estimated 5.5 million cases, with about 150,000 new diagnoses each year [*19*, *20*]. China faces a particularly high burden of liver disease, with over 300 million chronic liver disease patients. Notably, approximately 40% of these patients with cirrhosis suffer from Minimal Hepatic Encephalopathy (MHE), positioning China as the country most affected by liver disease globally [*21*].

1.1.1 Diagnosis and classification of Hepatic Encephalopathy

Symptoms of HE vary significantly in severity and therefore were classified according to the so-called West Haven criteria (WHC) into minimal HE and grades I through IV (Fig. 1.1) [*1*]. The classification of Grade I HE, as per these criteria, is subjective, often relying on the observations of caregivers or doctors familiar with the patient. Therefore, “overt HE” is generally used to describe cases showing clear symptoms like temporal disorientation or flapping tremor,

indicative of at least Grade II HE [*1*]. A subclinical variant of HE, known as MHE, is distinct from overt HE, but its diagnosis can be challenging as some symptoms akin to HE
grade I can also be found in patients without liver disease [6]. MHE is reported to be present in up to 50% of patients with chronic liver disease [*22*]. Given the absence of clear clinical symptoms, the detection of MHE primarily relies on psychometric and neuropsychological testing [*1*, *23*]. Conversely, Grade I HE, often detected by those close to the patient or through testing, falls under the category of covert HE, a term that implies subtler manifestations, yet includes symptomatic patients. Covert HE is distinct from MHE and lacks further grading. A notable aspect of the covert/ overt HE model is that symptoms such as disorientation and asterixis signify Grade II overt HE [*1*, *24*]. However, the term “overt” might be misleading, as patients with Grade I HE already show manifest symptoms, adding to the nomenclature's complexity [*1*].

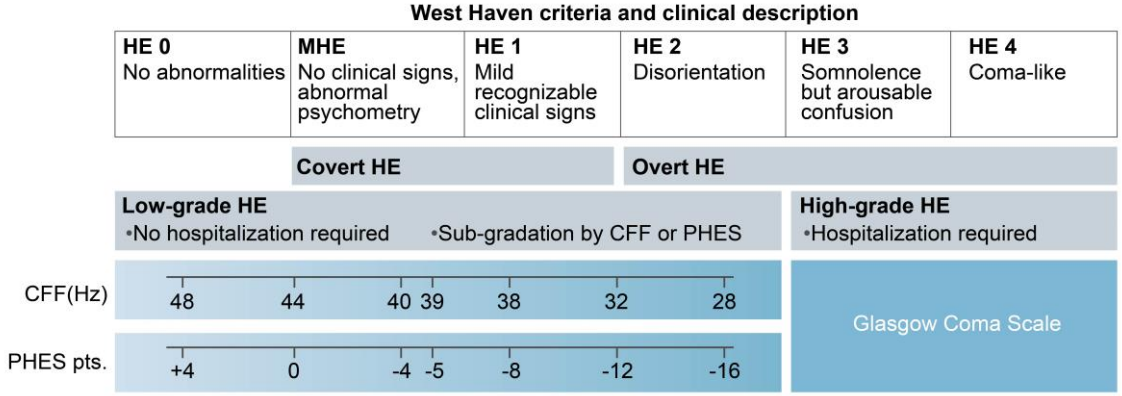

Figure 1.1: Classification of severity of HE. According to the West Haven criteria (WHC) [*8*], HE is classified into minimal HE (MHE) and HE stages 1-4. MHE only shows abnormalities when analysed by critical flicker frequency (CFF) and psychometric testing which yield the so-called “Psychometric Hepatic Encephalopathy Score” (PHES) MHE is characterized by a CFF of ≤ 39 Hz and a PHES score ≤ −5 [*1*]. (Reprinted with permission from Springer Nature, from Häussinger D. *et al*., 2022, Nature reviews, Disease primers. License No. 5597711487288).

A joint clinical practice guideline from the European Association for the Study of the Liver (EASL) and the American Association for the Study of Liver Disease (AASLD) suggests that the prevalence of HE could rise to 80% over a patient's follow-up period [*24*]. Meanwhile, overt HE is likely to manifest in 30-40% of cirrhotic patients during their entire clinical course of the

patients [*24*]. This condition not only significantly elevates the mortality but also places an enormous burden on patients, caregivers, and the healthcare system at large [*25*, *26*]. It is estimated that mild cognitive impairment from HE affects 60-80% of the cirrhotic population, substantially impairing daily functioning and reducing quality of life [*27*]. Current neurophysiological test methods aiding in HE diagnosis include the Psychometric Hepatic Encephalopathy Score (PHES) [*28*], computerized psychometric tests like the Stroop test [*29*] and SCAN test [*30*], the Continuous Reaction Time test (CRT) [*31*], the Inhibitory Control Test (ICT) [*32*], serum biomarkers [*33*]. Further diagnostical measures include, abdominal and brain imaging, electroencephalography (EEG), Critical Flicker Frequency (CFF) and blood ammonia levels [*1*, *34*, *35*].

The diagnosis of MHE has been complicated by a lack of standardization among the psychometric test batteries which are most frequently used and this has led to challenges in defining MHE [*6*]. Consequently, a revised classification of HE severity has been suggested, which classified includes MHE and previously recognized grades I and II of manifest HE under the umbrella of as "low-grade HE" [*1*]. This classification takes into account that techniques such as CFF and evoked potential recording can objectively identify low-grade HE [*36*]. Despite the lack of correlation between blood ammonia levels and the severity of HE, high blood ammonia levels have been suggested as a predictor of hospitalisation for HE [*37*]. For instance, a blood ammonia concentration exceeding 150 µmol/L in cases of acute liver failure, or surpassing 80 µmol/L in the context of cirrhosis, significantly increases mortality risk, thereby serving as a potential diagnostic marker for these conditions [*1*, *38*, *39*]. It is crucial to note that normal ammonia levels do not rule out the presence of HE, necessitating further diagnostic testing [*24*]. While 3-nitrotyrosine (3-NT) has been proposed as a serum biomarker for identifying mild HE in patients with alcoholic cirrhosis [*40*], its applicability across other liver cirrhosis etiologies remains unclear. There is also evidence suggesting that inflammation triggers episodes of HE in patients with liver cirrhosis. This has led to propose that inflammatory mediators, such as interleukins (IL)-6 and 18, may serve as potential biomarkers for the presence of HE in cirrhotic patients [*41*]. Since these inflammatory mediators are

influenced by a wide array of factors, and their specificity is relatively low, their reliability as biomarkers of HE in patients with liver cirrhosis remains to be proven.

1.1.2 Therapy of Hepatic Encephalopathy

Current therapeutic approaches aim at removing HE-triggering factors [*1*, *42*]. These include gastrointestinal or tissue bleeding [*43*], excessive dietary protein [*44*], infections [*45*], electrolyte imbalances [*46*], overuse of diuretics [*47*], drug use [*48*, *49*] and constipation [*50*]. Furthermore, portocaval shunting is removed by surgical procedures such as the transjugular intrahepatic portosystemic shunt (TIPS) [*51*].

The therapeutic landscape for HE is diverse and tailored to address its multifaceted pathophysiology. Central to HE management is the reduction of the neurotoxin ammonia [*1*]. Lactulose, a non-absorbable disaccharide, is important in this aspect. It reduces ammonia production by altering the gut environment, both in terms of microbial composition and pH, thereby decreasing its absorption [*52*]. This approach is often complemented with antibiotics like neomycin [*53*] and rifaximin [*54*], which further reduce ammonia-producing gut bacteria [*1*]. Simultaneously, nutritional strategies are employed, with a preference for plant-based proteins over animal proteins, owing to their lower potential for ammonia and neurotoxin production during digestion [*55*]. Zinc supplementation is another aspect, given its role in ammonia metabolism and the commonality of zinc deficiency in liver disease [*56*]. To mitigate the neurological manifestations of HE, benzodiazepine receptor antagonists [*57*] are used to normalize the increased GABAergic activity in the central nervous system [*1*]. Nutritional supplementation, particularly with branched-chain amino acids (BCAAs), supports overall patient health and may alleviate HE symptoms by modulating brain amino acid levels [*58*]. L-Ornithine-L-Aspartate plays a critical role in reducing blood ammonia levels by enhancing its conversion to urea and glutamine [*59*]. Beyond conventional treatments, HE management encompasses various off-label and experimental approaches [*1*]. These include polyethylene glycol [*60*], fecal transplantation [*61*], and adsorbing agents like AST-120 (kremezin) [*62*] or a

combination of micro-macrospheres (e.g. CARBALIVE^{TM}) [*63*], all targeting ammonia reduction through different mechanisms [*1*]. Ornithine phenylacetate [*64*] and glycerol phenylbutyrate [*65*] are used for their dual action in glutamine metabolism and ammonia reduction. Additionally, novel therapies such as albumin dialysis with the molecular adsorbents recirculating system [*66*] and the DIALIVE device [*67*] are being explored for their potential in reducing HE severity by targeting inflammation, a key factor in HE pathophysiology [*1*]. For cases where these interventions are ineffective, liver transplantation remains the only treatment option [*68*]. However, neurological impairment may not fully resolve after liver transplantation [*69*]. This has been suggested as a consequence of astrocyte senescence which may trigger irreversible structural changes in the brain [*4*, *69*]. This array of treatment options underscores the complex and interconnected nature of HE management, combining established methods with innovative research to improve patient outcomes [*1*].

1.1.3 Predisposing and precipitating factors of Hepatic Encephalopathy

HE manifests in the context of a dysfunctional liver, which either occurs acutely within hours or days, or chronically within months or even years [*70*]. While acute liver failure can be caused by liver toxins such as high doses of paracetamol [*71*], chronic liver damage, potentially progressing to liver cirrhosis, may be the result of hepatotropic viruses or prolonged alcohol abuse [*36*, *72*]. In these scenarios, the liver fails to sufficiently detoxify endogenous neurotoxic compounds which consequently bypass liver metabolism. These toxins can then cross the blood-brain barrier [*73*] and reach cells of the central neuronal system such as neurons, astrocytes, microglia and others [*74-76*].

Among the toxins which may impair the functions of these cells is ammonia, which is considered a major risk factor for the development of HE in patients with acute or chronic liver failure [*70*]. There are several risk factors that can trigger HE and which can be divided into predisposing and precipitating categories [*70*]. Factors predisposing to HE are multiple and intertwined, often resulting from complex changes in liver function [*1*]. A key determinant is

the type of liver disease, with alcohol-related cirrhosis presenting a notably higher risk compared to nonalcoholic, nonviral forms [*72*]. This disparity is highlighted by an adjusted hazard ratio (aHR) of 1.44 for alcohol-related cirrhosis. The extent of portosystemic shunting is another critical factor. A cumulative cross-sectional area exceeding 83 mm^2 in portosystemic shunts correlates with a higher HE risk and decreased survival [*77*]. Spontaneous portosystemic shunts in liver impairment patients are particularly problematic, increasing morbidity and mortality [*77*]. While TIPS increases HE incidence, strategic interventions, like using covered stents and early TIPS implementation, may mitigate this risk [*78*, *79*]. Noteworthy, the predisposing risk factors of HE can also be predicted by examining albumin [*80*] and bilirubin levels [*81*] and the Model for End-Stage Liver Disease (MELD) score [*82*]. A patient without prior HE episodes but with specific albumin and bilirubin profiles faces a substantial risk of HE within three years [*83*]. However, the MELD score, while informative for cirrhosis prognosis, doesn't always align with HE severity [*1*]. In examining the genetic risk factors of HE, a particular study explored the role of genetic variations in the glutaminase gene (GLS1) and highlighted the presence of a functional microsatellite, characterized by GCA repeats near the GLS1 promoter region. This study suggested that cirrhosis patients homozygous for the longer allele of this microsatellite might have a heightened propensity to develop overt HE [*84*]. However, a later study found no substantial evidence supporting the homozygous long genotype as a risk factor for HE [*85*]. In fact, the findings indicated that the heterozygote genotype protects against the development of HE [*85*]. Given these conflicting results, there is a clear need for additional studies to clarifying whether this genetic variation predisposes to develop HE in patients with liver cirrhosis.

Precipitating risk factors span various conditions or diseases, including metabolic acidosis [*1*], gut microbiota imbalance [*86*, *87*], variceal bleeding [*43*], constipation [*88*], small intestinal bacterial overgrowth (SIBO) [*50*], renal insufficiency [*89*], hyponatraemia [*76*], type 2 diabetes mellitus [*90*], epilepsy [*91*], advanced age [*92*], malnutrition and sarcopenia [*93*]. Medications commonly prescribed to cirrhosis patients, such as proton pump inhibitors (altering gut microbiota) for gastric ulcers [*48*, *49*], benzodiazepines and GABAergics (affecting central nervous system) for anxiety [*94*], and opioids (slowing intestinal motility) for pain [*95*], can

inadvertently contribute to the development of HE [*1*]. Additionally, aging further amplifies this risk due to an increased likelihood of polypharmacy, potentially enhancing the neurotoxic effects of ammonia [*92*]. Thus, risk assessment and management of HE should involve a comprehensive approach that addresses these diverse aspects [*1*].

The group of HE precipitating factors is extremely heterogeneous and for a long time the common action of these diverse factors to trigger HE remained elusive. However, in 1994 Professor Dr. Häussinger for the first time proposed astrocyte swelling and the induction of a so-called low-grade cerebral edema as a central mechanism that triggers HE in patients with liver cirrhosis [*96*, *97*]. Here, astrocyte swelling was proposed as a point of convergence of the actions of the heterogeneous group of HE-precipitating factors. In this regard, HE-precipitating factors will upregulate so-called HE-relevant factors such as ammonia, pro-inflammatory cytokines or benzodiazepines of the diazepam-type or induce hyponatremia which are all known to trigger astrocyte swelling [*98*]. For example, gastrointestinal bleeding leads to the digestion of blood-derived proteins which elevates ammonia levels [*99*]. Increasing dietary protein intake raises blood ammonia levels [*100*]. Moreover, systemic inflammation upregulates the levels of pro-inflammatory cytokines in the blood [*76*]. This paradigm for the first time explained how such complex neurological alterations observed in HE is precipitated by a such a heterogeneous set of factors.

1.1.4 Pathobiochemistry of hyperammonemia

Ammonia is considered a main toxin in the pathogenesis of HE [*101*]. This was evidenced by numerous studies which have highlighted ammonia as a critical factor in the neurophysiological alterations seen in liver failure and inherited urea cycle enzyme disorders [*42*, *102*]. The primary source of ammonia in the body is the metabolism of nitrogen-rich compounds, predominantly within the intestines and skeletal muscles [*103*, *104*]. Ammonia, a weak base with a pKa of 9.25 in water at 37 °C, exists mainly as protonated NH_4^+ at a physiological pH of 7.4, with less than 2% in the deprotonated (NH_3) form. The lipophilic

deprotonated ammonia can passively permeate cell membranes and cross the blood-brain barrier [*105*]. The protonated form NH_4^+ is transported by ion channels such as the sodium potassium chloride cotransporter 1 (NKCC1) [*105*]. In healthy individuals, ammonia is mainly produced in the small bowel by the action of enterocytic glutaminase and in the colon by gut bacteria [*1*, *106*]. Upon production, ammonia is detoxified in the liver via the urea cycle in periportal hepatocytes with low-affinity but high-capacity [*107*]. Urea is then excreted by the kidneys [*108*, *109*].

In the intricate landscape of liver function, a specialized subset of cells known as perivenous scavenger cells, predominantly the glutamine synthetase-positive (GS^+) hepatocytes, are pivotal in liver ammonia detoxification [*108*, *110*]. These cells are strategically located at the acinar efflux, enabling them to effectively trap and neutralise ammonium ions escaping from primary urea synthesis in the periportal areas [*108*]. This function is particularly important given the low affinity of the urea cycle initiating enzyme, carbamoyl phosphate synthetase 1 (CPS1), for ammonia and the generally low ammonium concentrations found in portal blood [*108*, *111*]. Perivenous scavenger cells play a multifaceted role in liver health. Through this dual ammonia-detoxification system, the liver typically maintains blood ammonia levels below 50 µM in humans [*109*, *112*].

While glutamine synthesis is a well-known ammonia detoxification pathway, these cells additionally regulate amino acid and nitrogen metabolism through further transporters and enzymes such as glutamate/ aspartate transporter II [*113*], ornithine aminotransferase (OAT1) [*114*], ammonium transporter Rh type B (RhBG) [*115*] and dicarboxylate uptake systems [*116*]. These distinct functions contribute to the maintenance of nitrogen balance and underscore the importance of perivenous scavenger cells in overall hepatic functionality [*108*]. In both mice and humans, the significance of perivenous scavenger cells in maintaining ammonia homeostasis is evident [*117*, *118*]. Mouse models with liver-specific GS deletion exhibit hyperammonemia, leading to neuronal and behavioral abnormalities, highlighting the critical role of hepatic GS in systemic ammonia regulation [*117*]. This is further exemplified in taurine transporter knockout mice, where impaired glutamine synthesis in the perivenous area,

attributed to the inactivation of GS and downregulation of RhBG, results in hyperammonemia [*119*]. Similar to inherited urea cycle disorders, patients with rare genetic GS deficiencies exhibit chronic hyperammonemia and reduced glutamine levels in body fluids [*120*]. Reduced protein levels of GS are also observed in patients with liver cirrhosis, often accompanied by chronic hyperammonemia [*118*].

In individuals with either spontaneous portosystemic shunts (SPSS) or cirrhosis, the liver's capacity to synthesize urea and glutamine, and consequently detoxify ammonia, is significantly compromised. This impairment results higher levels of ammonia in the systemic circulation [*121*, *122*]. Ammonia which is not efficiently cleared from the blood by the liver, can reach the brain and here it is metabolized to glutamine in astrocytes [*123*].

1.1.5 Role of astrocyte swelling in the pathogenesis of HE

In brain, astrocytes are vital for maintaining brain homeostasis by supporting the metabolism of neurons but also by actively participating in neurotransmission [*124*]. They are the predominant cells involved in ammonia metabolism [*125*, *126*]. Importantly, hyperammonemia as a consequence of liver dysfunction leads to excess formation of glutamine in the astrocytes. The resulting elevated glutamine levels triggers osmotic imbalances within the astrocytes [*127*]. This causes water to enter the cells to equilibrate the osmotic gradient, resulting in astrocyte swelling [*128-130*]. This swelling interferes with normal brain function and impairs neurotransmission [*131*], disturbs the blood-brain barrier [*105*], and potentially elevates intracranial pressure [*132*]. Of note, in animal models, the administration of the glutamine synthetase inhibitor methionine sulfoximine (MSO) entirely prevented the ammonia-induced astrocyte swelling and brain edema [*133*]. This further highlighted the importance of the astrocytes for the pathogenesis of HE and has led to focus on this cell type in search for a therapy. Beyond ammonia, other HE-relevant factors such as ligands of the peripheral-type benzodiazepine receptors (PBR) [*134-136*], pro-inflammatory cytokines [*137*, *138*] and

hyponatremia [*139*, *140*], have also been found to induce astrocyte swelling. These findings emphasize the central role of astrocyte swelling in the pathogenesis of HE.

In 1994 Häussinger *et al*. provided fundamental concept of the pathogenesis of HE by establishing astrocyte swelling and the formation of mild cerebral edema as hallmarks of HE in patients with liver cirrhosis [*96*]. Using proton magnetic resonance (^{1}H-MR) spectroscopy, this study revealed for the first time decreased levels of the osmolyte myo-inositol and increased levels of glutamine in brain of patients with liver cirrhosis and HE [*96*]. Given the localization of glutamine synthetase primarily in astrocytes [*127*], the decrease in inositol was interpreted as a compensatory volume regulatory response to the osmotic imbalance caused by glutamine synthesis within these cells [*96*]. Importantly, this low grade edema may escalate from mild to clinically overt when further osmotic disturbances are introduced by additional HE-precipitating factors (Fig. 1.2) [*6*]. Subsequent research unveiled a strong interplay between astrocyte swelling and oxidative/ nitrosative stress. Evidence of oxidative/ nitrosative stress was found in *in vitro* and in animal models of HE [*69*, *141*] and also in *post mortem* brain samples from patients with liver cirrhosis and HE [*137*]. This reciprocal relationship leads to protein modifications, RNA oxidation, changes in gene expression and signaling pathways, culminating in astrocytic/ neuronal dysfunction which are suggested to trigger cognitive and motoric symptoms of the patients [*1*, *142*, *143*].

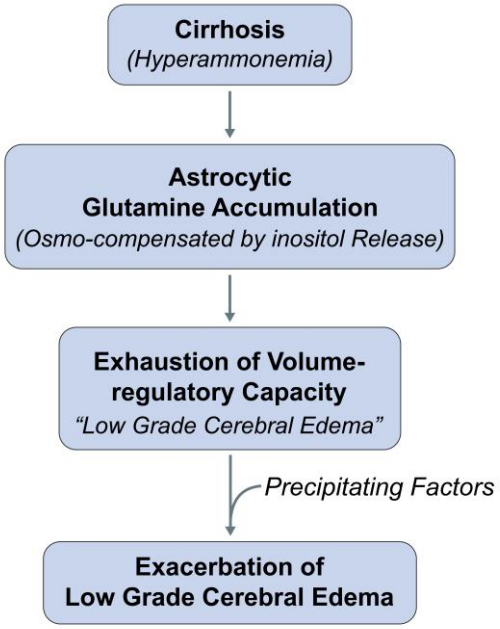

Figure 1.2: Hepatic encephalopathy and the generation of a low-grade cerebral edema. Hyperammonemia in patients with chronic liver failure leads to an accumulation of glutamine in astrocytes in the brain through the action of glutamine synthetase. The astrocytes can partially compensate the resulting osmotic stress through the release of organic osmolytes such as of myo-inositol. However, this depletes the available osmolyte pool and, triggers the generation of a low-grade cerebral edema. This makes the astrocyte susceptible to swelling-inducing effects of further HE-precipitating factors such as pro-inflammatory cytokines and others, which then may exacerbate the low-grade cerebral edema [*6*]. (Reprinted with permission from: Archives of Biochemistry and Biophysics, Häussinger, D., *et al.*, 2013; License No. 1382620-1).

1.1.6 Osmotic and oxidative/ nitrosative stress in HE

There is univocal evidence that ammonia triggers the formation of reactive oxygen species (ROS) and reactive nitrogen species (RNS) and thereby leads to oxidative/ nitrosative stress in astrocytes. This results in posttranslational protein modifications [*144*, *145*], oxidation of RNA [*6*, *141*] and of lipids [*146*, *147*], which were suggested to strongly impact on cellular physiology [*141*, *145*]. Importantly, *in vitro* studies showed that astrocyte swelling per se is sufficient to trigger ROS/ RNS formation in astrocytes [*6*, *148*, *149*]. Additional studies showed that further HE-relevant factors such as pro-inflammatory cytokines and benzodiazepines also trigger ROS/ RNS formation [*136*, *150*]. Given that HE-relevant factors trigger astrocyte swelling and ROS/ RNS formation and that astrocyte swelling in turn is sufficient to trigger ROS/ RNS formation,

Häussinger proposed that both are interrelated. He concluded that HE-relevant factors engage a self-reinforcing cycle in the astrocytes between osmotic and oxidative/ nitrosative stress [*151*, *152*]. This suggestion is further supported and extended by studies showing that HE-relevant factors cooperate in the induction of oxidative/ nitrosative and osmotic stress in cultured rat astrocytes [*12*, *149*, *153*, *154*]. Collectively, these studies provided a novel view on the pathogenesis of HE as a consequence of osmotic and oxidative/ nitrosative stress [*1*].

Further research shows that the interplay between astrocyte swelling and oxidative/ nitrosative stress alters mRNA and protein levels of osmoregulatory transporters [*155*]. Here, oxidative/ nitrosative stress was found to downregulate the sodium-dependent inositol transporter protein (SMIT) and the taurine transporter protein (TAUT), potentially exacerbating astrocyte dysfunction [*155*, *156*]. Here, NADPH oxidase mediates both ROS-induced swelling and the decline in SMIT and TAUT mRNA [*149*, *155*, *157*]. Importantly, SMIT mRNA was also decreased in the cerebral cortex of animal models of acute or chronic hyperammonemia [*155*].

The ammonia-induced swelling of the astrocyte *in vitro* was also proposed to result from an oxidative/ nitrosative stress-induced upregulation of the water channel protein, aquaporin (AQ) 4 [*158*, *159*]. However, the specific mechanisms driving the increase in AQP4 expression in response to ammonia are not fully understood and an involvement of AQ4 for brain edema formation in animal models of HE still remains a matter of controversial debate [*160*]. The potential cellular sources of cerebral ROS/ RNS in HE extend beyond astrocytes, with *in vitro* studies who identified neurons [*161*], microglia [*162*, *163*], fibroblasts [*69*] and endothelial cells [*164*]. Furthermore, there is evidence suggesting that reactive oxygen species originating outside the brain can contribute to cognitive impairment in HE [*165*, *166*]. In this regard, it was shown that manipulating ROS levels in the peripheral blood of bile duct ligated (BDL) or portacaval-shunted rats, either by scavenging ROS or by increasing ROS, was found to prevent or instigate the development of brain edema, respectively [*165*, *166*]. The potential synergistic effects between liver malfunction, hyperammonemia, and ROS originating outside the brain in

precipitating cerebral osmotic stress presents another layer of complexity in the pathogenesis of HE.

Reactive nitrogen species such as peroxynitrite ($ONOO^-$) trigger the nitration of tyrosine residues in proteins which serves as a surrogate marker of oxidative/ nitrosative stress [*167*]. Increased levels of 3-nitrotyrosine (3-NT) have been reported in the peripheral blood of patients with liver cirrhosis who have developed HE, underscoring the potential role of systemic oxidative stress in this condition [*40*, *168*].

1.1.7 Mechanisms underlying oxidative/ nitrosative stress in astrocytes in HE

During the recent years, considerable progress has been made *in vitro* and *in vivo* models of HE in identifying sources of ROS and RNS and the underlying molecular mechanisms [*136*, *150*, *154*, *169-171*]. Here, it was shown that the oxidative/ nitrosative stress triggered by HE-relevant factors originates from different cellular compartments such as the nucleus [*149*] or the mitochondria [*69*, *172*].

One significant mechanism involves the activation of *N*-methyl-D-aspartate receptors (NMDAR) in astrocytes (Fig. 1.3). The activation of ion channel through the binding of glutamate elevates intracellular calcium levels rise and triggers the formation of superoxide anion radical ($O_2^{\bullet-}$) and nitric oxide (NO) in astrocytes incubated with HE-relevant factors [*136*, *150*, *154*, *169*]. This was suggested a consequence of a membrane depolarization which removes the Mg^{2+} blockade of the NMDA-receptor [*173*, *174*]. The resulting elevation of the intracellular Ca^{2+} concentration triggers a vesicular release of glutamate through activation of the phospholipase A_2 (PLA2) and subsequent formation of prostanoids [*175*]. This glutamate release further raises intracellular Ca^{2+} levels through the activation NMDARs [*12*]. As a consequence of this amplification process, NADPH oxidase (NOX) isozymes 2 [*176*] and 4 [*4*] and neuronal nitric oxide synthase (nNOS) [*157*, *169*] become activated [*1*] and inducible nitric oxide synthase (iNOS) is upregulated [*136*, *177*]. NOX2, when activated, utilizes molecular oxygen and electrons from NADPH to generate $O_2^{\bullet-}$ [*176*, *178*]. iNOS and nNOS play a crucial

role in the ammonia-induced production of NO in astrocytes *in vitro* [*136*, *179*]. The rapid reaction of NO with $O_2^{\bullet-}$ results in the formation of $ONOO^-$, which can cause subsequently protein tyrosine nitration *in vitro* and *in vivo* [*136*, *141*, *180*].

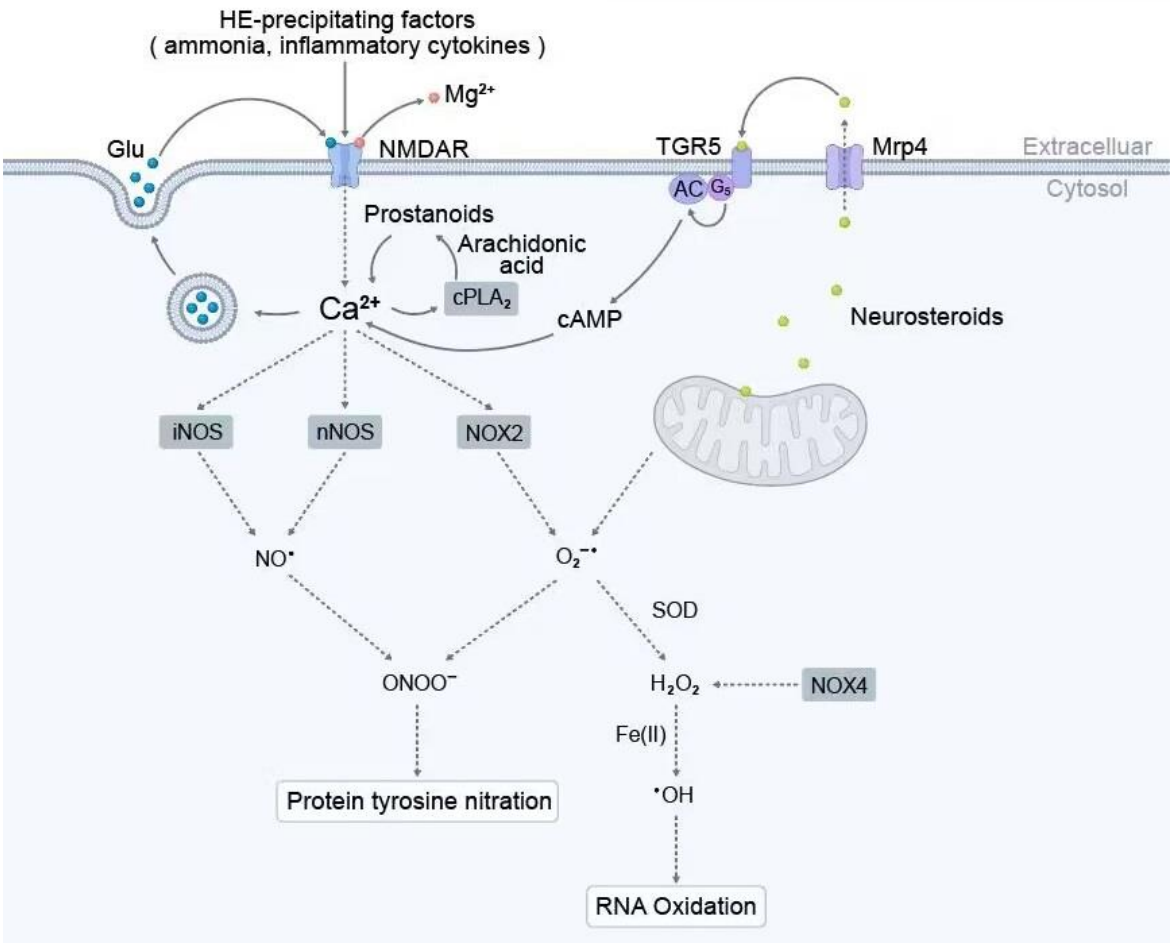

Figure 1.3: Mechanisms of oxidative/ nitrosative stress in astrocytes in HE. Activation of the NMDAR and exocytotic/vesicular release of glutamate triggers ROS and RNS formation in astrocytes incubated with HE-relevant factors. The vesicular glutamate release is triggered through arachidonic acid (ARA) release by cytoplasmic phospholipase A_2 (cPLA2) and the subsequent synthesis of prostanoids. This in turn leads to formation of NO and, $O_2^{-\bullet}$ which can recombine to form peroxynitrite ($ONOO^-$) [*12*]. Consequences of the RNOS formation are posttranslational protein modifications, oxidation of RNA and gene expression changes (Reprinted with permission from Rightslink: Archives of Biochemistry and Biophysics, Görg, B., *et al*., 2013a; License No. 1382749-1).

Exposure to ammonia triggers the production of ROS, primarily through the activation of NOX isoforms 2 and 4 [*154*, *176*]. *In vitro* studies demonstrated that exposure to ammonia containing or hypoosmotic cell culture media rapidly activates NOX2 in astrocytes via protein

kinase C (PKC) ζ phosphorylation within few minutes [*176*]. Additionally, NOX4 protein levels increase within 24 hours of ammonia exposure in cultured rat astrocytes [*4*]. Notably, NO and $O_2^{\bullet-}$, derived from NOS enzymes and NOX, respectively, contribute to cell swelling in ammonia-exposed astrocytes [*69*, *149*, *170*, *177*]. Interestingly, in animal models of chronic hyperammonemia both the basal and stimulated activities of nNOS in response to NMDAR activation are reduced in cerebellum [*181*]. Beyond NOX2 and 4, also glutaminase-mediated glutaminolysis was suggested to contribute to ammonia-induced $O_2^{\bullet-}$ formation in mitochondria [*69*, *170*]. This was suggested to trigger the mitochondrial permeability transition [*182*], which is paralleled by mitochondrial swelling [*69*, *183*]. Currently, the source of mitochondrial reactive oxygen species is unclear.

Recent studies further suggested that $O_2^{\bullet-}$ reacts with free ferrous iron (Fe^{2+}) ions, whose intracellular levels rise in ammonia-exposed astrocytes and thereby hydroxyl radicals are formed in the Fenton reaction [*69*] which may oxidize RNA [*6*, *141*]. Additionally, superoxide and nitric oxide may recombine to form $ONOO^-$, which can nitrate protein residues in proteins [*180*].

Neurosteroids activate the γ-aminobutyric acid ($GABA_A$) neurotransmitter receptor and thereby inhibit neuronal activity [*184*]. Enhanced GABAergic neurotransmission was suggested to underlie cognitive dysfunction in HE patients [*185*, *186*]. Importantly, the synthesis of neurosteroids involves the activation of the PBR and PBR binding sites were increased in brains of cirrhotic patients suffering from HE [*187*]. However, neurosteroids are also ligands of the G-protein-coupled bile acid receptor 1 (Gpbar-1, also known as TGR5), which was first recognized as a bile acid receptor in gastrointestinal and immune cells [*184*]. In brain, TGR5 expression is detected in astrocytes and neurons, and ammonia exposure *in vitro* was shown to downregulate both mRNA and protein levels of TGR5 in astrocytes [*184*]. TGR5 mRNA was also decreased in *post mortem* brain samples from patients with liver cirrhosis who had HE, but not in those who died without HE [*184*]. Since activation of the TGR5 triggers ROS formation in astrocytes and neurons *in vitro*, downregulation of TGR5 was interpreted to reflect a protective response [*184*]. In this regard, TGR5 downregulation may mitigate the neurosteroid-induced

ROS formation and cerebral oxidative stress in the brains of patients with liver cirrhosis and HE [*184*].

1.1.8 Consequences of oxidative/ nitrosative stress in HE

The vicious cycle between osmotic and oxidative/ nitrosative stress, which is triggered by HE-relevant factors, provokes numerous alterations in astrocytes *in vitro* [*154*, *175*, *179*, *188*]. Most of these alterations, which were proposed to contribute to the pathogenesis of HE, were also observed in *post mortem* brain samples from patients with liver cirrhosis and HE [*137*]. The following sections and Figure 1.4 describe these changes in detail.

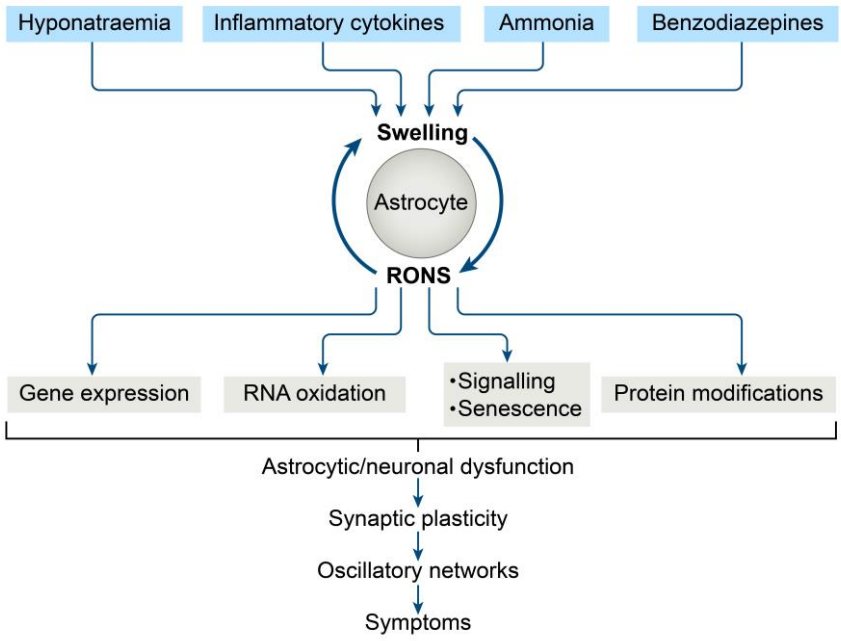

Figure 1.4: Pathogenetic model of hepatic encephalopathy. In astrocytes, HE-relevant factors trigger swelling and ROS/ RNS production, which are interdependent. This sets off a self-reinforcing cycle in which neuronal function is impaired. As a result, synaptic plasticity and oscillatory networks in the brain are disrupted, affecting motor and cognitive function, which is reflected in the symptoms of patients with HE [*1*]. (Reprinted from Rightslink with permission: Springer Nature, Nature reviews, Disease primers, Häussinger, D., *et al*., 2022; License No. 5597711487288).

HE-relevant factors strongly alter the expression of numerous genes in astrocytes *in vitro* [*4*, *137*, *143*]. The increased synthesis of NO, triggered by HE-relevant factors, leads to the release of Zinc ions (Zn^{2+}), which consequently triggers gene expression changes in the astrocyte [*137*, *151*]. Here, the rise in intracellular free Zn^{2+}, induced by ammonia and hypoosmotic cell culture media, prompts the nuclear accumulation of metal regulatory transcription factor 1 (MTF-1) and specificity protein 1 (SP1), which activates transcription of metallothionein (MT) 1/2 and the PBR mRNA [*179*, *189*]. While upregulation of MT1/2 may counteract toxic effects promoted by free Zn^{2+} ions, upregulation of the PBR was suggested to underlie enhanced neurosteroid synthesis [*179*].

A study by Dr. Görg, Dr. Bidmon and Prof. Dr. Häussinger in 2013 on *post mortem* human brain tissue confirmed many of the gene expression changes observed in astrocytes incubated with HE-relevant factors *in vitro* in patients with liver cirrhosis with HE [*137*]. Moreover, this study identified so far unknown HE-characteristic gene expression changes in the cerebral transcriptome in *post mortem* human brain samples from patients with liver cirrhosis [*137*]. Levels of a total of 1,012 genes were altered in patients with liver cirrhosis with and without HE [*137*]. The findings highlighted, that genes whose expression patterns were altered in HE, were implicated in oxidative stress defense (e.g. heme oxygenase-1 and peroxiredoxin-4) and related to cell proliferation (e.g. tumor suppressor protein 53 and lamin A/C) [*137*]. Interestingly, also many anti-inflammatory genes were upregulated in the cerebral cortex from patients with liver cirrhosis with HE such as peroxisome proliferator-activated receptor (PPAR)-α activity, which may counteract oxidative stress and inflammation in responses to endotoxemia [*137*, *190*]. Surprisingly, genes coding for pro-inflammatory cytokines and chemokines, such as IL-1β, IL-4, IL-10, IFN-γ and tumor necrosis factor α (TNF-α), were not significantly changed in the cerebral cortex of patients with or without HE [*137*]. This result corroborated findings from other studies showing unchanged pro-inflammatory cytokine mRNA levels in the cerebral cortex of animal models of HE or *post mortem* brain tissue from patients with liver cirrhosis with HE [*163*, *191*]. However, this does not rule out the possibility that pro-inflammatory cytokines may be upregulated in brain regions other than those studied in patients with cirrhosis and HE [*137*, *191*].

Extracellular neurosteroid levels are not exclusively governed by endogenous synthesis and metabolism [*192*], but also by their cellular transport systems such as by the MRP4 [*186*, *193*]. Interestingly, MRP4 protein levels were upregulated in astrocytes exposed to ammonia *in vitro* and in *post mortem* brain samples from patients with cirrhosis who had HE [*193*]. Therefore, it has been postulated that MRP4 may be involved in the release of neurosteroids from astrocytes, potentially contributing to the enhanced GABAergic neurotransmission observed in HE [*186*, *193*]. Ammonia, increased MRP4 protein levels in astrocytes *in vitro* in a dose- and time-dependent way, which was prevented by the glutamine synthetase inhibitor MSO [*193*]. Interestingly, inhibition of MRP4 with the chemical compound ceefourin 1 enhanced the ammonia-induced astrocyte senescence and upregulation of the oxidative stress surrogate marker heme oxygenase-1 (HO-1) [*193*]. Thus, upregulation of MRP4 may protect astrocytes by increasing the efflux of compounds such as of its substrate cyclic adenosine monophosphate (cAMP), which is known to inhibit astrocyte proliferation [*193*]. The same study also suggested that ROS/ RNS formation in astrocytes incubated with ammonia also activates PPARα, a transcription factor that regulates the expression of various genes involved in metabolism [*194*, *195*], inflammation [*196-198*], oxidative stress [*199*, *200*] and neurosteroid synthesis [*201*, *202*]. Importantly, MRP4 itself is among the genes whose transcription is controlled by PPARα [*193*].

Several HE models have been employed to assess the regulation of AQP-4, the most prevalent aquaporin in the brain and highly expressed in astrocytes [*158*, *203*, *204*]. Some studies support the hypothesis, that AQP-4 is involved in the development of brain edema in HE [*204-207*]. Treatment of cultured astrocytes with ammonia or in hyponatremic conditions resulted in upregulation of AQP4 [*158*]. Moreover, silencing the AQP-4 gene prevented the ammonia-induced cell swelling [*208*, *209*]. In a cerebral edema model, mice with an AQP-4 deletion exhibited significantly better survival rates than their wild-type counterparts. This underscores the critical role of AQP-4 in the pathogenesis of cerebral edema and offers potential therapeutic implications [*210*]. However, the relevance of AQ4 for the development of brain edema in HE is currently not fully understood and a matter of controversial debate [*160*].

Among the genes whose expression is altered in HE are also those coding for microRNAs (miRNAs) [*211*, *212*]. miRNAs are non-coding RNAs that play significant roles as post-transcriptional regulators of gene expression [*212*, *213*]. A recent study investigated miRNA and gene expression changes in ammonia-exposed rat astrocytes *in vitro* using microarray techniques [*212*]. The study identified 43 miRNAs that were downregulated and a total of 142 genes which were concomitantly upregulated in ammonia-exposed astrocytes. Interestingly, 43 of these genes were identified as potential targets of downregulated miRNA species [*212*]. The observed expression changes of these potential miRNA target genes in ammonia-exposed astrocytes were further confirmed by qPCR results. Among the miRNA species downregulated by ammonia, some identified who were predicted to target HO-1, which plays an important role for ammonia-induced senescence [*212*]. Further findings of this study suggested that upregulation of HO-1 is indeed a consequence of the downregulation of miRNAs miR-221-3p, -221-5p, -222-3p or -326-3p [*212*]. Moreover, downregulation of these miRNA species and upregulation of HO-1 was confirmed to contribute to the ammonia-induced astrocyte senescence [*212*]. Another study further suggested, that downregulation of miR326-3p releases the translational repression of NOX4 mRNA and thereby upregulates NOX4 protein [*4*]. The importance of these findings is indicated by the observation that HO-1 and NOX4 both contribute to ammonia-induced senescence [*212*]. This was suggested to be accomplished by HO-1 mediated upregulation of the intracellular levels of Fe^{2+} ions and NOX4-mediated hydrogen peroxide (H_2O_2) production, both of which may lead to the generation of hydroxyl radicals via the Fenton reaction, thereby contributing to oxidative stress in HE models [*4*].

In addition to miRNAs, long noncoding RNAs (lncRNAs), a type of noncoding RNA that comprises more than 200 nucleotides, have been implicated in the regulation of gene expression [*214*]. Numerous lncRNA levels changes were described in HE [*211*, *215*, *216*], such as in brain of BDL mice, an established animal model for HE [*217*]. Further investigations into the roles of these lncRNAs, such as of antisense RNA 1 (ZFAS1) and growth arrest-specific transcript 5 (GAS5), suggested their involvement in ammonia metabolism, as well as in apoptosis in neuronal cell lines [*217*]. However, whether this also applies to HE in brain in patients with liver cirrhosis are currently completely unknown and remain to be investigated.

Interestingly, oxidative/ nitrosative stress induced by HE-relevant factors in astrocytes also triggers nuclear swelling [*76*, *149*]. Currently, the precise mechanism as well as consequences thereof are not yet understood. However, nuclear swelling may originate from an activation of MAP kinases as it is observed during premature senescence in human fibroblasts [*218*]. Interestingly, MAP-kinases are also activated by ammonia in astrocytes *in vitro* [*136*, *153*]. This enlargement of the nucleus could potentially influence the regulation of gene transcription and nuclear transport mechanisms [*219*] by modulating chromatin density within the nucleus [*220*]. It therefore seems reasonable to speculate, that nuclear swelling observed in HE may relate to gene expression changes leading to astrocyte senescence.

The **oxidation of RNA** is a posttranscriptional modification of RNA and a consequence of oxidative/ nitrosative stress in astrocytes and neurons in HE [*117*, *141*]. Here, guanine becomes oxidized to 8-oxoguanosine [*117*, *141*, *221*]. This can impair the proper translation of messenger RNA, or when occurring in ribosomal RNA, inhibit ribosomal translation and thereby disrupt protein synthesis [*222*]. Oxidized RNA was found in astrocytes exposed to HE-relevant factors and in the cerebral cortex of hyperammonemic rats, where it was primarily located in perivascular astrocyte processes, neuronal somata and dendrites [*141*, *223*]. Here, it was suggested that by interfering with the proper translation of mRNA and thereby affecting protein synthesis, it may affect astrocytic and neuronal functions [*136*, *141*, *224*]. In ammonium acetate-treated rats, oxidized RNA was found in RNA transport granules in neurons in the cerebral cortex, where they are transported along neuronal dendrites to synapses [*141*]. As these granules transport RNA required for structural remodelling of the synapse after neuronal activity, the data suggest that RNA oxidation may impair synaptic plasticity in HE [*141*]. Also astrocytic RNA species were identified to become oxidized, such as the mRNA coding for the Na^+-dependent glutamate/ aspartate transporter 1 (GLAST) [*141*]. GLAST mRNA oxidation may underlie downregulation of GLAST protein in cultured astrocytes and in brain of animal models of HE [*225-227*]. Since GLAST critically contributes to glutamate clearance by astrocytes at the synaptic cleft, it was proposed that impaired neurotransmission in HE as a consequence of impaired glutamate homeostasis in HE may result from RNA oxidation [*141*]. Interestingly, the RNA quality control protein TROVE2 becomes upregulated in *in vitro* and animal models of HE

[*228*]. However, it remains unclear whether the upregulation of TROVE2 is a consequence of ammonia-induced RNA oxidation and whether it is involved in the degradation of oxidised RNA. Most importantly, increased levels of oxidised RNA were also found in *post-mortem* brain samples from cirrhotic patients with HE, but not in those from cirrhotic patients without HE [*137*, *143*, *98*].

Signaling pathways within astrocytes are essential for maintaining cerebral homeostasis and the proper functioning of the central nervous system [*69*]. However, in the context of HE many signaling pathways are altered due to osmotic and oxidative/ nitrosative stress [*98*, *229*]. This applies to extracellular signal-regulated kinases 1, 2 (ERK1/2), p38 mitogen-activated protein kinase (MAPK) and c-Jun N-terminal kinases (JNK) 1, 2, 3 [*136*, *145*, *153*]. The oxidative/ nitrosative stress-induced activation of these kinases was suggested to contribute to the ammonia-induced astrocyte swelling [*145*, *153*, *230*]. The p38 signaling pathway plays also a key role in regulating inflammation and cellular apoptosis [*69*, *231*, *232*]. Further research has illustrated that activation of p38 in ammonia-exposed astrocytes leads to phosphorylation and nuclear accumulation of tumor suppressor protein 53 (p53) [*4*, *69*]. This then activates the transcription of cell cycle inhibitory genes such as p21 and growth arrest and DNA damage inducible protein 45α (GADD45α) [*4*, *69*]. These changes lead to a halt in the cell cycle, which puts the astrocytes into a state of senescence [*4*, *142*]. There is also strong evidence for altered signaling pathways in the brain of animal models of HE, such as of the NO - cyclic guanylate monophosphate (cGMP) pathway [*233*, *234*]. This pathway becomes activated in neurons upon glutamate-induced activation of NMDA receptors [*131*]. The resulting increase in intracellular Ca^{2+} enables calmodulin to activate neuronal nitric oxide synthase and stimulates the synthesis of cGMP by soluble guanylate cyclase [*235*]. However, this pathway becomes impaired in both, the cerebellum and cortex of rats with hyperammonemia [*234*]. The stimulation of soluble guanylate cyclase by NO also appears to be reduced in cerebellum homogenates from individuals who succumbed to HE [*236*, *237*]. Therefore, it was proposed that drugs which were shown to normalize cGMP levels in brain in animal models of HE could be useful as therapeutics for the treatment of HE in humans [*234*]. These include the phosphodiesterase inhibitors zaprinast and sildenafil [*234*, *238*].

Senescence is triggered by ammonia-induced oxidative stress in astrocytes [*69*, *212*]. In this situation the cell cycle becomes arrested and the cell loses the ability to divide and to synthesize DNA [*239*] but remains viable. Hayflick and colleagues demonstrated that typical human diploid fibroblast cell strains cease dividing *in vitro* after a set number (40 - 60) of population doublings, known as the Hayflick limit, upon serial passaging [*240*]. This type of senescence was therefore termed replicative senescence and shown to result from progressive telomere shortening [*241-243*]. In so-called premature senescence, cells become arrested between G1/S phases of the cell cycle [*244*] and this may be triggered by a variety of intrinsic or extracellular stress. These include mitogenic signals, radiation, oxidative stress, chromatin disorganization, mitochondrial dysfunction, radiotherapy or chemotherapy drugs and inflammation [*245-249*]. In case of DNA damage and in order to prevent replication of errors, cells activate the DNA damage repair response, which inhibits cell proliferation by up-regulating two pathways, p53/p21 and p16INK4a/pRb [*250*], thereby coordinating the process of cellular senescence. Senescent cells also upregulate phospho-histone γ-H2AX (a sensitive marker of double stranded DNA damage), and secrete a discrete pattern of signaling factors and therefore adopt a so-called senescence-associated secretory phenotype (SASP) [*246*, *251*]. A widely used biomarker for replicative senescence is the upregulation of the senescence-associated β-galactosidase (SA-β-gal) whose activity is maximal at pH 6.0 [*252*, *253*]. As the most numerous cell type in the brain, astrocytes create a tissue-wide signaling network that regulates diverse brain functions and maintains brain homeostasis. Recent evidence suggests that the accumulation of senescent astrocytes contributes to the pathogenesis of neurodegenerative diseases [*254*]. This was suggested to result in a reduced synaptic density and impaired synaptic plasticity and neurotransmission [*255*]. In Alzheimer's disease, the senescent astrocytes showed a SASP phenotype which triggered β-Amyloid accumulation, hyperphosphorylation of Tau-proteins and the deposition of neurofibrillary tangles [*256*, *257*].

Building on previous findings, recent studies link ammonia exposure to astrocyte senescence in HE. The proposed mechanism involves oxidative stress-induced activation of the p53 signaling pathway, resulting in elevated expression of p21 and GADD45α [*4*, *69*]. Interestingly, GADD45α plays a critical role in DNA replication and repair by interacting with

proliferating cell nuclear antigen [*258*]. Interestingly, hippocampal memory and long-term potentiation are strongly impaired in GADD45α-deficient mice, which highlights the important function of this protein for the maintenance of cerebral function [*259*]. Importantly, upregulation of p53, p21 and GADD45α mRNA was also observed in cerebrocortical *post mortem* brain samples from patients with liver cirrhosis with HE, but not in those without HE [*69*]. Following research revealed, that the ammonia-induced astrocyte senescence is triggered by oxidative stress-dependent downregulation of a specific set of microRNAs which target HO-1 [*212*]. The resulting upregulation of HO-1 triggers endoplasmatic reticular stress and activates p53-dependent gene transcription presumably via the Fenton reaction [*4*].

Post-translational modifications (PTMs) represent chemical alterations that occur on specific amino acid residues following the biosynthesis of a protein [*260*]. Current research affirms that PTMs function as a biological mechanism to orchestrate the functionality of the proteome [*261*]. This control extends to protein folding [*262*] and stability [*263*], enzymatic activity [*264*], subcellular localization of proteins [*265*] and protein-protein interaction [*266*]. Various studies have shown that oxidative/ nitrosative stress induced by HE-relevant factors triggers or is associated with a wide range of PTMs in different protein species. These modifications include phosphorylation [*136*, *145*, *153*] as described above, protein tyrosine nitration [*136*, *150*, *154*], carbonylation [*267*, *268*], ubiquitination [*268*, *269*] and *O*-GlcNAcylation [*4*, *144*, *270*].

Tyrosine nitration represents a PTM which has gained much attraction in recent years. Reactive oxygen species such as superoxide may recombine with •NO or its derivatives to form $ONOO^-$ which decomposes. The decomposition products of $ONOO^-$ are capable of mediating the nitration of protein tyrosine, thereby triggering structural changes in proteins which may alter their functions [*271*]. Hypoosmotic cell culture media [*154*], ammonia [*136*], diazepam [*150*] and pro-inflammatory cytokines [*169*], have all been shown to trigger protein tyrosine nitration in astrocytes *in vitro*. Increased cerebral protein tyrosine nitration was also found in animal models of HE [*151*] such as in rats after ammonium acetate-treatment or after portal vein ligation [*136*, *221*]. Moreover, portacaval anastomosis has been shown to raise the

expression of NO synthases (nNOS and iNOS) and protein tyrosine nitration in rat brain in neurons and astrocytes [*272*, *273*]. Intriguingly, hyperammonemic mice lacking liver-specific GS also showed increased cerebral protein tyrosine nitration [*117*]. This latter study demonstrated that chronic hyperammonemia in absence of liver damage is already sufficient to trigger nitrosative stress and protein tyrosine nitration. Most importantly, increased cerebral protein in the brain tyrosine nitration was also found in *post mortem* brain samples from patients with liver cirrhosis who died in HE but not in those who had no HE [*143*].

In ammonia-exposed astrocytes glutamine synthetase (GS), ERK1, the PBR and the Na-K-Cl cotransporter (NKCC1) were found to be tyrosine-nitrated [*136*, *274*]. While GS nitration is associated with a loss of activity, nitration of the NKCC1 enhanced its transport activity [*136*, *274*]. Effects of protein tyrosine nitration on ERK1 and PBR are currently unknown. Importantly, an increase in GS tyrosine nitration and a decrease in GS activity has also been found in *post mortem* brain samples from patients with liver cirrhosis and HE [*143*]. *In vitro* studies suggested that GS nitration and inactivation could be reversed by a unknown enzymatic activity in spleen extracts from lipopolysaccharide (LPS)-treated rats, implying a potential regulatory role of GS nitration in the brain under oxidative stress [*275*]. This hypothesis is supported by the presence of a similar "denitrase" activity in brain extracts, which suggests that GS nitration does not simply reflect only ROS/ RNS-mediated protein damage but that it may serve as a mechanism regulating the catalytic activity of the protein [*275*]. Elevated tyrosine nitration of GS was also found in brains and livers of LPS-treated rats which implies that sepsis might exacerbate HE due to lowering the ammonia detoxification in liver and brain [*169*, *276*]. Currently, the question remains as to whether such conditions also induce GS tyrosine nitration in skeletal muscle. Given the diminished capacity of a dysfunctional liver to eliminate ammonia, the skeletal muscle emerges as a potential key site for glutamine synthesis-dependent ammonia detoxification [*277*]. Indeed, research on portocaval shunted rats suggested that liver dysfunction may lead to an increase in GS activity in skeletal muscle [*278*].

Na-K-Cl cotransporters (NKCCs), particularly NKCC1, have emerged as important players in brain edema formation [*279*], a key feature of several neurological diseases, including

Alzheimer's disease, Huntington's disease, Parkinson's disease and epilepsy [*280*]. Widely expressed in the central nervous system (CNS), NKCC1 regulates water homeostasis in astrocytes by driving the influx of sodium (Na), potassium (K), and chloride (Cl) ions, ultimately influencing cell volume and contributing to edema formation [*281*, *282*]. Importantly, experiments involving ammonia-exposed rat astrocytes have revealed nitration of the NKCC1 [*274*]. Similar to phosphorylation, also nitration of the NKCC1 enhanced its transport activity [*274*]. It was therefore suggested that activation of NKCC1 due to oxidative/ nitrosative stress may contribute to the ammonia-induced astrocyte swelling [*274*]. However, whether the NKCC1 also becomes nitrated in brains of hyperammonemic animals or in patients with liver cirrhosis with HE is currently unclear and remains to be investigated.

Ubiquitination is a PTM where ubiquitin is attached to proteins and which plays an integral role in protein degradation [*283*], cellular signaling [*284*] and endocytosis [*285*, *286*]. Also in cell culture and animal models of HE changes in the ubiquitin-proteasome system (UPS) were described [*268*, *269*]. The UPS plays a central role in eliminating misfolded or damaged proteins, thus contributing to overall cellular homeostasis [*268*]. In hyperammonemia animal models, oxidized proteins were significantly elevated in the hippocampus and this was paralleled by an increase in the levels of ubiquitinated proteins and proteasomal activity [*268*]. Complementary *in vitro* experiments revealed an increase in oxidized and ubiquitinated proteins, enhanced proteasomal activity, and elevated levels of antioxidant enzymes within mixed glial cultures and microglial cells incubated with ammonia [*268*]. This indicates that oxidative/ nitrosative stress in HE also damages proteins. However, potential consequences for protein homeostasis have not been studied in detail so far.

Protein carbonylation is a form of protein oxidation characterized by the introduction of carbonyl groups (such as aldehyde or ketone groups) into proteins [*287*]. It is a widely recognized marker of oxidative stress and damage and can trigger structural changes in the respective proteins. This may impair the biological functions of the affected protein and thereby contribute to various neuropathological conditions, such as multiple sclerosis [*288*], Alzheimer’s disease [*289*] and Parkinson's disease [*290*]. Increased levels of carbonylated

proteins were also observed in ammonia-exposed rat astrocytes, and it was suggested that the underlying oxidative stress originated from mitochondria [*269*]. A protein which was found to become carbonylated in ammonia-exposed astrocytes is the NKCC1 [*274*]. Similar to phosphorylation, also carbonylation of the NKCC1 enhanced its transport activity [*274*]. It was therefore postulated, that carbonylation of the NKCC1 may contribute to the swelling of astrocytes in HE [*279*]. Importantly, significantly elevated levels of carbonylated proteins were also found in the hippocampus of hyperammonemic mice [*268*]. Since the hippocampus plays a pivotal role for memory formation and learning, it was proposed that protein carbonylation may contribute to impaired cognitive functions in HE [*268*].

1.2 Protein *O*-GlcNAcylation

***O*-GlcNAcylation** is a PTM of proteins that involves the attachment of *O*-linked β-*N*-acetylglucosamine (*O*-GlcNAc) to the serine (Ser) and threonine (Thr) residues of nuclear [*291*], cytoplasmatic [*291*] and mitochondrial proteins [*292*]. This is a dynamic and reversible process, first identified by Torres and Hart in 1984, that holds a similar level of biological importance to protein phosphorylation [*10*, *293*, *294*]. The proteins modified by *O*-GlcNAcylation are predominantly cytoplasmic, nuclear and mitochondrial [*295*]. More than 5,000 proteins have been identified as being modified by *O*-GlcNAcylation, which unlike other forms of glycosylation, does not form higher oligosaccharides [*296*, *297*]. The process is tightly regulated by two key enzymes: *O*-GlcNAc transferase (OGT), which attaches the GlcNAc moiety to Ser/ Thr residues [*298*], and *O*-GlcNAcase (OGA), which removes the GlcNAc residue [*299*, *300*]. Both enzymes play a critical role in maintaining *O*-GlcNAc homeostasis within cells [*301*]. In some proteins, *O*-GlcNAcylation and phosphorylation sites are identical and consequently mutually exclusive [*302*]. It was therefore proposed, that this so-called “yin or yang” may have opposite effects on functions or interactions of the respective proteins [*302*]. Cellular protein *O*-GlcNAcylation was proposed to reflect nutrient availability, as this determines the synthesis of the donor substrate uridine diphosphate GlcNAc (UDP-GlcNAc) within the hexosamine biosynthetic pathway (HBP) [*10*, *295*]. Moreover, nutrient availability also modulates the levels

of OGT, OGA and respective adaptor proteins and substrates (Fig. 1.5) [*10*]. *O*-GlcNAcylation is widespread in the brain and the levels and the activity of OGT and OGA is significantly higher in the brain compared to peripheral tissues [*303*]. While *O*-GlcNAcylation is a highly dynamic process, the mechanisms governing the temporal control of *O*-GlcNAc signaling remain largely unknown. These findings underscore the critical importance of *O*-GlcNAcylation in cellular biology and hint at its potential role in neurological processes and diseases.

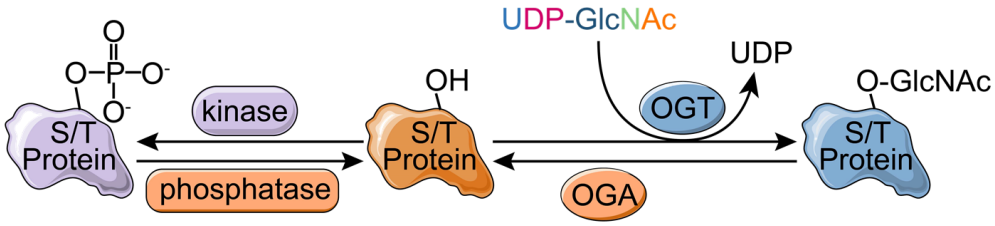

Figure 1.5: Dynamic relationship between phosphorylation and *O*-GlcNAcylation. Both phosphorylation and *O*-GlcNAcylation may occur on the same serine/threonine (Ser/ Thr) residues of proteins. The enzyme OGT catalyzes the addition and the enzyme OGA the removal of the sugar moiety. UDP-GlcNAc is the activated nucleotide sugar donor used by OGT catalyze the *O*-GlcNAcylation of proteins [*10*]. (Modified from Hart *et al*. 2011; License No. 1432374-1).

1.2.1 *O*-GlcNAc-transferase

The *O*-GlcNAc transferase (OGT) catalyzes the *O*-GlcNAcylation of proteins, by transferring the GlcNAc molecule from UDP-GlcNAc to the serine or threonine residues in proteins [*298*]. OGT exhibits significant conservation, as it is encoded by a single gene which shares 80% identity and found across various eukaryotic organisms [*304*]. In mammals, the OGT gene is located at chromosomal locus Xq13.1, a region linked to Parkinson's disease [*305*]. RNA sequencing studies have revealed that OGT deficiency affects the transcription of genes involved in the cell cycle, neurogenesis and neuronal development [*306*]. Furthermore, mutations and catalytic deficiencies in OGT have been associated with intellectual disabilities, highlighting a significant relationship between protein *O*-GlcNAcylation and neurological functions [*307*]. OGT comes in three distinct isomers: mitochondrial OGT (mOGT; 103 kDa), nucleocytoplasmic OGT (ncOGT; 116 kDa) and short OGT (sOGT; 78 kDa) [*304*] (Fig. 1.6). These isoforms differ in their numbers of tetratricopeptide repeats (TPRs), which are crucial for substrate recognition and interaction

[*308*]. mOGT is found in the mitochondria and contains 9 TPRs; ncOGT, which is located in the nucleus and is also found in the cytoplasm, contains 13.5 TPRs; and sOGT, which is also present in the cytoplasm and nucleus, contains 2.5 TPRs [*309*, *310*]. These OGT isomers have been found in a variety of cells and tissues ncOGT is strongly expressed in adult brain areas such as the prefrontal cortex and hypothalamus, while sOGT was found in kidney, liver, muscle, thymus, blood, salivary gland, ovaries, tonsils, placenta and pancreatic islet cells. mOGT has been found in fetal brain and lungs [*304*, *311*]. The mechanisms that allow a single OGT enzyme to recognize a wide range of protein substrates could involve context-dependent recruitment of OGT to these substrates by a series of conserved adaptor proteins and specific interactions with the TPR domain of OGT that vary depending on the substrate [*302*]. This highlights the functional complexity of OGT in cellular regulation and its potential role in a variety of biological processes and diseases.

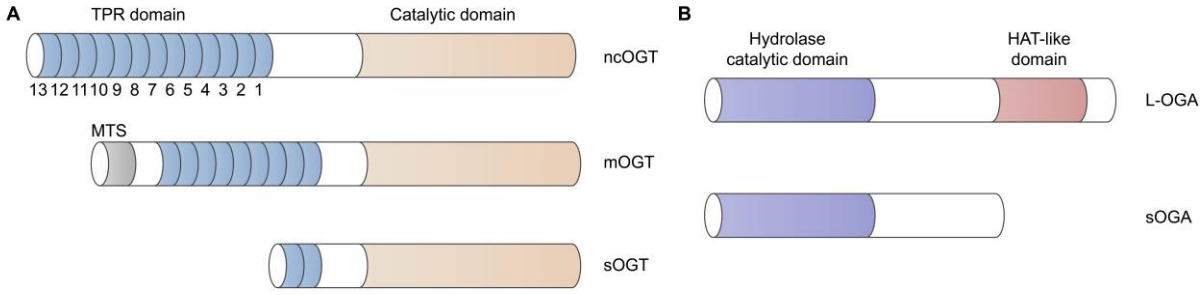

Figure 1.6: OGT and OGA subtypes and domain structure. (**A**) The three splice isoforms of OGT, ncOGT, mOGT and sOGT have different N-termini, but the same catalytic domains. Only mOGT contains a mitochondrial targeting sequence (MTS) in the N-terminal region. (**B**) The two splice isoforms of OGA, L-OGA and sOGA have different C-terminus. L-OGA has a putative HAT domain, whereas sOGA does not and instead has a distinct 15-amino-acid long C-terminal extension, according to information provided by [*9*]. (Modified from Ruan *et al*. 2013; License No. 1436659-1).

1.2.2 *O*-GlcNAcase

β-*N*-acetylglucosamindase, or *O*-GlcNAcase (OGA), is a critical enzyme involved in *O*-GlcNAc metabolism, catalyzing the specific removal of β-*O*-linked GlcNAc from modified proteins [*299, 312*]. This enzyme is conserved across eukaryotic species, particularly mammals, but does not exist in prokaryotes or yeast [*313*]. OGA has two distinct forms, the long OGA (L-OGA) and the

short OGA (sOGA) [*314*]. L-OGA, encoded by 16 exons, contains a unique N-terminal *O*-GlcNAcase domain and a C-terminal histone acetyltransferase (HAT)-like domain [*315*]. Conversely, sOGA, encoded by 10 exons, features an N-terminal hyaluronidase catalytic domain [*316*]. L-OGA is primarily localized in the cytoplasm, while sOGA resides in the nucleus [*317*]. Interestingly, high levels of OGA expression have been observed in neurons in the human brain, and an upregulation was noted in mammalian and rodent models of neurodegenerative diseases [*318*]. Inhibition of OGA was recently postulated to reduce tau aggregation by enhancing the *O*-GlcNAc modification of tau, which in turn prevents its hyperphosphorylation. This is particularly relevant for the pathogenesis of Alzheimer's disease where increased levels of aggregated tau are considered a hallmark of the disease [*319*]. Active OGA protein has also been identified in mitochondria [*319*]. Recent studies have begun to explore changes in the interaction partners of OGT and OGA under cellular stress conditions, suggesting that during stress, protein interactors could suppress OGA activity, leading to enhanced *O*-GlcNAcylation of distinct proteins [*320*]. In this regard, the joint action of OGA and fatty acid synthase (FAS) can inhibit the catalytic activity of OGA [*321*]. Earlier *in vitro* studies have confirmed that the catalytic domain of OGA is located at the N-terminus, while the C-terminus is vital for optimal enzymatic activity [*322*]. Intriguingly, *O*-GlcNAcylation, a dynamic modification affecting thousands of diverse proteins, is controlled by only OGT and OGA enzymes [*312*, *323*]. This remarkable specificity underscores their potential impact on diverse biological processes and disease states, including HE.

1.2.3 The hexosamine biosynthetic pathway (HBP)

The *O*-GlcNAcylation depends on the availability of the OGT substrate UDP-GlcNAc which is the product of the HBP (Fig. 1.7). External glucose is imported into the cell by glucose transporters which are embedded in the cell membrane [*324*]. It has been estimated that 2-3% of glucose taken up is channeled into the HBP, suggesting this pathway may play a significant regulatory role in glucose metabolism utilization. It was therefore postulated that the HBP may act as a intracellular glucose sensor which triggers a negative feedback loop [*325*]. Moreover,

there is a strong connection between the modification of proteins by *O*-GlcNAcylation and the transit of glucose through the HBP [*2*].

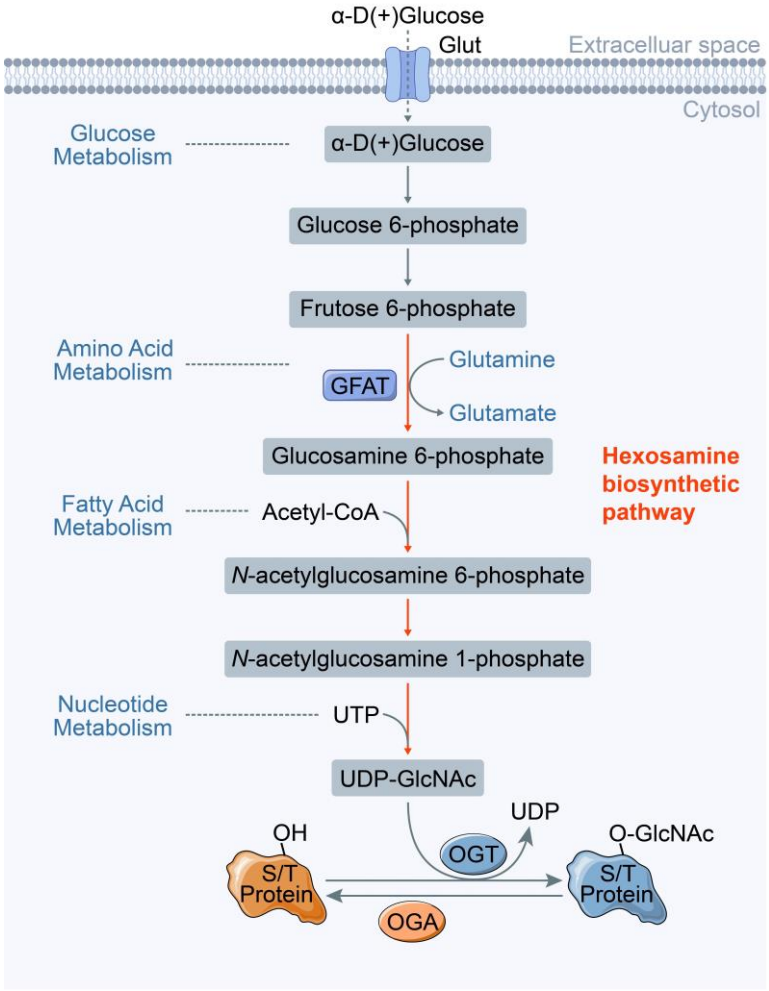

Figure 1.7: The hexosamine biosynthetic pathway (HBP). A small fraction of the glucose which enters the cell is converted to glucosamine-6-phosphate (GlcNAc-6-P) by glutamine: fructose-6-phosphate amidotransferase (GFAT), which is the rate limiting enzyme of the HBP pathway. In the following, GlcNAc-6-P is converted to UDP-GlcNAc, which is used by OGT as a substrate for adding GlcNAc to serine or threonine residues of target proteins. The *O*-GlcNAc moiety is removed from *O*-GlcNAc-modified proteins by *O*-GlcNAcase (OGA) [*2*]. (Modified from Hart *et al*. 2019; License No. 1436224-1).

Once glucose enters the HBP, it is phosphorylated to glucose-6-phosphate (G-6-P), which is then converted into fructose-6-phosphate (Fru-6-P). About 35% of this Fru-6-P is used alongside glutamine to form glucosamine-6-phosphate (GlcN-6-P) and glutamate, a reaction controlled by fructose-6-phosphate amidotransferase (GFAT). This enzyme catalyzes the rate-limiting step, consuming glutamine to generate GlcN-6-P and glutamate [*326*]. The remaining Fru-6-P is allocated for glycolysis. After this, the amine group of GlcN-6-P is acetylated by

acetyl-CoA to produce *N*-acetylglucosamine-6-phosphate (GlcNAc-6-P) which is further converted into *N*-acetylglucosamine-1-phosphate by *N*-acetylglucosamine-phosphate mutase (AGM). Finally, UDP-*N*-acetylglucosamine pyrophosphorylase (UAP) uses uridine triphosphate (UTP) to turn *N*-acetylglucosamine-1-phosphate into UDP-GlcNAc [*2*]. The GlcNAc from UDP-GlcNAc is utilized by OGT to modify the oxygen atom of the hydroxyl group of serine or threonine residues on the target protein. Importantly, UDP-GlcNAc is the exclusive donor for *O*-GlcNAcylation [*326*, *327*]. The HBP involves a variety of substances, including glucose (carbon source), glutamine (nitrogen donor), uridine (nucleotide for UDP-GlcNAc synthesis), acetyl-CoA (acetyl group donor), UTP (phosphoryl group donor) and ATP (energy source) [*2*, *328*]. This underlines the integrative role of UDP-GlcNAc in cellular processes that involve carbohydrate, amino acid, fatty acid and nucleotide metabolisms [*329*]. Besides serving as the donor nucleotide for *O*-GlcNAc modification of proteins, UDP-GlcNAc is also necessary for lipid and protein glycosylation within the ER [*327*]. High levels of UDP-GlcNAc result in the allosteric inhibition of GFAT, and the activity of GFAT is linked to several PTMs [*330*]. Incubating cells *in vitro* with glucose, glucosamine (which bypasses GFAT's allosteric inhibition), or OGA inhibitors such as PUGNAc can increase overall protein-*O*-GlcNAcylation [*325*, *331*].

1.2.4 Consequences of *O*-GlcNAcylation for protein function

Protein *O*-GlcNAcylation directly and dynamically interacts with many essential biological pathways, including translation [*332*, *333*], transcription [*334*, *335*], signaling cascades [*336*], protein folding [*337-340*], protein- protein interactions [*266*, *341*, *342*], cellular localization [*335*, *343*], protein transport [*344-346*], protein stability [*347*, *348*], protection of nascent polypeptide chains from ubiquitination [*349*], as well as Ca^{2+} handling [*350*] and Ca^{2+} channels [*351*]. Recent research has established that *O*-GlcNAcylation also influences the function of transcription factors such as p53 [*352*, *353*], c-myc [*354*], nuclear factor-κB (NF-κB) [*355*, *356*] and Sp1 [*357*, *358*], thereby affecting gene transcription. Interestingly, *O*-GlcNAcylation of Sp1 is linked to diabetes and its complications [*359*]. Earlier studies found that Sp1, a zinc finger transcription factor that binds GC-rich motifs in many promoters, exhibited increased *O*-GlcNAcylation due

to hyperglycemia. This directly influenced DNA binding and transcriptional activity [*360*, *361*], and enhanced the transcription of plasminogen activator inhibitor-1 (PAI-1), a protein implicated in diabetic cardiovascular disease onset [*362*]. In relation to diabetes, it has been shown that *O*-GlcNAcylation interferes with phosphorylation of Sp1 and thereby alters its intracellular localization and transcriptional activity [*363*]. Further studies showed that *O*-GlcNAcylation protects Sp1 from proteasomal degradation [*357*]. Furthermore, *O*-GlcNAcylation of Sp1 inhibits its interaction with other transcription factors, such as nuclear transcription factor Y (NF-Y) [*364*], organic cation transporter 1 (Oct1), Sp3 and Sp4 [*365*].

Besides Sp1, the activity of many other transcription factors is modulated by *O*-GlcNAcylation. This includes brain and muscle Arnt-like protein-1 (BMAL1) [*366*], carbohydrate-responsive element-binding protein (ChREBP) [*367*], forkhead box protein O1 (FoxO1) [*368*], liver X receptor (LXR)α [*369*], PPARγ coactivator-1 (PGC)-1α [*370*], PPARγ and others [*371*]. FoxO1, a key player in controlling hepatic glucose production, shows increased mRNA expression of glucose-6-phosphatase (G6Pase) and PGC1 [*372*] when *O*-GlcNAcylated [*373*, *374*]. Moreover, *O*-GlcNAcylation of FoxO1 promotes the expression of genes involved in ROS detoxification, providing a potential protective mechanism against the elevated ROS generation associated with increased glucose metabolism [*368*]. The impact of *O*-GlcNAcylation on nuclear pore (NUP) has been extensively studied. This suggests a potential role in regulating the nucleocytoplasmic trafficking [*344*, *375*, *376*]. High steady-state levels of *O*-GlcNAcylation on the nuclear pore complex (NPC) components contribute to the complex's stability by preventing its ubiquitination and degradation [*377*]. In studies focusing on *O*-GlcNAc modification within the cytosol and nucleus, the ubiquitin-activating enzyme has been found to be subject of *O*-GlcNAcylation [*378*]. This links protein *O*-GlcNAc glycosylation to protein ubiquitination, suggesting that the former may govern the latter [*378*].

The examples given above suggest, that alterations in protein *O*-GlcNAcylation may serve as an adaptive response to cellular stress, and failure in this process could precede disease onset [*379*]. OGT and OGA operate as a "buffer" system, fine-tuning the level of global *O*-GlcNAcylation by mutually interacting with each other's transcription and translation

processes [*295*]. Aberrant *O*-GlcNAcylation has been linked to numerous human diseases such as Alzheimer's disease [*303*, *380*], diabetes [*381*], cancer progression [*382*, *383*], stress response [*384*, *385*], immune response [*356*, *386*], and recently to HE [*4*].

1.2.5 Ammonia-induced protein *O*-GlcNAcylation

Recent studies have shown that ammonia triggers protein *O*-GlcNAcylation in rat astrocytes *in vitro* [*144*]. Except for GAPDH, no further protein species were identified who become *O*-GlcNAcylated in ammonia-exposed astrocytes [*144*]. Further evidence suggested that ammonia upregulates HO-1 in cultured astrocytes through protein *O*-GlcNAcylation [*4*]. Here, upregulation of HO-1 was suggested to be a consequence of the *O*-GlcNAcylation-dependent inhibition of the transcription of microRNAs such as miR326-3p, which were shown to target HO-1 mRNA (Fig. 1.8) [*4*]. This was thought to reduce microRNA-mediated transcriptional inhibition of HO-1 mRNA. Upregulation of HO-1, and also of NOX4 whose mRNA is also a predicted target of miR326-3p, triggered an oxidative stress-mediated activation of p53 and the p53-dependent transcription of cell cycle inhibitory genes p21 and GADD45a [*4*]. Most importantly, *post mortem* brain samples from liver cirrhosis patients with HE displayed elevated levels of senescence markers, HO-1, and glucose-regulated protein 78 (grp78 - an ER stress surrogate marker [*387*]), further supporting the link between cellular senescence and HE pathogenesis.

Additionally, increased *O*-GlcNAcylation of proteins was observed, suggesting potential involvement of this post-translational modification in HE [*4*]. These alterations were not found in samples from patients with liver cirrhosis without HE, thereby underscoring protein *O*-GlcNAcylation as a characteristic feature of HE [*4*]. Similar to what was observed in ammonia-treated rat astrocytes in Görg *et al*. (2019), increased protein *O*-GlcNAcylation was also observed in livers of mice treated with NH_4Cl *in vivo* [*388*, *389*]. In line with effects observed in ammonia-exposed rat astrocyte, it was also noted in mouse liver that enhanced *O*-GlcNAcylation was paralleled by increased glutamine and UDP-GlcNAc levels [*388*].

Interestingly, in mouse liver, the *O*-GlcNAcylation of CPS1 enhances the affinity of CPS1 for ammonia. Since CPS1 is pivotal in ureagenesis, these findings suggest that liver-based *O*-GlcNAcylation of CPS1 plays a critical role in the detoxification of ammonia [*388*].

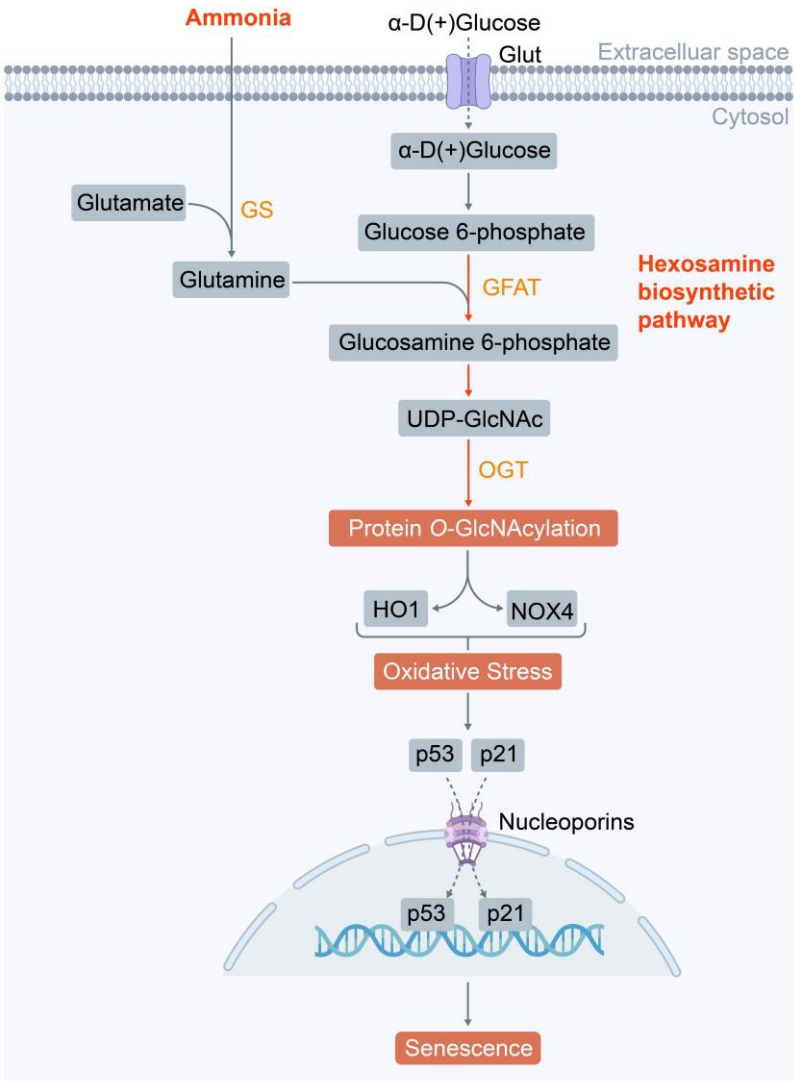

Figure 1.8: Glutamine formation triggers oxidative stress in astrocytes through protein *O*-GlcNAcylation. Ammonia is used by glutamine synthetase (GS) to form glutamine which is substrate of GFAT to produce glucosamine-6-phosphate in the hexosamine biosynthetic pathway (HBP). This is the rate-limiting step within the HPB which limits the synthesis of the nucleotide-sugar UDP-GlcNAc. UDP-GlcNAc is a substrate of OGT which catalyzes the *O*-linked β-D-N-acetylglucosamine at specific Ser/ Thr residues in proteins. The *O*-GlcNAcylation of so far unknown proteins in ammonia-exposed astrocytes inhibits the transcription of miR326-3p which in turn upregulates HO-1 and NOX4 protein levels. The resulting oxidative stress activates p53 and p21. This triggers the transcription of cell cycle inhibitory genes and thereby leads to astrocyte senescence [*4*]. (Redrawn with modifications from Görg, B., *et al*. 2019; License No. 5711240476051).

1.2.6 Techniques employed for the identification of *O*-GlcNAcylated proteins

Many different techniques have been utilized for the identification of *O*-GlcNAcylated proteins and intramolecular sites of protein *O*-GlcNAcylation. In this regard, *O*-GlcNAc modified proteins can be detected by Western blot analysis, immunofluorescence and immunohistochemistry. The most frequently used antibodies here are the clones CTD110.6 [*390*] and RL2 [*391*]. Though these approaches are technically straightforward, they fall short in specificity, lacking the ability to identify the exact protein or site of modification [*392*]. Currently, a dedicated OGT-specific consensus sequence for protein *O*-GlcNAcylation remains elusive. This lack of consensus limits the informative value of the widely used, potentially leaving a significant portion of *O*-GlcNAcylated proteins undetected [*296*]. There are also antibodies available who detect distinct *O*-GlcNAcylated protein species such as tau *O*-GlcNAcylated at serine 400 [*393*], histone H2B *O*-GlcNAcylated at serine 112 [*394*] and sirtuin-1 *O*-GlcNAcylated at serine 549 [*395*].

To overcome the limitations mentioned above, mass spectrometry (MS)-based proteomics were employed [*396*]. By coupling with enrichment strategies like lectin affinity chromatography or immunoaffinity purification, MS can detect even low-abundance *O*-GlcNAcylated proteins [*379*]. Given the scarcity and diversity of *O*-GlcNAcylation [*397*], an enrichment step using lectins such as wheat germ agglutinin (WGA) [*398*], aleuria aurantia lectin [*399*], and psathyrella velutina lectin [*400*] is required. This technique has been well-established through LC-ES/MS. However, their non-specific interactions with other glycans might reduce glycosylation detection sensitivity. Therefore, a treatment with peptide *N*-glycosidase F (PNGase F) is usually implemented to reduce potential interference with GlcNAc residues [*296*, *397*, *401*]. Moreover, various enzymatic labeling techniques were employed such as azide-alkyne cyclo addition („click-chemistry“) which allow labeling and visualization of *O*-GlcNAcylated proteins in cells [*402*]. By using synthetic azide or alkyne-modified sugars incorporated into cellular glycoproteins, these can be labeled with a fluorescent tag for detection by immunofluorescence [*401*]. In a chemoenzymatic labeling enrichment approach, *O*-GlcNAc residues are tagged with uridine diphosphate-azido-modified galactose (UDP-

GalNAz) using a modified galactosyltransferase GalT1(Y289L) [*403*]. *O*-GlcNAc-residues may also be tagged using metabolic chemical reporters (MCRs) like *N*-azidoacetylgalactosamine-tetraacylated (Ac4GalNAz) [*404*], *N*-(4-pentynoyl)-glucosamine-tetraacylated (Ac4GlcNAlk) [*401*] and 6-azido-6-deoxy-*N*-acetyl-glucosamine triacylated (Ac36AzGlcNAc) [*405*], which are converted to UDP-GalNAz and then epimerize to UDP-GlcNAz [*406*]. These techniques enable to purify proteins by tagging *O*-GlcNAc moieties with reactive groups and subsequent „click-chemistry“ reactions [*407*].

1.3 Heme oxygenase-1

Heme oxygenase (HO), also known as heat shock protein-32 (Hsp32), is a rate-limiting and stress-inducible enzyme for heme degradation in a wide range of human and mammalian tissues. Since its discovery in 1968 [*408*], a large number of studies provided compelling evidence that it has anti-inflammatory and anti-oxidative roles in numerous diseases [*409*]. HO-1 can catalyze the degradation of heme to biliverdin (BV), Fe^{2+} and carbon monoxide (CO) by utilizing reducing equivalents supplied from NADPH-cytochrome P450 oxidoreductase (Fig. 1.9) [*408*, *410*]. Biliverdin is subsequently reduced to bilirubin (BR) under the action of NAD(P)H-dependent biliverdin reductase (BVR). BR is an effective anti-oxidant that may protect cells from oxidative stress [*411-413*]. CO has vasodilatory and platelet anti-aggregatory properties [*414*, *415*]. Fe^{2+} ions which are released by HO-1 from heme may serve for the synthesis of hemoglobin in red blood cells. Importantly, Fe^{2+} ions may promote the formation of ROS in the so-called Fenton reaction and therefore must be sequestred to proteins to prevent ROS-mediated damage [*416*, *417*]. Therefore, the action of HO-1 may vary depending on the specific pathophysiological situation and thus may be beneficial as well as detrimental for the pathogenesis of the respective diseases [*418*]. This dichotomy is well described in the literature and known as “Janus-Face” of HO-1 [*419*, *420*].

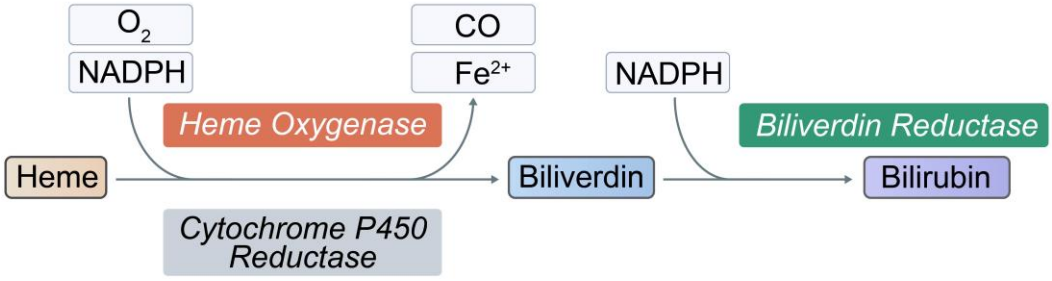

Figure 1.9: Schematic representation of the enzymatic degradation of heme. Heme oxygenase 1 cleaves heme to biliverdin (BV), ferrous iron (Fe^{2+}) and carbon monoxide (CO). This requires NADPH-cytochrome P450 reductase (CPR) as a co-factor. Biliverdin is then reduced to bilirubin by biliverdin reductase (BVR) [*5*]. (Modified from Abraham *et al*. 2008; License No. 1437807-1).

1.3.1 Structural properties of heme oxygenases

The HO family encompasses enzymes primarily located in the membrane of the endoplasmic reticulum. Within mammals, three distinct HO isoforms have been discerned: HO-1 [*421*], an inducible isoform, and two constitutive isoforms, HO-2 and HO-3 [*422*, *423*]. While these isoforms are products of separate genes, they share similar protein motifs necessary for substrate recognition and heme degradation [*424*]. The HO-1 isoform is a endoplasmic reticulum transmembrane protein which is composed of 288 amino acids and which has a molecular weight of approximately 32 kDa [*425*]. The structure involves an N-terminal domain accessible to the cytoplasm and a confined single transmembrane segment (TMS) situated at the C-terminal [*426*]. The TMS of HO-1 takes on an α-helical form, mirroring a hydrophobic core peptide signal [*427*]. Mutations within the TMS, such as of W270N increase its susceptibility to protein cleavage and consequently cause HO-1 degradation [*428*]. However, HO-1 may also be cleaved near to the TMS under physio- and pathophysiological conditions, thereby releasing a truncated variant which was suggested to translocate to the nucleus where it may enhance the transcription of antioxidative genes [*429*, *430*]. The human HO-1 gene, which is found on chromosome 22q12, is 1414 kb in length and contains 4 introns and 5 exons [*431*]. Here, the transcription depends on the length polymorphism of guanidine thymidine dinucleotide repeats in the promoter region [*432*]. Individuals with longer GT-repeat lengths demonstrate

both reduced HO-1 expression and antioxidant defense. This is due to a decreased transcription of HO-1 and reduced protein levels [*433*]. As opposed to HO-1, HO-2 contains 30 extra amino acids at the N-terminus and has a molecular weight of approximately 36 kDa. Uniquely, HO-2 integrates two heme regulatory motifs (HRMs), encompassing Cys-Pro sequences near the C-terminus (Fig. 1.10) [*434*]. While the precise function of these HO-2 domains remains undetermined, heme binding to HRMs in other proteins triggers the degradation of the respective proteins [*435*]. HO-3, which exhibits 90% amino acid homology with HO-2, is a less efficient heme catalyst [*436*]. In the nervous system, HO-2 and HO-3 are mainly expressed within neurons, and here they are unresponsive towards stress stimuli [*437*, *438*]. Interestingly, in the rat, HO-3 was exclusively found in astrocytes [*439*, *440*]. However, the precise function of HO-3 in the brain is currently not fully understood [*440*]. In humans, there is further evidence for the existence of another splice form of HO-1 which yields a 14 kDa HO-1 isoform. His variant is located in the cytoplasm and becomes upregulated by UV irradiation and by H_2O_2 [*441*]. This variant was shown to promote cell proliferation and to increase relative telomere length [*441*].

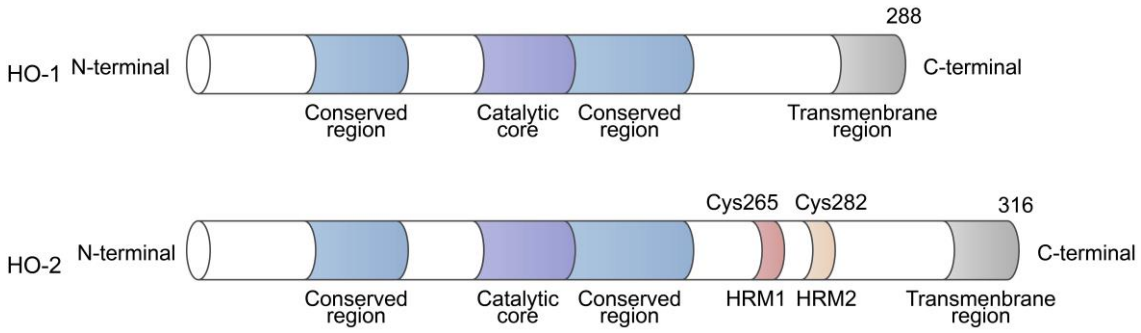

Figure 1.10: Schematic illustration of the domain structures of HO-1 and HO-2. HO-1 and HO-2 share identical regions such as the conserved region, the catalytic core and the transmembrane region. HO-2 contains additionally two heme regulatory motifs (HRMs) at the C-terminus [*7*]. (Modified from Muñoz-Sánchez *et al*. 2014; Open access).

1.3.2 Regulation of HO-1 gene expression

The regulation of HO-1 gene expression is a complex and multifaceted process. Various stimuli can upregulate HO-1 at the mRNA and protein level. These include heme [*442*, *443*], ROS/ RNS [*444-447*], heat stress [*448*, *449*], ultraviolet radiation [*450*, *451*], heavy metals [*452*, *453*], cytokines [*454*, *455*] and numerous pharmacological agents [*456*, *457*]. These diverse stimuli may act through distinct but potentially overlapping signal transduction pathways to influence the transcription of HO-1 [*414*, *458*, *459*]. The transcription of HO-1 involves key cis-acting elements within its promoter region, such as the antioxidant response element (ARE) [*460*], heme-responsive element (HERE) [*461*], antioxidant/ electrophile response elements (ARE/EpRE) [*462*], heat shock elements (HSEs) [*463*, *464*] and stress response elements (StRE) [*465*]. Various inducers stimulate these elements, which are then recognized by transcription factors such as nuclear factor erythroid 2-related factor 2 (Nrf2) [*466*], activator protein-1 (AP-1) [*467*, *468*], nuclear factor (NF)-κB [*469*] and heat shock factor-1 (HSF-1) [*470*]. This subsequently triggers the transcription of HO-1 gene. The transcription factor AP-1 is a member part of the basic region/ leucine zipper (bZIP) [*471*] which also includes nuclear factor-erythroid 2 (NF-E2) and Nrf-1 and -2 [*466*]. Among these, Nrf2 serves as a master regulator of the cellular antioxidant response, shielding cells from oxidative stress by controlling the expression of various antioxidant genes [*472*]. Under oxidative stress conditions, Nrf2 is activated and migrates into the nucleus where it binds to the ARE in the promoter regions of a host of antioxidant and cytoprotective genes including HO-1 [*473*]. This activation is triggered by mitogen-activated protein kinases (MAPKs), which are protein Ser/Thr kinases that can transmit extracellular signals from cytoplasm into the nucleus (Fig. 1.11) [*474-476*]. MAPKs, comprising ERK1/2, c-Jun N-terminal kinase (JNK) and p38, constitute a diverse signaling pathways implicated in numerous cellular processes [*153*, *477*]. In the context of liver diseases, MAPKs notably activate the Nrf2/HO-1 pathway and the transcription factor AP-1 [*478-480*], playing crucial roles in signal transduction by modulating gene transcription in the nucleus in response to changes in the cellular environment [*481*, *482*]. Consistently, constitutive activation of ERK and p38 pathway resulted in increased transcription of a HO-1 reporter gene [*483*, *484*].

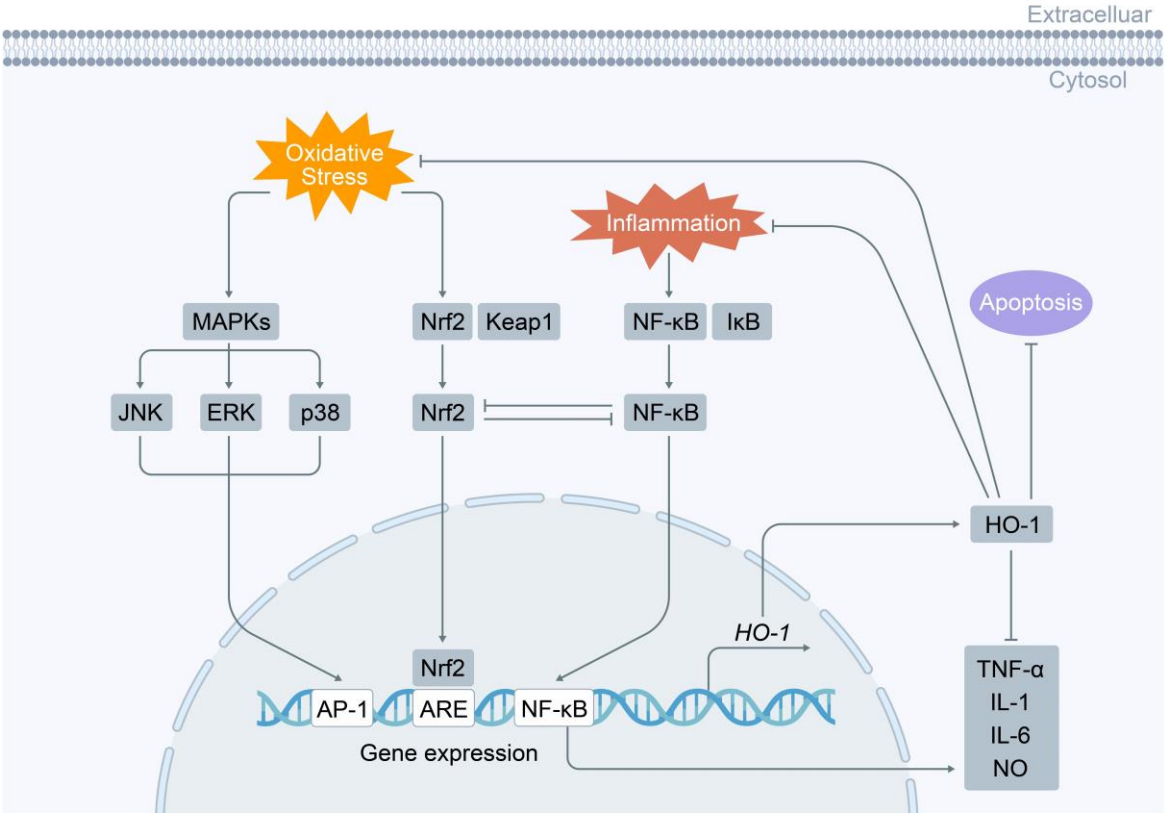

Figure 1.11: Schematic representation of mechanisms governing the transcription of heme oxygenase 1 (HO-1). HO-1 transcription is controlled by a variety of stress-related transcription factors, such as, AP-1, Nrf2 and NF-κB. Upon activation, these transcription factors may translocate to the nucleus where they bind to their respective promoter regions and activate the transcription of HO-1 [*11*]. This in turn may counteract oxidative stress and inflammation. (Modified from Waza *et al*. 2018; License No. 1440398-1).

CO is one of the products of heme catabolism by HO-1 [*485*]. Recently, an anti-apoptotic effect of CO and its relationship to MAPK were described [*476*, *486*]. The overexpression of HO-1 or the exogenous infusion of CO prevented tumor necrosis factor α (TNF-α)-induced apoptosis in murine fibroblasts [*487*]. CO can activate p38 MAPK and simultaneously inhibit ERK and the the transcription of proinflammatory cytokines in response to endotoxin. These results suggest that the anti-apoptotic and anti-inflammatory effects of CO depended on the modulation of the p38 MAPK pathway [*488*, *489*]. Importantly, the upregulation of HO-1 can in turn affect the transcription of a number of antioxidant enzymes, including superoxide dismutase (SOD), glutathione peroxidase (GSH-Px), and catalase, NAD(P)H-quinone oxidoreductase 1 (NQO1) and glucose-6-phosphate dehydrogenase (G6PDH) [*490-493*]. Here, HO-1 was suggested to stabilize transcription factors in the nucleus which in turn enhances their transcriptional activity [*430*, *492*].

1.3.3 Intracellular localization of heme oxygenase-1

Generally, HO-1 is attached to the smooth ER through a domain at its C-terminal end, with most of the protein structure located in the cytoplasm and oriented towards it [*426*, *494*]. However, under stress conditions, HO-1 can relocate to other cellular locations such as the plasma membrane [*429*, *495*], the nucleus [*496*, *497*], caveolae [*495*] and the mitochondria [*497-499*]. The subcellular location of HO-1 is dynamically regulated by post-transcriptional and post-translational alterations, which may also alter its catalytic activity [*430*].

Very early attempts to isolate HO-1 from rat liver suffered from substantial proteolytic breakdown during solubilization and purification [*500*]. However, HO-1 also becomes truncated under stress conditions in the cells (Fig. 1.12). Here, the proteolytic cleavage of full-length 32kDa HO-1 at the ER yields a 28 kDa truncated form [*430*]. Further evidence suggests that proteolytic cleavage of full-length HO-1 may yield at least two truncated HO-1 isoforms of 27/28 and 30 kDa size [*430, 500*]. In this regard, Hsu *et al*. suggested that signal peptide peptidase (SPP) is able to cleave the TMS in the C-terminus of HO-1 [*501*]. However, other evidence suggest that HO-1 may also be cleaved by cathepsin B (CatB) and calpain-1 and -2 [*430*, *502*].

The full-length HO-1 is composed of 288 amino acid residues and has a molecular size of 32 kDa whereas the truncated form (28 kDa) lacks the 23 amino acids [*428*]. In response to different stimuli such as hypoxia, hemin [*430*], or heme-hemopexin, HO-1 may be cleaved at the C-terminus which makes a conserved nuclear shuttling sequence (NSS) accessible [*430*]. Once liberated from the ER membrane, HO-1 may translocate to the nucleus, where it serves as a transcriptional enhancer for the transcription of antioxidant defense genes [*503*]. This was shown in mouse cells for a 28 kDa HO-1 variant, which was missing 53 amino acids of the C-terminus. This variant was found to bind to Nrf2 and thereby to prolong its transcriptional activity and to upregulate the levels of oxidative stress-responsive genes such as NQO1, CAT and G6PDH [*430*, *492*].

Oxidative stress induced by ultraviolet light or H_2O_2 was shown to upregulate a unique splice variant of HO-1 with a molecular size of approximately 14 kDa [*441*]. This variant exclusively

localizes to the cytoplasm, where it interacts with cytochrome P450 reductase (CPR), and biliverdin reductase, to catalyze the degradation of heme [*441*].

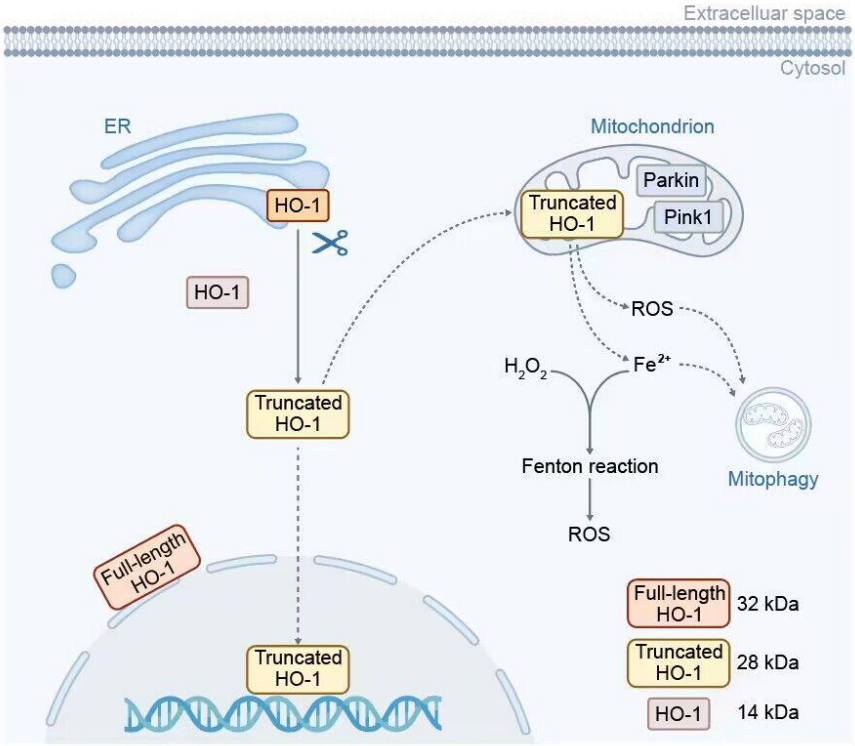

Figure 1.12: Intracellular localization of HO-1. Full-length HO-1 anchors at the smooth endoplasmic reticulum (ER) membrane following synthesis. Stress or pathological conditions can induce the trafficking of HO-1 to nucleus. Full-length and truncated HO-1 were also found in mitochondria. HO-1 influences biogenesis and dynamics of the mitochondria and mitophagy. Within the nucleus, both the full-length and truncated forms of HO-1 are present, regulating gene expression associated with angiogenesis, anti-apoptotic proteins, anti-oxidative enzymes, metastasis and mitochondrial biogenesis. The 14 kDa HO-1 present in the cytosol [*3*]. (Redrawn with modifications from Chiang *et al*. 2021; Open access).

Truncated HO-1 can also translocate to mitochondria, where it is catalytically active [*429*, *504*]. Here, it can trigger the PTEN-induced kinase 1 (PINK1)/ Parkinson protein 2 (PARK2) mitophagy pathway and ferroptosis (iron-dependent cell death) in an oxidative stress dependent way [*505*].

1.3.4 Homomerisation of heme oxygenase-1

Full-length HO-1 readily forms higher-order oligomers, which increases the catalytic activity compared to the respective HO-1 monomers [*428*]. The presence of the carboxy-terminal region (CTD) in full-length HO-1 is crucial for its oligomerization and the formation of stable multimeric structures. In line with this, truncated HO-1 does not oligomerize and exists as a monomer [*506*]. During oligomerization of HO-1, multiple HO-1 subunits assemble into larger, homomers/ multimeric structures [*507*]. It was originally proposed that HO-1 does not form multimers, which may occur via disulfide bridges, due to the absence of cysteine in its amino acid sequence [*437*]. However, following studies clearly demonstrated that HO-1 forms dimer and consecutively higher order homomeric HO-1 protein complexes at the ER membrane. This oligomerization was suggested to enhance its catalytic activity [*508*], stability [*428*], and to impact on the interaction with other proteins [*508*]. This oligomerization is triggered by the C-terminal TMS around amino acid (AA) position 270 of HO-1 as shown by site-specific mutagenesis experiments [*428*]. Here, TMS-TMS interactions at the ER stabilize HO-1 [*428*] and blocking HO-1 multimerization triggers its degradation [*428*]. Also data from Hwang *et al*. support the view that truncated HO-1 lacking the C-terminal domain is unable to form oligomers [*428*]. HO-1 also tends to form dimers within lipid vesicles in a TMS-dependent way [*509*]. The TMS region also interacts with CPR which further promotes the formation of HO-1 oligomers. Thus, this oligomeric state may also play a role in the catalytic function of HO-1, as it may facilitate the cooperative reaction needed for heme degradation and bilirubin synthesis [*428*]. Notably, the presence of CPR significantly enhances HO-1 oligomerization, particularly under hypoxic conditions [*510*]. This is thought to be mediated by CPR's ability to stabilize HO-1 against proteolytic cleavage by proteases, such as trypsin [*506*].

In summary, the transmembrane segment (TMS) of HO-1 functions not only as a membrane anchor but also facilitates the self-assembly of HO-1 in the endoplasmic reticulum (ER), thereby increasing its half-life and catalytic activity [*428*]. The significance of the TMS-TMS interaction in HO-1 has implications for pathophysiological conditions associated with

cellular stress, as genetic variations affecting this interaction may impact on disease progression.

1.3.5 Heme oxygenase-1 in hepatic encephalopathy

The role of HO-1 for cerebral dysfunction in HE is currently not fully understood. In the liver, HO-1 is believed to protect hepatocytes from oxidative stress [*511*]. However, excessive upregulation of HO-1 in the liver, particularly in the context of liver cirrhosis, may exacerbate liver damage [*512*, *513*]. Here HO-1 may rather trigger oxidative stress and apoptosis [*411*], processes that contribute to liver deterioration and aggravate liver cirrhosis [*512*, *513*].

Similar to its role in the liver, also in the brain HO-1 was shown to protect against oxidative stress [*514*, *515*]. However, in brain tissues and primary cultured brain cells, HO-1 protein and mRNA levels are upregulated by a variety of stressors such as by oxidative stress [*411*, *516*]. HO-1 mRNA or protein levels were also elevated in rat cerebral cortex in a variety of animal models of HE [*212*, *517-519*]. Here it was speculated that, upregulation of HO-1 in the brain of ammonium acetate-treated rats may relate to cerebral hyperemia under hyperammonemic conditions [*519*]. Studies on bile duct-ligated rats showed that systemic application of the HO-1 inhibitor zinc protoporphyrin IX (ZnPP) reduced cerebral AQP-4 protein levels and oxidative stress markers in the brain [*518*]. However, this was most likely due to extracerebral effects as ZnPP also reduced portal vein pressure and blood ammonia levels in the BDL rats [*518*]. In this regard, elevated HO-1 levels in the liver were suggested to contribute to the progression of liver cirrhosis [*512*].

Upregulation of HO-1 protein was also observed in ammonia-exposed astrocytes [*4*, *519*] and endothelial cells [*520*], but not in neurons [*519*]. Importantly, microarray analyses on *post-mortem* human brain samples taken from the cerebral cortex have recently established the relevance of these findings for the pathogenesis of HE in humans [*137*]. In this study, HO-1 mRNA levels were increased in samples of patients with liver cirrhosis who had HE. Moreover, compared to controls, HO-1 mRNA levels were not significantly different in samples from

patients with liver cirrhosis without HE [*137*]. This is in line with previous findings showing that oxidative stress markers are selectively upregulated in patients with liver cirrhosis and HE but not in those without HE [*143*]. Unfortunately, the cell types which contribute to the increased HO-1 mRNA levels in the brain in patients with liver cirrhosis with HE are currently unknown and remain to be identified.

Further studies in cultured astrocytes on the role of HO-1 in the pathogenesis of HE showed that ammonia triggers astrocyte senescence in a HO-1 and NADPH oxidase-dependent way [*141*]. This study suggested that ammonia upregulates HO-1 through protein *O*-GlcNAcylation-dependent downregulation of HO-1 mRNA targeting microRNAs [*212*]. Upregulation of HO-1 and NOX4 in ammonia-exposed astrocytes triggered oxidative stress in a ferrous iron-dependent way, presumalby via the Fenton reaction [*4*]. Consistent with this, HO-1 overexpression in astrocytes was shown to increase ROS production in a free ferrous iron-dependent manner [*411*]. The role of HO-1 in the pathogenesis of HE is currently only incompletely understood. However, given its important role for the induction of oxidative stress and senescence - it is reasonable to speculated that HO-1 may be a potential target for preventing brain dysfunction in HE.

1.4 Aim of the present study

Previous findings suggested that protein *O*-GlcNAcylation plays an important role for oxidative stress and senescence in ammonia-exposed cultured rat astrocytes and in the pathogenesis of hepatic encephalopathy in patients with liver cirrhosis and hepatic encephalopathy. However, protein species who are subject to protein *O*-GlcNAcylation in astrocytes remained unknown.

The aim of this study was to identify changes in the astrocytic *O*-GlcNAcome induced by ammonia and to investigate potential consequences for the function of proteins affected by *O*-GlcNAcylation. Further studies should determine whether hyperammonemia also triggers protein *O*-GlcNAcylation in the rat brain.

2. Materials and Methods

2.1 Materials

All materials used for the investigations described in the present thesis are listed below in the following sections 2.1.1 to 2.1.9.

2.1.1 Equipment

96-well PCR Plate	Applied Biosystems, Foster City, CA, USA
96-well Reaction Plate Framestar®	4titude, Berlin, Germany
Amersham ImageQuant™ 800 biomolecular imager	Cytiva, Thermo Fisher Scientific, Waltham, USA
Analytical balance 770 max.120 g	Kern&Sohn, Balingen-Frommern, Germany
Analytical balance 440-47N max.2000 g	Kern&Sohn, Balingen-Frommern, Germany
Biorad ChemiDoc Touch Imaging System	BioRad, München, Germany
Centrifuge 5415D	Eppendorf, Hamburg, Gemany
Centrifuge AHT 35R	Hettich, Tuttlingen, Germany
Centrifuge Rotina 420R	Hettich, Tuttlingen, Germany
CO_2-incubator Hera Cell 150	Heraeus, Hanau, Germany
Concentrator plus	Eppendorf, Hamburg, Gemany
Confocal laser scanning microscopy (LSM880)	Zeiss, Jena, Germany
Electrophoresis chamber	Biometra, Göttingen, Germany
Fluorescence microscope (Observer Z.1)	Zeiss, Jena, Germany
Gel Loading Syringe	Hamilton, Stockbridge, GA, USA
Magnetic Stirrer Heidolph™ MR2000	Heidolph, Schwabach, Germany
Microlitre pipette	Eppendorf, Hamburg, Gemany
Nanodrop®ND-1000	Peqlab Biotechnologie, Erlangen, Germany
Gel Loading Syringe	Hamilton, Stockbridge, GA, USA
Magnetic Stirrer Heidolph™ MR2000	Heidolph, Schwabach, Germany
Microlitre pipette	Eppendorf, Hamburg, Gemany
Nanodrop®ND-1000	Peqlab Biotechnologie, Erlangen, Germany
PH-Meter (330)	WTW, Weilheim, Germany
Phase-contrast microscopy (Axio Vert.A1)	Zeiss, Jena, Germany
Pipette controller (Pipetboy accu)	IBS Integra Biosciences, Fernwald, Germany
Polyethylene cell lifter Costar®	Corning Incorporated, Corning, NY, USA
Roller Mixer SRT1	Stuart Scientific, Staffordshire, England
Rotator DR-200	Carl Roth, Germany
Spectrophotometer Ultrospec 2100 pro	Amersham Biosciences, Freiburg, Germany
Thermoblock Thermomixer® 5436	Eppendorf, Hamburg, Gemany
Thermocycler	Eppendorf, Hamburg, Gemany
Ultrasonic processors UP50H	Hielscher, Teltow, Germany
Vacuum Safety Suction Systems HLC	Ditabis, Pforzheim, Germany
ViiA7™ Real-Time PCR	Applied Biosystems, Foster City, CA, USA

Vortex VM2	CAT, Staufen, Germany
Water Baths	Thermo Scientific, Walthm, MA, USA
ZetaView®	Particle Metrix, Inning, Germany

2.1.2 Consumable materials

Analytical balance 770	Kern&Sohn, Balingen-Frommern, Germany
Cell culture dishes Falcon®	Corning Incorporated, Corning, NY, USA
Cell culture dishes (60/100 mm)	Greiner bio-one, Kremsmünster, Austria
Cell culture flask Cellstar®	Greiner bio-one, Kremsmünster, Austria
Disposable plastic cuvettes	Sarstedt AG & Co, Nümbrecht, Germany
Disposable serological pipettes (5/10/25 mL)	Corning Incorporated, Corning, NY, USA
Eppendorf Safe-Lock Tubes (1.5/2 mL)	Eppendorf, Hamburg, Gemany
Filtropur s 0.2-syringe filter	Sarstedt, Nürnbrecht, Germany
Glass coverslip	Assistent, Sondheim, Germany
Ibidi µ-Dishes (35 mm, plastic, glass)	Ibidi, Gräfelfing, Germany
Magnetic Stirrer Heidolph™ MR2000	Heidolph, Schwabach, Germany
MatTek dishes (55 mm, plastic, glass)	MatTek Corporation, Ashland, USA
Microplate Seal Film for qPCR	4titude, Berlin, Germany
Microscope slides	Engelbrecht, Edermünde, Germany
Neubauer Counting Chamber	Marienfeld, Lauda Königshofen, Germany
Nitrocellulose Transfer Membranes Protran®	Whatman, Dassel, Germany
Parafilm M Labfilm	Pechiney, Chicago, IL, USA
Pipette tips	StarLab, Ahrensburg, Germany
Polystyrene Centrifuge Tube (15/50 mL)	Falcon, Heidelberg, Germany
QIAshredder collection tube	Qiagen, Hilden, Germany
Screw-Cap Microtubes 2 mL	Sarstedt, Nürnbrecht, Germany

2.1.3 Chemicals and substances

1,4-Dithiothreitol	Sigma-Aldrich, Taufkirchen, Germany
2-Mercaptoethanol	Carl Roth, Karlsruhe, Germany
β-Glycerophosphate	Carl Roth, Karlsruhe, Germany
β-Mercaptoethanol	Carl Roth, Karlsruhe, Germany
Acetic acid	VWR, Radnor, PA, USA
Agarose	Biozym, Hessisch Oldendorf, Germany
Alloxan monohydrate	Sigma-Aldrich, Taufkirchen, Germany
Aloxistatin/E64d	Monmouth Junction, NJ, USA
Ammonium acetate, NH_4Ac	AppliChem, Darmstadt, Germany
Ammonium persulfate, APS	Serva, Heidelberg, Germany
Adenosin triphosphate, ATP	Sigma-Aldrich, Taufkirchen, Germany
Biotin alkyne	Thermo Fisher Scientific, Waltham, MA, USA
Bromphenol blue	Carl Roth, Karlsruhe, Germany
Bovine serum albumin, BSA	Roche, Diagnostics, Penzberg, Germany

Chloroform	Merck, Darmstadt, Germany
$CuSO_4$	Thermo Fisher Scientific, Waltham, MA, USA
D-(+)-Glucosamine hydrochloride	Sigma-Aldrich, Taufkirchen, Germany
DAPI	Sigma-Aldrich, Taufkirchen, Germany
Deoxynucleotide (dNTP) solution mix	Qiagen, Hilden, Germany
Dimethylsulfoxid, DMSO	Sigma-Aldrich, Taufkirchen, Germany
3,3-Dithio-bis-(Sulfosuccinimidyl)propionat, DSP	Sigma-Aldrich, Taufkirchen, Germany
Ethidiumbromid	Carl Roth, Karlsruhe, Germany
Ethanol	Merck, Darmstadt, Germany
Fetal bovine serum albumin, FBS	Merck, Darmstadt, Germany
$FeCl_3$	Sigma-Aldrich, Taufkirchen, Germany
Glycine	Merck, Darmstadt, Germany
Glycerol	Merck, Darmstadt, Germany
Hemin	Sigma-Aldrich, Taufkirchen, Germany
Hoechst34580	Invitrogen, Karlsruhe, Germany
Hydroxylamine hydrochloride	Charlotte, NC, US
Imidazole hydrochloride	Sigma-Aldrich, Taufkirchen, Germany
Isopropanol (2-Propanol)	VWR Chemicals, Darmstadt, Germany
L-Glutamine	Sigma-Aldrich, Taufkirchen, Germany
Methanol	Merck, Darmstadt, Germany
$MgCl_2$	Merck, Darmstadt, Germany
$MnCl_2 \cdot 4H_2O$	Sigma-Aldrich, Taufkirchen, Germany
N-Glycosidase F	Roche, Diagnostics, Penzberg, Germany
Na_3AsO_4	Sigma-Aldrich, Taufkirchen, Germany
NaCl	Sigma-Aldrich, Taufkirchen, Germany
NaF	Sigma-Aldrich, St. Louis, MO, USA
NaOH	Sigma-Aldrich, Taufkirchen, Germany
Na_3VO_4	Sigma-Aldrich, Taufkirchen, Germany
NH_4Cl	Sigma-Aldrich, St. Louis, MO, USA
Nuclease-free water	Promega, Mannheim, Germany
Recombinant *O*-GlcNAc Transferase	R&D Systems, Minneapolis, MN, USA
UDP-GalNaz	Thermo Fisher Scientific, Waltham, MA, USA
UDP-GlcNAc sodium salt	Sigma-Aldrich, Taufkirchen, Germany
Paraformaldehyde, PFA	Merck, Darmstadt, Germany
Phosphate-buffered saline (with/without Ca^{2+}/Mg^{2+}), PBS	Invitrogen, Karlsruhe, Germany
Phenylmethylsulfonylfluoride, PMSF	Carl Roth, Karlsruhe, Germany
Ponceau S Staining Solution	Serva, Heidelberg, Germany
O-(2-Acetamido-2-deoxy-D-glucopyranosylidenamino) N-phenylcarbamate, PUGNAc	Sigma-Aldrich, Taufkirchen, Germany
Pyruvate	Merck, Darmstadt, Germany
Sodium dodecyl sulfate, SDS	Sigma-Aldrich, Taufkirchen, Germany
Streptavidin-coated agarose beads	Thermo Fisher Scientific, Waltham, MA, USA
SYBR Green	Invitrogen, Karlsruhe, Germany

Trichloroacetic acid, TCA	Sigma-Aldrich, Taufkirchen, Germany
Tetramethylethylenediamine, TEMED	Sigma-Aldrich, Taufkirchen, Germany
Tris(hydroxymethyl) aminomethane, TRIS	VWR Chemicals, Darmstadt, Germany
Tris-HCl	Carl Roth, Karlsruhe, Germany
Triton-X 100	Sigma- Aldrich, Taufkirchen, Germany
Trypsin/EDTA (0.05%/0.02% in PBS)	CytoGen, Wetzlar, Germany

2.1.4 Ready-to-use reagents

AllStars Negative Control siRNA	Qiagen, Hilden, Germany
DMEM Glutamax [+] 1.0 g/L D-glucose [Pyruvate] Gibco™	Invitrogen, Karlsruhe, Germany
Recombinant Gal-T1 (Y289L)	Thermo Fisher Scientific, Waltham, MA, USA
HiPerFect Transfection Reagent	Qiagen, Hilden, Germany
PBS (with/without Ca^{2+}/Mg^{2+})	Invitrogen, Karlsruhe, Germany
Recombinant rat heme oxygenase 1	Cusabio, Wuhan, China
Recombinant human *O*-GlcNAc transferase	R&D Systems, Wiesbaden, Germany
siRNA OGT (Rn_Ogt_1)	Qiagen, Hilden, Germany
siRNA OGT (Rn_Ogt_2)	Qiagen, Hilden, Germany
siRNA GFAT1 (Rn_MGC95214_1)	Qiagen, Hilden, Germany
siRNA GFAT2 (Rn_RGD1303097_2)	Qiagen, Hilden, Germany
Streptavidin-conjugated beads	Millipore, Merck, Darmstadt, Germany

2.1.5 Inhibitors

γ-secretase Inhibitor (Compound E)	MedChemExpress, Monmouth Junction, NJ, USA
cOmpleteTM Protease Inhibitor	Roche Diagnostics, Penzberg, Germany
ER-associated Protein Degradation Inhibitor Eeyarestatin I (ESI)	MedChemExpress, Monmouth Junction, NJ, USA
RNase Inhibitor	Ambion, Darmstadt, Germany

2.1.6 Kits

Bradford Assay Kit	Bio-Rad, München, Germany
Click-iT™ *O*-GlcNAc Enzymatic Labeling Kit	Thermo Fisher Scientific, Waltham, MA, USA
Click-iT™ Protein Analysis Detection Kit	Thermo Fisher Scientific, Waltham, MA, USA
Cytiva Amersham™ ECL™	Cytiva, Marlborough, MA, USA
N-Glykosidase F Deglycosylation Kit	Roche, Diagnostics, Penzberg, Germany
QuantiTect® Reverse Transcription Kit	Qiagen, Hilden, Germany
RNeasy® Micro Kit	Qiagen, Hilden, Germany
Western Lightning Plus ECL™	Amersham, Waltham, Netherlands

2.1.7 Antibodies

Table 2.1: Overview of the primary and secondary antibodies used in this thesis. (mAb: monoclonal antibody; pAb: polyclonal antibody).

Primary antibodies	Host species	Dilution	Supplier
Anti-α-Tubulin, mAb	Mouse	1:1,000	Sigma-Aldrich, Taufkirchen, Germany
Anti-GAPDH, mAb	Mouse	1:5,000	Meridian Life Science, Memphis, USA
Anti-GFPT1, mAb	Rabbit	1:1,000	Abcam plc., Cambridge, UK
Anti-GFPT2, mAb	Rabbit	1:1,000	Abcam plc., Cambridge, UK
Anti-GRP78/BiP, mAb	Mouse	1:5,000	BD, Bioscience, Heidelberg, Germany
Anti-GS, mAb	Mouse	1:5,000	BD, Bioscience, Heidelberg, Germany
Anti-HO-1, mAb	Rabbit	1:1,000	Abcam plc., Cambridge, UK
Anti-HO-1, pAb	Rabbit	1:1,000	Enzolifesciences, Lörrach, Germany
Anti-*O*-GlcNAc, mAb	Mouse	1:1,000	BioLegend, San Diego, CA, USA
Anti-*O*-GlcNAc, mAb [RL2]	Mouse	1:1,000	Abcam plc., Cambridge, UK
Anti-OGT, pAb	Rabbit	1:1,000	Abcam plc., Cambridge, UK

Secondary antibodies	Host species	Dilution	Supplier
Anti-mouse-IgG (ALEXA Fluor 488)	Donkey	1:200	Jackson Immunoresearch West Grove, PA, USA
Anti-rabbit-IgG (Cy3)	Donkey	1:200	Jackson Immunoresearch West Grove, PA, USA
Anti-rabbit-IgG (Cy5)	Donkey	1:200	Jackson Immunoresearch West Grove, PA, USA
Anti-mouse-IgG (FITC)	Goat	1:200	Jackson Immunoresearch West Grove, PA, USA
Anti-mouse-IgG (HRPOD)	Goat	1:5,000	Biorad, München, Germany
Anti-rabbit-IgG (HRPOD)	Goat	1:5,000	Dako, Hamburg, Germany

2.1.8 Buffer solutions

Protein lysis buffer
- 20 mmol/L Tris-HCl (pH 7.4)
- 140 mmol/L NaCl
- 2 mmol/L Ethylenediaminetetraacetic acid (EDTA)
- 2 mmol/L EGTA
- 0.42 g/L NaF
- 4,4 g/L Na-Pyrophosphate (10xH_2O)
- 0.2 g/L Na-ortho-vanadate

	β-glycerophosphate Prior to usage the following compounds were added: 1% (v/v) Triton X-100 cOmplete™ Protease Inhibitor Cocktail
10 x Transfer buffer	10 mmol/L SDS 3.86 mmol/L Glycine 4.78 mmol/L Tris-base 5,000 mL ddH_2O
1 x Transfer buffer	500 mL 10 x Transfer buffer 1,000 mL MeOH 3,500 mL ddH_2O
5 x Running buffer	1.73 mmol/L SDS 125 mmol/L Tris-base 1.25 mmol/L glycine
10 x Tris-buffered saline (TBS) buffer (pH 7.6)	1.98 mmol/L Tris-base 1.488 mmol/L NaCl
1 x TBST buffer	1 x TBS buffer 0.1% Tween 20
SDS-Polyacrylamid gel electrophoresis (PAGE) sample buffer	68 mmol/L Tris-HCl (pH 6.8) 3.4% SDS (w/v) 17.1% (v/v) glycerol 0.1% (w/v) bromophenol blue 200 mmol/L DTT

2.1.9 Oligonucleotide sequences for real-time PCR

Table 2.2: Nucleotide sequences of real-time PCR primers. Real-time PCR oligonucleotide sequences were synthesized by Eurofins Genomics Inc (Ebersberg, Germany).

mRNA Primer	Primer	Sequences 5'-3'	Accession number
CAT	Forward	ATG AAG CAG TGG AAG GAG CA	NM_012520.2
	Reverse	GGC CCC GCA GTC ATG ATA TT	
G6PDX	Forward	GCA AAC AGA GTG AGC CCT TC	NM_017006.2
	Reverse	GCT TGT AGG AGG CTG GAT CA	
HO-1	Forward	CGG CCC TGG AAG AGG AGA TAG	XM_039097470.1
	Reverse	CGA TGC TCG GGA AGG TGA AAA	
HPRT1 [1]	Forward	TGC TCG AGA TGT CAT GAA GGA	NM_012583.2
	Reverse	CAG AGG GCC ACA ATG TGA TG	
NQO1 [2]	Forward	TGG CCA ATT CAG AGT GGC ATT	NM_017000.3
	Reverse	AGA GTG GTG ACT CCT CCC AG	
SOD-1 [3]	Forward	AAT GTG TCC ATT GAA GAT CGT GTG A	NM_017050.1
	Reverse	GCT TCC AGC ATT TCC AGT CTT TGT A	

([1]Zemtsova *et al.,* 2011; [2]Huang *et al.,* 2018; [3]Winer *et al.,* 2013;)

2.1.10 Databases, software and world wide web-resources

AxioVision	ZEISS, Oberkochen, Germany
DAVID v6.8	National Institutes of Health, Maryland, USA
FIDJI	https://fiji.sc/ [*521*]
ImageJ v1.53k	National Institutes of Health, Maryland, USA
Image Lab™	Bio-Rad, München, Germany
MaxQuant v2.0	Max-Planck-Institute of Biochemistry, Germany
Microsoft 365™	Microsoft Corporation, Redmond, WA, USA
*O*GlcNAcPred-II	Jia, C., Zuo, Y., and Zou, Q. (2018) *O*-GlcNAcPRED-II: an integrated classification algorithm for identifying *O*-GlcNAcylation sites based on fuzzy undersampling and a K-means PCA oversampling technique. *Bioinformatics* 34, 2029-2036
OligoAnalyzer™ v3.1	https://eu.idtdna.com/pages/tools/oligoanalyzer
Primer-BLAST	National Center for Biotechnology Information (NCBI), http://www.ncbi.nlm.nih.gov/tools/primer-blast
Primer3web v4.1.0	http://primer3.ut.ee/
Prism9™	GraphPad Soft. Inc., San Diego, CA, USA
STRING v11.5	Global Biodata Coalition (https://globalbiodata.org/) and ELIXIR, Wellcome Genome Campus, Hinxton, Cambridgeshire, CB10 1SD, UK
YinOYang	Gupta, R., and Brunak, S. (2002) Prediction of glycosylation across the human proteome and the correlation to protein function. *Pac Symp Biocomput*, 310-322
ZEN Blue & Black	ZEISS, Oberkochen, Germany

2.2 Methods

2.2.1 Preparation and culture of rat cerebral cortical astrocytes

Primary cortical astrocytes were isolated from both brain hemispheres of newborn Wistar rats (0 - 3 days old). After decapitation, the scalp was removed and both cerebral hemispheres were dissected from the skull with a scalpel. The meninges were then removed using forceps and a stereoscopic loupe. The cerebral cortex was prepared from both hemispheres and the tissue was roughly chopped with a scalpel, transferred to 5 mL PBS (w/o Ca^{2+}/Mg^{2+}), and triturated with a Pasteur pipette with various opening diameters. The tissue suspension was then filtered through a nylon net filter and filled up with 20 mL of DMEM (1000 mg/L D-Glucose, GlutaMAX^{TM}) cell culture medium (10% penicillin / streptomycin and 10% FBS). After centrifugation (300 g / 5 min / 4 °C), the supernatant was completely removed and the pellet was aliquoted int o T75 cell culture flasks with 25 mL DMEM cell culture medium (10% penicillin / streptomycin and 10% FBS). The cell suspension was cultivated in an incubator (37 °C, 5% CO_2) for a period of 7 days. In order to remove contaminating microglia, oligodendrocytes and neurons from the cultures, flasks were shaken overnight at 200 rpm / 37 °C. After forming a confluent astrocyte layer, cells were washed with PBS without Ca^{2+}/Mg^{2+} and incubated in trypsin-EDTA (0.05% / 0.02% in PBS) for 5 min at 37 °C. Afterwards, the trypsin-EDTA-treated astrocytes were dislodged by gentle tapping and split into new T75 cell culture flasks at a ratio of 1:3 with 10 mL cell culture medium (DMEM + 10% FBS). Finally, the prepared astrocytes were transferred to culture dishes adequate for the planned investigations and cultured until the desired confluence was reached. New-born rats were obtained from the animal facility of the Central Unit for Animal Research and Animal Welfare Affairs of the University of Düsseldorf (Zentrale Einrichtung für Tierforschung und wiss. Tierschutzaufgaben (ZETT), Project Number O78/08). All animals were maintained according to the German Legislation for the Care and Use of Laboratory animals and the EU Directive 2010/63/EU. The astrocytes were prepared and/ or seeded by the technical assistants Michaela Fastrich, Vanessa Herbertz, Nicole Eichhorst or Torsten Janssen (Experimental Hepatology, Heinrich Heine University, Düsseldorf, Germany).

2.2.2 Transfection of cultured rat astrocytes with siRNA

Astrocytes were grown in 100 mm cell culture dishes until cells reached 70-80% confluency. Before astrocytes were transfected with the siRNA, cells were washed three times with FBS-free DMEM, and then fresh FBS-free DMEM was added after the final wash. First, the transfection reagent was prepared by mixing 140 µL of HiPerFect (Qiagen) with 308 µL FBS-free DMEM (total volume of 448 µL) in 2 mL Screw-Cap Microtubes (Sarstedt) which were briefly vortexed. A volume of 151.2 µL control siRNA (AllStars^{TM}, Qiagen; cat. no. 1027280) or an equal mixture of two OGT-targeting siRNAs (Rn_Ogt_1 and Rn_Ogt_2) or GFAT1 and GFAT2 siRNAs (Rn_MGC95214_1 and Rn_RGD: 1303097_2) were diluted each in 151.2 µL FBS-free DMEM (total volume of 453.6 µL) in 2 mL Screw-Cap Microtubes, respectively (Tab. 2.3). The respective siRNA mixtures were then combined with the transfection reagent (448 µL), gently tapped for 10 seconds and incubated for 10 min at RT. Subsequently, 128 µL of the siRNA/ HiPerFect mixture was added to the culture medium of each dish and gently mixed. Astrocytes were further incubated for 24 h at 37 °C and 5% CO_2. At the end of the incubation time, the cells were washed thrice with FBS-free DMEM and further processed for follow-up experiments as described in the Section 2.2.3.

Table 2.3: Reaction mixture for siRNA transfection reagent.

Components	Mix 1 [µL]	Mix 2 [µL]	Mix 3 [µL]
siRNA AllStars	151.2	-	-
siRNA OGT (1)	-	151.2	-
siRNA OGT (2)	-	151.2	-
siRNA GFAT1	-	-	151.2
siRNA GFAT2	-	-	151.2
FCS-free DMEM	302.4	151.2	151.2
Total reaction volume	453.6	453.6	453.6

2.2.3 Experimental treatment of cultured rat astrocytes

Astrocyte cultures with a confluence of 80-90% were employed for the experimental treatment. For synchronization and to minimize growth factor-mediated effects, astrocytes grown in DMEM+FBS were gently washed thrice with DMEM without FBS and cultured for another 24 h in FBS-free DMEM before experiments were conducted. Astrocytes were either left untreated or incubated with NH_4Cl (5 mM), hemin (5 µM) or D-glucosamine (GlcN, 8 mM) for the duration indicated in the respective figure and corresponding legend. Where indicated, astrocytes were pre-incubated with alloxan (1 mM; "Inhibitor 1", Fig. 2.1), before NH_4Cl was added. In separate experiments, compound E (1 µM), aloxistatin (E64d, 50 µM), eeyarestatin I (ESI, 20 µM) were added to astrocytes cultured for 48 h in absence or presence of NH_4Cl (5 mM) and further incubated for 24 h ("Inhibitor 2", Fig. 2.1).

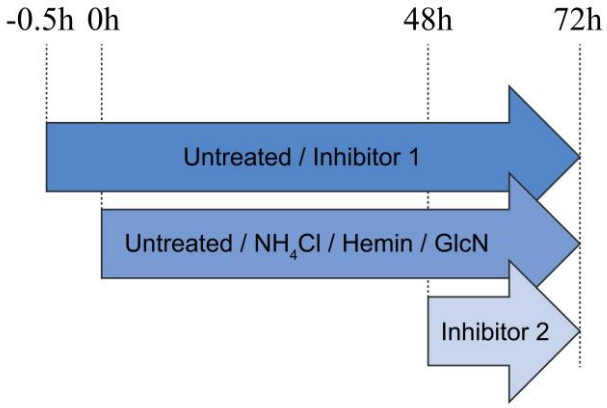

Figure 2.1: Schematic overview on the experimental treatment of the astrocytes. Astrocytes were left untreated or incubated with NH_4Cl (5 mM) for 72 h at 37 °C and 5% CO_2. In separate experiments astrocytes were pre-incubated for 30 minutes with the chemical compounds alloxan (Inhibitor 1). In separate experiments, the astrocytes were incubated for 48 h with NH_4Cl (5 mM) or were left untreated and then inhibitor 2 was added aloxistatin (50 µM), compound E (1 µM) or eeyarestatin (20 µM) and cells were cultured for another 24 h in absence or presence of NH_4Cl.

2.2.4 Hyperammonemia animal model

Effects of hyperammonemia on cerebral *O*-GlcNAc, GRP78 and HO-1 protein levels were investigated in protein lysate from rats after intraperitoneal injection of freshly prepared ammonia acetate (4.5 mmol/kg body weight) [*137*, *235*]. Controls received the vehicle (0.9%

NaCl). Twenty four hours after injection, rats were anesthetized and transcardially perfused with physiological saline and cerebral, hippocampus and cerebellum were dissected and samples were stored at -80 °C. Animal procedures were approved by the State Office for Nature, Environment and Consumer Protection, North Rhine-Westphalia, Germany (AZ 81-02.04.2019.A371). These samples were handed over to me for the preparation of protein lysates in protein lysis-buffer supplemented with 80 µM *O*-(2-Acetamido-2-deoxy-D-glucopyranosylidenamino)-N-phenylcarbamat (PUGNAc) and 0.1 % SDS (w/v). Lysates were ultrasonicated (Hielscher Ultrasonics) on ice, debris and insoluble components were removed by centrifugation and protein concentrations were measured using the Bradford assay.

2.2.5 Primer design for polymerase chain reaction (PCR)

Primer design is crucial with regard to specificity and sensitivity of detecting different mRNA species. Primer properties are determined by the number of bases, the GC content and the melting temperature (*Tm*-value). Target genes for PCR were selected from genomic databases and primer were designed using *Primer3web* version 4.1.0 (http://primer3.ut.ee/). Reverse and forward primers were optimized in silico to avoid secondary structures and less than 4 G or C repeats. For the designed primers, melting temperatures, secondary structures, and the formation of primer-dimers were estimated using *OligoAnalyzer*™ 3.1. All primers listed in Table 2.2 were purchased from Eurofins MWG Operon and had a melting temperature ranging from 52 °C to 60 °C. Target gene specificities were validated for each primer using BLAST (http://www.ncbi.nlm.nih.gov/tools/primer-blast).

2.2.6 Extraction of RNA from cultured rat astrocyte

RNA was isolated from cultured rat astrocytes using RNeasy kits according to manufacturer's instructions (Qiagen). Briefly, culture medium was aspirated from 100 mm culture dishes and cells were washed three times with ice cold PBS (w/o Mg^{2+}/Ca^{2+}). Cells were lysed in 700 µL of

RNA lysis buffer provided by Qiagen (RLT-buffer) supplemented with 1% β-mercaptoethanol and lysates were transferred into clean 1.5 mL reaction tubes and properly mixed. Lysates were then pipetted on QIAshredder spin columns (Qiagen) and centrifuged at 13,000 x g for 2 min at RT. The supernatant was transferred to a fresh tube and the sedimented insoluble cell fragments were discarded. The RNA was precipitated by adding an equal volume of 100% ethanol and mixed immediately by up and down pipetting. Following, the mixtures (650 µL) were transferred to RNeasy Mini spin columns (Qiagen) attached to 2000 µL collection tubes centrifuged for 15 seconds at 10,000 rpm and RT. After discarding the flow-through, 700 µL of RW1 buffer (Qiagen) was added to each RNeasy spin column, and columns were centrifuged for 15 seconds at 10,000 rpm and RT. Then, 500 µL of RPE buffer (Qiagen) was added to each RNeasy spin column and columns were centrifuged for 15 seconds at 10,000 rpm. The RNA was then dried on the column by 2 min centrifugation for 2 min at 10,000 rpm and RT. Following centrifugation, the RNeasy spin column was transferred to a new 1.5 mL collection tube. RNA was released from the membrane and collected by adding 50 µL of RNase-free water to the spin column followed by centrifugation for 1 min at 10,000 rpm and RT. The isolated RNA was stored at -80 °C until further use.

2.2.7 Quantification of RNA

The concentration and purity of the RNA in each total RNA preparation was determined using the NanoDrop™ 1000 Spectrophotometer (Thermo Scientific) by measuring the absorptions at 260 nm and 280 nm wavelengths. The ratio of both wavelengths indicates the purity of the RNA preparation and should be within the range of 1.9 - 2.1. Measurements were performed by putting equal amounts of sample (2 µL) on the NanoDrop™ measurement cell followed by measurement of the absorption at 260 nm and 280 nm wavelengths.

2.2.8 cDNA synthesis

Complementary desoxyribonucleic acid (cDNA) was produced using the First Strand cDNA synthesis kit (Qiagen, Hilden, Germany) of total RNA. Sample volumes containing 1 µg RNA were filled to a volume of 12 µL with RNase-free water and 2 µL of 7 × genomic DNA (gDNA). Wipeout buffer was added to eliminate gDNA according to the recipe in Table 2.4. Samples were incubated at 42 °C for 2 min. To reverse-transcription reaction components containing 1 µL of Quanti-Script reverse transcriptase (RTase), 4 µL of Quantiscript reverse transcription (RT)-Buffer, and 1 µL of RT Primer Mix were added and thoroughly mixed. The RT Primer Mix contains the four deoxynucleotide triphosphate (dNTPs), adenine (dATP), cytosine (dCTP), guanine (dGTP), and thymine (dTTP), and a universal oligonucleotide that permits cDNA synthesis from all sections of RNA transcripts [*522*]. In the next step, the mixture was incubated in a heating block at 42° C for 15 min and then at 95 °C for 3 min to start the cDNA synthesis. The samples were then adjusted with RNase-free water to yield a cDNA concentration of 10 ng/L. Genomic DNA contamination was measured by preparing a negative control, which contains all reaction components except the RTase. The samples were diluted 10 times with RNase-free water and stored at -20 °C.

Table 2.4: Reaction mixture for cDNA synthesis.

Components	Volumes [µL]
RNA (1 µg/µL)	12.0
7x gDNA Wipeout Buffer	2.0
Quantiscript Reverse Transcriptase	1.0
Quantiscript RT Buffer	4.0
RT Primer Mix	1.0
Total reaction volume	20.0

2.2.9 Quantitative real-time PCR

mRNA species were quantified by *real-time* PCR using the ViiA7™ Real-Time PCR Cycler System (Applied Biosystems) and GoTaq® qPCR Master Mix (Promega). SYBR® Green (Promega) was used as fluorescent reporter dye, which intercalates with double-stranded DNA. SYBR® Green emits light of the wavelength 521 nm when it is excitated by a 494 nm laser. The measurement of the emission enables to quantify the DNA content present at each *real-time* PCR cycle. All primers listed in Table 2.2 were adjusted to a concentration of 10 pmol/µL with RNase-free water. Hypoxanthine Phosphoribosyltransferase 1 (HPRT1) served as an endogenous reference and housekeeping gene used for the normalization of the respective target gene in each sample. For performing real-time PCR measurements, the following reaction mixtures listed in Table 2.5 were prepared.

Table 2.5: Reaction mixture for real-time PCR.

Components	Volumes [µL]
cDNA (10 ng/µL)	1.2
Forward primer (10 µM)	1.0
Reverse primer (10 µM)	1.0
2xSYBR® Green	12.5
RNase-free water	9.3
Total reaction volume	25.0

Samples were measured in 96-well reaction plates (Applied Biosystems) using a volume of 25 µL reaction mixture. Each gene of interest was analyzed in duplicate for each sample. The 96-well plate was sealed with adhesive PCR plate seal and the plate was transferred to the cycler. The *real-time* PCRs were carried out using the following listed in Table 2.6.

Table 2.6: Real-time PCR settings.

Step	Temperature [°C]	Time [s]	Cycles
Denaturation	50	120	1x
Denaturation	95	600	
Annealing	95	15	40×
Elongation	60	60	

At the end of the measurements, melting curve analyses were performed to determine the existence of nonspecific products and primer-dimers by gradually increasing the temperature and measuring the fluorescence signal after each increment. The detection threshold, i.e. where the amplification curve passed the detection limit, was calculated automatically by the ViiA7™ Real-Time PCR Cycler System and assigned as the cycle threshold (C_t) value for each sample. The C_t value was utilized to calculate the amount of the respective gene of interest in each sample. Gene expression levels were calculated using the $\Delta\Delta C_t$ method [*523*]. The ΔC_t was calculated by subtracting the C_t of the target sample from C_t for the endogenous control hypoxanthine-guanine phosphoribosyltransferase 1 (HPRT1) which served as a housekeeping gene [*524*].

2.2.10 Preparation of protein lysates from cultured rat astrocytes

At the end of the experiment, the cell culture medium was removed from the cell culture dishes. Astrocytes were washed three times with ice-cold PBS (w/o Ca^{2+}/Mg^{2+}) and protein was isolated by adding 300 µL protein lysis buffer and detaching the cells from the dishes using a cell scraper. The protein lysates were prepared using protein lysis buffer as described in section 2.1.8. Lysates were transferred into fresh reaction tubes, ultrasonicated on ice for 30 seconds and centrifugated at 20,000 x g and 4 °C for 20 min. Insoluble pelleted components were discarded and the supernatant was transferred into clean reaction tubes. The lysates were stored at -20 °C until further use.

2.2.11 Preparation of nuclear extracts from cultured rat astrocytes

Astrocytes were washed three times with ice cold PBS (w/o Mg^{2+}/Ca^{2+}) containing 100 µM sodium ortho-vanadate, detached using a cell scraper and pelleted by centrifugation (14,000 rpm for 2 min at 4 °C). Supernatants were discarded and pellets were incubated in 400 µL buffer containing 10 mM HEPES-KOH pH 7.9; 1.5 mM $MgCl_2$; 10 mM KCl; 0.5 mM DTT; 0.2 mM PMSF; 1 mM sodium orthovanadate for 10 min on ice. At the end of the incubation time, samples were centrifuged for 2 min at 14,000 rpm and 4 °C and supernatants containing the cytosolic fraction were discarded. Pellets were resuspended in 100 µL buffer containing 20 mM HEPES-KOH pH 7.9, 1.5 mM $MgCl_2$, 420 mM NaCl, 0.2 mM EDTA pH 8.0, 25% glycerol, 0.5 mM DTT, 0.2 mM PMSF and 1 mM sodium orthovanadate and incubated for 30 min on ice. At the end of the incubation, samples were centrifuged at 14,000 rpm and 4 °C for 2 min and supernatants were collected and stored at -80 °C until further use.

2.2.12 Preparation of supernatants from cultured rat astrocytes

Astrocytes were grown on 60- or 100-mm plastic dishes and treated as indicated in the respective figure legend. At the end of the incubation time, supernatants were collected and centrifuged at 20,000 x g and 4 °C for 10 min. Supernatants were transferred to an Eppendorf tube and volumes were narrowed using a centrifuge concentrator (Eppendorf Concentrator Plus, Eppendorf, Hamburg, Germany) at 37 °C for 60 min. Samples were resuspended in protein loading buffer and further used for Western blot analyses.

2.2.13 Western blot analyses

Sample preparation for Bradford assays and photometric measurements

Protein concentrations were measured using the Bradford assay which is based on an absorbance shift from 465 nm to 595 nm upon binding of the red-brown dye Coomassie Brilliant Blue to arginine, histidine, phenylalanine, tryptophan and tyrosine residues in proteins

at acidic pH. Protein determinations were carried out using an albumin-based standard curve with following concentrations: 0.125, 0.25, 0.5, 1, 1.5, 2 mg/mL. Protein samples were measured in Bradford reagent (Bio-Rad, Munich, Germany) diluted 1:5 in aqua bidest. 5 µL of each protein lysate were mixed with 995 µL of the diluted Bradford reagent in a clean reaction tube and briefly vortexed. After mixing, the total volume of 1,000 µL was transferred to plastic cuvettes and absorbances at a wavelength 595 nm were measured using a spectrophotometer (Ultrospec 2100 pro, Amersham Biosciences, Freiburg, Germany). Measurements were normalized to samples containing no protein. Each sample was measured in triplicate and mean values were calculated.

Polyacrylamide gel electrophoresis

Sample volumes containing equal amounts of protein were mixed with SDS-PAGE protein loading buffer (Section 2.1.8). Polyacrylamide (PAA) separating gels were prepared at PAA concentrations of 8, 10 and 12%. The composition of the separating and stacking gel mixtures are given in the following Table 2.7.

Protein lysates were transferred to 1.5 mL Eppendorf tubes and mixed with 20 µL of SDS-PAGE protein sample buffer. After heating to 95 °C for 3 min, samples were shortly centrifuged at 12,000 x g and cooled down on ice. Ten µL of standard molecular weight marker (Dual Color, Bio-Rad) and samples were loaded on PAA gels and gel electrophoresis (Bio-Rad, Munich, Germany) was performed using 1 x running buffer (Section 2.1.8). Samples were allowed to run into the stacking gel at a constant voltage of 90 V before the voltage was set to 140 V.

Table 2.7: Composition of separating and stacking gels.

Components	15 mL of separating gel [mL]			5 mL of stacking gel [mL]
	8 %	10 %	12 %	4 %
H_2O	6.9	5.9	4.9	3.4
30 % acrylamide	4.0	5.0	6.0	0.83
1.5 M tris (pH 8.8)	3.8	3.8	3.8	-
0.5 M tris (pH 6.8)	-	-	-	0.63
10 % SDS	0.15	0.15	0.15	0.05
10 % APS	0.15	0.15	0.15	0.05
TEMED	0.009	0.006	0.006	0.005
Total volume	15.009	15.006	15.006	4.965

Protein transfer on membrane

At the end of the electrophesis, gels were electroblotted to transfer the proteins from the gel onto the nitrocellulose membrane (Protran) using a semidry blotting procedure (Electroblotting Fastblot™, Biometra). The PAA-gel was laid on nitrocellulose membrane which first was wetted in aqua bidest and then in transfer buffer (Section 2.1.8). The membrane was placed on stacked filter papers pre-soaked with transfer buffer which were also placed on top of the PAA-gel. By this a layer was created consisting of filter papers, SDS-PAGE gel, nitrocellulose membrane and filter papers as indicated in Figure 2.2. Proteins were transferred onto the nitrocellulose membrane by applying a constant current of 0.8 mA per cm^2 for 90 minutes.

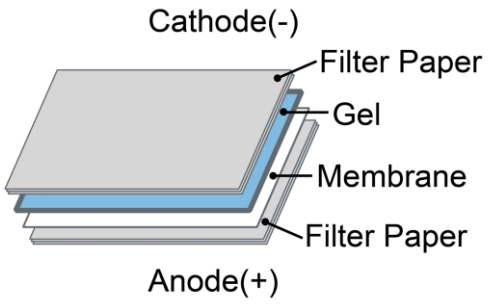

Figure 2.2: Scheme depicting the positioning of the PAA-gel, nitrocellulose and filter papers in the semi-dry blotting apparatus. The membrane is positioned in proximity to the positive electrode, whereas the gel is positioned near the negative electrode. The PAA-gel and the membrane are layered between stacks of filter paper wetted with transfer buffer.

Detection of protein species transferred to the nitrocellulose membrane

At the end of the blotting, the membrane was stained with Ponceau S Staining (Serva) to visualize transferred proteins in order to inspect whether the blotting was successful. The membrane was washed three times with tris-buffered saline (TBS) containing 0.1 % Tween-20 buffer and blocked in 5 % (v/v) bovine serum albumin (BSA) in TBS-T at RT for 1 h. Afterwards, the membrane was incubated with diluted primary antibodies (Tab. 2.1) in 1 x TBS containing 0.1 % Tween®20 (TBS-T) and 5 % (v/v) BSA or non- fat dry milk overnight at 4 °C under gentle agitation. At the end of the incubation, unbound antibodies were removed by washing the membrane three times with TBS-T. Finally, the membrane was incubated with appropriate secondary antibodies (Tab. 2.1) in TBS-T with 5 % BSA in TBS-T for 1 h at RT. At the end of the incubation, the membrane was washed three times with TBS-T each for 10 min at RT. Antibodies bound to the membrane were detected by probing the membranes with Western-Lightning plus ECL™ (Perkin Elmer). Briefly, luminol and peroxide solutions were mixed at a ratio of 1:1 and added to the membrane. Chemiluminescence was acquired and visualized using the ChemiDoc MP and Image Lab software (Bio-Rad, Munich, Germany) or the Amersham ImageQuant™ 800 biomolecular imager and control software v2.0.0 (Cytiva, Thermo Fischer Scientific). Chemiluminescence signals were quantified using the Image Lab (Bio-Rad) or ImageJ software. Where indicated, blots were reprobed with antibodies directed against GAPDH which served as a loading reference. Chemiluminescence intensities of proteins of interests were normalized to those of GAPDH.

2.2.14 *In vitro O*-GlcNAcylation of HO-1

In vitro O-GlcNAcylation was performed by incubating recombinant HO-1 (Cusabio, Wunhan, China) with purified OGT (R&D Systems, Wiesbaden, Germany) and UDP-GlcNAc (Sigma-Aldrich). *In vitro O*-GlcNAcylation of purified recombinant HO-1 (Cusabio, Wunhan, China) was carried out in 40 µL reaction buffer containing 33.5 mM Tris-HCl, pH 7.5, 0.67 mM DTT, 8.38 mM $MgCl_2$, 2.5 mM UDP-GlcNAc, 0.064 µg/µL HO-1 and 0.09 µg/µL OGT (R&D Systems, Wiesbaden, Germany). Samples were incubated for 90 min at 37 °C, mixed with protein loading

buffer and analysed by Western blot as indicated in the respective figure legend. For chemical crosslinking samples were incubated with dithio-bis(succinimidyl propionate) (DSP, 100 µM) for 10 min at 37 °C. For these experiments, *in vitro O*-GlcNAcylation was carried out in 25 mM HEPES (pH7.5) reaction buffer containing 10 mM $MgCl_2$. Recombinant HO-1 was either incubated without or with active or heat-inactivated (65 °C, 5 min) OGT, respectively. The reaction was terminated by addition of glycine (80 mM, 37 °C, 5 min, gentle shaking).

2.2.15 Click reaction on labelled proteins

„Click-chemistry" (azide/ alkyne click reaction and detection) was carried using the Click-iT™ *O*-GlcNAc Enzymatic Labelling System and the Click-iT™ Protein Detection Kit according to the manufacturer's protocol (Invitrogen, Thermo Fischer Scientific). Prior to Click-iT™ *O*-GlcNAc enzymatic labelling, N-glycans were removed by incubating the protein samples for 30 min at 37 °C with PNGase F. According to the protocol of manufacturer (Tab. 2.8), astrocytic protein lysates were incubated with the labelling reaction buffer containing 20 mM HEPES, pH 7.9, 18 megaOhm water, Click-iT™ *O*-GlcNAc enzymatic labeling buffer, 100 mM Manganese (II) chloride ($MnCl_2$), UDP-GalNAz and Gal-T1 (Y289L) overnight at 4 °C.

Table 2.8: Volumes for Click-iT™ enzymatic labeling reactions.

Components	Sample [µL]	Positive control [µL]
Proteins of interest: 2-5 µg in 1% SDS, 20 mM HEPES pH 7.9	40.0	-
α-crystallin control protein	-	4.0
18 megaOhm water	49.0	4.5
Labeling buffer (Component C)	80.0	8.0
$MnCl_2$ 100 mM (Component D)	11.0	1.5
UDP-GalNAz	10.0	1.0
Gal-T1 (Y289L) (Component B)	7.5	1.0
Total reaction volume	197.5	20.0

At the end of the incubation time, proteins were precipitated with methanol/ chloroform to remove excess UDP-GalNAz. Samples were centrifugated at 20,000 x g for 5 min at RT, supernatants were discarded and pellets were resuspended in 20 mM HEPES, pH 7.9 and heated for 10 min at 90 °C. Then, protein pellets were resuspended and incubated with 1% SDS in 50 mM Tris-HCl, pH 8.0 and Click-iT™ reaction buffer containing biotin alkyne solution. Next, Copper(II) sulfate ($CuSO_4$), Click-iT™ Reaction Buffer Additive 1 and Click-iT™ Reaction Buffer Additive 2 were added and samples were briefly vortexed and mixed for 20 min by gentle rotation. Azide-labelled proteins were precipitated using chloroform/ methanol in H_2O and samples were centrifugated at 20,000 x g for 5 min at RT. The upper aqueous phase was removed and the interface layer containing the proteins was collected and proteins were precipitated by addition of methanol. Samples were centrifuged at 20,000 x g for 5 min at RT, air dried for 15 min at RT and resuspended in precipitation buffer. Finally, biotin-labelled proteins were precipitated using streptavidin-conjugated beads.

2.2.16 Immunofluorescence analyses on cultured rat astrocytes

Immunofluorescence analyses were performed on astrocytes grown on MatTek™ glass bottom dishes (MatTek Life Sciences), or ibidi imaging dishes (µ-Dish, polymer coverslip, Ø 35 mm; ibidi Corporation). At the end of the incubation time, cells were fixed using methanol (Roth) for 3 min at RT and washed three times with PBS (w/o Ca^{2+}/Mg^{2+}). Following, cells were incubated with PBS (w/o Ca^{2+}/Mg^{2+}) containing 10 % BSA and 0.1 % Triton X-100 for 30 min at RT and incubated with primary antibodies directed against HO-1 (1:200) over night at RT in PBS (w/o Ca^{2+}/Mg^{2+}) + 10 % BSA. Excess antibodies were removed by washing the cells thrice with PBS (w/o Ca^{2+}/Mg^{2+}) before cells were incubated fluorochrome-coupled (Alexa-Fluor488) antibodies directed against rabbit IgG (1:200, Jackson Corp) for 2 h at RT. Nuclei were counterstained using Hoechst34580 (1:5,000). For labelling the ER, astrocytes were incubated with ER-Tracker™ Green (1 µg/mL; Thermo Fisher Scientific) for 10 min at 37 °C. Cells were washed three times with ice-cold PBS (w/o Ca^{2+}/Mg^{2+}) and fixed with freshly prepared

paraformaldehyde (Thermo Fisher Scientific) + glutaraldehyde (Sigma-Aldrich) (4% each) for 3 min at RT. Mitochondria were counterstained using MitoTracker™ DeepRed (Thermo Fisher Scientific) according to the protocol of the manufacturer. HO-1- staining was performed as described above except that Cy5 or Cy3 conjugated anti-rabbit IgG antibodies (Tab. 2.1) were used for labelling HO-1 antibodies, respectively. Images were acquired using the confocal laserscanning microscope LSM880 (Zeiss AG, Oberkochen, Germany). Signal intensities were quantified using *ImageJ* software (National Institutes of Health, Maryland, USA).

2.2.17 Chemical cross-linking of proteins

Protein-protein interactions were analysed by chemical cross-linking with dithio-bis(succinimidyl propionate) (DSP). Prior to use, DSP was dissolved in DMSO to obtain a 1 M stock solution. At the end of the experimental treatment of the astrocytes, cell culture medium was removed and astrocytes were washed twice with PBS (with Ca^{2+}/Mg^{2+}, 37 °C) before 5 mL of warm PBS containing 1 mM DSP was added to cells. After incubation of the astrocytes for 30 min at 37 °C and 5% CO_2, PBS was removed and excess DSP was quenched by washing the cells thrice with 20 mM Tris-HCl (pH 7.0) and subsequently with ice-cold PBS (w/o Ca^{2+}/Mg^{2+}). Lysates were harvested using protein lysis buffer supplemented with 80 µM PUGNAc and 0.1 % SDS and ultrasonicated on ice for 30 seconds. The protein concentrations were measured using Bradford reagent and equal amounts of protein were mixed with protein-loading buffer without DTT and further processed by SDS-PAGE (Fig. 2.3).

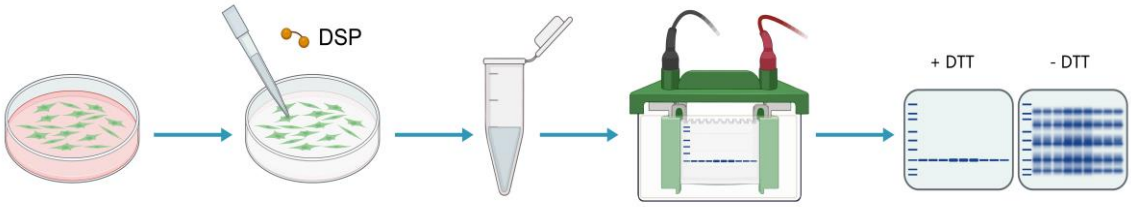

Figure 2.3: Cross-linking of astrocytic proteins and detection of crosslinked proteins by Western blot. Interacting proteins were detected using the membrane permeable cross-linker DSP. The crosslinking is reversed by addition of DTT (+) and accordingly, omission of DTT (-) allows to detect crosslinked proteins by SDS-PAGE and Western blot.

2.2.18 Epifluorescence microscopy

Epifluorescence microscopy was performed using the Cell Observer.Z1 (Zeiss AG, Oberkochen, Germany). Images were acquired using an LD LCI Plan-Apochromat 25x/0.8 Imm Korr DIC M27 set to water immersion and an AxioCamMR3. Images were acquired and processed using AxioVision software (Zeiss AG, Oberkochen, Germany).

2.2.19 Confocal laserscanning microscopy

Confocal laserscanning microscopy was performed as described recently [98] using the LSM880 (ZEISS, Oberkochen, Germany) and Plan-Apochromat objectives 40x/1.4 and 63x/1,4 Oil DIC M27 and immersion oil type 518F/24 °C. Images were acquired using ZEN Black software (ZEISS, Oberkochen, Germany).

2.2.20 Protein-protein interaction network analysis

Protein association networks and functional enrichments within the network were identified utilising the Search Tool for the Retrieval of Interacting Genes/Proteins (STRING). The STRING tool provides a database of known and predicted protein–protein interactions (https://string-db.org/). Analyses were conducted with consideration of both functional and physical protein

associations (full STRING network), derived from text mining, experimental, databases and co-expression analyses. Only interactions with a minimal interaction score of 0.900 (highest confidence) were considered, and proteins not associated with the network were excluded.

Functional protein association networks and functional enrichments in the network were identified using the *Search Tool for the Retrieval of Interacting Genes/Proteins* (STRING, version 11.5; Global Biodata Coalition (https://globalbiodata.org/); ELIXIR, Welcome Genome Campus, Hinxton, Cambridgeshire, CB10 1SD, UK). The STRING tool provides a database of known and predicted protein–protein interactions (https://string-db.org/). Analyses were performed with consideration of functional and physical protein associations (full STRING network), derived from text mining, experimental, database, and co-expression analyses. Interactions scoring 0.700 or above (high confidence) were considered.

2.2.21 Functional enrichment analysis of *O*-GlcNAcylated protein species

A computational investigation was conducted to examine the relationships between molecular functions (MF), cellular components (CC) and biological processes (BP) associated with *O*-GlcNAcylated protein species using the Database for Annotation, Visualization and Integrated Discovery (DAVID, National Institutes of Health, NIH, https://david.ncifcrf.gov/tools.jsp) [*525*]. *O*-GlcNAcylated protein species were uploaded to the DAVID platform and the enrichment analysis was performed against the background of rattus norvegicus. Enriched Gene Ontology (GO) categories for MF, CC and BP were identified. For statistical analysis P-Values were adjusted according to the Benjamini-Hochberg procedure [*526*] and terms showing a false discovery rate of < 0.05 were considered statistically significant. The top 10 most significant GO categories were selected for further analysis. Similarly, DAVID was used to identify the Kyoto Encyclopedia of Genes and Genomes (KEGG) pathways enriched with *O*-GlcNAcylated protein species (FDR < 0.05). The ggplot2 R package was used to generate bubble plots visualizing these enriched pathways. The enrichment ratio (Rich Factor) was used,

representing the ratio of observed proteins in a given pathway to the total number of protein species associated with that pathway.

2.2.22 Nanoparticle tracking analysis

Extracellular vesicles (EVs) were analysed using a ZetaView multi-parameter particle tracking analyser (Particle Metrix, Germany), as previously described [*527*]. The device employs a method of particle detection based on the phenomenon of Brownian motion [*528*]. This technique enables to detect and measure particles whose size is in the nanometre range. Prior to measuring the samples of interest, the measurement accuracy of the ZetaView was verified by measuring nanoparticles with a diameter of 125 nm. The camera was adjusted to ensure that the particles were in sharp focus, and the camera sensitivity was set to an appropriate level. Samples were diluted in particle-free PBS to achieve a particle count in the range of 1 - 9 x 10^7 p./mL (or 250 to 300 particles per visual field). The script control function was employed to record five 30-second videos for each sample, incorporating a sample advance and a 5-second delay between each recording.

2.2.23 Analysis of enriched *O*-GlcNAcylated proteins using quantitative mass spectrometry

Cultured astrocytes were incubated in the presence or absence of NH_4Cl (5 mM, 72 h) and *O*-GlcNAcylated proteins were biotin-labeled using click-iT™ and precipitated using streptavidin-beads (Section 2.2.15). For each sample, two protein aliquots were taken from which one was labelled in presence and the other in absence of biotin. The latter served to control for endogenous biotinylated proteins. Biotin-labeled proteins and respective controls were prepared and analysed by quantitative mass spectrometry. Four samples per group were prepared from individual astrocyte culture dishes: control without biotin labelling, NH_4Cl-treated without biotin labeling, control with biotin labelling, and NH_4Cl treated with biotin labelling. The samples were loaded onto a polyacrylamide gel and separated with a running distance of approximately 5 mm. Following staining with Coomassie Brilliant Blue, bands

containing protein were washed, reduced with dithiothreitol, alkylated with iodoacetamide, and digested with trypsin. The resulting peptides were then prepared for mass spectrometric analysis in 0.1% (v/v) trifluoroacetic acid, as previously described [*529*]. The tryptic peptides were separated using a C18 column and an Ultimate 3000 Rapid separation system (Thermo Fisher Scientific), following the procedure described in [*530*] except that the liquid chromatography-based peptide separation was performed using a 60-minute gradient. The separated peptides were injected directly into a QExactive Plus mass spectrometer (Thermo Fisher Scientific) via an electrospray nano-source interface. Tandem mass spectrometry was used to analyse the peptides in data-dependent positive mode: first, survey spectra were recorded in the orbitrap (resolution: 140000, automatic gain control target: 3000000, maximum ion time: 50 ms, scan range: 200 to 2000 m/z, profile mode); second, up to twenty two- and threefold charged precursors were selected by the quadrupole (4 m/z isolation window), fragmented by higher energy collisional dissociation (normalized collision energy: 30) and fragment spectra were recorded in the orbitrap (resolution: 17500, automatic gain control target: 100000, maximum ion time: 50 ms, scan range: 200 to 2000 m/z, centroid mode). Already fragmented precursors were excluded from repetitive fragmentation for the next 10 seconds.

Data analysis to identify and quantify proteins was performed using MaxQuant Version 1.6.12.0 (Max Planck Institute of Biochemistry) using standard parameters unless otherwise stated. The “match between runs” feature as well as label-free quantification was enabled and 29951 rattus norwegicus sequences (UP000002494) downloaded on 23th January 2020 from the UniProt Knowledgebase used as sequence entries for database searches. The carbamidomethylation at cysteines was considered to be a fixed and the oxidation of methionine and protein N-terminal acetylation as a variable modification. Protein identification data and label-free quantification-based intensities were processed using Perseus 1.6.6.0 (Max Planck Institute for Biochemistry). Only proteins identified with at least two different peptides and three valid quantitative values in at least one group were considered. Contaminants and proteins identified 'by site' were removed. For statistical analysis, label-free quantification intensities were log2 transformed, missing values filled with

values drawn from a downshifted normal distribution (width 0.3 standard deviations, down-shift 1.8 standard deviations) and subsequently, a two way ANOVA and pairwise comparisons using the significance analysis of microarrays method (5% false discovery rate, S0 =0.1) based on Student's t-tests [*531*] were calculated. The mass spectrometric analyses were carried out by the Molecular Proteomics Laboratory, BMFZ, Heinrich Heine University, Düsseldorf, Germany (Dr. Gereon Poschmann, Prof. Dr. Kai Stühler) and the description of the methods for mass spectrometry analysis were provided by Dr. Gereon Poschmann.

2.2.24 Analysis of heme oxygenase 1 glycosylation using mass spectrometry

Recombinant purified rat heme oxygenase 1 ($HO\text{-}1_{rec}$) was analyzed with and without prior OGT catalyzed *O*-linked N-acetyl-D-glucosaminidation. Proteins were separated by polyacrylamide-gelelectrophoresis, proteins were stained and prepared for mass spectrometric analysis by tryptic digestion as described above. Tryptic peptides were separated via liquid chromatography and injected into the mass spectrometer as described in Section 2.2.23. Mass spectrometric analysis was performed on a Fusion Lumos mass spectrometer (Thermo Fisher Scientific) which operated in data-dependent positive mode: precursor spectra were recorded in the Orbitrap analyser (resolution: 60,000, automatic gain control target: 100,000, maximum ion time: 50 ms, scan range: 400 to 1800 m/z, profile mode), subsequently, 2-10 charged precursors were selected by the quadrupole (1.6 m/z isolation window), fragmented and analysed in the linear ion-trap part of the instrument (scan rate: rapid, automatic gain control target: 10,000, maximum ion time: 35 ms, centroid mode). Fragmentation was carried out both with higher energy collisional dissociation and collision-induced dissociation and separate spectra recorded for each fragmentation technique. The maximum cycle time was 2 seconds, already fragmented precursors were excluded for the next 60 seconds.

Protein and peptide identification was carried out with MaxQuant version 2.0.3.0 essentially using standard parameters if not stated otherwise. The carbamidomethylation at

cysteines was used as fixed and methionine oxidation, protein N-terminal acetylation as well as serine and threonine linked N-acetylglucosamine as variable modifications. For the latter one, a neutral loss of 204.09 was considered as well the respective oxonium ion and fragmentation products as diagnostic fragment ions (126.055 $[HexNAc\text{-}C_2H_6O_3]^+$, 138.055 $[HexNAc\text{-}CH_6O_3]^+$, 144.066 $[HexNAc\text{-}C_2H_4O_2]^+$, 168.066 $[HexNAc\text{-}2H_2O]^+$, 186.076 $[HexNAc\text{-}H_2O]^+$ and 204.087 $[HexNAc]^+$. The sequence information from the P06762 heme oxygenase 1 entry as well as 5073 Komagataella phaffii entries (UP000000314) were downloaded from the UniProt KB on 15th December 2019 and used for database searches. The mass spectrometric analyses were carried out by the Molecular Proteomics Laboratory, BMFZ, Heinrich Heine University, Düsseldorf, Germany (Dr. Gereon Poschmann, Prof. Dr. Kai Stühler). The description of the methods for mass spectrometry analyses were provided by Dr. Gereon Poschmann.

2.2.25 Statistical analysis

Statistical analyses were performed with data derived from at least 3 independent astrocyte preparations or 5 independent animals as indicated in the legend of the respective figure or table. Measurements are presented as mean values and each independent data point is represented by a single dot in the respective graph. Number of independent experiments are indicated in the respective figure legends. Normal Gaussian distribution was tested using the Shapiro-Wilk test and variances were compared using the F-test. Depending on the number of groups to be compared, Student´s t-test, Mann-Whitney or the Wilcoxon test or one-way ANOVA followed by the indicated *post* hoc test were applied. The statistical tests used for the analysis of the data are provided in respective figure legend. A p-value < 0.05 was considered statistically significant.

3. Results

3.1 Identification of *O*-GlcNAcylated protein species in cultured rat astrocytes

3.1.1 Effects of ammonia on protein *O*-GlcNAcylation

Previous research demonstrated increased *O*-GlcNAcylation of so far unknown proteins in rat astrocytes which were incubated with ammonium chloride (NH_4Cl). Interestingly, the magnitude of this effect was modulated by both, the ammonia concentration and the exposure time [*144*]. Using the CTD110.6 antibody and Western blot analysis, *O*-GlcNAcylated proteins were detected in the molecular weight range 25 to 250 kDa [*144*].

The experiments described here were performed using the RL-2 and anti-*O*-GlcNAc antibody which was raised against purified *O*-GlcNAcylated nuclear proteins. The experiments were performed on the same well-established rat astrocyte cultures used in previous investigations [*532*]. Astrocytes were incubated with 5 mM NH_4Cl for 72-hours [*4*, *69*, *144*] an ammonia concentration which was univocally demonstrated to be non-toxic in prior studies [*4*, *69*, *136*, *212*, *519*, *533-535*]. Western blotting analyses with the RL-2 antibody showed increased protein *O*-GlcNAcylation in astrocytes incubated with NH_4Cl when compared to controls (Fig. 3.1A). The majority of *O*-GlcNAcylated proteins detected by the RL-2 antibody exhibited molecular weights between 50 and 250 kDa, with a smaller fraction between 25 and 50 kDa. Notably, the most pronounced increases were observed in protein species of approximately 65-70 kDa. Densitometric analysis confirmed a significant (about ≈ 2-fold) increase in the overall protein *O*-GlcNAcylation levels upon ammonia treatment (Fig. 3.1B). These results are in line with previous findings where an increase in protein *O*-GlcNAcylation was observed in ammonia-exposed rat astrocytes by Western blot using the CTD110.6 antibody [*144*].

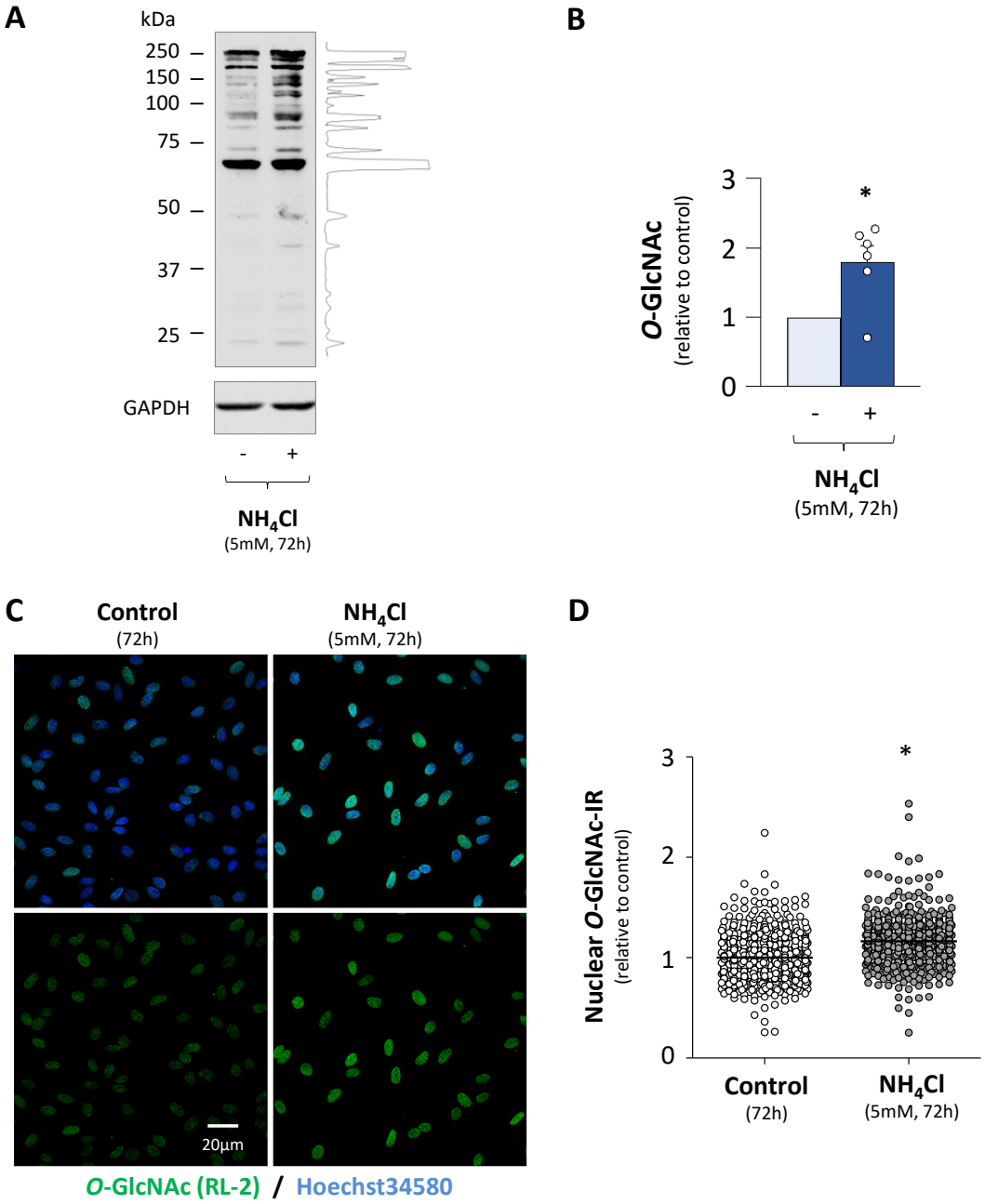

Figure 3.1: Effects of ammonia on protein *O*-GlcNAcylation in cultured rat astrocytes. (**A**) Western blot analysis of *O*-GlcNAcylated proteins in protein lysates derived from astrocytes incubated for 72 h with 5 mM NH_4Cl and from controls using the RL2 anti-*O*-GlcNAc antibody. *O*-GlcNAc immunoreactivities (IR) in astrocytes exposed to NH_4Cl as demonstrated in a chemiluminogram (right hand of the blot). (**B**) *O*-GlcNAc IR was normalized to GAPDH IR and levels in NH_4Cl-treated astrocytes are presented as fold of controls (N=6 independent experiments). (**C**) Investigation of *O*-GlcNAc by immunofluorescence analysis. *O*-GlcNAc (green) and Hoechst34580 (blue). (**D**) Nuclear anti-*O*-GlcNAc IR was quantified and normalized to the respective nuclear area using ImageJ/FIJI. A total of 620 and 676 nuclei from controls or NH_4Cl-treated astrocytes from three independent preparations were analyzed, respectively. Statistical analysis was performed using Student´s t-test. *: Statistically significantly different to untreated controls ($p<0.05$).

To further confirm the Western blot results obtained using the anti-RL-2 antibody, we performed immunofluorescence (IF) analyses and fluorescence microscopy. In line with the Western blot analyses, also the anti-*O*-GlcNAc immunofluorescence was significantly increased in the astrocytes incubated with NH_4Cl when compared to controls (Fig. 3.1C, D). Here, the anti-*O*-GlcNAc immunoreactivity was predominantly nuclear (Fig. 3.1C).

3.1.2 Profiling *O*-GlcNAcylated protein species in untreated and ammonia-exposed astrocytes using „click-chemistry“

Based on these findings, we further examined which proteins species were affected by *O*-GlcNAcylation. For this, we utilized „click-chemistry“ for labelling of *O*-GlcNAcylated protein species with a biotin. This technique is in particular specific and sensitive and allows the labelling of those protein species that are *O*-GlcNAcylated only in minute amounts [*536*, *537*].

In order to identify the ammonia-induced changes in protein *O*-GlcNAcylation, two technical approaches were employed in order to detect the *O*-GlcNAcylated protein species. First, *O*-GlcNAcylated protein species were tagged using biotin and detected the labelled protein by Western blot using peroxidase-coupled streptavidin-HRP (Fig. 3.2A). In a second approach, we purified the biotin-labeled protein species with streptavidin-coated agarose beads prior to the detection with peroxidase-coupled streptavidin-HR (Fig. 3.2B). Both methods consistently showed numerous *O*-GlcNAc-labelled proteins in the molecular weight range of 50-250 kDa. In comparison to the controls, astrocytes exposed to NH_4Cl exhibited a 2-fold increase in the abundance of biotin-labelled proteins, as indicated by the respective chemiluminescence intensities (Fig. 3.2C). It is of significant importance to note that samples subjected to „click-chemistry“ in absence of biotin did not demonstrate aforementioned signals (Fig. 3.2B). This finding corroborates the efficacy of the technical approach to detect and purify *O*-GlcNAcylated proteins and excludes that the observed signals originate from endogenously biotinylated proteins [*538*]. Furthermore, these findings are also consistent with those derived from the Western blot analyses using the RL-2 antibody. The aforementioned

„click-chemistry“ approach was validated through its efficacy and sensitivity in the labelling and purification of *O*-GlcNAcylated protein species in cultured rat astrocytes.

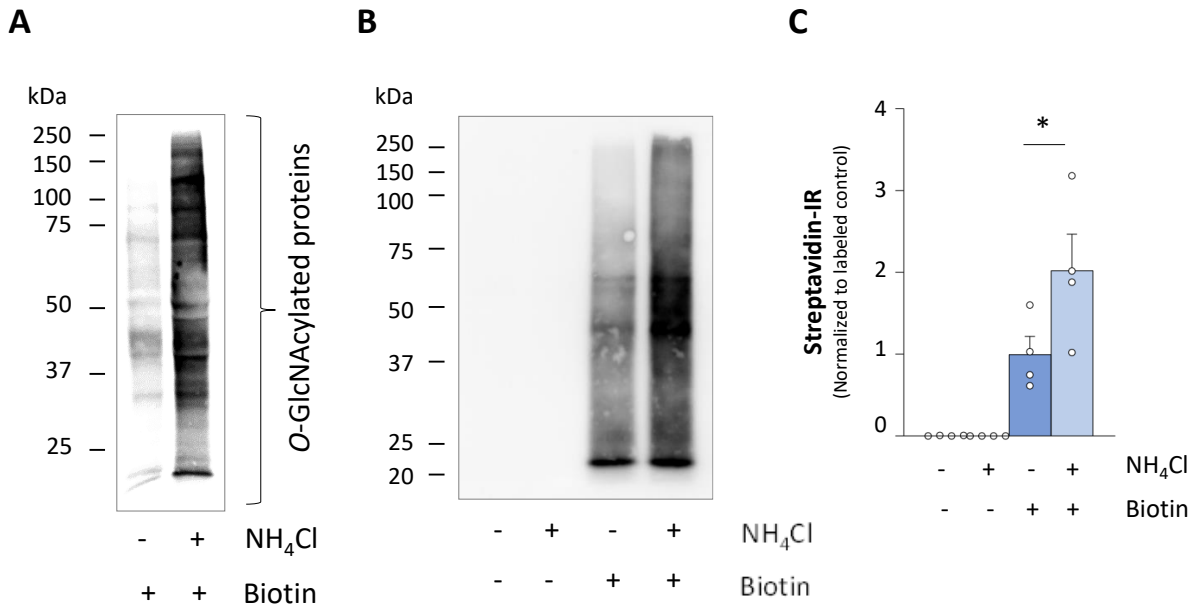

Figure 3.2: Labelling and purification of *O*-GlcNAcylated protein species in protein samples from cultured rat astrocytes. Cultured astrocytes were either left untreated or incubated with NH_4Cl (5 mM, 72 h). Using click-chemistry, *O*-GlcNAcylated proteins in protein samples were labelled with biotin (**A**, **B**) and analysed without (**A**) or after purification by streptavidin-coated beads (**B**) by Western blot. (**C**) Signal intensities were analysed by densitometric analysis. As for control, samples were labelled in absence of biotin (N=4; paired Student´s t-test). *: statistically significantly different to untreated controls ($p<0.05$).

3.1.3 Ammonia alters the *O*-GlcNAcylation of protein species of the astrocytic *O*-GlcNAcome

Using mass spectrometry, a total of 335 *O*-GlcNAcylated protein species were identified in samples from cultured astrocytes in samples of controls and NH_4Cl-exposed astrocytes whose levels were significantly higher with regard to their respective labelling controls (Fig. 3.3A, Tab. 3.1). Of all the identified protein species, about 88% (295 proteins) were exclusively found in NH_4Cl-exposed astrocytes, while 5% (16 proteins) were solely identified in controls. The remaining 7% (24 proteins) were present in both groups (Fig. 3.3A). Functional protein association networks in the *O*-GlcNAcylated protein species were then analyzed using the STRING proteomic database [*539*]. Analysis of the subcellular distribution revealed a

predominant enrichment of *O*-GlcNAcylated proteins of the cytoplasm, cytosol and mitochondria and to lower extent also of the cytoskeleton or endoplasmic reticulum (Fig. 3.3C).

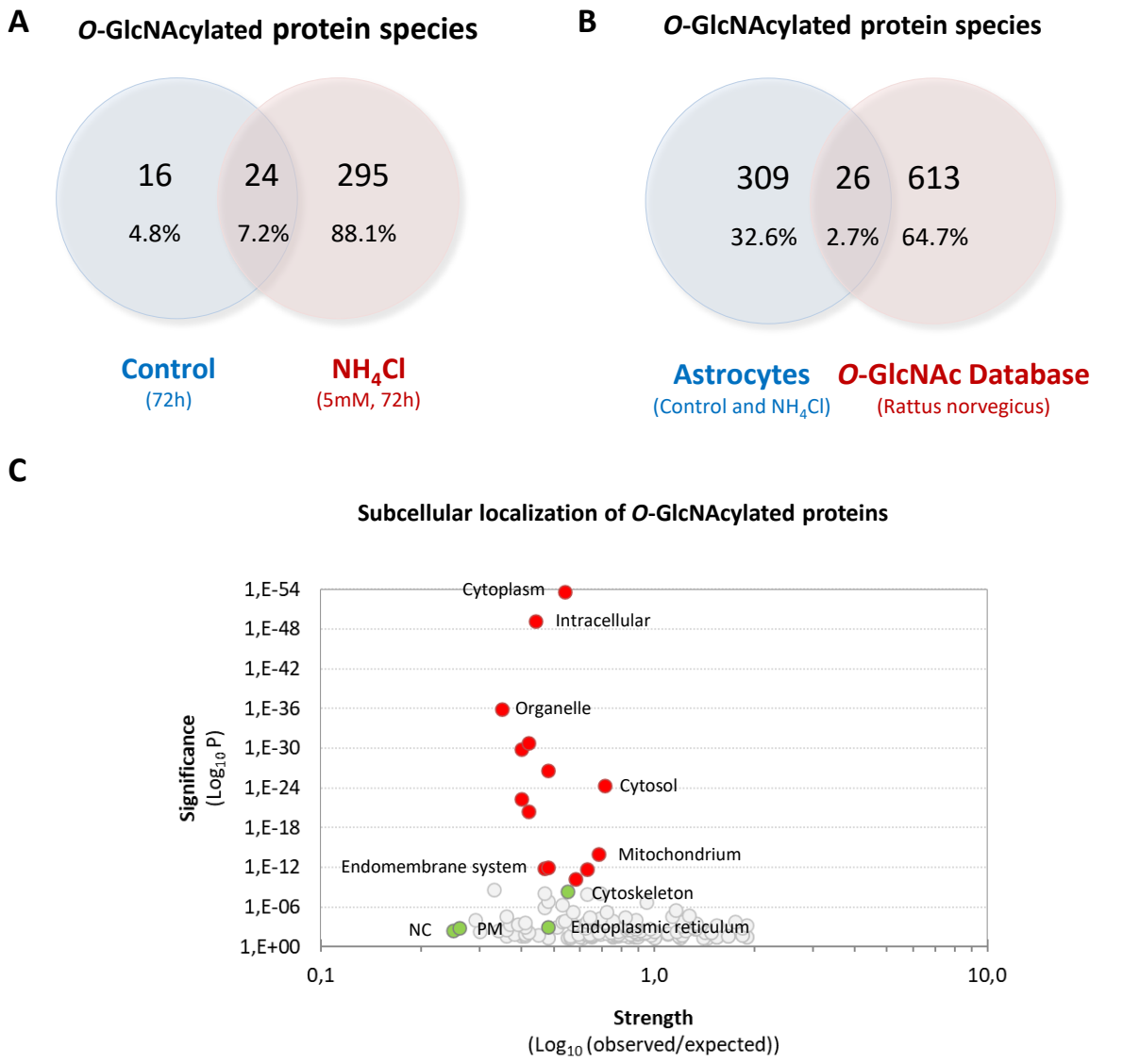

Figure 3.3: Bioinformatic analyses on *O*-GlcNAcylated protein species in rat astrocytes. (**A**) Comparison of *O*-GlcNAcylated protein species whose level were significantly above the respective background control in astrocytes incubated with NH_4Cl (5 mM, 72 h) and in untreated controls (72 h). (**B**) Comparison of the identified *O*-GlcNAcylated protein species with the *O*-GlcNAc reference datasets of the *O*-GlcNAc Database v1.2 for rattus norvegicus. (https://www.oglcnac.mcw.edu). (**C**) The subcellular compartments of the identified *O*-GlcNAcylated protein species were annotated using STRING protein-protein interaction network analysis. The significance was determined using P-values corrected for multiple testing (Benjamini-Hochberg). ER: Endoplasmic reticulum; PM: Plasmamembrane; NC: Nucleus. Red dots: P-value ≤1,E-10; green dots: selected categories (P-value <1,E-10).

Table 3.1: *O*-GlcNAcylated protein species in cultured rat astrocytes. Cells were either left untreated or incubated with NH_4Cl (5 mM) for 72 h. *O*-GlcNAcylated protein species were biotin-labeled by Click-iT™ labeling, isolated by affinity purification using streptavidin-beads and identified by mass spectrometry. As for control, labeling experiments were performed in absence of biotin ("Control background" and "NH_4Cl background"). All proteins are listed whose abundance was significantly higher in controls and cells incubated with NH_4Cl compared to the respective background control. In a third analysis, all proteins are listed whose *O*-GlcNAcylation level were significantly different in astrocytes incubated with NH_4Cl (5 mM, 72 h) compared to controls (72 h). (N=4; paired Student´s t-test/ Significance Analysis of Microarray). *: statistically significantly different compared to untreated controls.

„Control" vs "Control background"									
Aldh4a1	Cyb5r3	B4galt5	Gnas	Cars	B4galt1	Map1a	Gla	Rpl6	Entpd2
Ston1	Slc25a11	Gna11	Pdia4	Map4	Pcyox1	Dhrs1	Gcn1l1	Ptpn9	Gnai1
Asl	Esyt1	Gbp2	Sec31a	Cndp2	Scpep1	Rpl15	Itgb1	Dctn1	Vta1
A0A0G2JUZ5		Gna13	Atp1b3	Iqgap2	Pafah1b1	Lrp1	Ppp2r4	Sec24c	Vars
Lrrc59									

„NH_4Cl" vs "NH_4Cl background"									
Gdi2	Actn1	Ivd	Ldhb	Fscn1	Xpnpep1	Cyb5r3	Mapk3	Tubb5	Mapk1
Anxa1	Idh3a	Arpc1b	Eno2	Wars	Hsd17b4	Hspa4	Tln1	Hadha	Ldha
Pdlim5	Ddx5	Oat	Idh2	Ganab	Hsp90aa1	Iqgap1	Atp1a1	Cct4	Tuba1b
Cct6a	Acadl	Vat1	Nnt	Cltc	Aldh1a1	Myh14	Tubb6	Gnas	Cyc1
Cct8	Sptbn1	Ahcy	Nars	Cpne1	Hsd17b10	Lrp1	Cand1	Maob	Myh10
Cct7	Sqrdl	Sfxn1	Cars	Decr1	Aldh6a1	Acss2	Ddx1	Eef2	Abat
Cct2	Ctsa	Dnpep	Esd	Ap2a1	Serpinb6	Pgm1	Eif3l	Nisch	Snx27
Cct3	Dnaja1	Txnrd1	Hk1	Rab18	Rac1;Rac3	Itgav	Rpl10a	Copb1	Prpf8
Cct5	Ehd2	Man2c1	Pgd	Gcdh	Dync1li2	Atp2a2	Acot2	Hadh	Mthfd1
Myo1c	Aldh1l1	Slc44a2	Pkm	Uggt1	Rangap1	Psmd5	Atl3	Pfn2	Eif3b
Mprip	E9PT22	Map1a	Gla	Cryz	Dync1h1	Stip1	Ipo9	Pfkm	Sfxn3
Farsb	Map4	Rbm39	Pfkl	Gart	Ppid;Ppidl1	Ppp6c	Gbe1	Me1	Aox1
Ogdh	Plcd1	Kpna4	Gba	Dlst	Slc25a12	Sec24c	Tpm4	Me2	Sbds
Pfkp	Coro7	Slc16a1	Rab21	Ogt	Ppp1r12a	Huwe1	Dhx9	Acaa2	Impa1
Aimp1	Psme2	Gcn1l1	Dpp7	Usp9x	Snrnp200	Vps35	Dhrs1	Dbnl	Ap1b1
Psmb5	Ampd3	Vwa5a	Isyna1	Jup	S100a10	Sf3b3	Psmd1	Alg2	Ptpn9
Lonp1	Acsbg1	Ctnnb1	Sorbs3	Ufl1	Apoa1bp	Csad	Copa	Ppm1f	Itga7
Tuba1c	Sntb1	Ppp1cc	Hspa1a	Rpl3	Aldh18a1	Ctbp1	Cpt2	Etf1	Arvcf
Gpnmb	Psmd8	Prkar2a	Sacm1l	Rars	Pafah1b1	Ipo5	Gbp2	Asns	Esyt1
Cops3	Llgl1	Sec31a	Ppp2r4	Aars	Q5U2Q3	Uqcrc2	Fkbp2	Gsto1	Synpo
Dbn1	Cndp2	Lancl1	Sec22b	Eprs	Fam129b	Rtcd1	Psmd13	Dnm2	Snd1

Table 3.1 (continued)

„NH_4Cl“ vs “NH_4Cl background”									
Itgb1	Parp3	Ctnnd1	P56571	Fasn	Rpl5;Rpl5l1	Hnrnpf	Dctn1	Cpt1a	Matr3
Arpc2	Psma4	B4galt1	Uap1l1	Sars	Adh4;Adh5	Acad9	Ddb1	Ubr4	Api5
Shmt2	Vta1	D3ZSF3	Slc27a1	Tars	Ndufv1	Echs1	Prmt1	Tmed7	Aadat
Gna13	Copg1	Ank2	Suclg1	Nsf	Iqgap2	Rnpep	Cotl1	Oplah	Acly
Xpo1	Lta4h	Ttll12	Myo6	Fn1	Cyb5r1	Rtcb	Rpn2	Arcn1	Hexb
Lamp2	Stat3	Hyou1	Sec23a	Gars	Ap2m1	Aco1	Stat1	Itpa	Tln2
Dpysl5	Ap2a2	Myo1d	Mars	Iars	Cyfip1	Gstt2	Lamp1	Lama5	Dpp3
Pgm3	Rpl23	Scn7a	Sccpdh	Sri	Psma3	Psmd6	Cse1l	Ppp2r2a; Ppp2r2d	
Tnpo1; Tnpo2		Tubb4b; Tubb4a		Ahcyl1; Ahcyl2		Eif2s3; Eif2s3y		Kras; Nras; Hras	
Ube2d2; Ube2d3		Ptges3;Ptges3l1		Gapdh;LOC685186; Gapdh-ps2		A0A0G2JVG3		Ipo7	
LOC100911597; Myh9		Ephb2; Epha6; Epha4; Ephb4; Ephb3; Ephb1; Epha7						RGD1311756	
Paics; LOC100359876		LOC100361854; Rps26; RGD1565117				Prps1; Prps2; Prps1l1			
Rps3; RGD1560831		LOC100912210; Rps25; LOC100911337				LOC100362640; Rps4x;Rps4y2			
LOC691716; Rps15a		Rps23;RGD1563570; RGD1563705				Map4k4; Mink1; Tnik			
A0A0G2JT86; A0A0G2JVT8		Rpl9;RGD1561928; LOC100910002				Pdxk;RGD1566085			
Acta2;Actg2		A0A0G2KAM4		A0A0G2KAI8		RGD1562301		A0A0G2JUZ5	

„NH_4Cl“ vs “Control”									
Idh3a	Wars	Myh10	Oat	Itgav	Dync1h1	Rpl10a	Eef2	Cct2	Nars
Gcdh	Atp2a2	Shmt2	Jup	Sntb1	Apoa1bp	Etf1	Itga7	Farsb	Pfkl
Asns	Suclg1	Rtcb	Ipo5	Tln2	Aldh18a1	Eprs	Hexb	Cops3	Aars
Hyou1	Lama5	Lamp1	Iars	Itga2b	D3ZSF3	Psmb3	Scn7a	Mars	Pgm3
Rpl18	Ctsb	Ctsd	Tagln	Puf60	Atp6v1a	Rps9	Palld	Tgm2	H2afy
Ctsc	Hcfc1	Myl6	Cp	Psmd12	Hsp90b1	Hspa9	Lrpprc	Ap3b1	Glud1
Eif3a	Lasp1	Oxct1	Dld	Hspa5	Rhoc	Acta2; Actg2			
LOC100360413; Eef1a1; LOC100360150									

When compared to untreated controls, the *O*-GlcNAcylation levels of 51 protein species were increased and those of 17 species were decreased in astrocytes incubated with NH_4Cl (5 mM, 72 h) (Fig. 3.4A, B, Tab. 3.2). For further in-depth examination of the 68 *O*-GlcNAcylated proteins we performed a STRING database analysis which assigned proteins species to cytoplasmic (e.g., Oat and Lamp1), mitochondrial (e.g., Glud1 and Dld), lysosomal (e.g., Lamp1

and Ctsb), ribosomal (e.g., Rpl10a and Rpl18), polysomic (e.g., Eef2 and Myh10) and ER compartments (e.g., Hsp90b1 and Hyou1) (Fig. 3.4C, Tab. 3.3).

Of note, out of the 68 proteins, 29 did not show significantly higher levels compared to the respective background control of untreated or NH_4Cl-treated astrocytes. This may reflect an insufficient statistical power of the analysis due to an insufficient number of experiments and high a variance resulting from this.

We next compared the identified *O*-GlcNAcylated proteins in controls and astrocytes with NH_4Cl (5 mM, 72 h) to the entries in the current version (v1.2) of the *O*-GlcNAcome database (Fig. 3.3B, Tab. 3.2) [*297*]. The *O*-GlcNAcome database includes a total of 19026 proteins from 49 different species. Here, *O*-GlcNAcylated proteins in rattus norvegicus account for only 639 proteins. Interestingly, only a small fraction of 28 *O*-GlcNAcylated protein species identified in the astrocytes matched with the entries in the *rattus norvegicus O*-GlcNAcome database. Therefore, our dataset may provide a basis for further refinement and expansion of the current *O*-GlcNAcome database for rats [*299*, *302*].

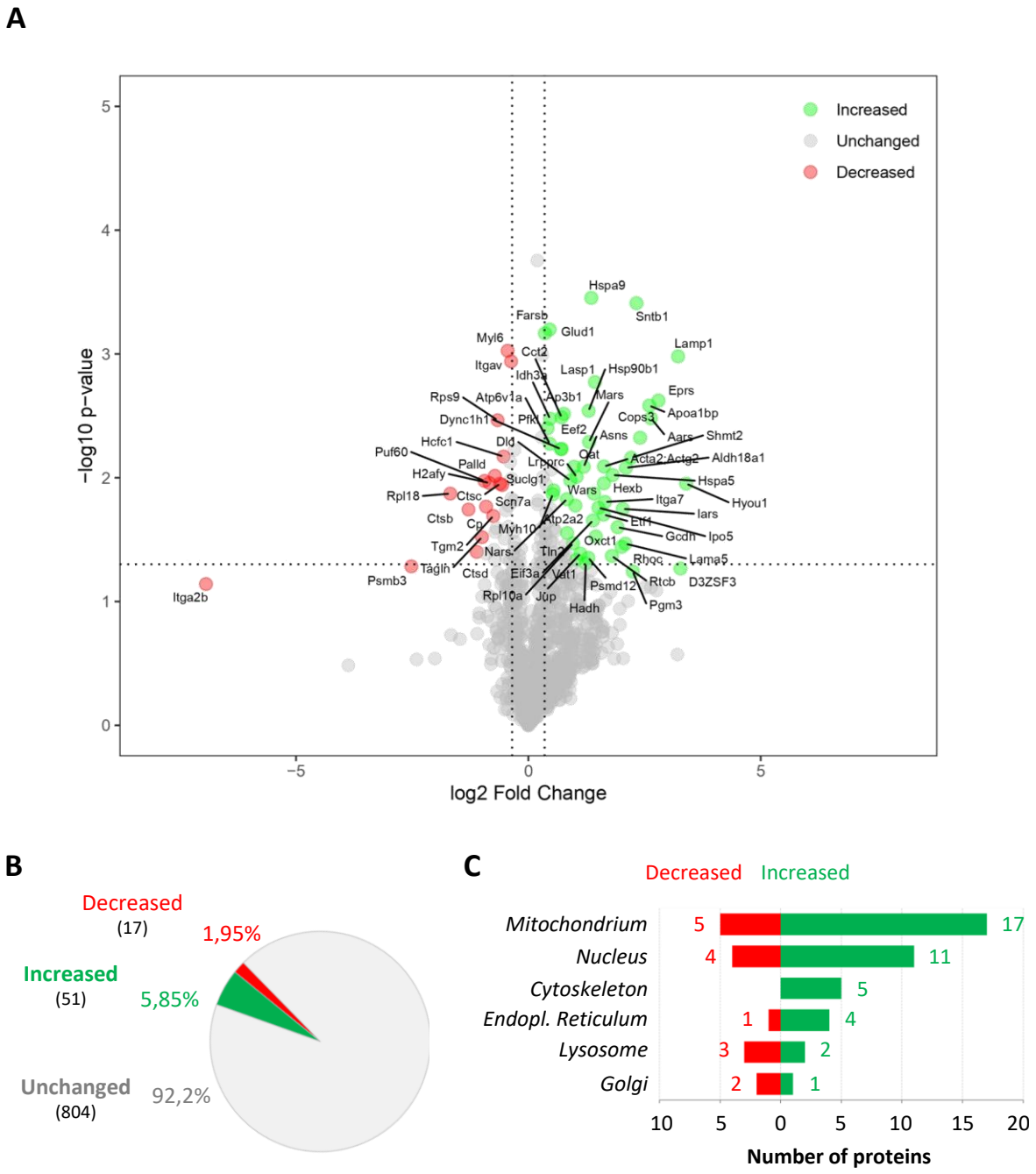

Figure 3.4: Mass spectrometric analysis of purified click chemistry-labelled proteins. (**A**) Illustration of protein *O*-GlcNAcylation level changes in NH_4Cl-exposed astrocytes compared to controls. (**A**) Relative *O*-GlcNAcylation level changes of distinct protein species in NH_4Cl-exposed (5 mM, 72 h) astrocytes compared to controls (72 h). Proteins showing significantly increased or decreased *O*-GlcNAcylation in astrocytes incubated with NH_4Cl compared to controls are indicated by green or red dots, respectively. (**B**) Illustration of protein *O*-GlcNAcylation level changes in NH_4Cl-exposed astrocytes compared to controls in a pie chart. (**C**) Protein species with altered *O*-GlcNAcylation levels in NH_4Cl-exposed astrocytes were assigned to cellular compartments using STRING functional enrichment analysis. (N=4; paired Student´s t-test/ Significance Analysis of Microarray). *: statistically significantly different compared to untreated controls ($p<0.05$).

Table 3.2: Comparison with *O*-GlcNAc database. This table compares *O*-GlcNAcylated protein species in controls (72 h) and astrocytes incubated with NH_4Cl (5 mM, 72 h) whose level were above the respective background control (see Tab. 3.1) with those of the rattus norvegicus reference dataset available in the *O*-GlcNAc Database v1.2 (www.oglcnac.mcw.edu).

Protein species exclusively found in rat astrocytes (this study)									
VTA1	ITGB1	PICALM	SSR1	SEC24C	ALDH4A1	GLA	SEC31A	PTPN9	PPP2R4
RPL6	GCN1L1	IQGAP2	STON1	GNAI1	B4GALT5	GNA11	PDIA4	LRP1	ENTPD2
CARS	CYB5R3	LRRC59	GBP2	GNAS	SCPEP1	ASL	ATP1B3	VARS	RPL15
GSTO1	MATR3	CTNNB1	DNM2	GBE1	PCYOX1	ESD	ESYT1	GNA13	DHRS1
PSMD1	IARS	ITGAV	TAGLN	LMAN1	XPNPEP1	FN1	MPRIP	UBR4	ATL3
SEC23A	ALDH1L1	AP1B1	TPM4	UFL1	PRKAG1	ME1	USP9X	EPRS	SARS
ACSBG1	SPTBN1	VWA5A	PFKM	CSAD	B4GALT1	OGT	ANK2	TARS	AADAT
RPL24	SUCLG1	TUBA1C	H2AFY	AP2M1	PRKAR2A	ME2	DBN1	EIF5B	RPL18
SQRDL	RAB5C	ARVCF	PGM3	ACAD9	HIST1H1E	GBA	API5	COTL1	PSMD13
UAP1L1	MARS	GANAB	TLN2	PFN2	APOA1BP	SRI	CYC1	AP2A1	SNTB1
CSE1L	IPO7	D3ZSF3	GCDH	TMED7	SLC44A2	ITPA	ITGA2B	FKBP2	CTNND1
ADSS	TTLL12	CPNE1	CYFIP1	PSMD8	FAM129B	DHX9	IPO9	IPO5	MYO6
E9PT22	SF3B3	MYH14	AOX1	HSPA4	PCDH17	CCT7	HEXB	SCN7A	NARS
AMPD3	IMPA1	STAT1	LAMA5	SND1	MTHFD1	CCT8	PRPF8	WARS	CLTC
LLGL1	ALG2	RNPEP	DECR1	IQGAP1	ALDH6A1	CCT5	COPA	ACO1	DLST
EIF3L	PSMB5	PSMD5	SNX27	PLCD1	DYNC1H1	DDB1	GART	VPS35	TLN1
CYB5R1	ACSS2	ACAA2	EEF2	ANXA1	ARPC1B	OAT	DPP3	CORO7	STIP1
HSPA1A	ACACA	ATP2A2	ENO2	ATP1A1	TXNRD1	HK1	AHCY	NPM1	FASN
LAMP1	ECHS1	PSMA4	MAPK3	COPB1	S100A10	PKM	MAOB	PSMA3	LAMP2
LTA4H	GSTT2	UQCRC2	P56571	STAT3	ALDH1A1	RPL3	ABAT	AARS	GDI2
RPL23	RPL10A	VAT1	MAPK1	DNAJA1	SLC16A1	PFKL	PPP1CC	TUBB5	IDH2
OPLAH	PGM1	CCT6A	COPG1	NISCH	SLC27A1	RARS	EIF3B	AIMP1	SEC22B
TUBB6	Q5U2Q3	DNPEP	KPNA4	RBM39	HSD17B4	PFKP	RAB18	ETF1	SBDS
PARP3	SHMT2	OGDH	DDX46	NDUFV1	MAN2C1	ASNS	PRMT1	ITGA7	CCT2
HYOU1	PSME2	SFXN1	DDX1	SORBS3	PDLIM5	PGD	HADHA	MYO1D	MYO1C
PPP6C	ARCN1	RTCD1	FARSB	SCCPDH	SERPINB6	NNT	RAB21	PCCB	COPS3
ISYNA1	PSMD6	HNRNPF	LANCL1	TUBA1B	SACM1L	GARS	GPNMB	LONP1	CRYZ
DPYSL5	UGGT1	PPM1F	XPO1	DPP7	HADH	DDX5	ACTN1	RTCB	CCT3
CCT4	DBNL	JUP	CTSA	A0A0G2JUZ5		SLC25A11		PAFAH1B1	
PPP1R12A		SLC25A12		DYNC1LI2		A0A0G2KAI8		A0A0G2KAM4	
HSD17B10		ALDH18A1		RGD1311756		SNRNP200		RANGAP1	
HIST1H4B		HSP90AA1		RGD1562301					

Table 3.2 (continued)

Protein species found in rat astrocytes and included in *O*-GlcNAc Database									
MAP4	DCTN1	MAP1A	CNDP2	HUWE1	SYNPO	NSF	RPN2	ARPC2	ACLY
PHB2	CTBP1	IDH3A	SFXN3	MYH10	ACOT2	LDHA	IVD	ACADL	AP2A2
CPT2	CPT1A	LDHB	FSCN1	CAND1	EHD2	CRYM	A0A0G2JVG3		

Table 3.3: Changes in the abundances of *O*-GlcNAcylated protein species in cultured rat astrocytes induced by ammonia. Astrocytes were either incubated with NH_4Cl (5 mM) or left untreated (control) for 72 h. *O*-GlcNAcylated protein species were biotin-labeled using Click-iT™, purified by streptavidin affinity purification and identified by mass spectrometry. The table lists protein species whose abundancies were statistically significantly different in cultured rat astrocytes incubated with NH_4Cl (5 mM, 72 h) compared to untreated controls (72 h). Data are based on four independent experiments. Statistical analysis was performed using paired t-tests and significance analysis of microarrays (SAM) approach. A false discovery rate (FDR) of 5% and S0 set to 0.1 were applied along with a permutation based FDR and q-value calculation [*540*]. -Log p-value: Transformed p-value highlighting statistical significance. q-value: FDR-adjusted p-value, indicating the likelihood of false positives. Difference: Magnitude of change in protein abundance between treated and control groups. t-statistic: Measure of difference between groups relative to data variability. The mass spectrometric analyses were carried out by the Molecular Proteomics Laboratory, BMFZ, Heinrich Heine University, Düsseldorf, Germany (Dr. Gereon Poschmann, Prof. Dr. Kai Stühler).

Gene	Protein names (Protein IDs)	-Log p-value	q-value	Difference	t-statistic
Rpl18	**60S ribosomal protein L18** (A0A0H2UHS7; P12001)	1.87	0.00	-1.68	-4.00
Rps9	**40S ribosomal protein S9** (P29314; A0A0G2K4C4; M0RB65; D3ZV50)	2.46	0.0115385	-0.66	-3.72
Puf60	**Poly(U)-binding-splicing factor PUF60** (A0A0H2UHZ6; Q9WV25)	1.97	0.0214286	-0.94	-3.56
Ctsb	**Cathepsin B; Cathepsin B light chain; Cathepsin B heavy chain** (Q6IN22;P00787)	1.74	0.0289412	-1.29	-3.45
H2afy	**Core histone macro-H2A.1** (A0A140TAB4; Q02874; B1WC28)	1.96	0.0273333	-0.84	-3.37
Myl6	**Myosin light polypeptide 6** (A0A0G2K6J5; B2GV99; Q64119; A0A0G2JWE1; D3ZHA7; P16409)	3.03	0.0265946	-0.45	-3.33
Palld	**Palladin** (F1M265;P0C5E3;D4A7X7;A0A0G2K046)	2.02	0.0246	-0.72	-3.25
Cp	**Ceruloplasmin** (G3V7K3; A0A0G2K9I6; P13635; CON_ ENSEMBL:ENSBTAP00000031900)	1.74	0.0289412	-1.29	-3.45
Hcfc1	**Host cell factor 1** (D3ZN95)	2.17	0.0372766	-0.533	-2.97
Ctsc	**Dipeptidyl peptidase 1; Dipeptidyl peptidase 1 exclusion domain chain; Dipeptidyl peptidase 1 heavy chain;Dipeptidyl peptidase 1 light chain** (P80067)	1.95	0.0430833	-0.61	-2.92

Table 3.3 (continued)

Gene	Protein names (Protein IDs)	-Log p-value	q-value	Difference	t-statistic
Itgav	**Integrin subunit alpha V** (F1LZX9;A0A0G2JVZ6)	1.87	0.04136	-0.37	-2.85
Tgm2	**Protein-glutamine gamma-glutamyltransferase 2** (Q9WVJ6)	1.70	0.0397692	-0.76	-2.82
Scn7a	**Sodium channel protein** (F1LQQ7)	1.94	0.0430545	-0.56	-2.80
Tagln	**Transgelin** (A0A0G2JWK7; P31232)	1.52	0.0422857	-1.00	-2.80
Psmb3	**Proteasome subunit beta type-3** (P40112;D3Z8J0)	1.28	0.0415439	-2.52	-2.79
Ctsd	**Cathepsin D;Cathepsin D 12 kDa light chain; Cathepsin D 9 kDa light chain; Cathepsin D 34 kDa heavy chain; Cathepsin D 30 kDa heavy chain** (Q6P6T6;P24268)	1.40	0.0534603	-1.11	-2.66
Itga2b	**Integrin subunit alpha 2b** (D3ZXC1)	1.14	0.0502687	-6.94	-2.62
Myh10	**Myosin-10** (G3V9Y1; Q9JLT0)	1.87	0.0495294	0.52	2.62
Jup	**Junction plakoglobin** (Q6P0K8)	1.39	0.0510303	1.12	2.64
Psmd12	**Proteasome (Prosome, macropain) 26S subunit, non-ATPase, 12** (Q5XIC6)	1.35	0.0518154	1.29	2.65
Pgm3	**Phosphoacetylglucosamine mutase** (B2RYN0;D3ZFX4)	1.24	0.052625	2.25	2.65
Rpl10a	**60S ribosomal protein L10a** (P62907; D3Z9F6; F1LYQ7)	1.47	0.048129	0.96	2.68
Suclg1	**Succinyl-CoA ligase [ADP/GDP-forming] subunit alpha, mitochondrial** (A0A0H2UHE1; P13086)	1.90	0.048918	0.54	2.70
Tln2	**Talin 2** (D4A3B0; D3ZA84; D3ZT58; D3ZE09)	1.55	0.0497333	0.83	2.71
Pfkl	**ATP-dependent 6-phosphofructokinase, liver type** (P30835)	2.40	0.0452203	0.41	2.73
Eef1a1[1]	**Elongation factor 1-alpha; Elongation factor 1-alpha 1** (M0R757; P62630; F1M6C2; P62632)	2.07	0.046	0.50	2.75
D3ZSF3	**Peptidyl-prolyl cis-trans isomerase** (D3ZSF3)	1.27	0.0438519	3.27	2.82
Atp6v1a	**H(+)-transporting two-sector ATPase** (D4A133; A0A1W2Q6N0)	2.27	0.0390189	0.46	2.82
Rtcb	**tRNA-splicing ligase RtcB homolog** (Q6AYT3)	1.37	0.040549	1.80	2.85
Farsb	**Phenylalanine--tRNA ligase beta subunit** (Q68FT7)	3.17	0.0422041	0.36	2.87

Table 3.3 (continued)

Gene	Protein names (Protein IDs)	-Log p-value	q-value	Difference	t-statistic
Idh3a	**Isocitrate dehydrogenase [5] subunit, mitochondrial; Isocitrate dehydrogenase [NAD] subunit alpha, mitochondrial** (F1LNF7; Q99NA5)	2.48	0.0297391	0.47	3.02
Rhoc	**Ras homolog family member C** (A0A0G2K6E0; B2RYP0; Q5XIM3)	1.44	0.0304	2.01	3.07
Oxct1	**Succinyl-CoA:3-ketoacid coenzyme A transferase 1, mitochondrial** (B2GV06)	1.53	0.0310909	1.45	3.08
Nars	**Asparagine-tRNA ligase** (F1LPV0; F1LML0; Q4KLM9)	1.83	0.031814	0.83	3.14
Lama5	**Laminin subunit alpha 5** (F1MAN8)	1.47	0.0333659	2.09	3.15
Atp2a2	**Sarcoplasmic/endoplasmic reticulum calcium ATPase 2** (P11507; Q64578; A0A0G2K9N9; G3V9U7; D3ZHJ6; P18596)	1.78	0.0252308	1.01	3.28
Eif3a	**Eukaryotic translation initiation factor 3 subunit A** (Q1JU68)	1.65	0.0258947	0.39	3.33
Gcdh	**Glutaryl-CoA dehydrogenase** (D3ZT90)	1.60	0.0281143	1.92	3.43
Glud1	**Glutamate dehydrogenase 1, mitochondrial** (P10860)	3.20	0.0181818	0.46	3.50
Dld	**Dihydrolipoyl dehydrogenase, mitochondrial** (Q6P6R2)	1.98	0.01875	0.90	3.51
Dync1h1	**Cytoplasmic dynein 1 heavy chain 1** (M0R9X8; F1LRT9; P38650)	2.23	0.0193548	0.70	3.51
Etf1	**Eukaryotic peptide chain release factor subunit 1** (Q5U2Q7)	1.70	0.02	1.62	3.56
Eef2	**Elongation factor 2** (P05197)	2.23	0.0206897	0.72	3.56
Ipo5	**Importin 5** (D4A781; M0RB74)	1.76	0.0222222	1.51	3.63
Lrpprc	**Leucine-rich PPR motif-containing protein, mitochondrial** (F1LM33; Q5SGE0)	2.01	0.012	1.04	3.75
Itga7	**Integrin alpha-7;Integrin alpha-7 heavy chain;Integrin alpha-7 light chain;Integrin alpha-7 70 kDa form** (Q63258;D4A051)	1.80	0.00	1.65	3.82
Wars	**Tryptophan-tRNA ligase, cytoplasmic; T1-TrpRS; T2-TrpRS** (D3ZSF3)	1.87	0.00	1.41	3.83
Oat	**Ornithine aminotransferase, mitochondrial** (P04182)	2.09	0.00	0.98	3.83

Table 3.3 (continued)

Gene	Protein names (Protein IDs)	-Log p-value	q-value	Difference	t-statistic
Iars	**Isoleucine--tRNA ligase** (F1LS86; A0A0G2JVL8; A0A0G2JZH2)	1.75	0.00	2.03	3.84
Cct2	**T-complex protein 1 subunit beta** (Q5XIM9)	2.49	0.00	0.71	3.91
Ap3b1	**AP-3 complex subunit beta** (D3ZIF5;A0A0G2JWD6)	2.52	0.00	0.76	4.10
Asns	**Asparagine synthetase [glutamine-hydrolyzing]** (P49088)	2.09	0.00	1.19	4.12
Hexb	**Beta-hexosaminidase subunit beta** (F1LR87;Q6AXR4)	1.96	0.00	1.62	4.18
Hspa5	**78 kDa glucose-regulated protein** (P06761)	2.02	0.00	1.81	4.48
Acta2; Actg2	**Actin, aortic smooth muscle; Actin, gamma-enteric smooth muscle** (A0A0G2K4M6; P62738; P63269)	2.09	0.00	1.63	4.54
Mars	**Methionine--tRNA ligase, cytoplasmic** (D3Z941)	2.29	0.00	1.31	4.72
Aldh18a1	**Aldehyde dehydrogenase 18 family, member A1** (D3ZIE9)	2.08	0.00	2.10	4.81
Hyou1	**Hypoxia up-regulated protein 1** (Q6P136; Q63617)	1.95	0.00	3.40	4.82
Shmt2	**Serine hydroxymethyltransferase** (Q5U3Z7)	2.16	0.00	2.21	5.12
Hsp90b1	**Endoplasmin** (Q66HD0; A0A0A0MY09; A0A0G2K4I4)	2.54	0.00	1.30	5.32
Cops3	**COP9 signalosome complex subunit 3** (Q68FW9)	2.32	0.00	2.41	5.77
Lasp1	**LIM and SH3 domain protein 1** (Q99MZ8)	2.77	0.00	1.43	6.17
Aars	**Alanine-tRNA ligase, cytoplasmic** (P50475)	2.48	0.00	2.64	6.49
Apoa1bp	**NAD(P)H-hydrate epimerase** (B0BNM1)	2.58	0.00	2.60	6.86
Eprs	**Glutamyl-prolyl-tRNA synthetase** (A0A0G2JZI2; Q6TXE9)	2.62	0.00	2.80	7.16
Hspa9	**Stress-70 protein, mitochondrial** (F1M953; P48721)	3.45	0.00	1.35	7.79
Lamp1	**Lysosome-associated membrane glycoprotein 1** (P14562; A0A0U1RRS9)	2.98	0.00	3.22	9.12
Sntb1	**Syntrophin, beta 1** (D3ZWC6)	3.41	0.00	2.33	10.07

([1]The gene Eef1a1 is associated with two LOC-IDs: LOC100360413 and LOC100360150. These can be employed as search queries to retrieve its record online, even if the Eef1a1 symbol undergoes changes.)

3.1.4 Pathway enrichment analysis and interaction networks of the identified *O*-GlcNAcylated protein species

To identify protein-protein interaction networks which are established by the *O*-GlcNAcylated protein species, STRING database analyses were performed [*541*]. Here, all protein species were included, whose level were above the background in controls and NH_4Cl-treated astrocytes (Tab. 3.1). Of note, protein species may interact in several ways: while some engage in direct physical interactions, others interact indirectly, relying on intermediary proteins to facilitate the connection. Every associated protein is connected by a line, each with a distinct colour that denotes the method of interaction detection, as described by a comprehensive list of detection methods. This allowed us to construct a STRING network encompassing *O*-GlcNAcylated protein species in our rat astrocyte cultures (Fig. 3.5A). The network analysis revealed a variety of protein networks of diverse pathways. These include tRNA aminoacylation, protein folding and chaperones complex, myosin II complex, coat protein complex I (COPI) coated vesicle membrane, membrane coat, sphingolipid metabolism and lysosome, microtubule dependent trafficking, nucleocytoplasmatic transport complex, actin filament organization, carbon metabolism, pyruvate metabolism, fatty acid beta oxidation, glutamine family amino acid metabolic process, 5S rRNA binding and proteasome (Fig. 3.5A). The corresponding proteins functionally related to transport processes, amino acid and energy metabolism and were involved in protein biosynthesis and degradation pathways (Fig. 3.5A, Tab. 3.4).

The STRING analysis was further applied to identify protein-protein interaction networks which are established by protein species, whose *O*-GlcNAcylation levels changed upon NH_4Cl in the astrocytes. Similar to the approach mentioned above, these analyses included biological functions and signalling pathways which are potentially affected by the NH_4Cl-induced changes in the *O*-GlcNAcylation of distinct proteins. Notably, five functional groups emerged from the network analysis: endoplasmic reticulum chaperone complex, glutamine family amino acid metabolism, translation, lysosome and translation (Fig. 3.5B). These data show that the changes in astrocytic *O*-GlcNAcome that are induced by ammonia relate to biochemical pathways that have recently been proposed to underlie ammonia toxicity in astrocytes.

A

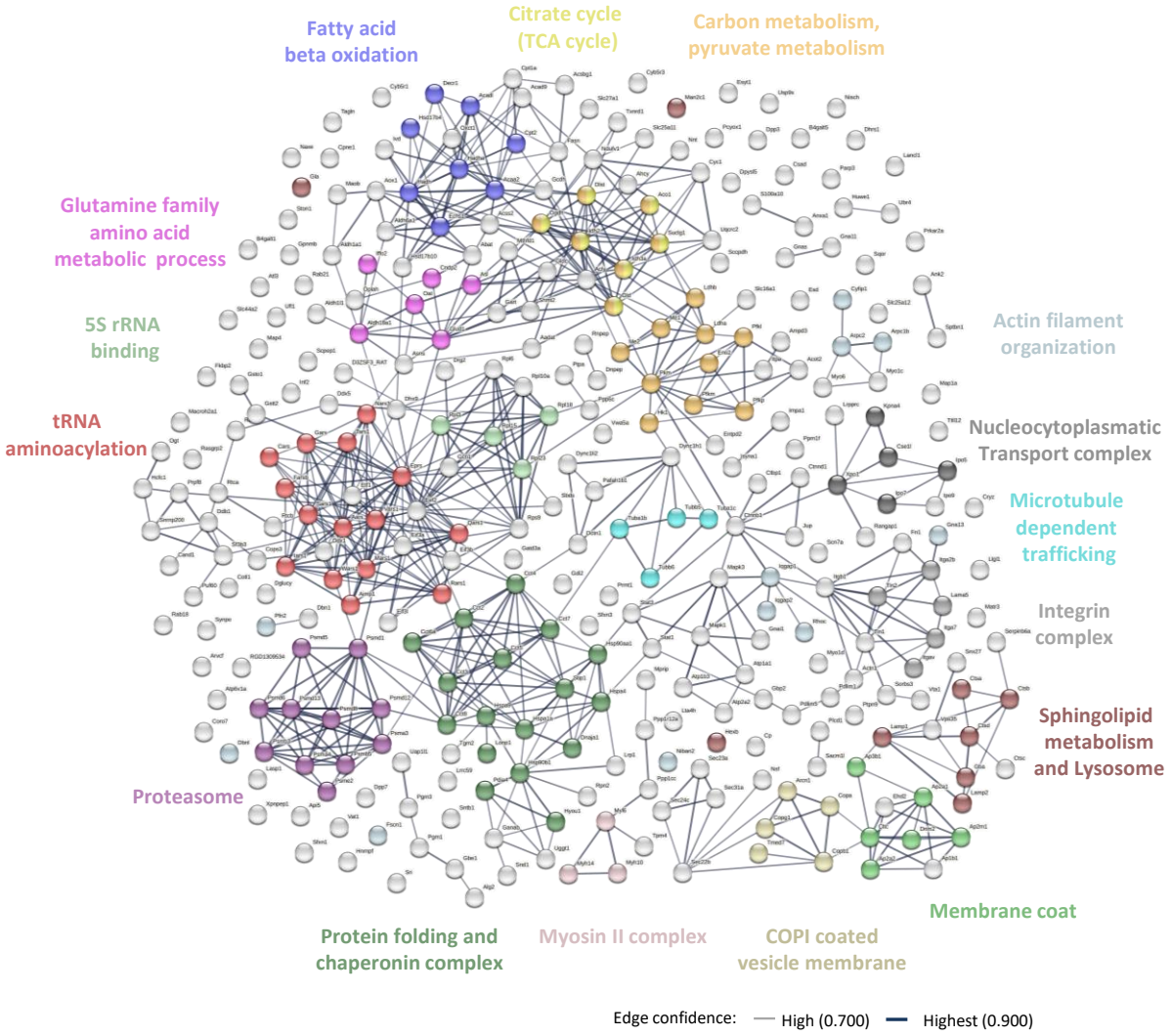
Fatty acid beta oxidation
Citrate cycle (TCA cycle)
Carbon metabolism, pyruvate metabolism
Glutamine family amino acid metabolic process
5S rRNA binding
Actin filament organization
tRNA aminoacylation
Nucleocytoplasmatic Transport complex
Microtubule dependent trafficking
Integrin complex
Sphingolipid metabolism and Lysosome
Proteasome
Membrane coat
Protein folding and chaperonin complex
Myosin II complex
COPI coated vesicle membrane
Edge confidence:
High (0.700)
Highest (0.900)

B

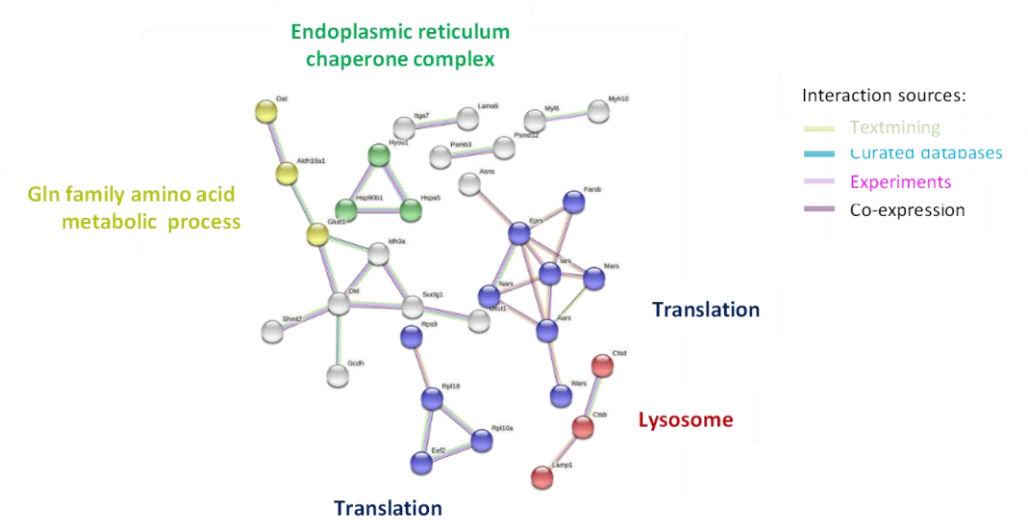
Endoplasmic reticulum chaperone complex
Gln family amino acid metabolic process
Translation
Lysosome
Translation
Interaction sources:
Textmining
Curated databases
Experiments
Co-expression

Figure 3.5: STRING network analysis of proteins constituting the astrocytic *O*-GlcNAcome. (**A**, **B**) Identification of STRING network clusters constituted by (**A**) *O*-GlcNAcylated protein species identified by Click-iT™ chemistry whose level were above their respective background control. (**B**) Protein species whose *O*-GlcNAcylation levels changed upon NH_4Cl treatment compared to controls (STRING database; https://string-db.org/). Clusters of nodes represent distinct biological pathways/processes. Yellow nodes indicate the glutamine family amino acid metabolic process; violet nodes relate to translation; red nodes are associated with lysosomes; and green nodes signify the endoplasmic reticulum chaperone complex. Blue nodes represent proteins involved in the KEGG signaling pathway. Each node represents a single protein species, and connecting lines illustrate protein-protein interactions. Line colors denote the evidence type supporting the interaction: text-mining (yellow), curated databases (teal), experimental findings (purple) and co-expression (grey).

Table 3.4: Subcellular localization of ammonia-responsive *O*-GlcNAcylated protein species. This table summarizes the subcellular localization of protein networks based on the Gene Ontology Cellular Component (GOCC) terms enriched with proteins exhibiting ammonia-induced changes in *O*-GlcNAcylation. The data were obtained from STRING functional enrichment analysis and analyzed using a false discovery rate (FDR) correction (Benjamini-Hochberg method) to account for multiple testing [*526*].

Term Description (Term ID)	Count	Strength	FDR	Matching Proteins
Protein-containing complex (0032991)	30 of 2846	0.57	5.42e-08	Rpl10a, Pfkl, Cops3, Rtcb, Itgav, Suclg1, Lrpprc, Dld, Lama5, Shmt2, Glud1, Idh3a, Psmb3, Atp2a2, Hspa5, Etf1, Ctsd, Rpl18, Cct2, Rps9, Hsp90b1, Hyou1, Eef2, Jup, Hexb, H2afy, Itga7, Myh10, Eif3a, Dync1h1
Intracellular (0005622)	39 of 5194	0.42	9.91e-08	Rpl10a, Pfkl, Cops3, Lasp1, Wars, Rtcb, Suclg1, Lrpprc, Dld, Shmt2, Glud1, Ctsb, Idh3a, Psmb3, Tgm2, Ctsc, Oat, Atp2a2, Aars, Hspa5, Apoa1bp, Etf1, Lamp1, Hspa9, Ctsd, Rpl18, Cct2, Rps9, Hsp90b1, Hyou1, Eef2, Jup, Hexb, H2afy, Puf60, Myh10, Eif3a, Oxct1, Dync1h1
Cytoplasm (0005737)	33 of 3657	0.5	9.91e-08	Rpl10a, Pfkl, Lasp1, Suclg1, Lrpprc, Dld, Shmt2, Glud1, Ctsb, Idh3a, Tgm2, Ctsc, Oat, Atp2a2, Aars, Hspa5, Apoa1bp, Etf1, Lamp1, Hspa9, Ctsd, Rpl18, Cct2, Rps9, Hsp90b1, Hyou1, Eef2, Jup, Hexb, Myh10, Eif3a, Oxct1, Dync1h1
Cellular anatomical entity (0110165)	41 of 6475	0.35	3.26e-06	Rpl10a, Pfkl, Cops3, Lasp1, Rtcb, Itgav, Suclg1, Lrpprc, Dld, Lama5, Shmt2, Glud1, Ctsb, Idh3a, Cp, Tgm2, Ctsc, Oat, Atp2a2, Aars, Hspa5, Apoa1bp, Etf1, Lamp1, Hspa9, Ctsd, Rpl18, Cct2, Rps9, Hsp90b1, Hyou1, Eef2, Jup, Hexb, H2afy, Puf60, Itga7, Myh10, Eif3a, Oxct1, Dync1h1
Intracellular organelle (0043229)	32 of 4198	0.43	6.84e-06	Rpl10a, Cops3, Lasp1, Suclg1, Lrpprc, Dld, Glud1, Ctsb, Idh3a, Tgm2, Ctsc, Oat, Atp2a2, Hspa5, Apoa1bp, Lamp1, Hspa9, Ctsd, Rpl18, Cct2, Rps9, Hsp90b1, Hyou1, Eef2, Jup, Hexb, H2afy, Puf60, Myh10, Eif3a, Oxct1, Dync1h1

Table 3.4 (continued)

Term Description (Term ID)	Count	Strength	FDR	Matching Proteins
Organelle (0043226)	33 of 4534	0.41	9.18e-06	Rpl10a, Cops3, Lasp1, Rtcb, Suclg1, Lrpprc, Dld, Glud1, Ctsb, Idh3a, Tgm2, Ctsc, Oat, Atp2a2, Hspa5, Apoa1bp, Lamp1, Hspa9, Ctsd, Rpl18, Cct2, Rps9, Hsp90b1, Hyou1, Eef2, Jup, Hexb, H2afy, Puf60, Myh10, Eif3a, Oxct1, Dync1h1
Intracellular membrane-bounded organelle (0043231)	26 of 3168	0.46	5.55e-05	Cops3, Suclg1, Lrpprc, Dld, Glud1, Ctsb, Idh3a, Tgm2, Ctsc, Oat, Atp2a2, Hspa5, Apoa1bp, Lamp1, Hspa9, Ctsd, Rps9, Hsp90b1, Hyou1, Jup, Hexb, H2afy, Puf60, Eif3a, Oxct1, Dync1h1
Mitochondrion (0005739)	12 of 644	0.81	6.47e-05	Suclg1, Lrpprc, Dld, Glud1, Ctsb, Idh3a, Tgm2, Oat, Hspa5, Apoa1bp, Hspa9, Oxct1
Membrane-bounded organelle (0043227)	27 of 3716	0.41	0.00026	Cops3, Rtcb, Suclg1, Lrpprc, Dld, Glud1, Ctsb, Idh3a, Tgm2, Ctsc, Oat, Atp2a2, Hspa5, Apoa1bp, Lamp1, Hspa9, Ctsd, Rps9, Hsp90b1, Hyou1, Jup, Hexb, H2afy, Puf60, Eif3a, Oxct1, Dync1h1
Mitochondrial matrix (0005759)	6 of 149	1.15	0.00095	Suclg1, Lrpprc, Glud1, Idh3a, Oat, Hspa9
Endoplasmic reticulum chaperone complex (0034663)	3 of 11	1.98	0.0013	Hspa5, Hsp90b1, Hyou1
Polysome (0005844)	4 of 45	1.49	0.0017	Rpl10a, Rpl18, Eef2, Myh10
Tricarboxylic acid cycle enzyme complex (0045239)	3 of 13	1.91	0.0017	Suclg1, Dld, Idh3a
Catalytic complex (1902494)	11 of 775	0.7	0.0017	Pfkl, Suclg1, Dld, Shmt2, Glud1, Idh3a, Psmb3, Hspa5, Ctsd, Hexb, Dync1h1
Membrane-enclosed lumen (0031974)	11 of 828	0.67	0.0026	Suclg1, Lrpprc, Glud1, Idh3a, Oat, Hspa5, Hspa9, Rps9, Hsp90b1, Hyou1, H2afy
Organelle lumen (0043233)	11 of 828	0.67	0.0026	Suclg1, Lrpprc, Glud1, Idh3a, Oat, Hspa5, Hspa9, Rps9, Hsp90b1, Hyou1, H2afy
Intracellular organelle lumen (0070013)	11 of 825	0.67	0.0026	Suclg1, Lrpprc, Glud1, Idh3a, Oat, Hspa5, Hspa9, Rps9, Hsp90b1, Hyou1, H2afy
Ribonucleoprotein complex (1990904)	7 of 300	0.91	0.0027	Rpl10a, Lrpprc, Rpl18, Rps9, Eef2, Myh10, Eif3a
Cytosol (0005829)	11 of 913	0.63	0.0052	Rpl10a, Pfkl, Tgm2, Hspa5, Rpl18, Cct2, Rps9, Hsp90b1, Eef2, Jup, Myh10

Table 3.4 (continued)

Term Description (Term ID)	Count	Strength	FDR	Matching Proteins
Intracellular non-membrane-bounded organelle (0043232)	14 of 1502	0.51	0.0068	Rpl10a, Lasp1, Lrpprc, Tgm2, Hspa9, Rpl18, Cct2, Rps9, Eef2, Jup, H2afy, Myh10, Eif3a, Dync1h1
Non-membrane-bounded organelle (0043228)	14 of 1526	0.51	0.0077	Rpl10a, Lasp1, Lrpprc, Tgm2, Hspa9, Rpl18, Cct2, Rps9, Eef2, Jup, H2afy, Myh10, Eif3a, Dync1h1
Polysomal ribosome (0042788)	3 of 29	1.56	0.0084	Rpl10a, Rpl18, Eef2
Vacuole (0005773)	6 of 267	0.9	0.0099	Dld, Ctsb, Ctsc, Lamp1, Ctsd, Hexb
Smooth endoplasmic reticulum (0005790)	3 of 35	1.48	0.0130	Hspa5, Hsp90b1, Hyou1
Oxidoreductase complex (1990204)	4 of 94	1.17	0.0130	Dld, Shmt2, Glud1, Idh3a
Mitochondrial tricarboxylic acid cycle enzyme complex (0030062)	2 of 7	2.0	0.0197	Suclg1, Idh3a
Side of membrane (0098552)	5 of 202	0.94	0.0207	Ctsb, Atp2a2, Lamp1, Jup, Myh10
Endoplasmic reticulum lumen (0005788)	3 of 44	1,38	0.0210	Hspa5, Hsp90b1, Hyou1
Lysosome (0005764)	5 of 208	0.93	0.0220	Ctsb, Ctsc, Lamp1, Ctsd, Hexb
Lytic vacuole (0000323)	5 of 211	0.92	0.0227	Ctsb, Ctsc, Lamp1, Ctsd, Hexb
Ribosome (0005840)	4 of 127	1.04	0.0311	Rpl10a, Rpl18, Rps9, Eef2

To further decipher potential functional consequences of ammonia-induced *O*-GlcNAcylation, Gene Ontology (GO) and Kyoto Encyclopedia of Genes and Genomes (KEGG) pathway enrichment analyses were performed. These analyses included protein species whose *O*-GlcNAcylation level in NH_4Cl-treated astrocytes were above the background control (Tab. 3.1). GO enrichment analysis identified 1,978 significantly enriched GO categories (p-

value < 0.05) encompassing 659 biological processes, 658 cellular components and 661 molecular functions.

Within the enriched biological processes, protein stabilization (FDR = 1.10 x 10^-10) was the most prominent category. Additionally, processes related to telomere maintenance such as "positive regulation of establishment of protein localization to telomere" (FDR = 5.25 x 10^-9) and "positive regulation of telomere maintenance via telomerase" (FDR = 9.43 x 10^-9) (Fig. 3.6A, Suppl. Tab. 1). The most enriched terms in the molecular function category included "protein binding" (FDR = 1.82 x 10^-12), "NAD binding" (FDR = 2.24 x 10^-12) and "ATP binding" (FDR = 5.04 x 10^-12). Furthermore, the GO analysis revealed significant enrichment of *O*-GlcNAcylated protein species in specific cellular components: The most enriched categories included "cytosol" (FDR = 4.35 x 10^-19), "mitochondrion" (FDR = 3.56 x 10^-13) and "cytoplasm" (FDR = 2.71 x 10^-9), supporting the notion of predominant localization within these compartments (Fig. 3.6A, Suppl. Tab. 1).

KEGG pathway enrichment analysis identified ten key metabolic pathways significantly enriched with *O*-GlcNAcylated protein species (Fig. 3.6B, Suppl. Tab. 2). These pathways included glycolysis/ gluconeogenesis, fatty acid degradation, branched-chain amino acid degradation (valine, leucine and isoleucine), purine metabolism, pentose phosphate pathway, galactose metabolism, citrate cycle (TCA cycle), fatty acid elongation, cysteine and methionine metabolism and fructose and mannose metabolism. The observed enrichment provides evidence that protein *O*-GlcNAcylation may play a role in regulating cellular metabolism in the presence of NH_4Cl. Furthermore, ten protein species (MAPK1, MAPK3, Hras;Kras, Rac1, Ctnnb1, Stat3, Itgb1, Tuba1b, Stat1, Tubb4b;Tubb4a) emerged as recurrent hits across multiple enriched pathways.

The findings from the GO analyses are in line with the findings of the STRING network analysis and indicate that the astrocytic *O*-GlcNAcome of ammonia-exposed astrocytes is strongly enriched for biological functions and molecular pathways related to sugar, nucleotide, amino and fatty acid metabolism. Furthermore, among the *O*-GlcNAcylated proteins an enrichment was noted for cytosolic and mitochondrial proteins.

A

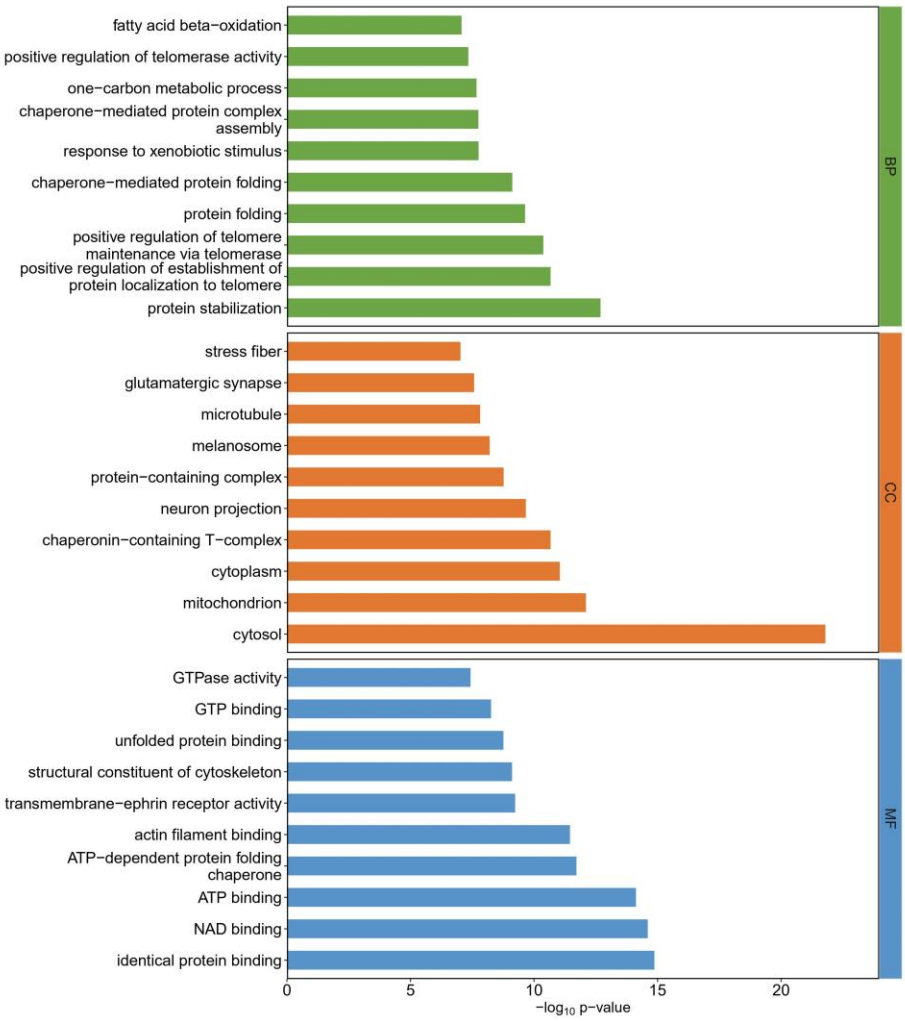
fatty acid beta−oxidation
positive regulation of telomerase activity
one−carbon metabolic process
chaperone−mediated protein complex assembly
response to xenobiotic stimulus
chaperone−mediated protein folding
protein folding
positive regulation of telomere maintenance via telomerase
positive regulation of establishment of protein localization to telomere
protein stabilization
BP
stress fiber
glutamatergic synapse
microtubule
melanosome
protein−containing complex
neuron projection
chaperonin−containing T−complex
cytoplasm
mitochondrion
cytosol
CC
GTPase activity
GTP binding
unfolded protein binding
structural constituent of cytoskeleton
transmembrane−ephrin receptor activity
actin filament binding
ATP−dependent protein folding chaperone
ATP binding
NAD binding
identical protein binding
MF
0
5
10
15
20
−log10 p−value

B

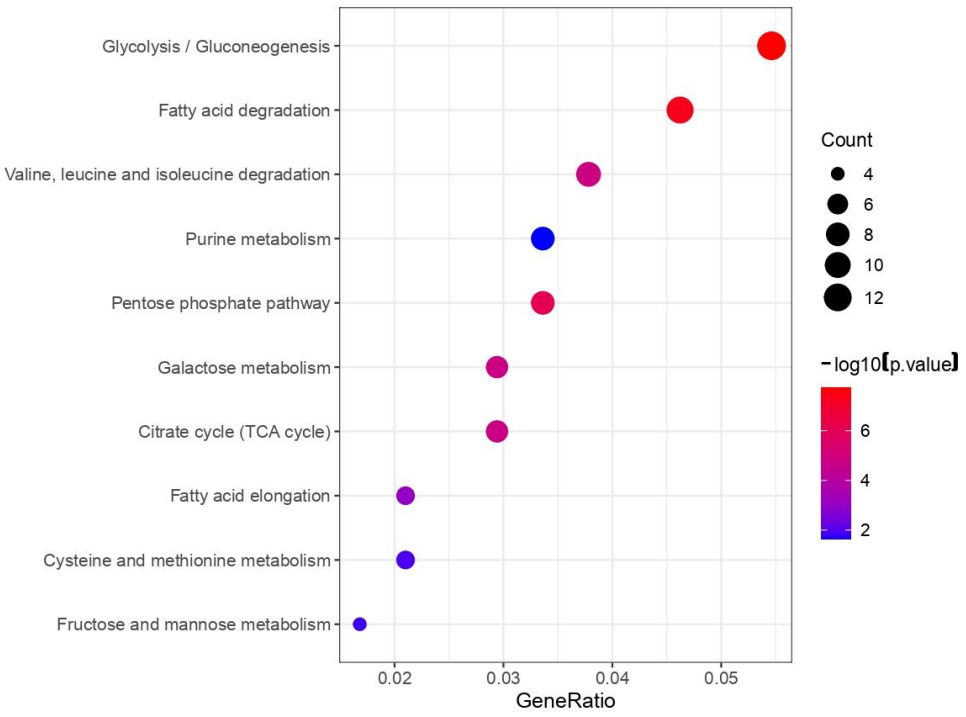
Glycolysis / Gluconeogenesis
Fatty acid degradation
Valine, leucine and isoleucine degradation
Purine metabolism
Pentose phosphate pathway
Galactose metabolism
Citrate cycle (TCA cycle)
Fatty acid elongation
Cysteine and methionine metabolism
Fructose and mannose metabolism
0.02
0.03
0.04
0.05
GeneRatio
Count
4
6
8
10
12
−log10[p.value]
6
4
2

Figure 3.6: Functional enrichment analysis of *O*-GlcNAcylated protein species. (**A**) Gene Ontology (GO) analysis revealed significant associations with various GO categories for biological processes (BP, green colour), cellular components (CC, orange colour) and molecular functions (MF, blue colour). GO terms are sorted by corrected p-value ($p < 0.05$), with the most significant terms listed first). (**B**) KEGG pathway enrichment identified pathways enriched with *O*-GlcNAcylated proteins (p-value < 0.05 and q-value < 0.05). The x-axis represents the ratio of enriched target proteins to the total number of proteins in each pathway. The y-axis depicts the specific pathways. Dot size indicates the number of enriched genes in each pathway. Color intensity reflects the corrected p-value, with red indicating higher significance and blue indicating lower significance.

3.2 Effects of ammonia on the *O*-GlcNAcylation of HO-1 in cultured rat astrocytes

3.2.1 Ammonia triggers the *O*-GlcNAcylation of full length and truncated HO-1 in cultured rat astrocytes

Previous studies have demonstrated that HO-1 protein is barely detectable in normal brain tissue. However, under conditions of oxidative stress, there is a significant increase in HO-1 protein levels [*411*]. This also applies to cultured rat astrocytes when incubated with NH_4Cl (5 mM, 72 h) [*212*, *519*]. To investigate whether HO-1 protein is modified by *O*-GlcNAcylation, „click-chemistry“ and affinity purification, and Western blot analysis were performed. The results showed that *O*-GlcNAcylation of the full-length HO-1 (monomer) increased by approximately 10-fold in NH_4Cl-exposed astrocytes compared to controls (Fig. 3.7A, B). Besides the full-length HO-1 monomer which has a molecular weight of approximately 32 kDa, a second anti-HO-1 IR band was detected in astrocytes incubated with NH_4Cl (5 mM, 72 h). This band has an approximate molecular weight of about 28 kDa and corresponds to truncated HO-1 which is devoid of the Linker and ER-transmembrane region (Fig. 3.7C). The *O*-GlcNAcylation of truncated HO-1 was about 3-times higher in astrocytes incubated with NH_4Cl compared to controls (Fig. 3.7A, B).

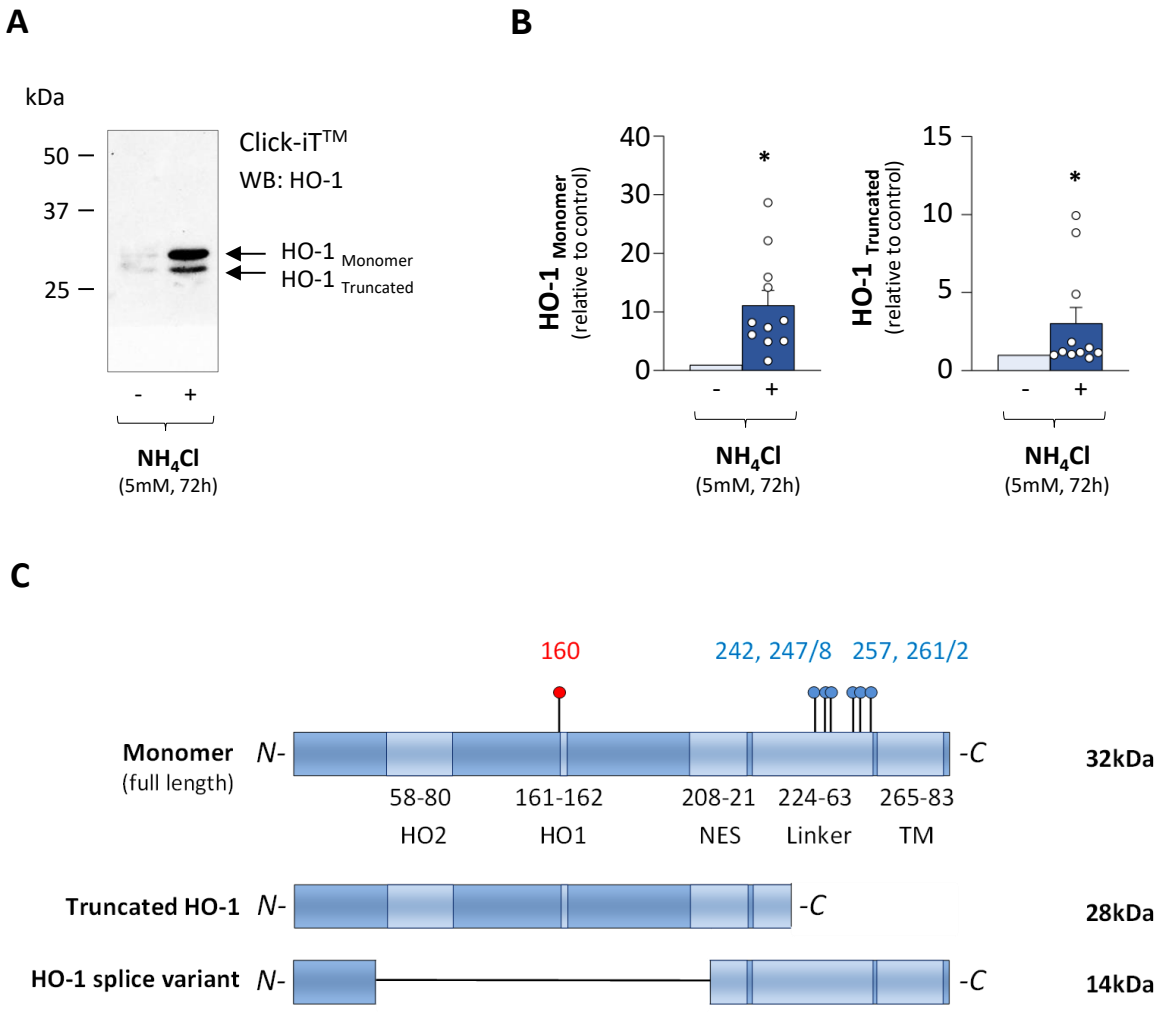

Figure 3.7: Effects of ammonia on HO-1 *O*-GlcNAcylation in cultured rat astrocytes. (**A**) Cells were cultured for 72 h in the absence (control) or presence of NH_4Cl (5 mM). *O*-GlcNAcylated proteins were labelled by Click-iT™ chemistry and affinity purified and HO-1 was detected by Western blot analysis. (**B**) Densitometric quantification of anti-HO-1 signal intensities. Anti-HO-1 IR levels in astrocytes incubated with NH_4Cl are expressed relative to untreated controls. Wilcoxon matched-pairs signed rank test was used for the statistical analysis. *: statistically significantly different compared to untreated controls. (N=11). (**C**) Potential *O*-GlcNAcylation sites as predicted by YinOYang and *O*GlcNAcPred-II bioinformatic analyses are indicated by pin points in rat HO-1 protein. HO-2/ HO-1: heme oxygenase 2 or 1 binding sites; NES: nuclear export sequence; Linker: linker region; TM: transmembrane domain.

3.2.2 Mass spectrometry analysis of *in vitro O*-GlcNAcylated purified rat HO-1

In order to identify potential *O*-GlcNAcylation sites in HO-1, we utilized YinOYang [*542*] and *O*-GlcNAcPred-II [*543*] bioinformatics tools. These platforms predicted seven *O*-GlcNAcylation sites within the HO-1 protein of rattus norvegicus (Tab. 3.5 and 3.6, Fig. 3.8A). Notably, six of these sites are nestled within the linker region unique to the full-length variant of HO-1, which is absent in its truncated counterpart. As opposed to this, serine at position 160 (Ser^{160}) is present in both HO-1 variants (Fig. 3.7C). Ser^{160} lies within a conserved LPSSGEG motif across rodents (Fig. 3.8B), and primates and resides within the HO-1 homodimerization interface (Fig. 3.8C). This suggests that *O*-GlcNAcylation of HO-1 at Ser^{160} could affect the dimerization of HO-1 which is crucial for its catalytic activity.

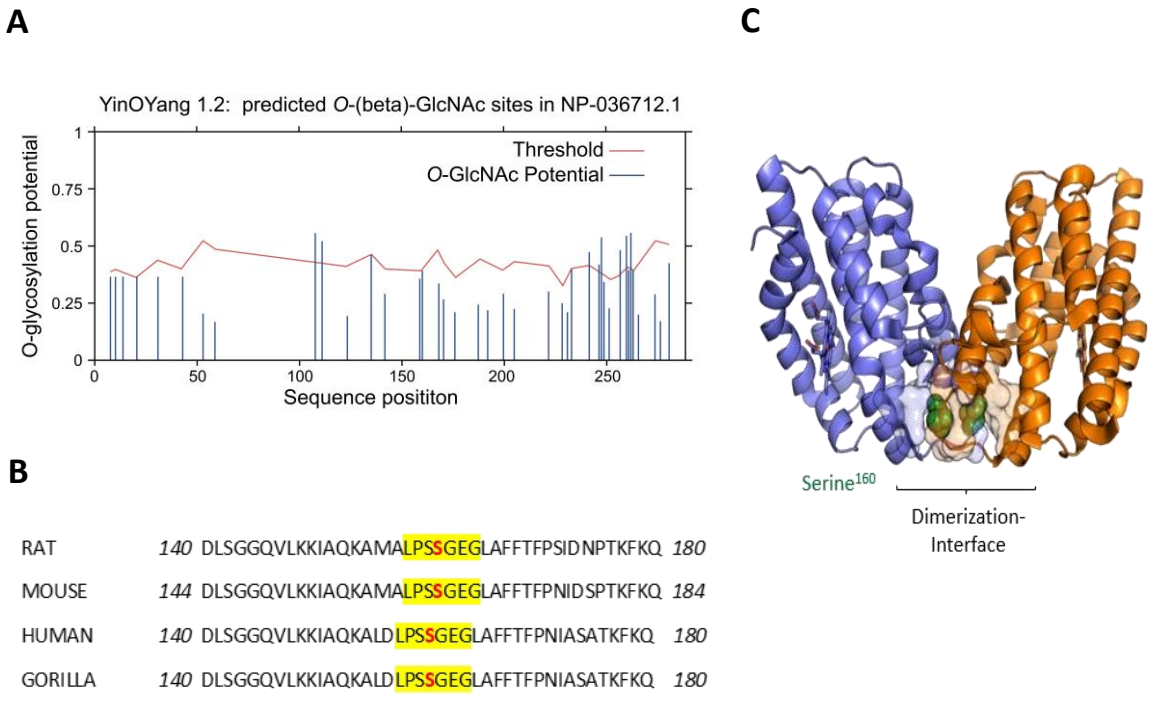

Figure 3.8: Bioinformatic prediction of HO-1 *O*-GlcNAcylation sites. (**A**) *O*-GlcNAcylation potential of serine and threonine residues of rattus norvegicus HO-1 as predicted by YinOYang (v1.2). (**B**) Amino acid sequence alignment of Ser^{160} in rat, mouse, human and gorilla HO-1. (**C**) Schematic visualization of the 3D structure of two HO-1 subunits forming a homodimer with Ser^{160} highlighted at the dimerization interface. The two HO-1 monomers are colored differently and Ser^{160} is shown as sphere-model (Provided by Dr. Michele Bonus, Institute of Pharmaceutical and Medical Chemistry, Heinrich Heine University, Düsseldorf).

Table 3.5: Prediction of *O*-GlcNAcylation sites in HO-1 protein. The prediction was performed on NP_036712.1 heme oxygenase 1 (rattus norvegicus) using *O*-GlcNAcPred-II [*543*].

No.	Window	Position	PositiveOrNegative
1	XXXXMERPQLDSMSQDLSEALKE	8	negative
2	XXMERPQLDSMSQDLSEALKEAT	10	negative
3	RPQLDSMSQDLSEALKEATKEVH	14	positive
4	SQDLSEALKEATKEVHIRAENSE	21	negative
5	ATKEVHIRAENSEFMRNFQKGQV	31	negative
6	EFMRNFQKGQVSREGFKLVMASL	43	negative
7	VSREGFKLVMASLYHIYTALEEE	53	negative
8	KLVMASLYHIYTALEEEIERNKQ	59	negative
9	YGPHWQEAIPYTPATQHYVKRLH	108	negative
10	HWQEAIPYTPATQHYVKRLHEVG	111	negative
11	HYVKRLHEVGGTHPELLVAHAYT	124	negative
12	THPELLVAHAYTRYLGDLSGGQV	135	negative
13	AHAYTRYLGDLSGGQVLKKIAQK	142	negative
14	KKIAQKAMALPSSGEGLAFFTFP	159	negative
15	KIAQKAMALPSSGEGLAFFTFPS	160	positive
14	KIAQKAMALPSSGEGLAFFTFPS	159	negative
15	KIAQKAMALPSSGEGLAFFTFPS	160	positive
16	LPSSGEGLAFFTFPSIDNPTKFK	168	negative
17	SGEGLAFFTFPSIDNPTKFKQLY	171	negative
18	AFFTFPSIDNPTKFKQLYRARMN	176	negative
19	KFKQLYRARMNTLEMTPEVKHRV	188	negative
20	LYRARMNTLEMTPEVKHRVTEEA	192	negative
21	LEMTPEVKHRVTEEAKTAFLLNI	200	negative
22	EVKHRVTEEAKTAFLLNIELFEE	205	negative
23	IELFEELQALLTEEHKDQSPSQT	222	negative
24	QALLTEEHKDQSPSQTEFLRQRP	229	negative
25	LLTEEHKDQSPSQTEFLRQRPAS	231	negative
26	TEEHKDQSPSQTEFLRQRPASLV	233	negative
27	SQTEFLRQRPASLVQDTTSAETP	242	positive
28	LRQRPASLVQDTTSAETPRGKSQ	247	positive
29	RQRPASLVQDTTSAETPRGKSQI	248	positive
30	QRPASLVQDTTSAETPRGKSQIS	249	positive
31	ASLVQDTTSAETPRGKSQISTSS	252	negative
32	DTTSAETPRGKSQISTSSSQTPL	257	positive
33	SAETPRGKSQISTSSSQTPLLRW	260	negative
34	AETPRGKSQISTSSSQTPLLRWV	261	positive
35	ETPRGKSQISTSSSQTPLLRWVL	262	positive
36	TPRGKSQISTSSSQTPLLRWVLT	263	negative
37	PRGKSQISTSSSQTPLLRWVLTL	264	positive
38	GKSQISTSSSQTPLLRWVLTLSF	266	negative
39	SSQTPLLRWVLTLSFLLATVAVG	274	negative
40	QTPLLRWVLTLSFLLATVAVGIY	276	negative
41	RWVLTLSFLLATVAVGIYAMXXX	281	positive

Table 3.6: Predicted *O*-GlcNAcylation sites in heme oxygenase-1. This table summarizes the predicted *O*-GlcNAcylation sites in heme oxygenase-1 protein (NP_036712.1) using YinOYang 1.2 software (DTU Health Tech, Lyngby, Denmark; https://services.healthtech.dtu.dk/services/YinOYang-1.2/ [*542*]).

SeqName	Residue	*O*-GlcNAc	Potential	Thresh. (1)	Thresh. (2)
NP_036712.1	108 T	++	0.5696	0.4288	0.5283
NP_036712.1	111 T	++	0.5311	0.4212	0.5181
NP_036712.1	160 S	+	0.4016	0.3962	0.4845
NP_036712.1	233 T	+	0.4087	0.4050	0.4963
NP_036712.1	242 S	+	0.4717	0.4137	0.5080
NP_036712.1	247 T	+	0.4322	0.3945	0.4822
NP_036712.1	248 T	++	0.5333	0.3720	0.4519
NP_036712.1	257 S	++	0.4712	0.3714	0.4511
NP_036712.1	260 S	++	0.5334	0.4012	0.4912
NP_036712.1	261 T	+	0.4144	0.4013	0.4914
NP_036712.1	262 S	++	0.5608	0.4015	0.4916

3.2.3 Mapping of *O*-GlcNAcylation sites in *in vitro O*-GlcNAcylated HO-1 by mass spectrometry

To identify *O*-GlcNAcylation sites in HO-1, recombinant HO-1 ($HO\text{-}1_{rec}$) was *in vitro O*-GlcNAcylated using recombinant *O*-GlcNAc transferase (OGT_{rec}) (Fig. 3.9A). As shown by Western blot analysis, anti-*O*-GlcNAc immunoreactivity of $HO\text{-}1_{rec}$ significantly increased in samples incubated with OGT_{rec} compared to those who were incubated without OGT_{rec} (Fig. 3.9B). Subsequent mass spectrometry analysis identified 32 peptides from $HO\text{-}1_{rec}$, achieving a 81% sequence coverage. Notably, OGT_{rec} treatment resulted in a mass shift indicative of N-acetylglucosamine modification within the AMALPSSGEGLAFFTFPSIDNPT peptide, mapping serine residues 159 or 160, which was absent in untreated samples (Fig. 3.9C). Importantly, the analysis could not distinguish between serine residues 159 and 160 as the modification site. Of note, a similar mass shift was not observed in any other of the fragmented HO-1 peptides. Nevertheless, the technical approach cannot rule out the existence of additional *O*-GlcNAcylation sites in HO-1, which may be the consequence of specific chemical properties and detection limits.

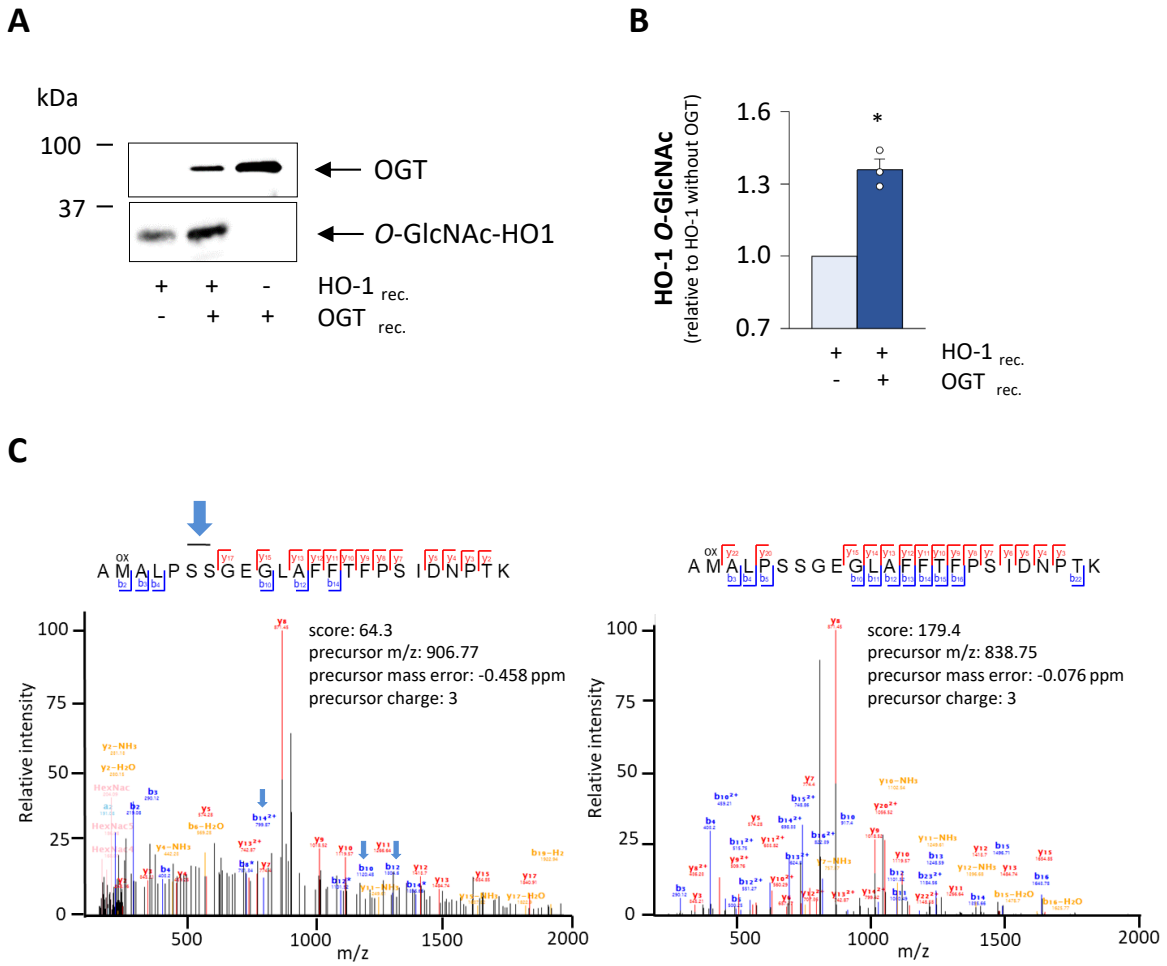

Figure 3.9*: Identification of O*-GlcNAcylation sites in *in vitro O*-GlcNAcylated rat recombinant HO-1. (**A**) HO-1_{rec} was subjected to *in vitro O*-GlcNAcylation as described above and in materials and methods. *O*-GlcNAcylation of HO-1 was detected by Western blot using anti-*O*-GlcNAc antibodies and (**B**) anti-*O*-GlcNAc IR were quantified by densitometric analysis. Intensities found in OGT_{rec}-treated samples are expressed as fold of what was found in samples incubated without OGT_{rec}. Statistical analysis: Student´s t-test. *: statistically significantly different to untreated controls. (N=3). (**C**) Identification of *O*-GlcNAcylation sites in *in vitro O*-GlcNAcylated HO-1_{rec} by mass spectrometry. Left: *O*-linked N-acetylglucosamine modification is indicated by a mass shift (blue arrows) at serines 159 or 160 and also by diagnostic fragment ions m/z 204.09, 186.08, 168.07 (marked in pink). Right: the unmodified peptide variant was found in OGT_{rec}-treated and untreated samples. “Ox”: oxidized methionine (frequently occurring during sample preparation).

3.2.4 Effects of NH_4Cl, hemin and GlcN on protein levels of HO-1 variants in cultured rat astrocytes

Previous studies in cultured rat astrocytes have exclusively reported effects of NH_4Cl on protein levels of full length HO-1 (32 kDa) [*4, 519*]. In the present study, we extended these investigations by analyzing effects of NH_4Cl on protein levels of full length and truncated HO-1. For this, we performed Western blot analyses in astrocytes incubated with NH_4Cl (5 mM) for 24-72 h and compared the effects to those of established HO-1 inducers, hemin (5 µM) [*430*] and GlcN (8 mM) [*4*]. Levels of the previously investigated 32 kDa HO-1 monomer were greatly increased at all time points and among all treatments analysed. Besides, two additional anti-HO-1 IR bands of lower molecular weight were detected (Fig. 3.10A). The second band had a molecular weight of approximately 20 kDa and may correspond to a so far unknown truncated variant. In astrocytes incubated with NH_4Cl or GlcN, the 28 kDa truncated variant 1 was only weakly detected and variant 2 was barely detectable. However, both variants were clearly detected in astrocytes incubated with hemin at all time points analyzed (Fig. 3.10B). It is important to note here, that the detection of truncated HO-1 variants was strongly dependent on the signal to noise ratio and the abundance of HO-1 protein in the respective samples (Fig. 3.10A). This especially accounted for truncated variant 2, whose level were the lowest of all three detected HO-1 variants.

To ascertain whether the upregulation of these truncated HO-1 variants is paralleled by changes in HO-1 transcription, HO-1 mRNA was quantified by qPCR. As shown in Fig. 3.11, HO-1 mRNA significantly increased at all time points analyzed in astrocytes incubated with NH_4Cl (5 mM), hemin (5 µM) or GlcN (8 mM). However, these changes were similar in astrocytes incubated with NH_4Cl and hemin and even tended to be higher in astrocytes incubated with GlcN at 72 h and 96 h. The results indicate that post-transcriptional mechanisms are responsible for the observed differences in HO-1 monomer and both truncated HO-1 protein level in astrocytes incubated with NH_4Cl, hemin and GlcN.

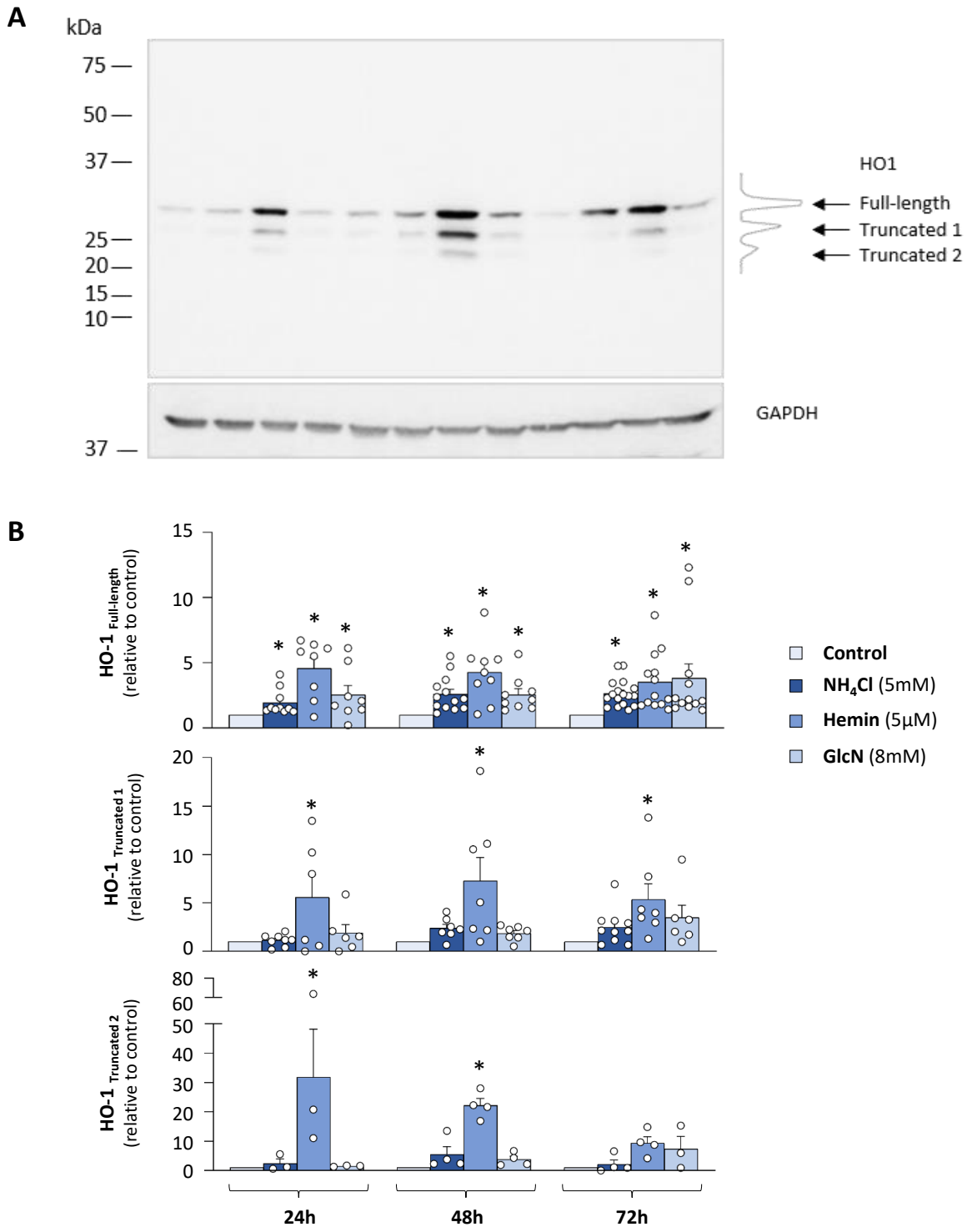

Figure 3.10: Effects of NH_4Cl, hemin and GlcN on HO-1 protein levels in cultured rat astrocytes. Astrocytes were cultured for 24, 48 or 72 h in absence (control) or presence of NH_4Cl (5 mM), hemin (5 µM) or GlcN (8 mM). (**A**) Western blot analysis was performed using antibodies against HO-1 and GAPDH. The right panel shows a representative chemiluminogram of HO-1 protein bands in hemin-treated astrocytes (48 h) with full-length and truncated variants 1 and 2 indicated. (**B**) Anti-HO-1 immunoreactivity (IR) was quantified by densitometry and normalized to GAPDH levels. Data are presented as relative HO-1 protein levels in astrocytes treated with NH_4Cl, hemin or GlcN compared to untreated controls (N=3-8). Statistical analysis was performed using the appropriate test (Kruskal-Wallis or Friedman). *: Significantly different compared to untreated controls.

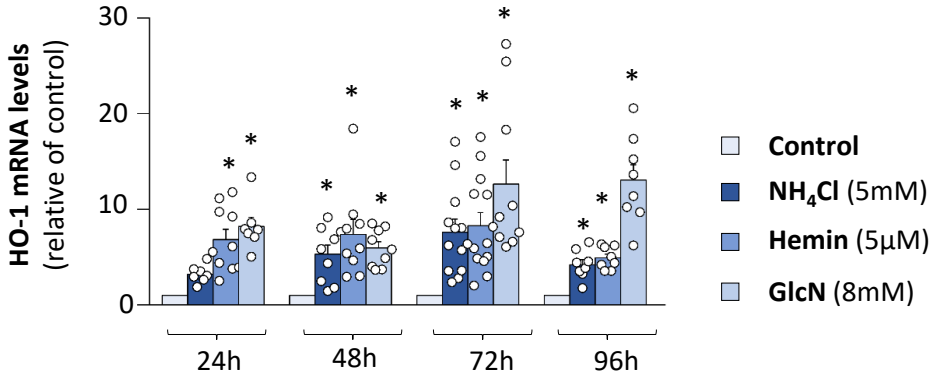

Figure 3.11: Effects of NH_4Cl, hemin and GlcN on HO-1 mRNA in cultured rat astrocytes. Culture rat astrocytes were incubated for 24, 48, 72 or 96 h with NH_4Cl (5 mM), hemin (5 µM) or GlcN (8 mM). At the end of the experiment, RNA was isolated and used to assess HO-1 mRNA levels by qPCR. mRNA levels of HO-1 were normalized to those of the housekeeping gene HRPT1 and are expressed relative to the respective controls. Statistical analyses were performed using ANOVA, Friedman or Kruskal-Wallis each followed by Dunn´s multiple comparison test. *: statistically significantly different to untreated controls ($p<0.05$). N=7-13.

Protein levels of the full-length HO-1 and of both truncated HO-1 variants strongly correlated among each other when all treatments and time points were included in the analysis (Fig. 3.12A). Here correlation coefficients ranged between r=0.68 and 0.85 with p-values below 10^-4 to 10^-10 (Fig. 3.12A). These results suggest, that compared to controls the treatments generally increased both full-length and truncated HO-1 proteins proportionally. This was also examined individually for each treatment by comparing the relative proportions of full-length and truncated HO-1 variants in relation to total HO-1. Here, the proportions of full-length HO-1 and both truncated variants in relation to total HO-1 were similar in astrocytes incubated with NH_4Cl (5 mM) or GlcN (8 mM) for 24, 48 or 72 h. However, in astrocytes incubated with hemin, the proportion of full-length HO-1 decreased, while those of both truncated variants increased at 24 and 48 h (Fig. 3.12B). This suggests that hemin induces a disproportionate increase in truncated HO-1 compared to total HO-1. Nevertheless, the precise mechanisms underlying this effect remain unknown and require further investigation.

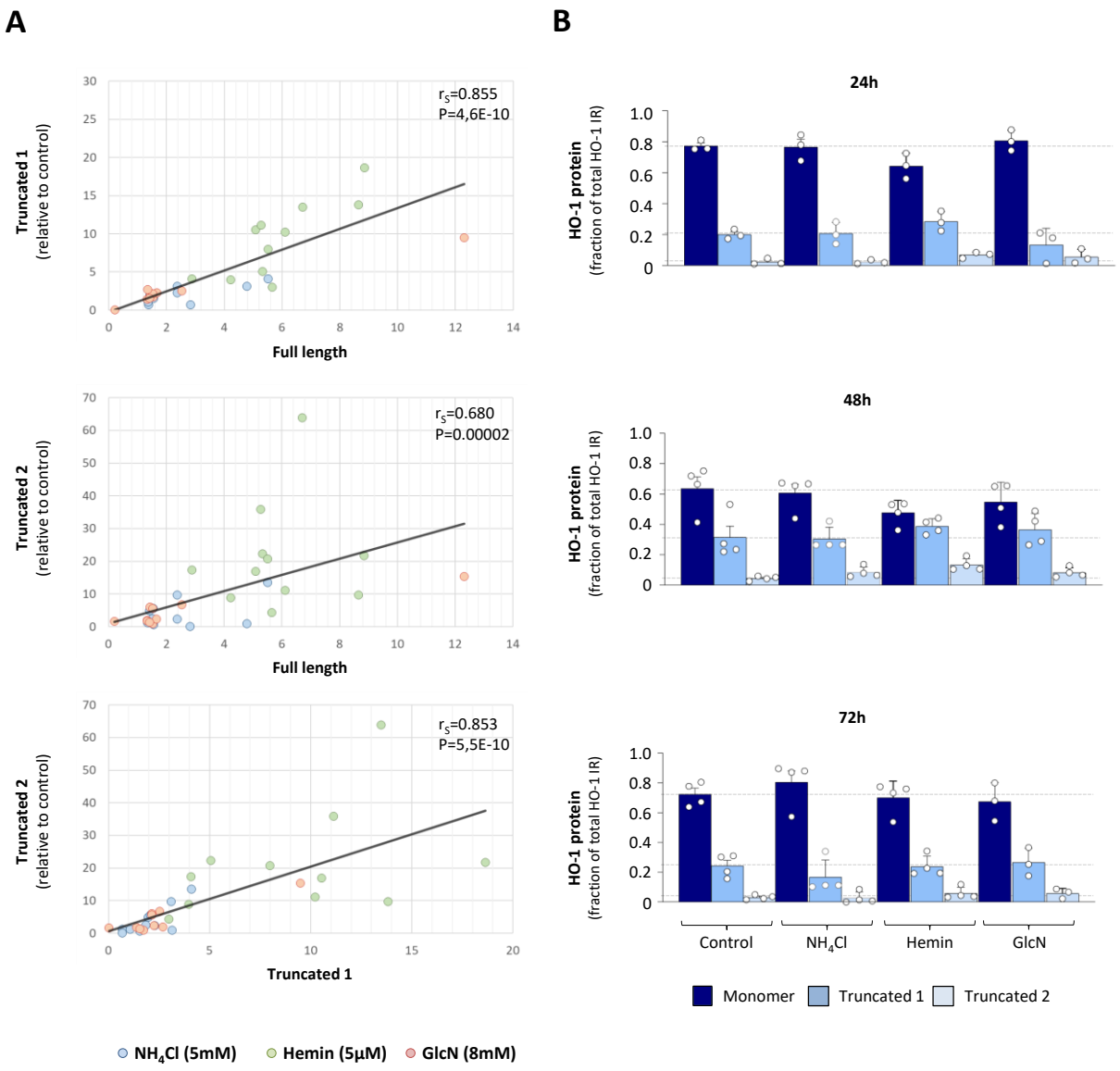

Figure 3.12: Correlation and distribution analyses of full-length and truncated HO-1 variants in astrocytes incubated with NH_4Cl, hemin and GlcN. (**A**) Protein levels of full-length and truncated HO-1 variants in NH_4Cl, hemin and GlcN exposed astrocytes (24, 48 and 72 h) were analyzed using Spearman's rank correlation coefficient (rs). The corresponding p-value (P) indicates statistical significance (two-tailed test). Paired values (in total N=31 and per group N=3-4) are shown. (**B**) Distribution of full-length and truncated variants of HO-1 protein in untreated astrocytes (control) or astrocytes incubated with NH_4Cl (5 mM), hemin (5 µM) or GlcN (8 mM). The bar graphs illustrate the arithmetic mean values and the standard error of the mean (SEM), with each individual data point represented by a dot.

3.2.5 Effects of NH_4Cl, hemin and GlcN on the formation of HO-1 homo- and heteromers

HO-1 can form higher-order complexes either by homomerisation or through the interaction with other protein species (heteromerisation) [*506*]. To assess this in the astrocytes, we crosslinked interacting proteins in the astrocytes using the DTT-cleavable linker dithiobis(succinimidyl propionate) (DSP) [*428*]. When such samples were analysed by Western blot in absence of DTT, multiple anti-HO-1 IR bands were detected. According to their respective molecular weights and references from the literature [*506*], the anti-HO-1 IRs are suggested to reflect truncated (V) (28 kDa), monomeric (IV) (32 kDa), dimeric (III) (64 kDa), trimeric (II) (96 kDa), and oligomeric (I) (>250 kDa) HO-1 (Fig. 3.13A). The level of these homomers most strongly increased in astrocytes incubated with NH_4Cl (5 mM) and to lesser extent also in those incubated with hemin (5 µM) and GlcN (8 mM) (Fig. 3.13B). Interestingly, the relative increase of the individual HO-1 IR signals was time dependent. While higher order HO-1 homomers (bands I-III) showed the highest increase already at 24 h, those of the band IV -V were highest at 48 h and 72 h (Fig. 3.13B). Unexpectedly, in these DSP-treated samples also the levels of truncated HO-1 (band V) were significantly elevated in astrocytes incubated with NH_4Cl (Fig. 3.13A). This is at variance with the Western blot data of protein samples taken where no cross-linking was performed described above (Fig. 3.10A). The underlying reason is currently unclear and requires further investigation. Furthermore, in addition to the most prominent observed HO-1 IR bands, numerous further bands exhibiting a comparably lower signal intensity were observed, with molecular weights spanning the whole molecular range between 25-250 kDa (Fig. 3.13A). It is unlikely that these signals correspond to HO-1 homomers, given that their molecular weights are not multiples of the monomer. These signals most likely reflect HO-1 monomers or homomers which interact with other protein species and therefore are considered heteromeric protein-HO-1 complexes. Further investigations are required to identify potential interacting proteins.

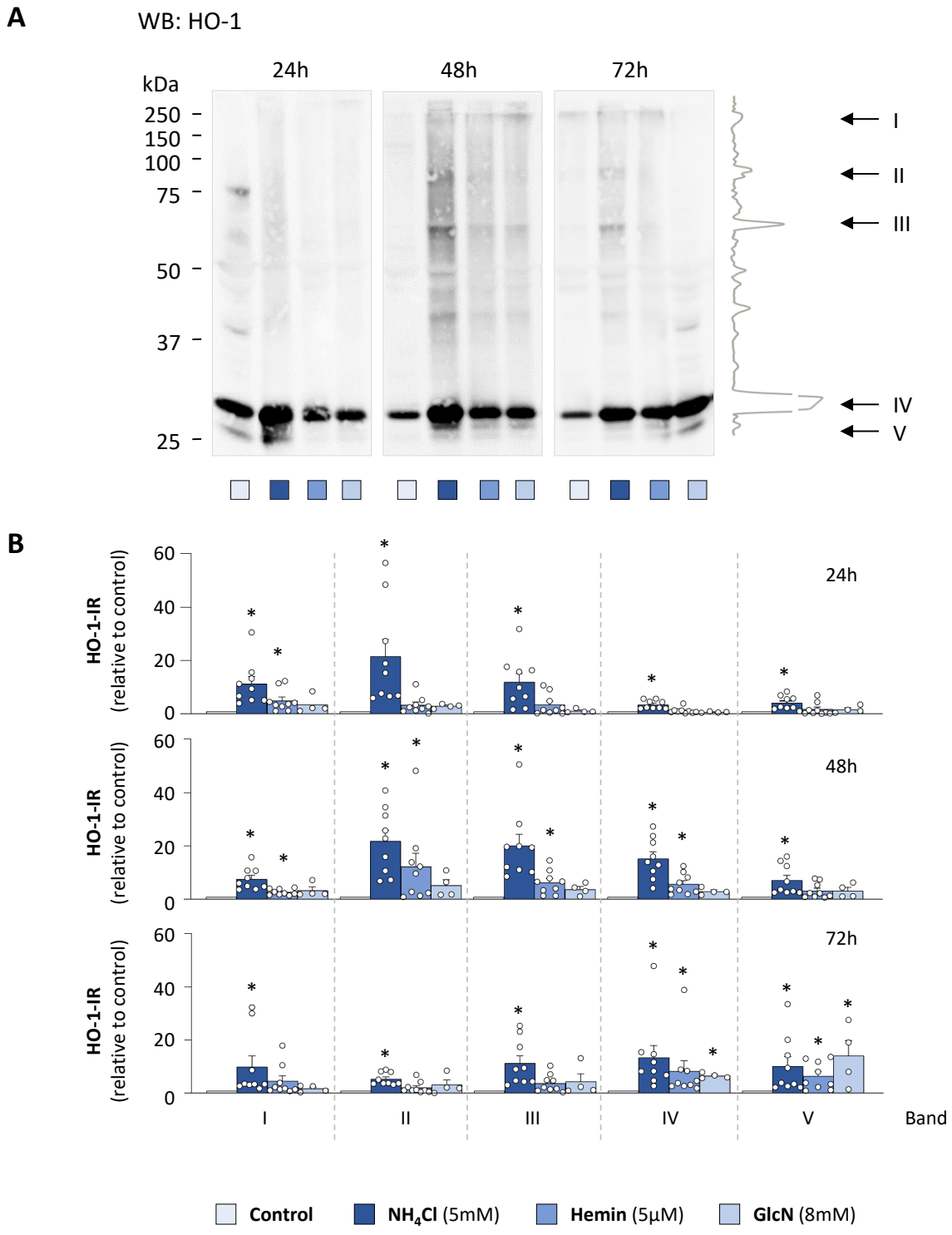

Figure 3.13: Analysis of HO-1 protein-protein interactions in astrocytes incubated with NH_4Cl, hemin and GlcN. (**A**) Time-dependent analysis of HO-1 protein interactions: astrocytes were incubated with NH_4Cl (5 mM), hemin (5 µM) or GlcN (8 mM) for 24, 48 or 72 h or left untreated for the indicated time (control). At the end of the experimental treatment, proteins were cross-linked with DSP and analysed by Western blot. Distinct bands corresponding to the molecular weights of truncated HO-1 (V, 28 kDa) or HO-1 monomer (IV, 32 kDa), dimer (III, 64 kDa), trimers (II, 96 kDa) and oligomers (I, >250 kDa) are indicated by arrowheads. (**B**) Densitometric analysis quantified prominent HO-1 immunoreactive (IR) bands. Statistical analysis was performed using Kruskal-Wallis and Dunn's multiple comparison test (*: $p < 0.05$ compared to untreated controls, N=4-9).

To explore potential regulation of HO-1 protein-protein interactions by NH_4Cl, hemin and GlcN, we performed correlation analysis. Here, the protein levels of most anti-HO-1 IR bands did not correlate with each other (Fig. 3.14). This was only observed for HO-1 IR bands III and I in astrocytes incubated with NH_4Cl (24 h) and hemin at (24 and 48 h) and for HO-1 IR bands I and III in astrocytes incubated with hemin for 72 h (Fig. 3.14). Importantly, levels of HO-1 monomer (band IV, Fig. 3.13A) did not correlate with those of any other HO-1 IR band. These findings suggest that HO-1 homomer formation is independent from HO-1 transcription and translation. However, the underlying mechanisms remain currently unclear and require further investigation.

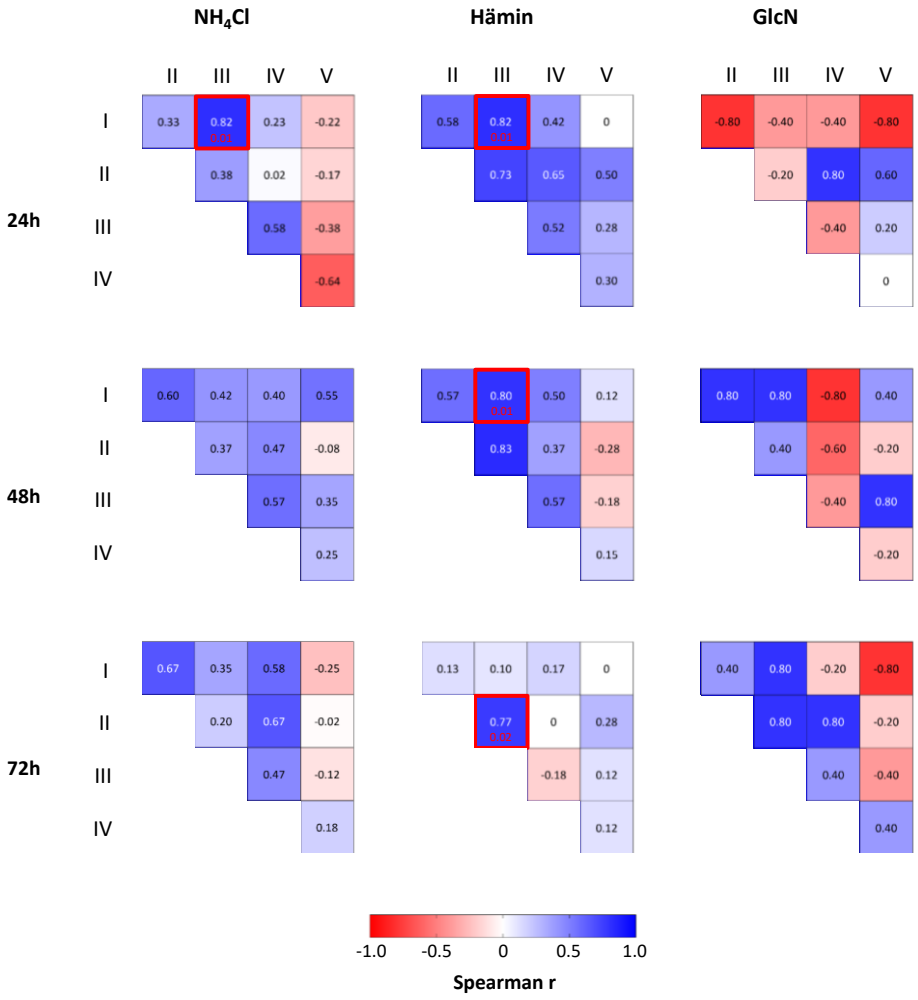

Figure 3.14: Correlation analysis of HO-1 protein-protein interactions in astrocytes incubated with NH_4Cl, hemin and GlcN. Astrocytes were cultured in absence (control) or presence of NH_4Cl (5 mM), hemin (5 µM) or GlcN (8 mM) for 24, 48 or 72 h. At the end of the experimental treatment, cells were cross-linked with DSP (refer to Fig. 3.13A for band identification) and analyzed by Western blot for HO-1. Spearman's rank correlation coefficients were calculated for the protein levels of the different HO-1 IR bands across treatments and time points. The heatmap depicts these correlation coefficients, with significant correlations (p-value < 0.05) highlighted in red. (N=4-9).

To verify that the anti-HO-1 IR bands represent protein-protein interactions, we resolved DSP-cross-linked proteins by dithiothreitol (DTT). This was exemplarily carried out in samples incubated with NH_4Cl, where HO-1 homomers were most pronounced. Incubation of the protein samples with DTT resulted in the complete abolition of signals corresponding to higher- molecular- weight HO-1 IR bands, while the signal corresponding to the monomer and truncated HO-1 remained unaltered (Fig. 3.15A). These findings suggest that NH_4Cl, and to a lesser extent hemin and GlcN, trigger the formation of HO-1 protein-protein complexes in cultured rat astrocytes.

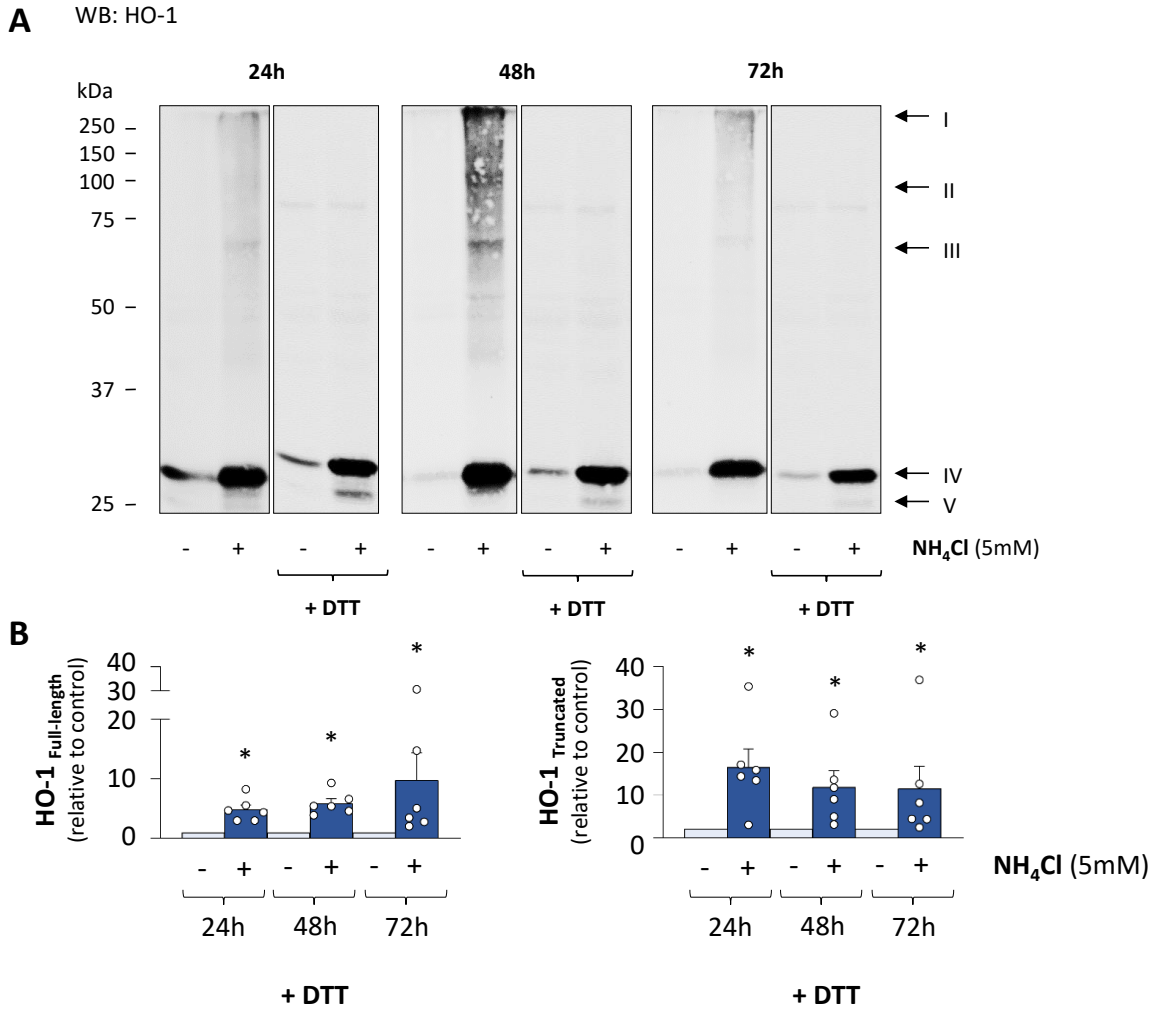

Figure 3.15: Reversibility of DSP-induced cross-linking of HO-1 protein-protein interactions. Astrocytes were cultured without (control) or with NH_4Cl (5 mM) for 24, 48 or 72 h. At the end of the incubation, interacting proteins were cross-linked with DSP (refer to Methods for details). (**A**) Protein samples were prepared for Western blot with (+) or without (-) 200 mM DTT and analysed by Western blot using anti-HO-1 reactive antibodies. Anti-HO-1 immunoreactive (IR) bands corresponding to truncated HO-1 (V, 28 kDa), HO-1 full-length/ monomer (IV, 32 kDa), and higher molecular weight HO-1 complexes (I-III) are indicated by roman letters. (**B**) Densitometry was used to quantify the full-length/ monomer (IV) and truncated (V) HO-1 IRs in DTT-treated samples. Statistical analysis was performed using the Wilcoxon rank-sum test (*: $p<0.05$ compared to control, N=6).

To further examine whether incubating the astrocytes with NH_4Cl triggers the formation of high molecular weight HO-1 complexes, confocal laser-scanning microscopy (CLSM) was performed. The CLSM immunoreactive spots were categorised based on their respective pixel sizes in the x, y and z dimensions which is considered a voxel (Fig. 3.16A, Fig.3.16B). Incubating the astrocytes with NH_4Cl (5 mM, 72 h) significantly increased the total number of HO-1 IR voxels (Fig. 3.16B). Importantly, the cumulative frequency plot of the anti-HO-1 IR voxels revealed that smaller voxels contribute relatively less to overall voxels in NH_4Cl-exposed astrocytes. This suggests that NH_4Cl promotes the formation of larger HO-1 complexes.

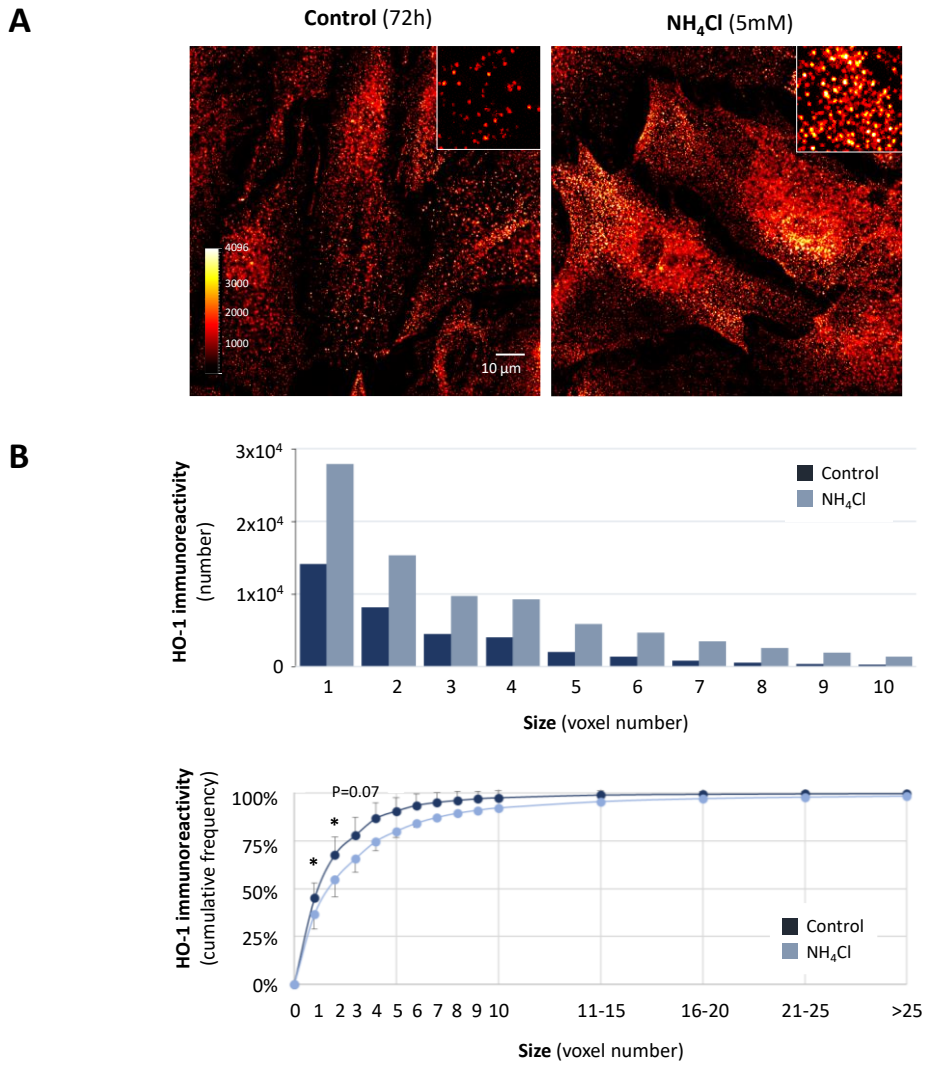

Figure 3.16: Distribution of HO-1 IR in cultured rat astrocytes. (**A**) Astrocytes were incubated with NH_4Cl (5 mM) or were left untreated for 72 h, fixed and HO-1 was analyzed by immunofluorescence and confocal laserscanning microscopy. Anti-HO-1 IR signal intensities are false color coded. The inset highlights an electronically magnified region. (**B**) Quantification of HO-1 voxel size distribution: The graph above illustrates the number of voxels that are immunoreactive to HO-1 across various size ranges. The graph below shows the cumulative frequency of HO-1 immunoreactive voxels in relation to their size.

3.2.6 Effects of protein *O*-GlcNAcylation inhibition on HO-1 protein-protein complex formation

To investigate the role of *O*-GlcNAcylation in HO-1 complex formation, we used knockdown strategies targeting proteins critical for protein *O*-GlcNAcylation, such as OGT (Fig. 3.17A) and GFAT1/2 (Fig. 3.17E) [*4*] or inhibited OGT using alloxan (Fig. 3.17I) [*544*]. Furthermore, in order to enhance the separation of higher-molecular-weight HO-1 complexes, the 4% SDS-PAGE gel was extended in length (Fig. 3.17C, G). The results of these analyses indicated that the levels of the HO-1 homomers were elevated by NH_4Cl in AllStars siRNA control-treated astrocytes (Fig. 3.17C, G). siRNA-mediated knockdown of GFAT1/2 or OGT (Fig. 3.17A, B, E, F) significantly reduced levels of higher-molecular-weight HO-1 bands (Fig. 3.17 C, D, G, H). Consistent with previous reports [*4*], knockdown of OGT or GFAT1/2 also decreased full-length HO-1 protein levels (Fig. 3.17C, D, G, H). A similar effect was observed in astrocytes incubated with the OGT inhibitor alloxan (Fig. 3.17I, J). These findings suggest that protein *O*-GlcNAcylation contributes to the formation of HO-1 homo- and heteromers in astrocytes incubated with NH_4Cl.

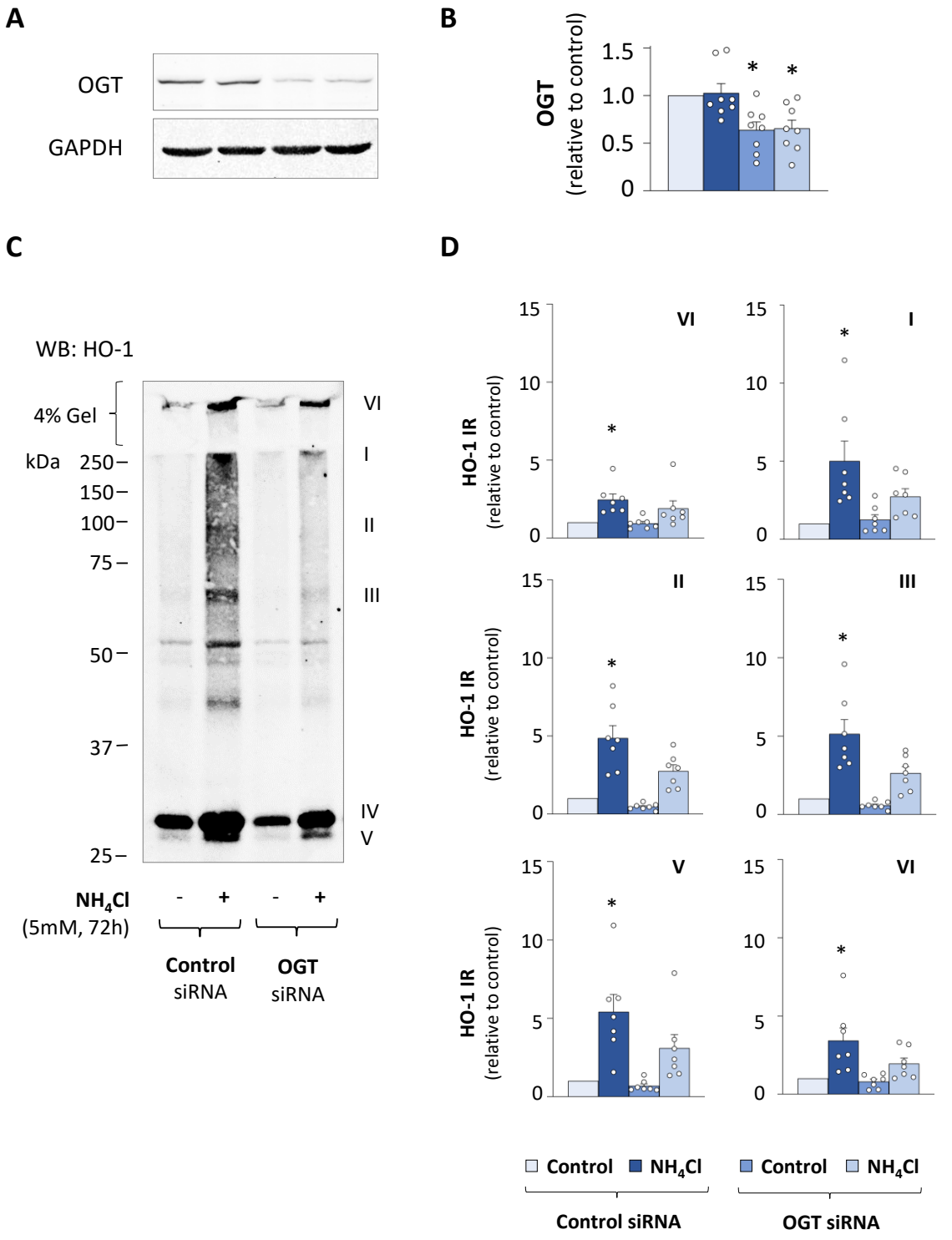
A
OGT
GAPDH
B
OGT
(relative to control)
1.5
1.0
0.5
0
*
*
C
WB: HO-1
4% Gel
kDa
250
150
100
75
50
37
25
VI
I
II
III
IV
V
NH4Cl
(5mM, 72h)
-
+
-
+
Control
siRNA
OGT
siRNA
D
HO-1 IR
(relative to control)
15
10
5
0
VI
I
II
III
V
VI
*
Control
NH4Cl
Control siRNA
OGT siRNA

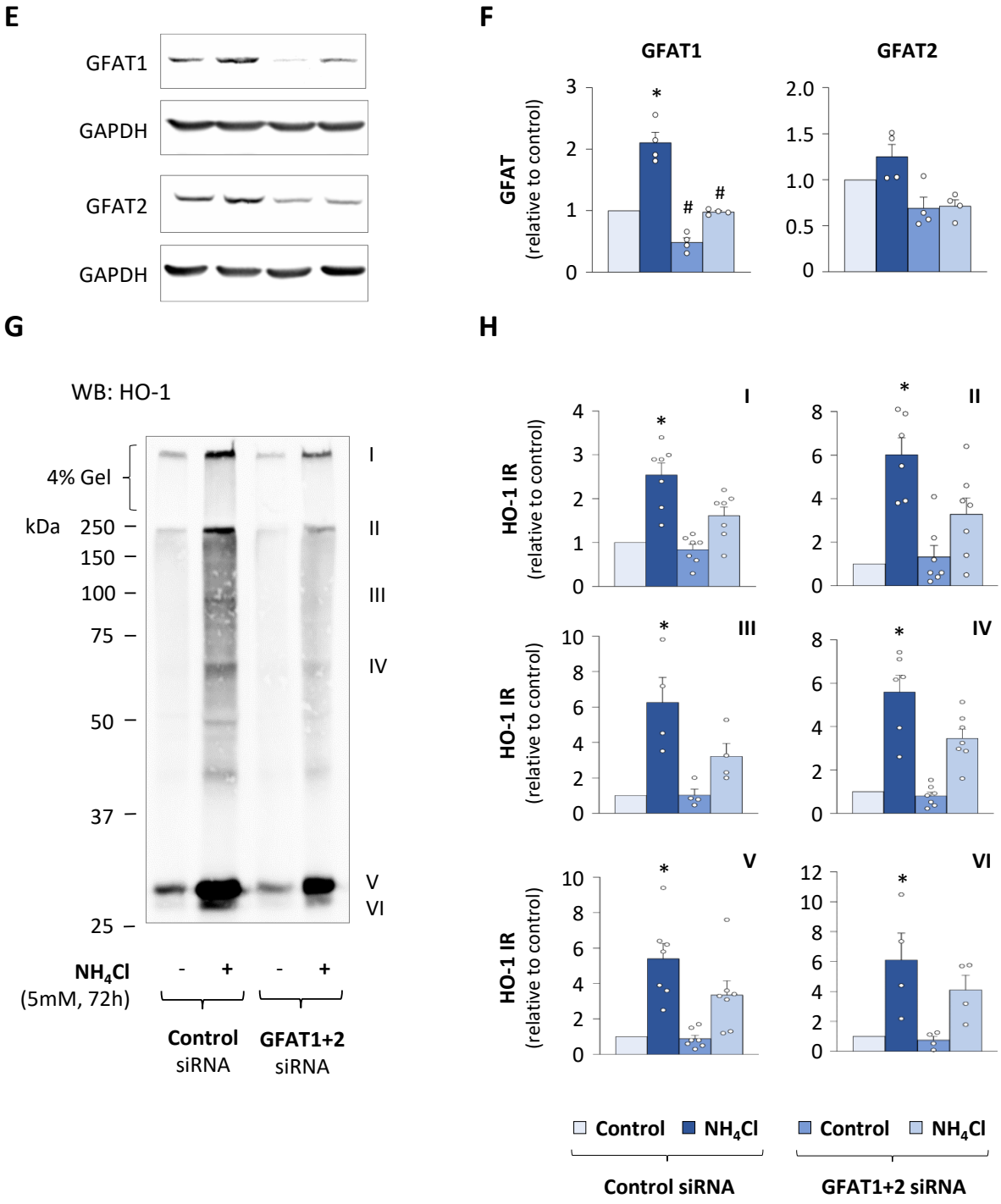
E
GFAT1
GAPDH
GFAT2
GAPDH
F
GFAT1
GFAT2
GFAT (relative to control)
G
WB: HO-1
4% Gel
kDa
250
150
100
75
50
37
25
I
II
III
IV
V
VI
NH4Cl (5mM, 72h)
- + - +
Control siRNA
GFAT1+2 siRNA
H
HO-1 IR (relative to control)
Control
NH4Cl
Control siRNA
GFAT1+2 siRNA

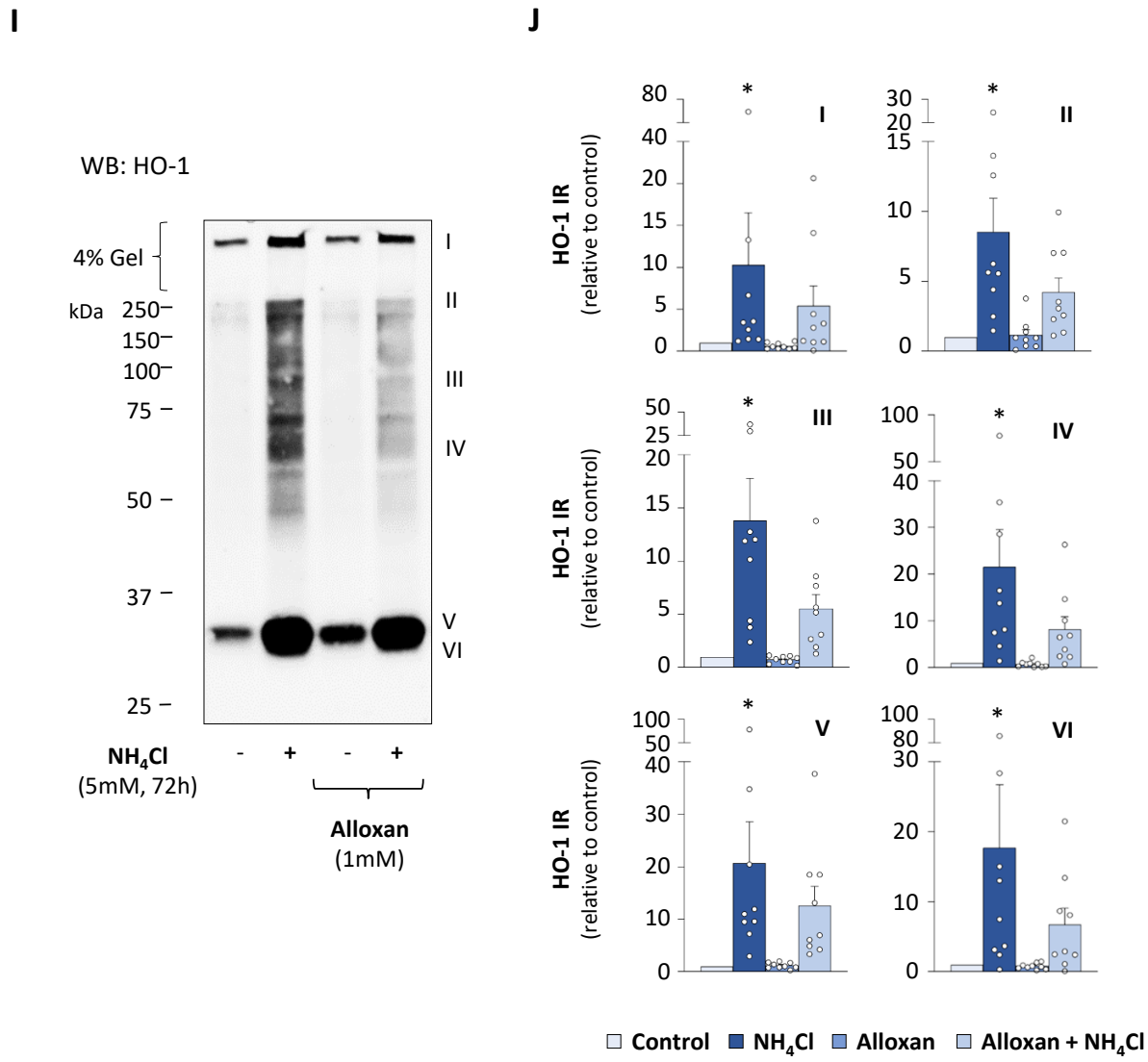

Figure 3.17: Effects of inhibition of protein *O*-GlcNAcylation on HO-1 protein-protein interactions in cultured rat astrocytes. (**A**-**H**) Astrocytes were pre-treated with control siRNA, or siRNA targeting OGT or GFAT1+2 for 24 h before cells were incubated with or without NH_4Cl (5 mM) for another 72 h. OGT (**A**, **B**) and GFAT1/2 (**E**, **F**) proteins were analysed by Western blot and quantified by densitometry. GAPDH was used for the normalization of OGT and GFAT1/2 protein levels. (**C**) Analyses of HO-1 protein by Western blot in astrocytes treated with DSP to cross-link interacting proteins (refer to methods). Prominent anti-HO-1 IR bands indicated by roman letters and were quantified by densitometric analysis (**C**, **D**, **G**, **H**, **I**, **J**). Astrocytes were pre-treated with the OGT inhibitor alloxan (1 mM, 30 min) before cells were further incubated with or without NH_4Cl (5 mM) for another 72 h. Statistical analysis was performed using ANOVA and Friedman multiple comparison test (**B**, **D**, **F**, **H**, **J**). *: statistically significantly different to untreated controls. (B: N=8; D/H: N=7; F: N=4; J: N=9).

3.2.7 Interaction of HO-1 and OGT *in vitro*

In order to investigate whether HO-1 homomers also form *in vitro*, purified recombinant HO-1 and OGT proteins were incubated in UDP-GlcNAc containing reaction buffer. At the end of the incubation, proteins in close proximity to each other were covalently cross-linked using DSP. Aliquots from each sample were taken up in sample buffer without DTT and subjected to separate Western blot analyses of HO-1 and OGT. Here, higher and lower order protein complexes were separated by combining gels of two different PAA concentrations (4% followed by 10%). The analysis of HO-1 showed a complex pattern of HO-1 IR bands with molecular weights ranging between 25 to above 250 kDa (Fig. 3.18A). In absence of OGT, two major bands were detected between ~25-37 kDa (band VI) and 50-75 kDa (band V), corresponding to a molecular weight potentially indicative of HO-1 monomer and dimer, respectively (Fig. 3.18A). Additional HO-1 IR bands were observed between 75-250 kDa with band III and IV showing the strongest intensities (Fig. 3.18A). In HO-1 and OGT co-incubated samples, two additional bands (I and II) became visible with a molecular weight far above 250 kDa within the 4% PAA gel. At the same, the intensities of bands III and IV were reduced (Fig. 3.18A, C). Importantly, heat-inactivation (65°C, 5 min) of OGT prior to incubation with HO-1 inhibited both, the increase in the HO-1 IR bands I and II and partly the decrease in bands III and IV (Fig. 3.18A, C). In absence of HO-1 only a single OGT IR band was detected far above 250 kDa within the 4% PAA gel. When OGT was co-incubated with HO-1 multiple anti-OGT reactive bands became visible. Interestingly, the molecular weights of these bands (Fig. 3.18B) partially overlapped with those found in the HO-1 Western blot analyses (Fig. 3.18A).

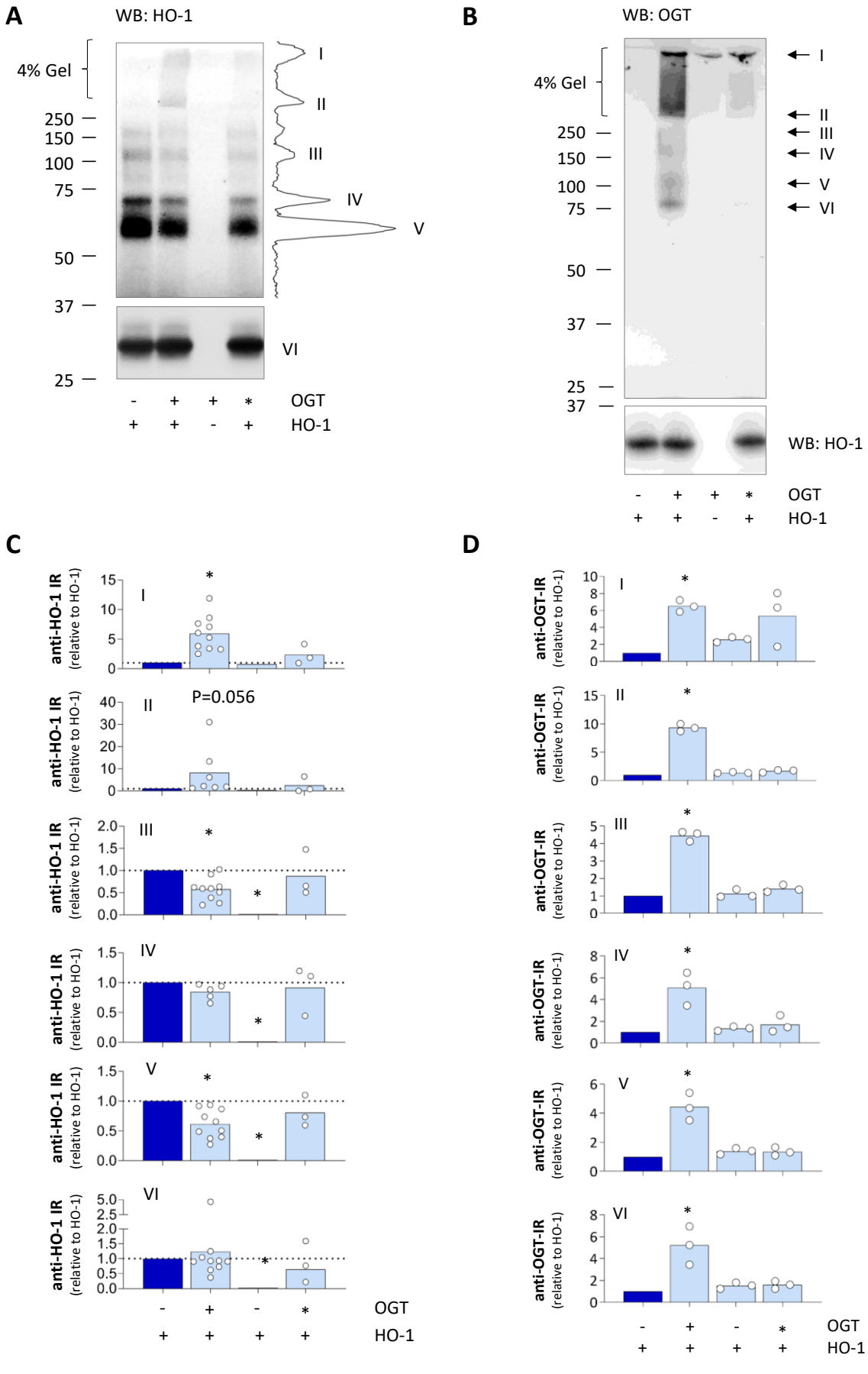
A
WB: HO-1
4% Gel
250
150
100
75
50
37
25
I
II
III
IV
V
VI
- + + *
+ + - +
OGT
HO-1
B
WB: OGT
4% Gel
250
150
100
75
50
37
25
37
I
II
III
IV
V
VI
WB: HO-1
- + + *
+ + - +
OGT
HO-1
C
anti-HO-1 IR
(relative to HO-1)
I
II
P=0.056
III
IV
V
VI
- + - *
+ + + +
OGT
HO-1
D
anti-OGT-IR
(relative to HO-1)
I
II
III
IV
V
VI
- + - *
+ + + +
OGT
HO-1

Figure 3.18: Interaction of OGT and HO-1 *in vitro*. Recombinant rat HO-1 was incubated without OGT (control), with OGT, or with heat-inactivated OGT (*). Samples were then cross-linked, incubated with DSP and analysed by Western blot for HO-1 (**A**) or OGT (**B**) Prominent bands are indicated by roman letters. (**C**, **D**) Densitometric quantification of prominent anti-HO-1 or OGT immunoreactive bands. Statistical analysis was performed by Kruskal-Wallis and Dunn's multiple comparison test. *: statistically significant different compared to untreated controls ($p<0.05$). n.s.: not statistically significant different. (N=3-10).

Here, a prominent anti-OGT immunoreactive band was detected at 75 kDa (band VI). This molecular weight corresponds well to the expected molecular weight of the recombinant OGT protein which was used in the experiments (Fig. 3.18B). Up to a molecular weight of 250 kDa three additional bands (III-V) were detected (Fig. 3.18B). Two high molecular weight OGT IR were detected above 250 kDa, and a wide smear of inseparable OGT IR was present between them. Similar to HO-1, heat-inactivation (65°C, 5 min) of OGT prior to incubation with HO-1 inhibited the changes described before (Fig. 3.18B). In these samples, the OGT immunoreactivity resembled that of samples of OGT incubated in the absence of HO-1. Interestingly, the intensity of the OGT IR band I was lower in absence of HO-1 (Fig. 3.18C, D), suggesting that OGT may be stabilized by HO-1.

For further Western blot analyses, aliquots of the same samples were prepared in running buffer containing DTT to resolve the DSP-induced cross-linking of proteins. One major and two minor anti-HO-1 immunoreactive bands with slightly different molecular weights were detected in the 25-37 kDa molecular weight range (Fig. 3.19). The reason for the slight difference in the molecular weights of the two minor anti-HO-1 immunoreactive bands is currently unknown. Moreover, two distinct anti-OGT immunoreactive bands were detected, both of which had lower intensities in samples lacking HO-1 (Fig. 3.19). It is currently unclear, whether the band with lower molecular weight is a fragment of the one with higher molecular weight (Fig. 3.19).

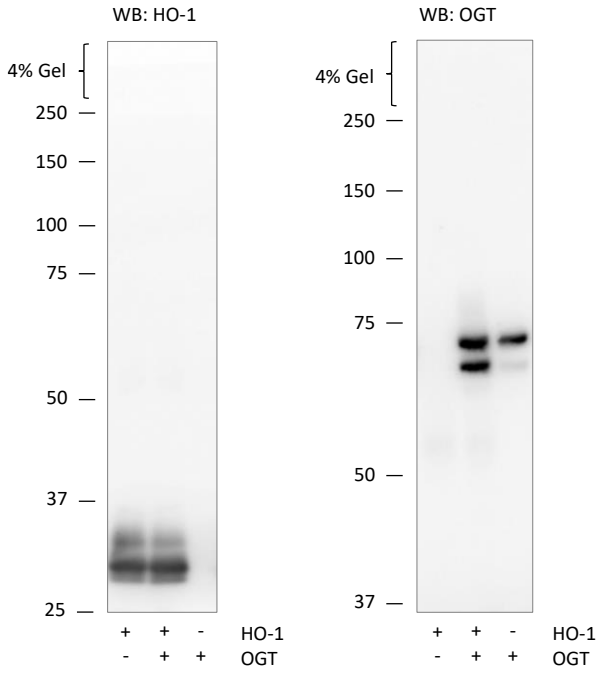

Figure 3.19: Resolution of DSP-induced cross-linking of recombinant HO-1 and OGT. Purified recombinant HO-1, HO-1 co-incubated with OGT or OGT alone were subjected to *in vitro O*-GlcNAcylation and DSP cross-linking. Samples were then resolved in protein loading buffer containing 200 mM DTT on a 7.5% polyacrylamide gel (14 cm running front) and analyzed by anti-HO-1 and anti-OGT Western blots, respectively.

These analyses suggest, that HO-1 interacts with OGT *in vitro*. The molecular weights of the anti-HO-1 and anti-OGT immunoreactive bands are similar, indicating that both proteins form the higher molecular weight complex. Unfortunately, the composition of these higher molecular weight complexes is currently unknown. Consequently, the results of these experiments do not permit a clear prediction of whether the interaction of HO-1 and OGT triggers the formation of HO-1 homers. It is noteworthy that OGT formed high molecular weight complexes in the absence of HO-1. This finding is consistent with studies, where it was demonstrated that in rat liver the purified OGT had a molecular weight of more than 340 kDa [*545*]. This molecular weight resulted from heteromeric OGT complexes composed of two alpha and one beta subunits.

3.3 Intracellular distribution of HO-1 in cultured rat astrocytes incubated with NH_4Cl, hemin or GlcN

Recent studies suggested that truncation liberates HO-1 from the ER membrane and thereby triggers translocation to other cellular compartments such as mitochondria [*546*, *547*] or the nucleus [*430*, *492*]. Therefore, effects of HO-1 induction by NH_4Cl, hemin or GlcN on intracellular localization of HO-1 were investigated. Immunofluorescence analyses and fluorescence microscopy showed that the treatments did not uniformly increase the protein levels of HO-1 in all astrocytes (Fig. 3.20A, B). This suggests these agents may differentially affect the distribution of HO-1 subpopulations. Irrespective of the experimental condition, nuclear HO-1 immunoreactivity was weak compared to the cytosol. When the astrocytes were incubated with NH_4Cl, hemin or GlcN, nuclear HO-1 immunoreactivity increased in a time-dependent way (Fig. 3.20A, B). Of note, this immunofluorescence analysis cannot discriminate between full-length (32 kDa) and truncated (28 kDa) HO-1.

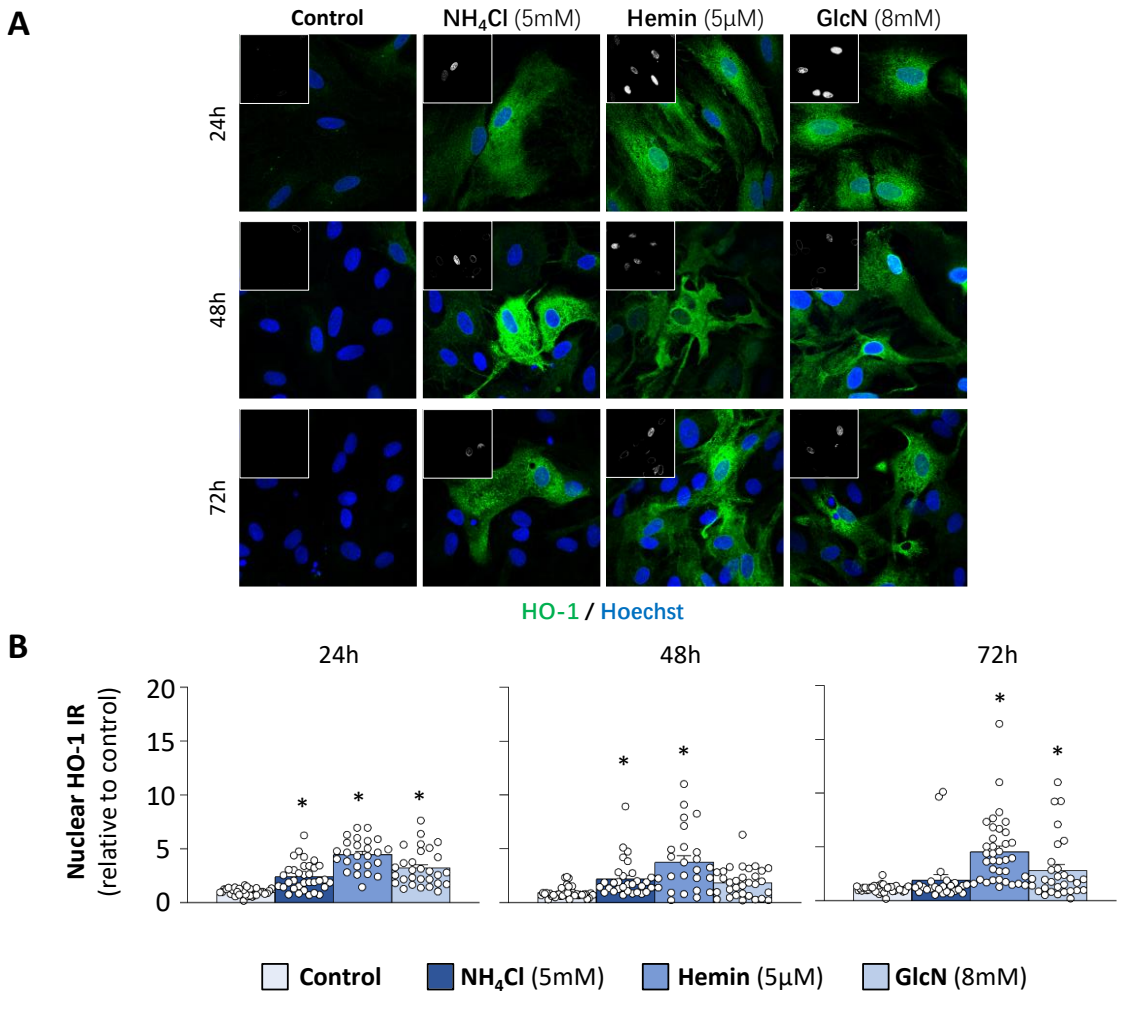

Figure 3.20: Effects of NH_4Cl, hemin and GlcN on nuclear HO-1 immunoreactivity in cultured rat astrocytes. Astrocytes were incubated with NH_4Cl (5 mM), hemin (5 µM), or GlcN (8 mM) or were left untreated (control) for 24, 48 and 72 h. (**A**) Immunofluorescence analysis of HO-1 (green) and Hoechst34580-labelled nuclei (blue) using confocal laser scanning microscopy. Representative images are shown. (**B**) The nuclear HO-1 immunofluorescence intensity of each individual astrocyte is represented by a dot. Statistical analysis was conducted using ANOVA and Dunn´s multiple comparison test. *: statistically significantly different compared to untreated controls ($p<0.05$). Nuclei are from 2 (GlcN, 48 h) or 3 (all other conditions) independent astrocyte preparations. Therefore, (GlcN, 48 h) data was excluded from statistical analysis.

To extend these investigations, further co-localization analyses were performed using organelle-specific dyes such as ER-Tracker™ Green and Mito-Tracker™ Deep Red to visualize the ER and mitochondria, respectively. Vital cells were incubated with the appropriate dyes, then fixed and processed for HO-1 immunofluorescence analysis. Of note, ER-Tracker™ Green is in general considered not to be well suited for fixation and subsequent immunofluorescence analysis. However, in the experiments of the present study ER-Tracker™ Green fluorescence was retained and its intensity was higher in astrocytes incubated with NH_4Cl (Fig. 3.21A). This is consistent with previous Western blot results from others, showing an upregulation of the sulfonylurea receptor 1 which is targeted by ER-Tracker™ Green in ammonia-treated astrocytes [*548*]. A significant, yet partial overlap was noted between ER-Tracker™ Green and anti-HO-1 immunofluorescence (Fig. 3.21A). No co-localization was observed between HO-1 and Mito-Tracker™ Deep Red but with Hoechst34580 in astrocytes incubated with NH_4Cl (Fig. 3.21B).

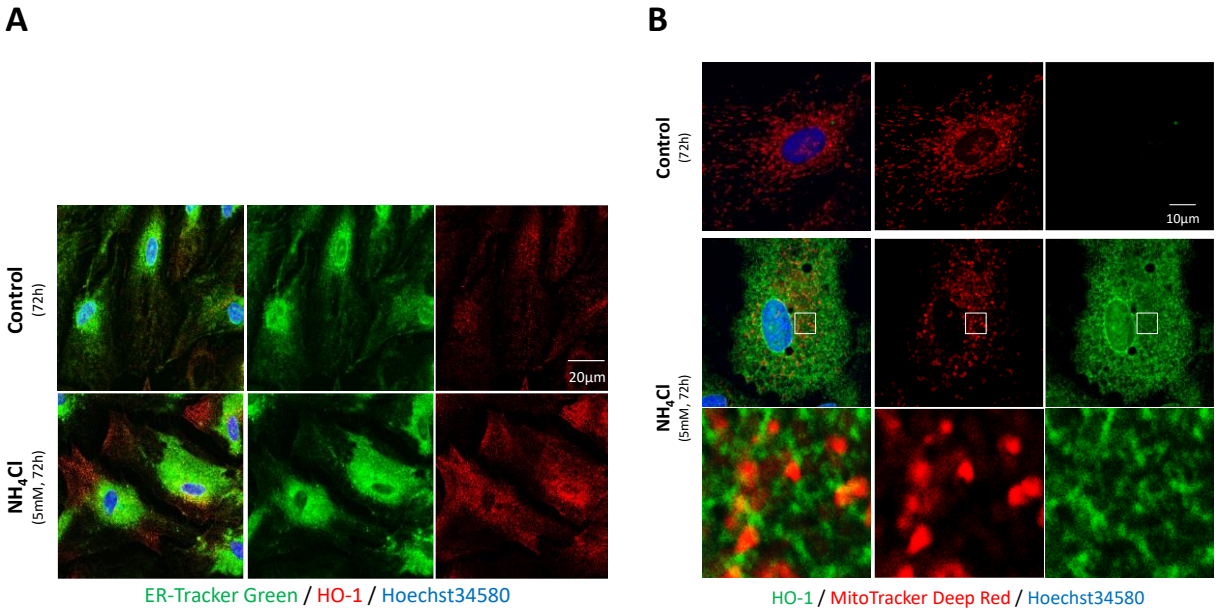

Figure 3.21: Subcellular localization of HO-1 in cultured rat astrocytes. Astrocytes were cultured for 72 hours with NH_4Cl (5 mM) or were left untreated (control). The endoplasmic reticulum was stained using ER-Tracker™ Green (**A**), mitochondria were stained with Mito-Tracker™ Deep Red (**B**) and HO-1 was detected by immunofluorescence. Images were acquired using confocal laser scanning microscopy as described in the materials and methods section.

Consistent with the increased nuclear HO-1 IR observed by immunofluorescence (Fig. 3.20A, B), Western blot analysis of nuclear protein fractions revealed significantly increased levels of full-length HO-1 in astrocytes treated with NH_4Cl, hemin or GlcN (Fig. 3.22A). Levels of truncated HO-1 (28 kDa) were significantly higher in nuclear lysates prepared from astrocytes incubated with hemin (48 and 72 h) and NH_4Cl (72 h) but not in those incubated with GlcN (Fig. 3.22A). Notably, astrocytes treated with hemin showed a significantly greater increase in the level of the truncated HO-1 protein in the nucleus compared to those incubated with NH_4Cl.

To investigate whether the increase in nuclear levels of truncated HO-1 enhances the transcription of Nrf2-dependent genes, qPCR analyses were performed. For this, we selected Nrf2 target genes formerly shown to be upregulated upon nuclear accumulation of truncated HO-1 [*430*, *492*]. The analyses showed, that CAT and SOD-1 mRNA levels remained unchanged across all treatments (Fig. 3.22B). From all selected genes, only the mRNA G6PDX increased in astrocytes incubated with NH_4Cl (72 and 96 h). In astrocyte incubated with GlcN the mRNAs of G6PDX and NQO1 were elevated at all time points analyzed (48, 72 and 96 h; Fig. 3.22B). In

contrast, in astrocytes incubated with hemin, no significant changes in the mRNA of any of the genes analysed were observed. Here, only a trend towards upregulation of G6PDX and NQO1 mRNA was noted at 24 h (Fig. 3.22B). Taken together, these findings do not support a significant role of nuclear truncated HO-1 for the transcription of Nrf2-dependent target genes. However, the findings do not rule out, that truncated HO-1 may account for the upregulation of further genes whose transcription is controlled by Nrf2.

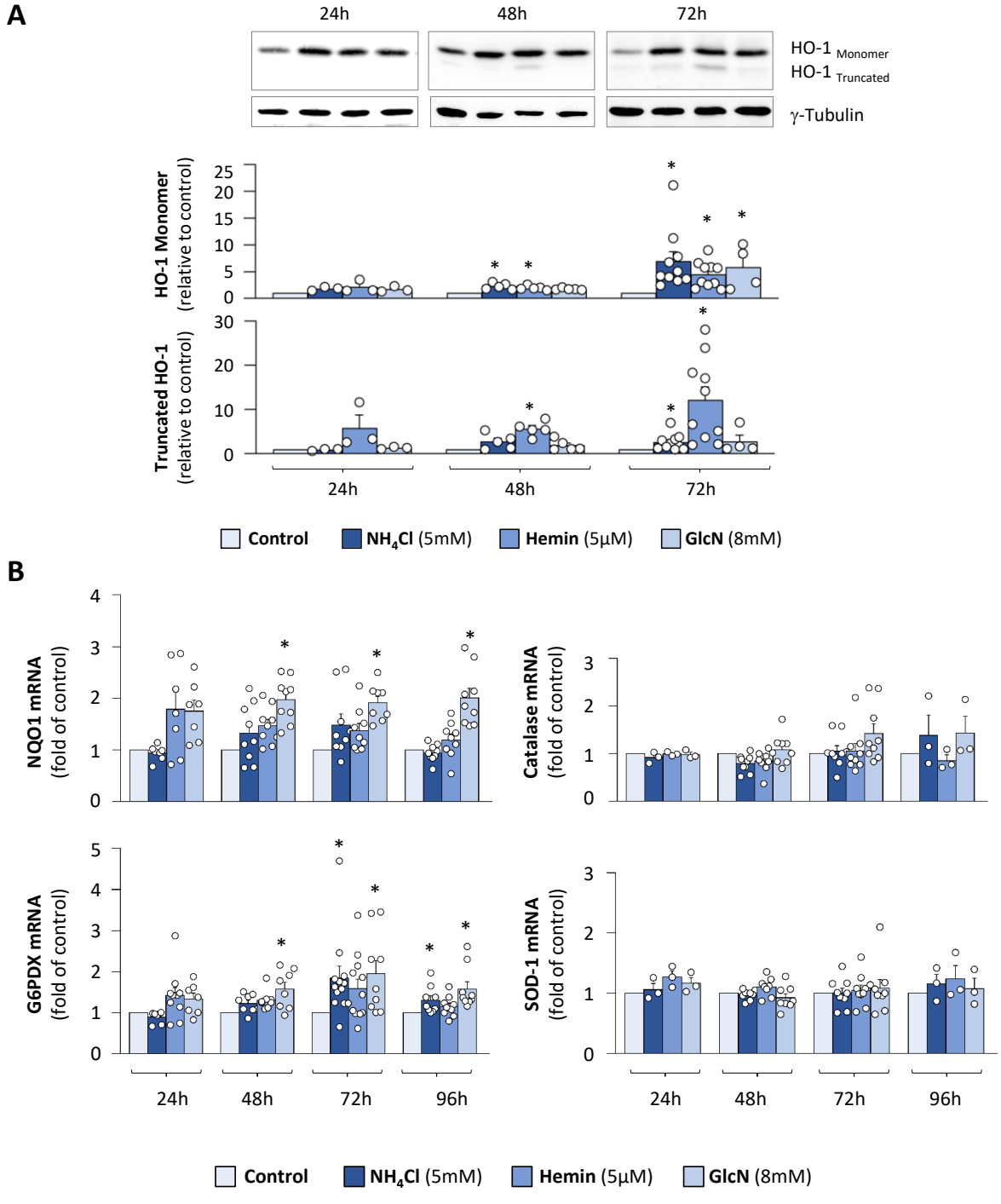

Figure 3.22: Nuclear levels of HO-1 protein and expression of Nrf2 target genes. (**A**) Nuclear protein extracts from astrocytes treated with NH_4Cl (5 mM), hemin (5 µM) or GlcN (8 mM) were subjected to Western blot analysis to determine the levels of nuclear HO-1 and γ-tubulin (loading control). HO-1 levels were quantified by densitometry and normalized to γ-tubulin. Each dot represents an independent experiment. (**B**) qPCR analysis of G6PDX, NQO1, catalase and SOD-1 mRNA in astrocytes incubated with NH_4Cl, hemin or GlcN. mRNAs of the respective genes were normalized to the housekeeping gene HPRT1 and are expressed relative to controls. Statistical analysis was performed using ANOVA, Friedman or Kruskal-Wallis each followed by Dunn´s multiple comparison test. *: statistically significantly different compared to untreated controls ($p<0.05$). n.s.: not statistically significantly different.

To determine whether truncated HO-1 is enriched in nuclear protein preparations, we examined the ratio of full-length to truncated HO-1 (Fig. 3.23). It is important to note that the protocol used here includes nuclear membranes, which originates from the ER membrane which in turn contains high levels of full-length HO-1. The analyses revealed an even lower abundance of truncated HO-1 relative to those of full-length HO-1 in the nuclear protein preparations of astrocytes incubated with NH_4Cl and GlcN. In astrocytes incubated with hemin, the proportions of truncated and full-length HO-1 were similar to control conditions. The results indicate that there is no significant enrichment of nuclear truncated HO-1 in relation to total HO-1 protein levels under the experimental conditions described here.

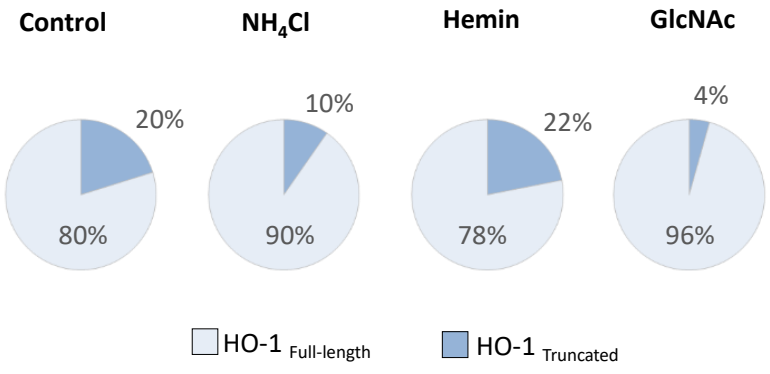

Figure 3.23: Proportion of nuclear full-length and truncated HO-1. Astrocytes were cultured for 24, 48, or 72 h with NH_4Cl (5 mM), hemin (5 µM), GlcN (8 mM), or were left untreated (control). Nuclear protein preparations were analyzed by Western blot for HO-1. The ratio of full-length to truncated HO-1 was quantified by densitometry (see Figure 3.22B).

3.4 Protein *O*-GlcNAcylation dependence of the ammonia-mediated increases of truncated HO-1 protein in the cell culture supernatant

Recent studies have suggested that HO-1 may be released from astrocytes via extracellular vesicles [*549*]. To investigate this, we analyzed HO-1 protein levels in the supernatants of astrocyte cultures using Western blot analysis.

Irrespective of the experimental treatment, truncated HO-1 was significantly enriched in the supernatant compared to full-length HO-1 (Fig. 3.24A). NH_4Cl (5 mM) and GlcN (8 mM) significantly increased truncated HO-1 levels in the supernatant, while hemin showed a trend towards an increase (Fig. 3.24A). While the level of full-length HO-1 in the supernatant was not significantly affected by any of the treatments, a clear trend was observed in astrocytes incubated with NH_4Cl or GlcN (Fig. 3.24A).

The effect of *O*-GlcNAcylation on HO-1 protein levels in the supernatant was investigated in astrocytes that were pre-treated with control siRNA, or with siRNA targeting GFAT1 and 2 or OGT. The analyses demonstrated that NH_4Cl had a significant effect on truncated HO-1 levels in the supernatant of astrocytes treated with control siRNA. However, this effect was not observed in astrocytes pre-treated with GFAT1+2 or OGT siRNAs (Fig. 3.24B). The results indicate that the release of truncated HO-1 induced by NH_4Cl is dependent on protein *O*-GlcNAcylation. It is noteworthy that NH_4Cl did not demonstrate a clear inhibitory effect on the protein levels of truncated HO-1 in the supernatant of astrocytes treated with GFAT1+2 siRNA, despite not showing a significant increase. The precise cause of this phenomenon is currently unclear. However, it may be indicative of the fact that, under the selected experimental conditions, UDP-GlcNAc levels remain sufficient to trigger the release of truncated HO-1.

In summary, the findings demonstrated that NH_4Cl-induces the release of truncated HO-1 in a way that depends on the *O*-GlcNAcylation of yet unknown proteins.

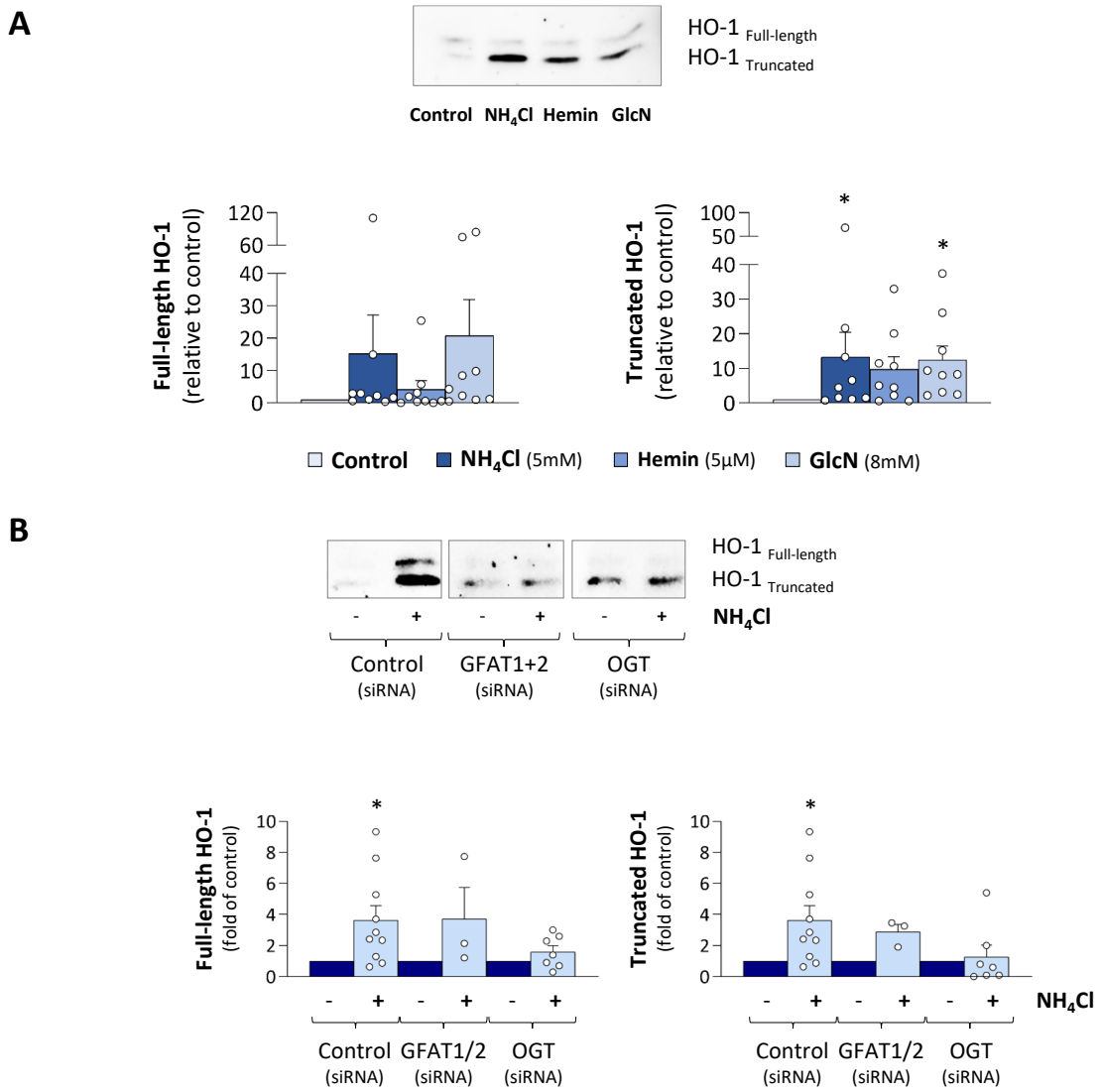

Figure 3.24: Impact of NH_4Cl, hemin, and GlcN on extracellular HO-1 protein levels. Astrocytes were cultured for 72 hours with either no treatment (control), NH_4Cl (5 mM), hemin (5 µM), or GlcN (8 mM). (**A**) Detection of HO-1 in the supernatant by Western blot analysis. (**B**) Impact of *O*-GlcNAcylation on NH_4Cl-induced HO-1 in the supernatant. Astrocytes were pre-incubated with control siRNA (AllStars), or siRNAs targeting GFAT1+2 or OGT for 24 h before cells were further incubated with NH_4Cl (5 mM, 72 h). Levels of HO-1 were analyzed by Western blot. Statistical analyses were performed using Student's t-Test or Wilcoxon test. (**A**) *: statistically significantly different compared to untreated controls ($p<0.05$), sample size: N=9). (**B**) *: statistically significantly different compared to control siRNA + NH_4Cl treatment ($p<0.05$), sample size: N=3-9.

To determine whether increased truncated HO-1 in the supernatants was linked to enhanced vesicular release, we analyzed the abundance of EVs in the supernatants of the astrocyte cultures (Fig. 3.25A, B). Quantification of the particle numbers and size revealed no significant differences in astrocytes treated with NH_4Cl, hemin or GlcN compared to untreated controls (Fig. 3.25B). This suggests that the elevated extracellular levels of truncated HO-1 are unlikely to be a consequence of increased vesicular release from the astrocytes.

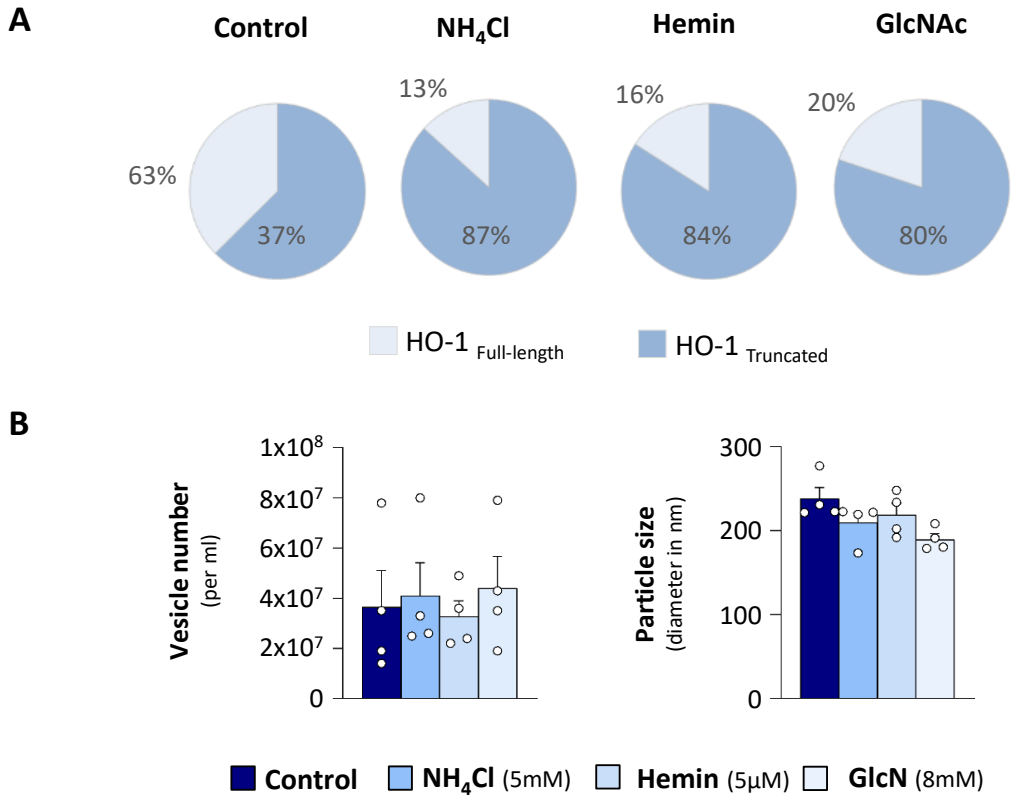

Figure 3.25: Proportion of full-length and truncated HO-1 and abundance of extracellular vesicle in the supernatant of cultured rat astrocytes. Astrocytes were cultured with NH_4Cl (5 mM), hemin (5 µM) or GlcN (8 mM) for 24, 48 or 72 hours or left untreated. Culture supernatants were prepared as described in the Materials and Methods section. (**A**) Western blot and densitometric quantification were used to analyse the relative amounts of full-length and truncated HO-1 protein. (**B**) Analysis of extracellular vesicles in number and size in the supernatants using the particle analyser as described in the Materials and Methods section. Statistical analyses were performed using Friedmann and Dunn's multiple comparison test. Sample size: N=4.

The objective of the subsequent experiments was to investigate whether the elevated levels of extracellular truncated HO-1 were a consequence of increased proteolytic cleavage of ER-anchored HO-1. Several cysteine proteases, including γ-secretase, CatB, calpains, signal SPP, and valosin-containing protein (p97), have been suggested to cleave HO-1 in human cell lines [*430*, *550*, *551*]. To investigate whether any of these proteases are involved in the NH_4Cl-mediated release of truncated HO-1, we incubated the astrocytes with the cysteine protease inhibitors Compound E and Aloxistatin (E64d), and the p97 inhibitor Eeyarestatin 1 (ESI). In order to prevent the toxic effects of prolonged inhibition of the respective proteases on the cells, protease inhibitors were added 48 hours after the incubation with NH_4Cl for another 24

h. None of these chemical compounds significantly inhibited the release of full-length or truncated HO-1 under these experimental conditions into the supernatant (Fig. 3.26A, B). Although the levels of truncated HO-1 in the astrocytes treated with E64d did not show a significant increase in the supernatant after NH_4Cl, a clear tendency was recognizable.

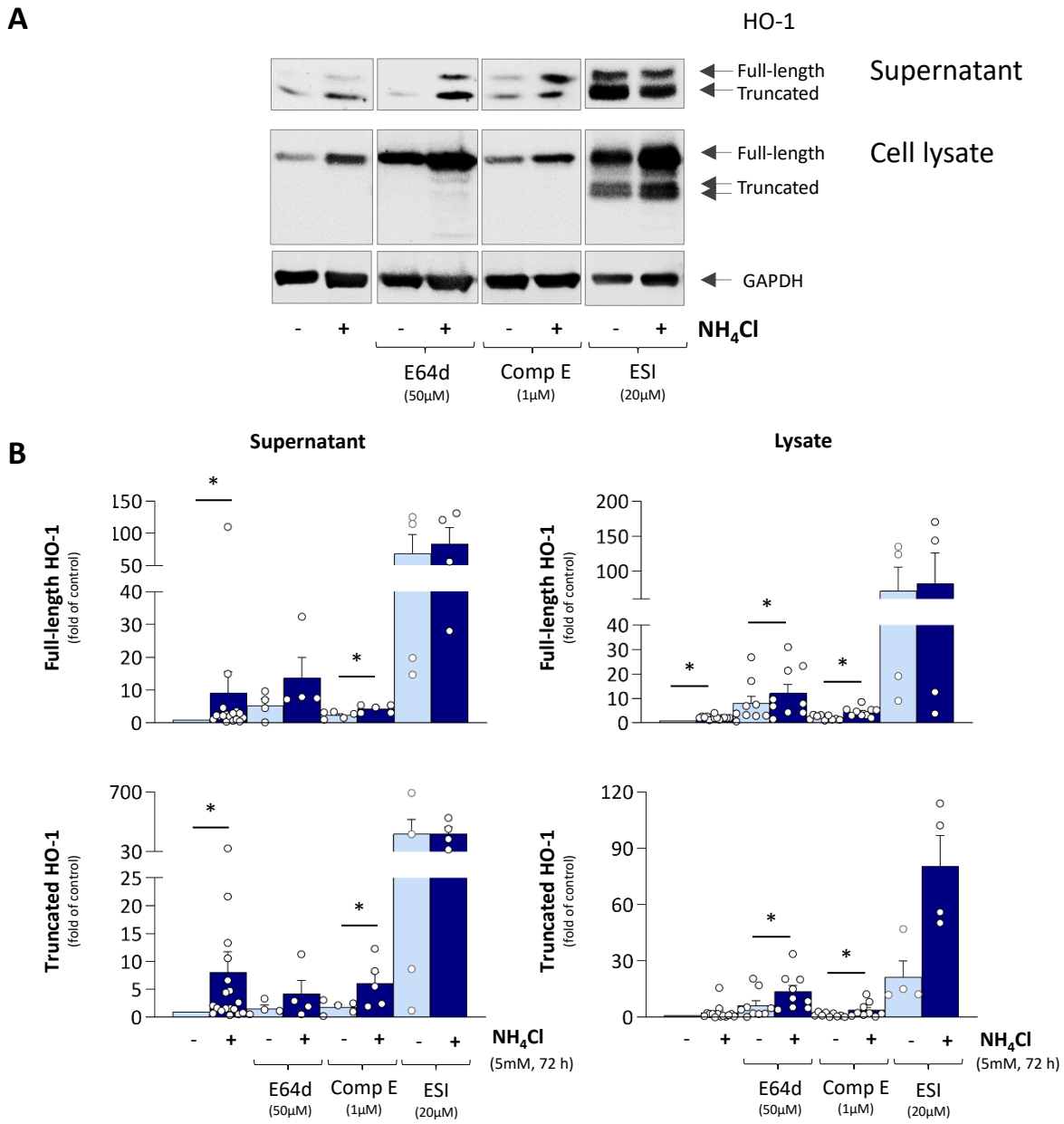

Figure 3.26: Effects of protease inhibitors on extracellular and intracellular HO-1 protein levels in cultured rat astrocytes. Astrocytes were incubated with NH_4Cl (5 mM) for 48 h before cysteine protease inhibitors (Compound E, 5 µM; E64d, 50 µM) or the ER-associated degradation (ERAD) inhibitor eeyarestatin 1 (ESI, 20 µM) were added and cells were incubated for another 24 h. (**A**) Full-length and truncated HO-1 protein were analyzed in cell culture supernatants and cellular lysates by Western blot and quantified by densitometry. (**B**) Statistical analyses were performed using Student's t-Test or Wilcoxon test. *: statistically significantly different compared to untreated controls ($p<0.05$). Each dot represents an independent experiment. Sample size: 4-14.

Inhibiting the ER-resident protease p97 with ESI strongly increased both intracellular and extracellular levels of full-length and truncated HO-1. Furthermore, many additional, HO-1 reactive signals were observed in astrocytes incubated with ESI (Fig. 3.27). It is of note that all of the protease inhibitors demonstrated the capacity to increase full-length and truncated HO-1 protein in the absence of ammonia. This suggests that their involvement in the cleavage of HO-1 is unlikely, and instead points to an important role for the degradation of full-length and truncated HO-1.

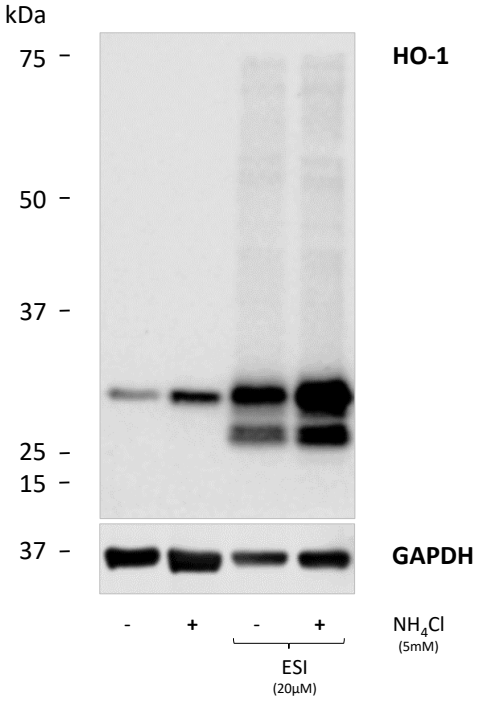

Figure 3.27: Impacts of cysteine protease and ERAD inhibitors on NH_4Cl-induced upregulation of HO-1 in cultured rat astrocytes. Astrocytes were cultured for 72 hours either without (control) or with 5 mM NH_4Cl present. After 48 hours, cells were cultured for a further 24 hours with E64d (50 μM), Comp E (5 μM), or ESI (20 μM) as indicated. Western blot analysis of HO-1 protein was performed on astrocyte protein lysates.

Besides proteases, also reactive oxygen species (ROS) can cleave proteins in a non-enzymatic manner. The potential for ROS-mediated non-enzymatic cleavage of HO-1 was investigated using purified recombinant rat HO-1. HO-1 was incubated with hydrogen peroxide (H_2O_2) or a combination of ferric chloride ($FeCl_3$) and DTT. The latter generates hydroxyl radicals ($^{\bullet}OH$) [*552*, *553*]. The incubation of OH-1 with either H_2O_2 or $FeCl_3$ + DTT resulted in a decrease

in full-length HO-1 (band II, Fig. 3.28A, B). At the same time, $FeCl_3$ + DTT but not H_2O_2 led to the appearance of anti-HO-1 reactive bands (I, IV and V) with molecular weights around 65 kDa, 20 kDa and below 20 kDa, respectively (Fig. 3.28A, B). It is of note that none of the treatments resulted in an increase in the band observed at approximately 28 kDa (band III, Fig. 3.28A, B), which corresponds to the molecular weight of truncated HO-1. This suggests that H_2O_2 and •OH does not cleave HO-1 at the N-terminal site which leads the formation of truncated HO-1. These findings suggest that •OH may trigger HO-1 aggregation and fragmentation *in vitro*, but this does not generate the truncated form observed in NH_4Cl-treated astrocytes.

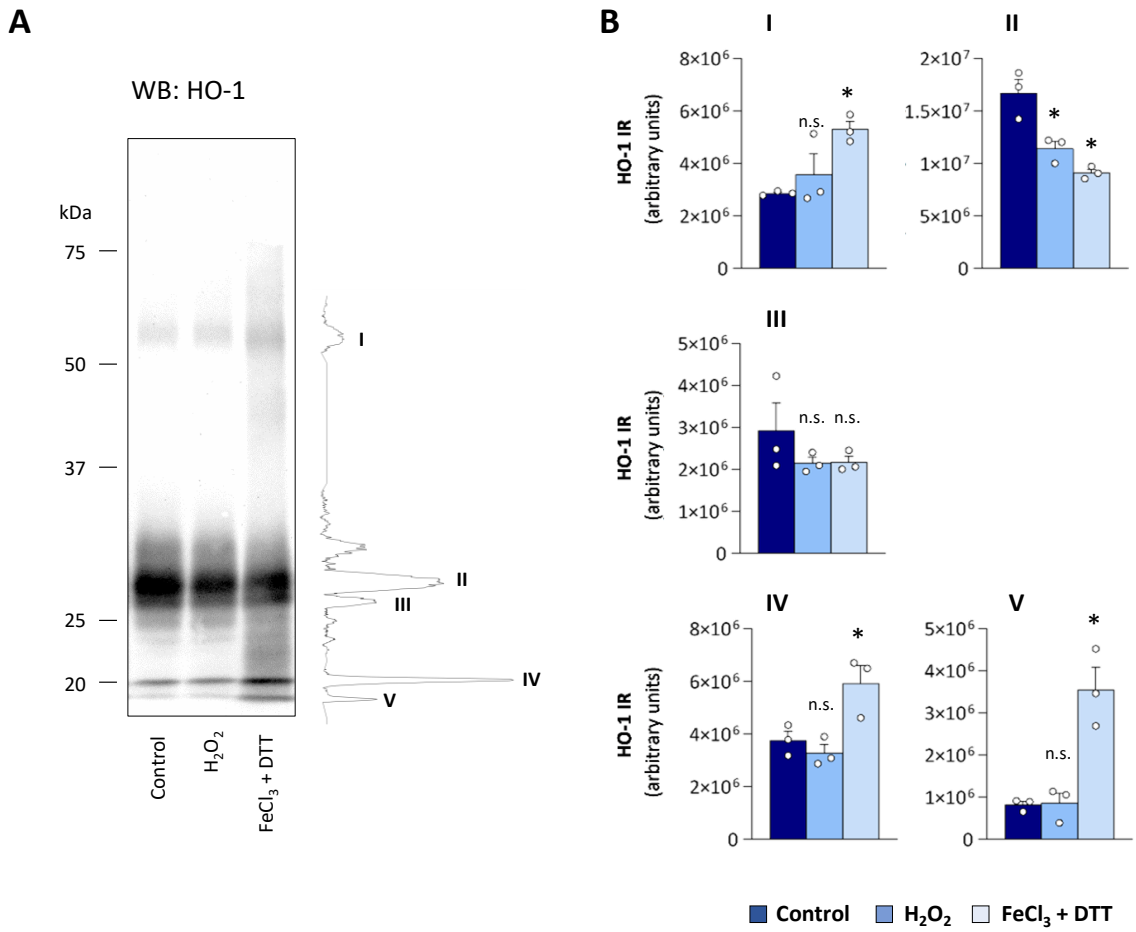

Figure 3.28: Reactive oxygen-induced fragmentation and aggregation of HO-1 *in vitro*. Purified rat HO-1 was incubated with hydrogen peroxide (H_2O_2, 500 µM) or a combination of ferric chloride ($FeCl_3$, 50 µM) and DTT (10 mM) to generate hydroxyl radicals (•OH) as indicated in the Materials & Methods section. Untreated HO-1 was used as a control. Samples were analyzed by Western blot using anti-HO-1 antibodies. (**A**) Anti-HO-1 immunoreactive (IR) bands are shown. Band II represents full-length HO-1, while bands I, IV and V represent major additional HO-1 IR bands. (**B**) Densitometric quantification of anti-HO-1 IR from Western blots. Statistical analysis was performed by Ordinary one-way ANOVA and Dunnett's multiple comparison test. *: Statistically significantly different compared to untreated controls ($p<0.05$). n.s.: not statistically significantly different (N=3).

In summary, ROS-mediated non-enzymatic cleavage of HO-1 may affect the stability of HO-1. However, it does not explain the increased levels of truncated HO-1 observed in the supernatant of astrocytes incubated with NH_4Cl.

3.5 Cerebral protein *O*-GlcNAcylation, HO-1 and GRP78 in hyperammonemic rats

To investigate, whether hyperammonemia also upregulates protein *O*-GlcNAcylation, HO-1 and GRP78 protein in rat brain *in vivo*, we challenged male Wistar rats with a single dose of NH_4Acetate (4.5 mmol/kg body weight). This experimental treatment was shown before to induce oxidative/ nitrosative in the brain of rats. Since memory and motor functions are severely impaired in HE, the analyses were carried out in brain tissue prepared from the hippocampus and cerebellum [*136*, *155*, *168*].

The results of the Western blot analysis showed a significant increase in protein *O*-GlcNAcylation in both brain regions of NH_4Acetate treated rats (Fig. 3.29A). Compared to hippocampal lysates, *O*-GlcNAc signals were much stronger in cerebellar protein lysates (Fig. 3.29B). Moreover, the molecular weights of the *O*-GlcNAcylated protein species differed substantially between the two brain regions (Fig. 3.29A).

In both brain regions, hyperammonemia did not affect the levels of glutamine synthetase (GS) and glutamine-fructose amidotransferases (GFAT1, 2) as show by Western blot (Fig. 3.29C). Both proteins are cruical for the synthesis of the OGT substrate UDP-GlcNAc. Interestingly, the enzyme responsible for *O*-GlcNAcylation, OGT, was downregulated in the hippocampus and unchanged in the cerebellum of NH_4Ac-treated rats. Moreover, GFAT1 was not detectable in hippocampal protein lysates (Fig. 3.29C, D). Thus, the lower levels of *O*-GlcNAcylated proteins in the hippocampus of NH_4Acetate-treated rats compared to the cerebellum were associated with lower levels of proteins that are crucial for protein *O*-GlcNAcylation.

Previous studies have linked protein *O*-GlcNAcylation to the upregulation of GRP78, an ER stress marker, and suggested a role in oxidative stress and senescence in HE [*4*, *136*]. Since protein *O*-GlcNAcylation upregulates HO-1 protein, which induces ER stress *in vitro*, the levels

of HO-1 and GRP78 were analysed in protein samples taken from hippocampus and cerebellum of control and NH_4Acetate-treated rats.

As shown by Western blot analysis, HO-1 and GRP78 were significantly upregulated in the cerebellum but remained unchanged in the hippocampus of NH_4Ac-treated rats compared the respective controls (Fig. 3.29E, F). These results show that hyperammonemia upregulates protein *O*-GlcNAcylation in the hippocampus and cerebellum. However, only in the cerebellum but not in the hippocampus, this upregulation was paralleled by increased levels of HO-1 and GRP78 protein.

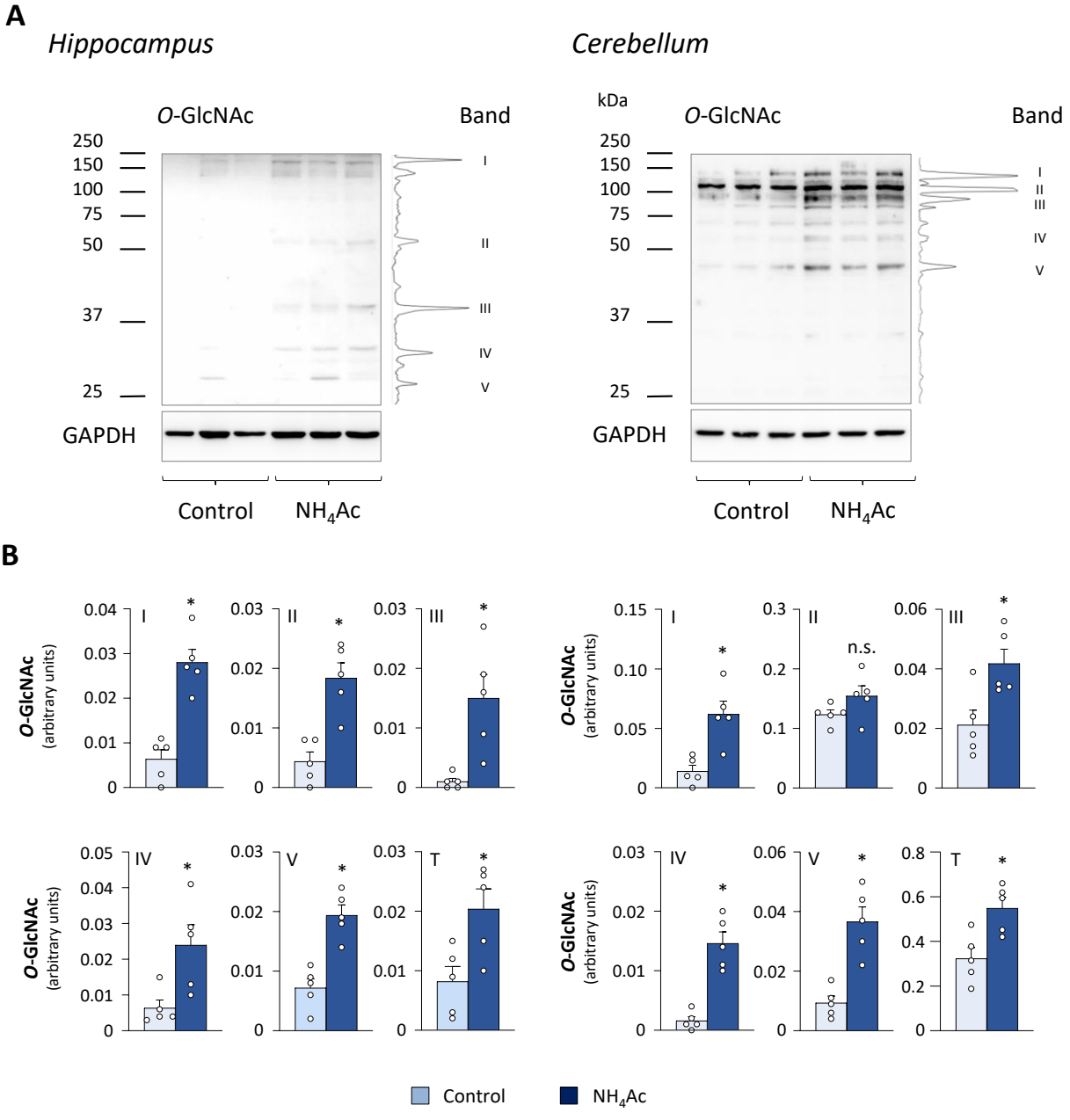

C

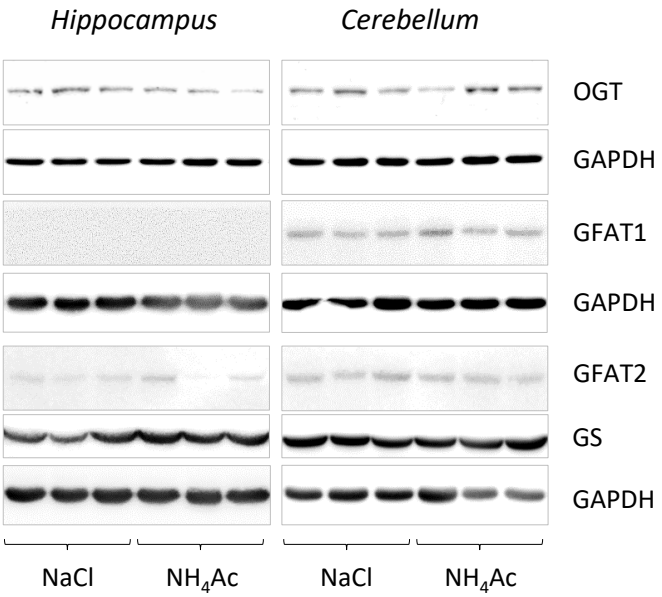

D

Hippocampus

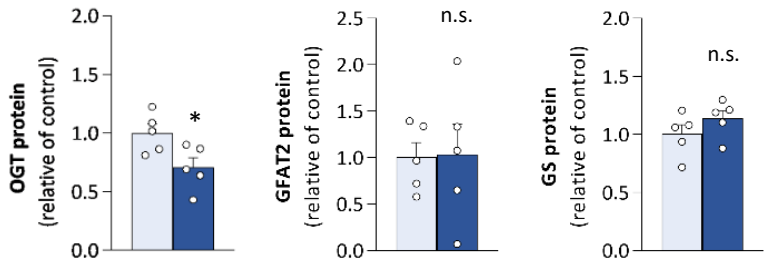

Cerebellum

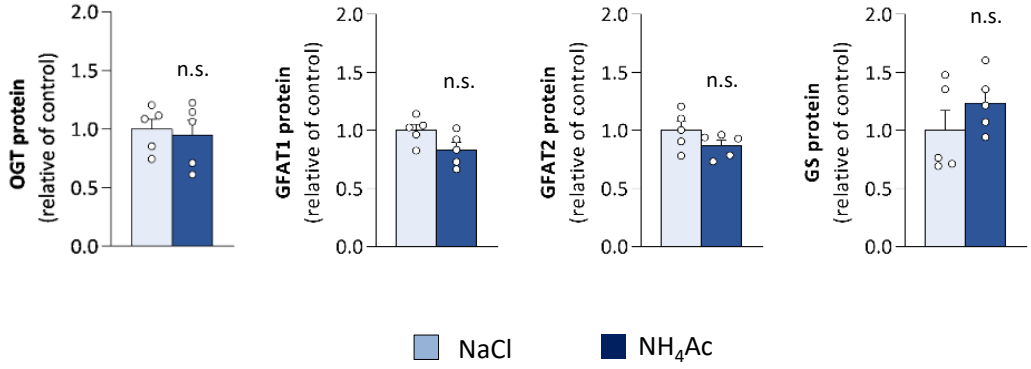

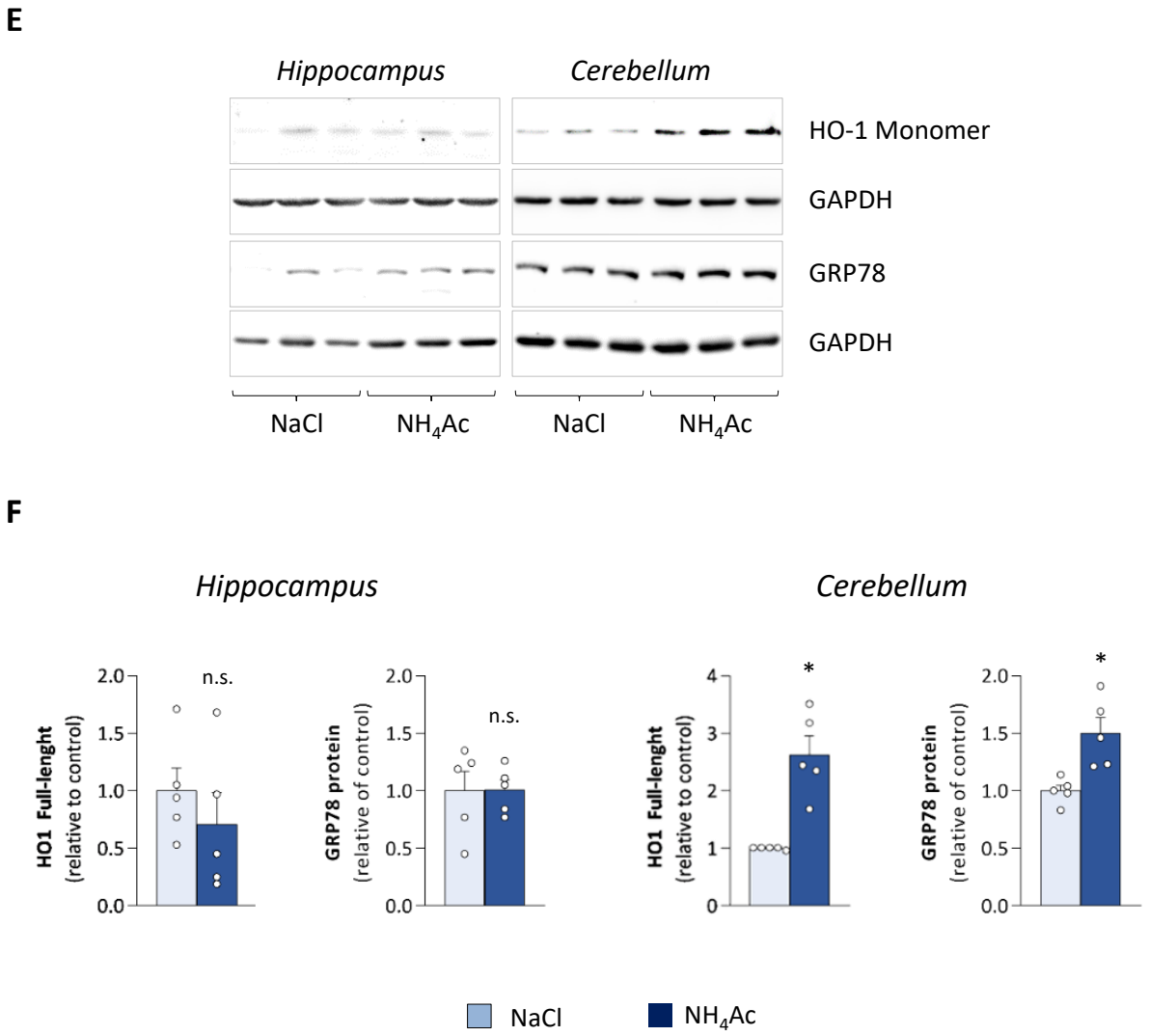

Figure 3.29: Effects of hyperammonemia on protein *O*-GlcNAcylation, HO-1 and GRP78 in the rat brain. Wistar rats were given either NH_4Ac (4.5 mmol/kg body weight) or a vehicle control (NaCl, 0.9%). After 24 hours, the rats were sacrificed, and protein lysates were prepared from the hippocampus and cerebellum for Western blot analysis. Analysis of protein *O*-GlcNAcylation by Western blot (**A**). Quantification of protein *O*-GlcNAcylation levels was performed using densitometry for individual protein species and total *O*-GlcNAc levels (**B**). Anti-*O*-GlcNAc immunoreactive (IR) bands with highest intensities are indicated by roman numerals (I-V) in the chemiluminogram (**A**). "T" represents the sum of signal intensity for all *O*-GlcNAcylated protein species. (**C**,**D**) Western-blot analysis of proteins involved in protein *O*-GlcNAcylation: OGT, GFAT1, GFAT2 and GS (**C**). (**E**, **F**) Western blot analysis and densitometric quantification of HO-1 and GRP78 protein (**E**). GAPDH was used as a loading control and for intensity normalization of the respective target protein. Statistical analysis was performed using either Student's t-test or Mann-Whitney test, as appropriate. *: statistically significantly different to untreated controls ($p<0.05$). n.s.: not statistically significantly different (N=5).

4. Discussion

4.1 Ammonia-induced protein *O*-GlcNAcylation in astrocytes

Protein *O*-GlcNAcylation was recently discovered as a posttranslational protein modification which relates to ammonia-induced oxidative stress in cultured rat astrocytes. Here, the *O*-GlcNAcylation of so far unknown proteins downregulates the transcription of miRNAs which target HO-1 and Nox4 [*4*, *144*]. This triggers the oxidation of RNA and induces senescence, which both are suggested to contribute to the pathogenesis of HE [*4*]. However, except for GAPDH protein species whose *O*-GlcNAcylation level change in response to ammonia the astrocytes remained unknown [*4*, *144*]. This study addresses the aforementioned knowledge gap by providing a comprehensive analysis of the astroglial *O*-GlcNAcome and by characterizing effects of ammonia on it.

Here, over 300 protein species of the rat astrocyte *O*-GlcNAcome were identified. Importantly, bioinformatic analyses revealed that many of the *O*-GlcNAcylated proteins are involved in energy metabolism such as in fatty acid oxidation, pyruvate metabolism and the citrate cycle (Fig. 3.5A). These findings are consistent with findings from the literature in other cell types and strengthen a crucial role of protein *O*-GlcNAcylation in energy metabolism and nutrient sensing [*554*].

With regard to earlier investigations, the present study revealed for the first time that ammonia not only increases, but also decreases the *O*-GlcNAcylation of a subset of protein species in the astrocytes [*144*]. This reflects the advantage of the current MS-based analytical approach, which has higher precision and sensitivity compared to the Western blot analyses used in previous studies [*144*]. Accordingly, these findings suggest a much more complex interaction between ammonia and protein *O*-GlcNAcylation in the astrocytes as previously assumed. However, it is currently unclear whether the reduced levels of the respective *O*-GlcNAcylated proteins are simply due to downregulation of the respective proteins, which requires further investigation.

Many of the protein species whose *O*-GlcNAcylation levels were altered by ammonia relate to mitochondria (Fig. 3.4C). Therefore one may speculate, that the altered protein *O*-

GlcNAcylation relates to the well-known ammonia-induced mitochondrial dysfunction in cultured rat astrocytes [*555*, *556*]. The latter is characterized by mitochondrial swelling [*69*], inhibition of respiratory chain activity [*557*, *558*], mitochondrial oxidative stress [*69*, *559*], and induction of the mitochondrial permeability transition [*182*]. In line with this assumption, excessive *O*-GlcNAcylation of mitochondrial proteins has been shown to impair activities of complexes I, III and IV, mitochondrial calcium levels and ATP synthesis [*292*]. This finding would argue for an increased protein *O*-GlcNAcylation as the cause for mitochondrial dysfunction in ammonia-exposed cultured rat astrocytes. However, one may also speculate that altered protein *O*-GlcNAcylation in ammonia-exposed astrocytes is a consequence thereof and may serve to counteract mitochondrial dysfunction. Further studies are required to clarify whether and if, how the *O*-GlcNAcylation of mitochondrial proteins relate to mitochondrial dysfunction in ammonia-exposed astrocytes.

Ammonia toxicity in astrocytes and in HE is closely linked to glutamine metabolism [*1*], on the one hand *via* glutamine synthetase-mediated glutamine synthesis and on the other by glutaminase-dependent hydrolysis of glutamine [*69*, *560*]. With regard to glutamine metabolism-related proteins, our data show an increased *O*-GlcNAcylation of glutamate dehydrogenase 1 (Glud1). Glud1 catalyzes the conversion of glutamate to α-ketoglutarate and is found in the cytosol and in mitochondria [*561*]. Regarding the latter, the Glud1 substrate glutamate is supplied through hydrolysis of glutamine by glutaminase [*562*]. The impact of ammonia on a-ketoglutarate levels in astrocytes in brain remains poorly understood and is a matter of controversial debate [*563*]. In rats four weeks after portocaval shunting (PCS), levels of a-ketoglutarate were unaltered in the cerebral cortex [*564*] but elevated in cerebral spinal fluid [*565*, *566*]. While the impact of the *O*-GlcNAcylation of Glud1 in ammonia-exposed astrocytes is currently unknown, one may speculate that it may increase the stability and half-life of Glud1. Currently, it remains to be investigated whether the *O*-GlcNAcylation affects Glud1 residing in the cytosol or in mitochondria, or in both cellular compartments.

The present study further identified several *O*-GlcNAcylated protein species in the astrocytes, which are associated with the synthesis and degradation of proteins. These include

many t-RNA aminoacyl synthetases who are central for protein biosynthesis and cellular viability [*567*, *568*]. The *O*-GlcNAcylation of these tRNA aminoacyl synthetases, such as WARS, was strongly enhanced in ammonia-exposed astrocytes. The significance of their *O*-GlcNAcylation is currently unclear but may increase their half-life possibly by interfering with their ubiquitination. Of particular interest here is the ratio of *O*-GlcNAcylation to non-*O*-GlcNAcylated protein. An increased proportion of the former could already indicate that the *O*-GlcNAcylated tRNA aminoacyl synthetases have an increased half-life compared to the non-*O*-GlcNAcylated tRNA aminoacyl synthetases. Besides these proteins, levels of *O*-GlcNAcylated ribosomal proteins Rpl18 and Rps9 were decreased and those of Rpl10A were increased by ammonia in cultured rat astrocytes (Fig. 3.4A, C, Tab. 3.3). It is noteworthy that the *O*-GlcNAcylation of other than the aforementioned ribosomal proteins has been previously demonstrated and postulated to positively influence translation and the biogenesis of ribosomes [*332*]. The significance of changes in the levels of *O*-GlcNAcylated ribosomal proteins Rpl18, Rps9 and Rpl10A for protein biosynthesis in ammonia-treated astrocytes is currently unknown and needs further investigation. However, it is tempting to speculate that their *O*-GlcNAcylation may relate to the oxidation of ribosomal and messenger RNA in ammonia-exposed astrocytes which was suggested to inhibit or impair protein translation [*141*]. However, further research is required to clarify the role of protein *O*-GlcNAcylation for translation in ammonia-exposed rat astrocytes and in brain in patients with liver cirrhosis and HE.

Using protein cluster analysis, we noted among the proteins of the astrocytic *O*-GlcNAcome an enrichment of proteasomal and lysosomal protein species (Fig. 3.5B, Tab. 3.3). Ammonia was found to increase the *O*-GlcNAcylation of the proteasomal subunits PSMB3 and PSMD12 and the lysosomal proteins LAMP1 and to reduce the *O*-GlcNAcylation of the lysosomal protein Cathepsin D (Fig. 3.4A, Tab. 3.3). Interestingly, at the same time - ammonia enhances proteasomal [*269*, *569*] and inhibits lysosomal degradation [*570*] in cultured rat astrocytes. However, this was suggested to be a consequence of an ammonium-induced pH-change [*571*, *572*]. Whether this is also relates of altered *O*-GlcNAcylation of the protein species mentioned above is currently unknown. While PSMB3 is a catalytically inactive structural subunit of the

catalytic chamber of the 20S proteasome [*573*], the PSMD12 is a non-ATPase subunit of the 19S regulatory proteasome [*574*], which delivers the peptide for degradation to the 20S subunit. Thus, the ammonia-induced *O*-GlcNAcylation may affect both, the 20S and 19S complexes of the 26S proteasome at the same time. Unfortunately, consequences of this for proteasomal activity are currently unknown. Interestingly, the *O*-GlcNAcylation of the ATPase subunits of the 19S proteasome inhibits proteasomal degradation [*575*].

Consequences of altered *O*-GlcNAcylation of cathepsin D (CatD) and LAMP1 for lysosomal activity are currently also unknown. However, it is known that *O*-GlcNAcylation of the catalytically inactive CatB is critical for its maturation from the inactive pre-CatB into the active form [*576*, *577*]. Similar to CatB also CatD is synthesized as an inactive prepro-form that is converted into the mature form in lysosomes [*578*]. Therefore, one may speculate that a decreased *O*-GlcNAcylation may reduce the levels of mature CatD and thereby impair lysosomal activity in ammonia-exposed astrocytes. However, further research is required to clarify a potential role of ammonia-induced changes in the *O*-GlcNAcylation of lysosomal proteins for the degradation of cellular macromolecules in the astrocytes.

Further evidence from our study suggested that ammonia alters the *O*-GlcNAcylation of ER-resident proteins in cultured rat astrocytes. Here, the *O*-GlcNAcylation of heat shock protein 5 (hspa5), which is also known as glucose regulated protein 78 (GRP78), was increased under ammonia. GRP78 is an endoplasmic reticulum chaperone that plays a central role in protein quality control and which regulates protein folding and degradation of misfolded proteins [*579*]. Previous studies have shown that ammonia triggers ER stress in cultured rat astrocytes which leads to upregulation of GRP78 ([*4*, *69*, *142*] and this study Fig. 2C; Fig. S3E [*4*]). This is paralleled by a disturbed *N*-glycosylation of proteins which takes place in the ER. However, consequences of the increased *O*-GlcNAcylation of proteins in the ER chaperone complex in response to ammonia are currently unclear. One may speculate that GRP78 is upregulated as a consequence of an *O*-GlcNAcylation-mediated decreased ubiquitination which may increase its half-life. However, upregulation of GRP78 by ammonia is also regulated at the transcriptional level. Therefore, it seems unlikely that the increased *O*-GlcNAcylation of

GRP78 is solely responsible for the upregulation of GRP78 protein in ammonia-treated rat astrocytes. Thus, further research is required to clarify the role of *O*-GlcNAcylation for ER-stress in ammonia-exposed rat astrocytes and in the brain of patients with liver cirrhosis and HE.

Interestingly, some of the proteins which we identified to become *O*-GlcNAcylated in the astrocytes are present in various cellular compartments. For example, Suclg1 [*580*] and Glud1 [*561*] are both present in the cytoplasm and in mitochondria. This may hint at a potential crosstalk between these compartments. Since cytosolic and mitochondrial OGT may differ with regard to their substrate specificity [*302*], one may speculate that the respective protein species may only become *O*-GlcNAcylated in one of both compartments. In this case, protein *O*-GlcNAcylation of the respective protein species would indicate its compartmental origin. This is similar to what is known from other post translational modifications such as the phosphorylation of signaling proteins. For example, p53 may become phosphorylated in the cytosol and the nucleus by different kinases. However, phosphorylation of p53 at serine^{392} takes place exclusively in the nucleus, where it triggers its nuclear accumulation and enhances the transcription of p53-dependent target genes [*4*]. However, whether the *O*-GlcNAcylation of Suclg1 and Glud1 also depends upon subcellular localization is currently unclear and remains to be established.

4.2 Ammonia-induced *O*-GlcNAcylation of HO-1 in cultured astrocytes

Recent publications have highlighted an important role of HO-1 and of protein *O*-GlcNAcylation for the pathogenesis of HE (for reviews see [*1*, *76*]). In the present study we found that truncated and full-length HO-1 themselves undergo *O*-GlcNAcylation in ammonia-treated cultured rat astrocytes (Fig. 3.10A, B). In this context, it is important to note that in ammonia-treated astrocytes, the increase in *O*-GlcNAcylated HO-1 was considerably higher compared to the increase in HO-1 protein levels suggesting that the former does not merely reflect the upregulation of the protein.

Using *in vitro O*-GlcNAcylated recombinant HO-1 and mass spectrometry we found that OGT interacts with HO-1 and triggered the *O*-GlcNAcylation of HO-1 serine residue 159 or 160 (Fig. 3.9A-C). Importantly, these serine residues reside in the center of the HO-1 dimerization interface. In cultured rat astrocytes, *O*-GlcNAcylation of HO-1 was paralleled by increased levels of HO-1 homo- and heteromers (Fig. 3.17C, G, I). This phenomenon was blocked either by inhibiting UDP-GlcNAc synthesis or OGT activity (Fig. 3.17A, E). In line with this, also increasing intracellular *O*-GlcNAc levels by incubating the astrocytes with GlcN led to the formation of HO-1 homo- and heteromers, albeit to a lesser extent than ammonia (Fig. 3.10A, B). These results indicate that protein *O*-GlcNAcylation triggers the homomerization of HO-1 and the interaction with further proteins. However, this does not necessarily mean, that it is a consequence of the *O*-GlcNAcylation of HO-1 itself. Instead, it may also represent a secondary effect of the *O*-GlcNAcylation of other, yet unknown protein species. This needs to be addressed in further investigations in cultured astrocytes in which a mutated HO-1 variant is expressed which cannot be *O*-GlcNAcylated at serine residues 159 or 160 but which is still able to dimerize. Unfortunately, mutations of serine residues 159 and 160 of HO-1 have also not yet been found in humans, so that it is not possible to deduce any functional consequences from this either. Similar to the disproportional increase of HO-1 *O*-GlcNAcylation and HO-1 protein level as mentioned above, also the increase in HO-1 homomeric complexes was not proportional to that of HO-1 protein in ammonia-treated rat astrocytes. This implies that the formation of HO-1 homomers is not simply an effect of the upregulation of HO-1 protein in ammonia-treated astrocytes.

While there is clear evidence that HO-1 monomers interact with each other via the dimerization interface, endogenous factors which favour or inhibit this process are currently unknown (Fig. 4.1). A relevant example can be drawn from orthodenticle homeobox 2 (OTX2), which plays a role in several brain disorders. Elevated intracellular levels of OTX2 trigger its oligomerization, which is subsequently degraded by autophagy. Interestingly, *O*-GlcNAcylation of two serine and one threonine residues in OTX2 blocks the interaction between OTX2 monomers, thereby preventing their lysosomal degradation [*581*]. Similarly, *O*-GlcNAcylation has been shown to sterically hinder the interaction of other proteins with their binding

partners. For instance, the transcription factors c-Myc, P53, and Sp1 are known to experience such effects [*352*, *582*, *583*].

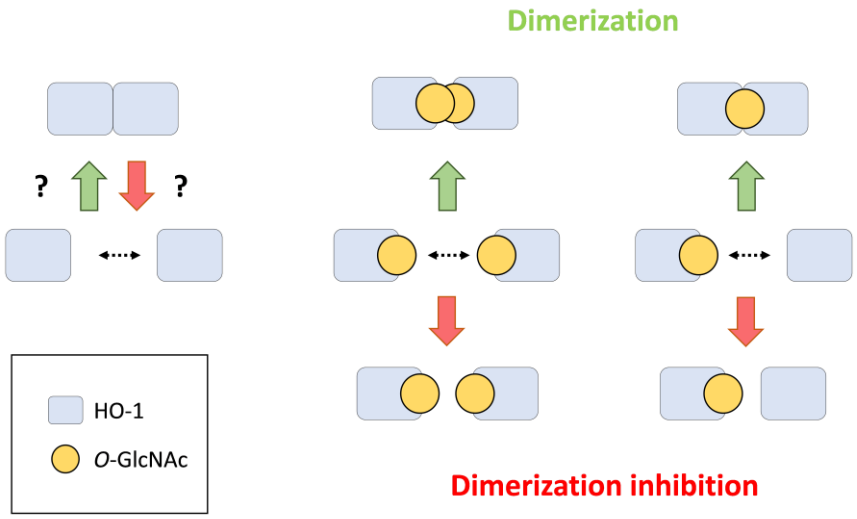

Figure 4.1: Schematic representation of potential the effects of HO-1 *O*-GlcNAcylation on HO-1 dimerization. Two HO-1 monomeric proteins which reside at the ER membrane can interact via their dimerization sites. The *O*-GlcNAcylation of HO-1 may affect this process, depending on whether one or both putative dimerization partners are modified by it.

In the case of c-Myc, it has been proposed that this blocks the access of kinases that mediate phosphorylation in the neighborhood of the *O*-GlcNAcylation site [*584*, *585*]. This prevents interaction with co-factors that are required for c-Myc to bind to DNA target sequences, consequently leading to the suppression of transcription of target genes. In the case of p53, it is proposed that *O*-GlcNAcylation suppresses the binding of p53 to the co-activator p300 [*586*]. This may result in a reduction in the transcription of genes that are essential for the repair of DNA damage or the induction of apoptosis [*587*]. Furthermore, it is postulated that *O*-GlcNAcylation of P53 impedes its interaction with ubiquitinating enzymes, such as MDM2 [*352*]. Consequently, the stability of P53 is increased. With regard to SP1, it is discussed that its *O*-GlcNAcylation inhibits the interaction with histone-modifying enzymes that modify chromatin [*588*]. These include, for example, histone acetyltransferases (HATs).

The inhibition of these interactions subsequently influences the chromatin structure and thus also gene expression.

Conversely, there are also a number of examples in which *O*-GlcNAcylation has been observed to promote or facilitate interactions with other proteins, rather than impeding them. Nevertheless, it remains unclear whether the interaction partners engage in direct interactions with the sugar. It is generally assumed that *O*-GlcNAcylation alters the protein's conformation, thereby enhancing its interaction with the target protein. This interaction can occur with other proteins, including those of the NPC, tau, FOXO1, CREB, and NF-κB [*370*, *376*, *589-591*].

O-GlcNAcylation of nucleoporins (NUPs) has been demonstrated to enhance the interactions between the various nucleoporins that constitute the nuclear pore complex. In the absence of *O*-GlcNAc, the interactions would be less robust, leading to a reduction in the stability of the pore complex. The *O*-GlcNAcylation of these proteins thus facilitates the formation of a functional nuclear pore complex [*376*]. TAU is a microtubule-associated protein. *O*-GlcNAcylation of TAU has been demonstrated to facilitate interactions between TAU and microtubules, thereby promoting the stability of the microtubule network. This modification facilitates the interaction of TAU with microtubules and prevents hyperphosphorylation, which is a key factor in the formation of neurofibrillary tangles and is a significant contributor to Alzheimer's disease pathogenesis [*589*]. FOXO1 is a transcription factor that plays a role in regulating the cell cycle and metabolism [*368*]. *O*-GlcNAcylation of FOXO1 has been demonstrated to enhance the transcription of target genes by facilitating improved interaction with co-activators [*370*]. Similarly, this is also discussed in the context of NF-κB, whose transcriptional activity influences inflammatory processes in particular [*591*]. CREB is a transcription factor that plays a pivotal role in the regulation of gene expression in response to cellular signals. Its *O*-GlcNAcylation can promote its interaction with co-activators such as CBP (CREB-binding protein), which in turn influences the growth and differentiation of cells [*590*].

Moreover, the temporal dynamics of HO-1 homomerization are unclear and also whether this is reversible or not. However, it is well conceivable that this process may depend on the

O-GlcNAcylation of the dimerization interface of the HO-1 monomers. In this regard, the effect of *O*-GlcNAcylation on the interaction of the HO-1 monomers may depend on whether only one or both HO-1 monomers are *O*-GlcNAcylated. For example, an *O*-GlcNAcylated HO-1 molecule may well interact with a non-*O*-GlcNAcylated HO-1, while not interacting with a second *O*-GlcNAcylated HO-1 molecule due to steric hindrance. However, it is also possible that the monomers even dimerize when both are *O*-GlcNAcylated (Fig. 3.13A, B). On the other hand, the *O*-GlcNAcylation of one or two HO-1 monomers may even block HO-1 dimerization. This question could be addressed in future studies using cells expressing HO-1 labelled with fluorescent tags which then are analyzed by superresolution and FRET-microscopy and co-immunoprecipitation and Western blot analysis.

Currently, there is clear evidence that mutations in the transmembrane segment of HO-1 which resides in the ER membrane, inhibits HO-1 homomerization [*428*]. Interestingly, our bioinformatic analyses did not predict any *O*-GlcNAcylation site within this transmembrane segment (Fig. 3.7C, Tab. 3.5, Tab. 3.6) and no such was found by our mass spectrometry investigations. Since HO-1 homomerization increases the stability and catalytic activity of the complex compared to the respective HO-1 monomers [*496*], the present findings may have important implications for ammonia-induced oxidative stress and senescence in astrocytes and for cerebral dysfunction in HE.

The ammonia-induced *O*-GlcNAcylation also triggered the formation of HO-1 heteromers but the interacting proteins were not identified. Already a variety of protein species has been shown to interact with HO-1 under different experimental conditions. These include CPR, poly (ADP-ribose) polymerase, poly (ADP-ribose) glycohydrolase, ubiquitin, caveolin, chromosome region maintenance 1 (CRM1), SPP, CatB, calpain-1, p300/cyclic AMP response element-binding protein and histone deacetylases [*430*, *496*, *510*]. Importantly, the respective interaction and also functional consequences thereof rely on the intracellular localization of HO-1. For example, under hypoxic conditions truncated HO-1 can translocate to the nucleus where it enhances the transcription of antioxidant genes by stabilizing Nrf2 [*430*]. The protein species interacting with HO-1 in the ammonia-treated astrocytes are currently unknown as well as the mode of interaction. Here it remains to be clarified, whether the *O*-GlcNAcylation

of HO-1 or of the interacting protein or of both triggers their interaction. Moreover, the interaction may also be mediated through the *O*-GlcNAcylation of another protein species which may serve as a kind of adapter (Fig. 4.2). It is further unclear, whether HO-1 interacts with further protein species through *O*-GlcNAcylation of the dimerization interface or other *O*-GlcNAcylated serine or threonine residues which were eventually not identified in our mass spectrometry analyses. When considered that more *O*-GlcNAcylation sites are present in HO-1, the respective site may even determine which protein species interact with HO-1.

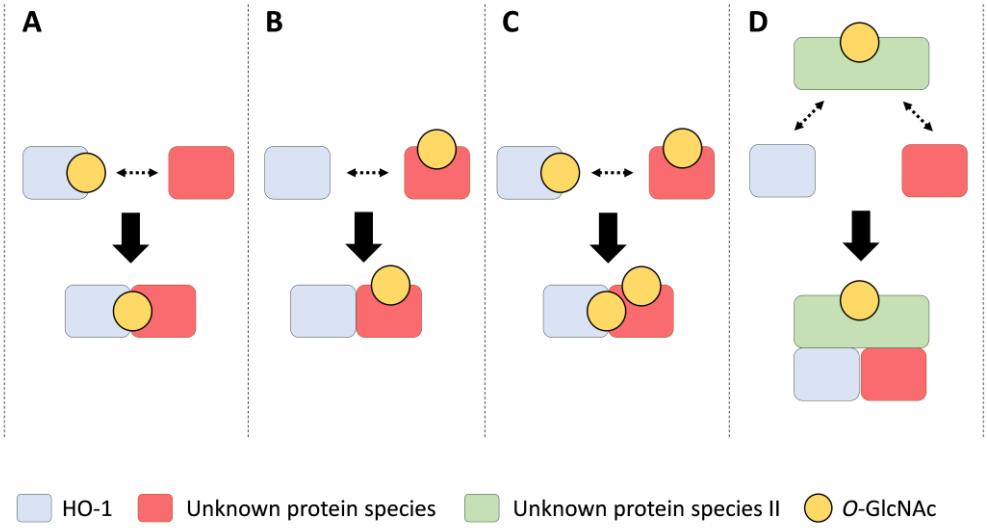

Figure 4.2: Schematic representation of potential effects of protein *O*-GlcNAcylation on HO-1 heteromerization. HO-1 heteromerization may be triggered by *O*-GlcNAcylation of HO-1 itself (**A**), or the interacting protein (**B**) or of both of them (**C**) or through the *O*-GlcNAcylation of a third protein (**D**).

Unraveling these mechanisms by which protein *O*-GlcNAcylation enables HO-1 to form homo- and heteromers may broaden our understanding on the toxic effects of ammonia to astrocytes. This may also help to identify novel therapeutic targets for mitigating ammonia-induced cerebral dysfunction in HE.

4.3 Ammonia enhances the release of truncated HO-1 from astrocytes in an *O*-GlcNAcylation-dependent way from astrocytes

In the present study, 3 distinct anti-HO-1 immunoreactive proteins with molecular weights of approximately 32, 28 and 20 kDa were detected in cultured rat astrocytes. The former two clearly relate to the HO-1 monomer and the 28 kDa truncated HO-1, respectively. However, the 20 kDa HO-1 protein, whose levels were rather low compared to the other two, has not been described so far. There is clear evidence, that the subcellular distribution of the full-length (32 kDa) and the truncated 28 kDa HO-1 variant differs. While the full-length HO-1 resides mainly within the ER membrane and was also occasionally found in mitochondria, the 28 kDa truncated was detected in the nucleus [*429*]. The data of the present study show, that ammonia elevates HO-1 protein levels in the ER, the nuclear membrane and also within the nucleus but not in mitochondria of the astrocytes (Fig. 3.20A, B, Fig. 3.21A, B, Fig. 3.22A). The by far strongest nuclear upregulation of HO-1 was observed in hemin-treated astrocytes (Fig. 3.10A, B). Interestingly, neither ammonia nor hemin led to an increase in the nuclear ratio between 28 kDa and 32 kDa HO-1. This argues against a specific enrichment of the truncated variant in the nucleus (Fig. 3.23). This is likely due to the fact, that nuclear membranes may also contain 32 kDa HO-1 and these membranes are co-enriched by the preparation of the nuclear fraction. In line with this, nuclear extracts devoid of nuclear membranes were strongly enriched for 28 kDa truncated HO-1 when cells were exposed to hypo- or hyperoxia or hemin [*430*, *492*]. The latter studies also clearly indicated that the nuclear accumulation of HO-1 enhanced the transcription of Nrf2-regulated genes in immortalized mouse embryonic fibroblasts [*430*, *492*]. This is in contrast to our observations showing no consistent upregulation of Nrf2-regulated genes in cultured rat astrocytes who were incubated with hemin but also not in those who were incubated with ammonia (Fig. 3.11). This may be explained by insignificant nuclear levels of truncated HO-1 which are insufficient to stabilize Nrf2-dependent gene transcription. These low nuclear 28 kDa HO-1 levels in NH_4Cl, hemin and GlcN-treated astrocytes may also reflect the nuclear export of 28 kDa HO-1 [*430*]. However, it may also indicate that enhanced Nrf2-dependent gene transcription is not solely triggered by nuclear accumulation of truncated HO-1, but rather requires additional factors. This is

suggested by the fact that the investigations mentioned above were performed in immortal cells which strongly differ with regard to primary cells as used in our study. Further research is needed to elucidate the precise role of truncated HO-1 in the nucleus in ammonia, hemin and GlcN-treated astrocytes.

Compared to the nucleus, protein levels of 28 kDa truncated HO-1 were strongly increased and enriched in the supernatants of ammonia-, hemin- or GlcN-treated astrocytes (Fig. 3.24A, Fig. 3.25A). Importantly, inhibiting protein *O*-GlcNAcylation blocked the ammonia-induced release of truncated HO-1 (Fig. 3.24B). Whether the hemin and GlcN-induced HO-1 release is also triggered by protein *O*-GlcNAcylation is currently unknown and remains to be determined. The way HO-1 is released from cells in general is yet not fully clear, but recent studies suggested that HO-1 is present in extracellular vesicles [*549*]. However, neither ammonia, hemin nor GlcN changed the number of EVs or their size in the supernatant of cultured rat astrocytes (Fig. 3.25B). This may suggest that the vesicles contain increased amounts of truncated HO-1. Besides the truncated 28 kDa HO-1 also full-length HO-1 becomes upregulated in the supernatants of ammonia, hemin and GlcN-treated astrocytes (Fig. 4.3). This may further argue for a vesicular release, since full-length HO-1 is anchored to lipid bilayer membranes which vesicles are formed of.

Interestingly, the findings discussed above may have potential relevance for the diagnosis of HE in patients with liver cirrhosis, as HO-1 was also detected in various human biofluids within EVs. These vesicles were mostly derived from the central nervous system (CNS) [*592*] and patients with neurodegenerative disease were found to have increased levels of HO-1 protein in their serum [*593*]. However, numerous other release mechanisms may account for the release of truncated HO-1 such as secretory autophagy. The latter enables the secretion of cytosolic proteins which are lacking N-terminal signal peptides required for secretion by the conventional secretory pathway.

Importantly, cerebral HO-1 mRNA levels were elevated in patients with liver cirrhosis and HE, but not in those without HE [*4*]. It is possible that this is also accompanied by an increased translation of the protein. In this case, HO-1 could be released from brain and its level may

increase in the serum of HE patients. This raises the intriguing possibility that serum HO-1 may serve as a biomarker for the presence of HE in patients with liver cirrhosis.

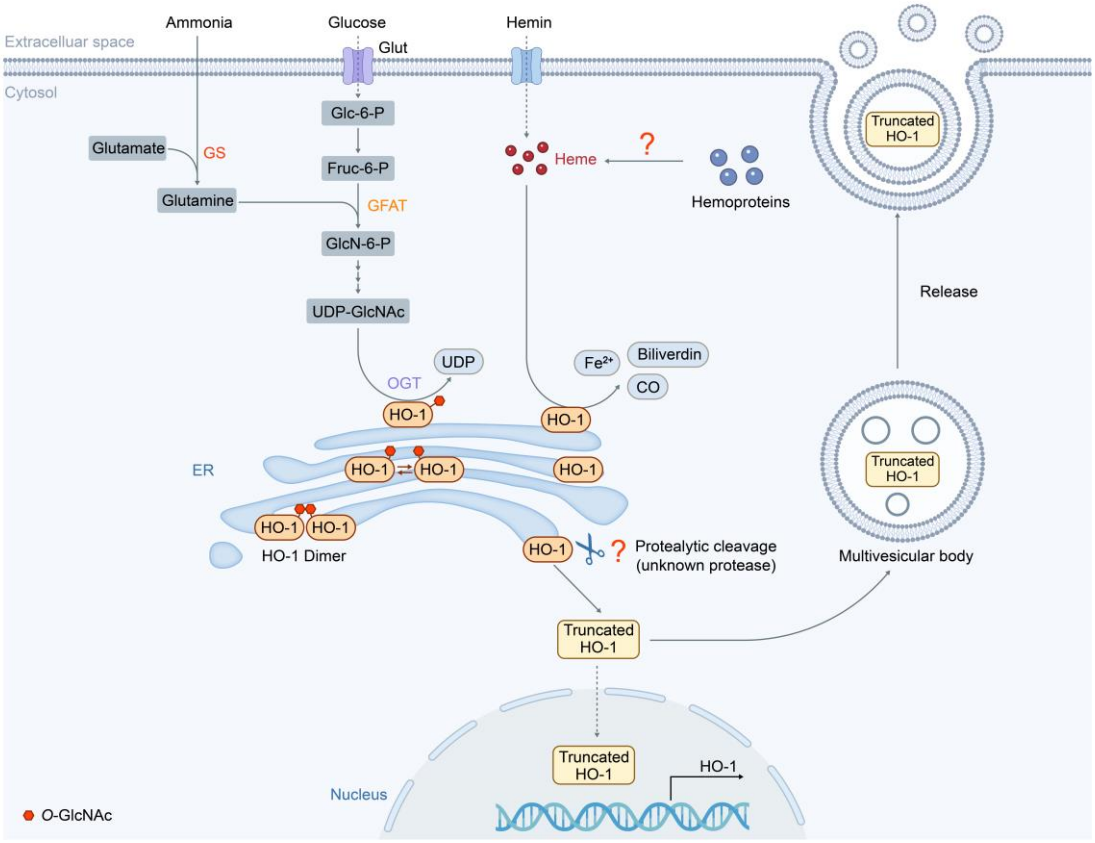

Figure 4.3: Effects of ammonia on intracellular localization and secretion of HO-1. Ammonia elevates the synthesis of UDP-GlcNAc by increasing the synthesis of glutamine in astrocytes. This triggers the *O*-GlcNAcylation of a variety of protein species including full-length HO-1. The latter resides in the ER membrane and its *O*-GlcNAcylation is associated with the formation of HO-1 homomers. HO-1 monomers are cleaved by a currently unknown protease which leads to the generation of truncated 28 kDa HO-1. This cleavage leads to the liberation of HO-1 from the ER into the cytoplasm which then translocates into the nucleus and is being secreted in vesicles into the extracellular space.

In further investigations we aimed to unravel the mechanism underlying the truncation of the full-length 32 kDa HO-1 into the 28 kDa form by ammonia in the astrocytes. Previous studies on several cell lines suggested that full-length HO-1 may be cleaved by a variety of cysteine proteases. These include γ-secretase, calpain, CatB, SPP and p97, the latter of which is part of endoplasmic reticulum-associated degradation (ERAD) pathway [*430*, *550*, *551*]. However, under the experimental setup used in the present study we found no evidence that

these proteases were involved in the NH_4Cl-induced truncation and increased secretion of truncated HO-1 in the astrocytes (Fig. 3.26A). As opposed to the aforementioned findings, we observed that p97 does not cleave full-length HO-1 in the cultured astrocytes. Instead, the inhibition of p97 led to an accumulation of the 28 kDa truncated HO-1 (Fig. 3.27). Moreover, also full-length HO-1 accumulated when p97 was inhibited, which is in line with the current view that full-length HO-1 is degraded by p97 and the ERAD pathway [*594*]. Interestingly, p97/ ERAD inhibition also induced multiple anti-HO-1 immunoreactive signals in Western blot of molecular weights higher than that of the monomer (Fig. 3.26A, B). These signals are most likely indicative of polyubiquitinated HO-1 monomers which are directed to degradation [*594*, *595*].

Importantly, some of the protease inhibitors per se tended to, or even significantly increased the levels of full-length and 28 kDa truncated HO-1 in absence of ammonia. This clearly argues against a role of these proteases for truncation of HO-1 but rather indicates their involvement in its degradation. Therefore, further research is needed to investigate by which mechanism HO-1 is cleaved and released from astrocytes upon ammonia.

In further experiments, it was investigated whether the ammonia-induced increase in extracellular 28 kDa truncated HO-1 could be due to a ROS-mediated cleavage, which may occur at specific amino acid residues [*492*]. This question was addressed *in vitro* using purified recombinant HO-1 incubated with H_2O_2 or hydroxy radical generating compounds. The latter indeed led to the degradation of full-length HO-1, thereby yielding two major fragments of 20 and 15 kDa (Fig. 3.28A, Band II). However, an increase of a 28 kDa fragment was not observed in these experiments which makes it unlikely that reactive oxygen species truncate full-length HO-1 in ammonia-treated rat astrocytes. It is noteworthy, that these experiments do not fully cover the much more complex situation in ammonia-treated astrocytes which includes further reactive oxygen and nitrogen species such as peroxynitrite and its decomposition products and others [*136*]. Interestingly, in the *in vitro* experiments hydroxyl radicals also triggered the formation of covalent higher molecular weight HO-1 complexes (Fig. 3.28A, B). These complexes are most likely triggered through a hydroxyl radical-mediated oxidation of histidine

residues which facilitate a covalent cross-linking between oxidized residues on distinct HO-1 molecules [*596*].

Further research is required to identify the way by which ammonia increases extracellular levels of 28 kDa truncated HO-1. The consequences for neighboring astrocytes or other cells of the nervous system or of other organs also remain to be determined.

In the present study, we identified a 20 kDa HO-1 variant in the astrocytes which is distinct from the well-documented 28 kDa C-terminal truncated [*597*] and the 14 kDa splicing forms [*441*]. This raises intriguing questions regarding the structure, cellular localization and potential functions of the 20 kDa variant. While the 14 kDa form predominantly resides in the cytoplasm, the 28 kDa form exhibits a nuclear localization [*496*]. However, in the present study significant amounts of the 20 kDa variant were only observed in hemin, but not in ammonia or GlcN-treated astrocytes. Therefore, one may speculate that the 20 kDa truncated HO-1 variant is rather unlikely to play an important role in ammonia toxicity and the pathogenesis of HE. However, the insignificant levels of this 20 kDa HO-1 variant in ammonia and GlcN-treated astrocytes may also reflect the detection limit of our analyses. This possibility is supported by the observation that hemin treatment, which upregulated the 20 kDa HO-1 most of all experimental treatments, also induced the strongest upregulation of full-length HO-1 (Fig. 3.10A, B). Moreover, the levels of full-length HO-1 and both forms of truncated HO-1 strongly and positively correlated across all treatment conditions. This may indicate that the processing of the full-length HO-1 and the truncation in general is similar under all experimental treatments.

4.4 Hyperammonemia induced protein *O*-GlcNAcylation and upregulation of HO-1 in rat brain

In contrast to the aforementioned *in vitro* studies on ammonia-treated astrocytes [*4, 144*], it has not yet been investigated whether hyperammonemia is sufficient to trigger protein *O*-GlcNAcylation in rat brain. This is also of particular importance regarding the interpretation of previous findings which showed increased protein *O*-GlcNAcylation in *post mortem* brain

tissue from patients with liver cirrhosis and HE [*4*]. Here, blood ammonia levels as well as comorbidities varied in these patients [*4*]. Previous studies already showed, that *O*-GlcNAcylated protein level strongly differ between different mouse brain regions. Highest levels of *O*-GlcNAcylated proteins were found in the cerebellum and much lower amounts in the hippocampus [*598*]. These findings were similar to our observations in rat brain and may be explained by absence of GFAT1 and lower OGT protein levels when compared to the cerebellum (Fig. 3.29C, D).

Hyperammonemia strongly increased the levels of *O*-GlcNAcylated proteins in the cerebellum but only slightly in the hippocampus (Fig. 3.29A, B). Interestingly, GFAT1 or 2 protein levels did not change in hyperammonemic rats (Fig. 3.29C, D). This may indicate that substrate availability for the synthesis of UDP-GlcNAc within the hexosamine biosynthetic pathway may be the limiting factor for protein *O*-GlcNAcylation in rat brain. These results are in contrast to findings from cultured rat astrocytes where ammonia upregulated GFAT1 and 2 [*4*]. These differences can be explained by technical limitation of the Western blot technique, in which cell type-specific differences cannot be differentiated. To address this question, immunofluorescence analyses or single cell analyses on dissociated brain cells could be performed in future studies.

Protein *O*-GlcNAcylation was suggested to upregulate HO-1 protein in ammonia-exposed rat astrocytes [*4*]. The present study shows that HO-1 is upregulated in the cerebellum, but not in the hippocampus of hyperammonemic rats (Fig. 3.29E, F). Unchanged HO-1 protein level in the hippocampus of hyperammonemic rats may be due to several reasons. First, the low protein *O*-GlcNAcylation level in the hippocampus may be insufficient to upregulate HO-1. Moreover, protein species which upregulate HO-1 protein in the hippocampus may be *O*-GlcNAcylated in the cerebellum, but not in the hippocampus. Furthermore, the Western blot analysis may be insufficient to detect subtle changes which are present in the astrocytes in the tissue protein lysates from the hippocampus.

Surprisingly, truncated HO-1 was not detected in cerebral protein lysates from either control or hyperammonemic rats from any brain region analyzed. This may suggest that similar

to the *in vitro* findings on cultured rat astrocytes, truncated HO-1 may also be released from the cells in the brain and transported with the blood stream. Consistent with previous reports demonstrating that HO-1 triggers ER stress in ammonia-exposed astrocytes [*4*], also the ER stress marker GRP78 was significantly upregulated in the cerebellum, but not the hippocampus, of hyperammonemic rats (Fig. 3.29E, F).

Interestingly, in mice, decreased cerebral *O*-GlcNAcylation due to genetic ablation of OGT was found to affect motor skills and cause ataxia, extensor rigidity, and posture abnormalities [*599*]. This was suggested a consequence of oxidative stress which was triggered by mitochondrial dysfunction [*599*]. In view of these findings, one may speculate, that contrary to what was found in ammonia-exposed astrocytes *in vitro*, increased protein *O*-GlcNAcylation in the cerebellum of hyperammonemic rats may rather protect against oxidative stress. However, genetic ablation of OGT will abolish the *O*-GlcNAcylation of all proteins of the *O*-GlcNAcome in all cerebral cell types at the same time. This must disturb multiple cellular pathways and cell-cell interactions simultaneously and therefore does not allow to draw the conclusion that protein *O*-GlcNAcylation per se protects against oxidative stress.

4.5 Targeting protein *O*-GlcNAcylation and HO-1 for the treatment of HE in patients with liver cirrhosis

The present findings are in line with previous studies who strengthened the view that targeting protein *O*-GlcNAcylation may be promising for the treatment of HE. Here, inhibition of protein *O*-GlcNAcylation in astrocytes may prevent NOX4-dependent oxidative stress and senescence which both were suggested to underlie cerebral dysfunction in HE [*1*, *4*, *69*, *76*, *142*]. However, non-specific systemic inhibition of protein *O*-GlcNAcylation is likely to cause unwanted side effects in organs other than the brain. For example, a recent study suggested an important role of protein *O*-GlcNAcylation for urea synthesis in the liver. Here it was shown that *O*-GlcNAcylation of CPS1 enhances its catalytic efficiency and increases ammonia detoxification in the liver, thereby reducing blood ammonia levels [*388*]. In view of these findings, global

inhibition of protein *O*-GlcNAcylation in patients with impaired liver function may further decrease the ability of the liver to detoxify ammonia.

It is also currently unclear, whether HO-1 may serve as a therapeutic target for the treatment of HE in patients with liver cirrhosis. Interestingly, systemic inhibition of HO-1 by zinc protoporphyrin lowered portal vein pressure, decreased ammonia levels in both plasma and brain, ameliorated the upregulation of HO-1 in brain and cerebral edema in bile duct ligated rats [*513*]. These findings suggest, that beneficial effects of HO-1 inhibition outside the brain such as in the liver are underlying the cerebral improvements observed in this animal model. However, these effects may be specific to animal model, and knockout animal models would be needed to assess how cerebral HO-1 contribute to the pathogenesis of HE. Unfortunately, studies employing such animal models are currently missing. It further remains to be investigated, whether truncated HO-1 which is released from astrocytes in a protein *O*-GlcNAcylation-dependent way contributes to cerebral dysfunction in HE.

The present findings raise the intriguing possibility that truncated HO-1 may serve as a biomarker for cerebral dysfunction in patients with liver cirrhosis and therefore for the presence of HE. Accordingly, this may be an important tool for early diagnosis and monitoring of disease progression. Such investigations must target HO-1 originating from the brain by isolating astrocyte-secreted extracellular vesicles as shown earlier for neurodegenerative diseases [*549*]. In this way, HO-1 which originates from other dysfunctional organs of patients with liver failure can be excluded from the analysis.

4.6 Limitations of the present work

In the present study, over 300 protein species were identified that were *O*-GlcNAcylated in cultured rat astrocytes by mass spectrometry. This requires further verification by other technical approaches such as by detecting the respective protein species in Click-iT-purified samples by Western blot. Unfortunately, this approach will not detect systematic errors resulting from the technical approach purifying *O*-GlcNAcylated proteins by the Click-iT. A more

reliable approach would be to immunoprecipitate the protein species to be tested and to confirm its *O*-GlcNAcylation by mass spectrometry or by anti-*O*-GlcNAc Western blot. Both methods are well suited to confirm the *O*-GlcNAcylation of a single protein, but technical issues limit their use to prove the opposite. It is clear that physicochemical properties of a protein or protein fragment may impair its detectability. This issue may also apply to the fact that HO-1 was not detected by MS in Click-iT purifications of ammonia-treated astrocytes but reproducibly detected when samples were analysed by anti-HO-1 Western blot. Regarding mass spectrometry, it is possible that with this technique one may not detect the glycosylated variant, although the corresponding non-glycosylated form is easily found. However, also Western blot analysis may produce false-negative results, as the epitopes that are recognized by the available antibodies directed against *O*-GlcNAc (CD110.6 and RL-2) are not clearly defined and may not be common to every *O*-GlcNAcylated protein. Moreover, no consensus sequence for *O*-GlcNAcylation has been identified to date.

The mass spectrometry data for the control and NH_4Cl-treated samples were not analyzed in pairs, and no fold-value was calculated for each independent preparation. As a result, different *O*-GlcNAcylation levels in the various preparations or experiments may significantly affect the statistics. The discrepancy between the number of protein species identified in the comparison of the samples 'NH_4Cl' vs 'NH_4Cl background' (over 300) and the number of significantly different protein species in the comparison of 'control' and 'NH_4Cl' (approximately 70) may be attributed to the inherent variability observed in the data.

Additionally, some protein species that were significantly increased in the NH_4Cl-treated samples compared to the control were not significantly increased when NH_4Cl-treated samples were compared to the respective background control. This may also be explained by an insufficient statistical power.

It is important to note that the MS analysis did not take into account the levels of different protein species, which may explain why some protein species showed less *O*-GlcNAcylation after exposure to ammonia. In this instance, the observed reduction in *O*-GlcNAcylation may simply reflect a reduction in the amount of protein for the respective species. Correspondingly,

an increase in the amount of a protein species could lead to a higher amount of *O*-GlcNAcylated protein. However, this cannot account for the increased *O*-GlcNAcylation of HO-1 observed in this study, as the *O*-GlcNAcylation was not directly proportional, but rather disproportionate to the increase in HO-1 protein quantity. Here, it further remains to be investigated, whether the *O*-GlcNAcylation of HO-1 alters its catalytic activity. In view of findings from the literature, one would assume that the increased homomerization of HO-1 in ammonia-treated astrocytes may enhance its stability and catalytic activity.

It is further important to clarify in future studies which protein species interact with HO-1 in ammonia-treated rat astrocytes. According to our Western blot analyses, HO-1 interacts with a large number of other proteins in addition to itself. Further investigations are currently underway using a tagged HO-1 that can be easily precipitated. Here, HO-1 variants were produced in addition to the wild-type form, with mutations introduced to prevent or mimic *O*-GlcNAcylation at the putative *O*-GlcNAcylation sites serine 159 and serine 160. This will clarify, whether the interaction of HO-1 with itself and other proteins relies on the identified *O*-GlcNAcylation site close to the dimerization site.

Future studies will also have to investigate consequences of the release of truncated HO-1 (28 kDa) on neighboring cells. It is conceivable that this may trigger pleiotropic effects and either induce oxidative and ER stress and senescence or has anti-inflammatory actions as suggested before. This could be tested by overexpressing and purifying the truncated HO-1 and applying it to astrocyte cultures.

Further investigations are necessary to determine which protein species are affected by altered *O*-GlcNAcylation in the brains of animal models of HE and in the brains of liver cirrhosis patients with HE. Once this has been established, potential consequences of the altered cerebral *O*-GlcNAcylation for cerebral dysfunction in HE can be investigated by *in vitro* and *in vivo* experiments. It is suggested, that this will greatly enhance our understanding on the role of cerebral *O*-GlcNAcylation on the pathogenesis of HE.

5. Literature

[1] Häussinger, D., Dhiman, R.K., Felipo, V., Görg, B., Jalan, R., Kircheis, G., Merli, M., Montagnese, S., Romero-Gomez, M., Schnitzler, A., Taylor-Robinson, S.D., & Vilstrup, H. (2022). "Hepatic encephalopathy." *Nat Rev Dis Primers*. 8(1): p.43. 10.1038/s41572-022-00366-6.

[2] Hart, G.W. (2019). "Nutrient regulation of signaling and transcription." *J Biol Chem*. 294(7): p.2211-2231. 10.1074/jbc.AW119.003226.

[3] Chiang, S.K., Chen, S.K., Chang, L.C. (2021). "The Role of HO-1 and Its Crosstalk with Oxidative Stress in Cancer Cell Survival." *Cells*, 10(9):2401. 10.3390/cells10092401.

[4] Görg, B., Karababa, A., Schütz, E., Paluschinski, M., Schrimpf, A., Shafigullina, A., Castoldi, M., Bidmon, H.J., Häussinger, D. (2019). "*O*-GlcNAcylation-dependent upregulation of HO1 triggers ammonia-induced oxidative stress and senescence in hepatic encephalopathy." *J Hepatol*. 71(5): p.930-941. 10.1016/j.jhep.2019.06.020.

[5] Abraham, N.G. and Kappas, A. (2008). "Pharmacological and clinical aspects of heme oxygenase." *Pharmacol Rev*. 60(1): p.79-127. 10.1124/pr.107.07104.

[6] Häussinger, D. and Sies, H. (2013). "Hepatic encephalopathy: clinical aspects and pathogenetic concept." *Arch Biochem Biophys*. 536(2): p.97-100. 10.1016/j.abb.2013.04.013.

[7] Munoz-Sanchez, J. and Chanez-Cardenas, M.E. (2014). "A review on hemeoxygenase-2: focus on cellular protection and oxygen response." *Oxid Med Cell Longev*. p.604981. 10.1155/2014/604981.

[8] Conn, H.O., Leevy, C.M., Vlahcevic, Z.R., Rodgers, J.B., Maddrey, W.C., Seeff, L., Levy, L.L. (1977). "Comparison of lactulose and neomycin in the treatment of chronic portal-systemic encephalopathy." A double blind controlled trial. *Gastroenterology*. 72(4 Pt 1): p.573-83.

[9] Ruan, H.B., Singh, J.P., Li, M.D., Wu, J., Yang, X. (2013). "Cracking the *O*-GlcNAc code in metabolism." *Trends Endocrinol Metab*. 24(6): p.301-9. 10.1016/j.tem.2013.02.002.

[10] Hart, G.W., Slawson, C., Ramirez-Correa, G., Lagerlof, O. (2011). "Cross talk between *O*-GlcNAcylation and phosphorylation: roles in signaling, transcription, and chronic disease." *Annu Rev Biochem*. 80: p.825-58. 10.1146/annurev-biochem-060608-10251.

[11] Waza, A.A., Hamid, Z., Ali, S., Bhat, S.A., Bhat, M.A. (2018). "A review on heme oxygenase-1 induction: is it a necessary evil." *Inflamm Res*. 67(7): p.579-588. 10.1007/s00011-018-1151-x.

[12] Görg, B., Schliess, F., Häussinger, D. (2013). "Osmotic and oxidative/nitrosative stress in ammonia toxicity and hepatic encephalopathy." *Arch Biochem Biophys*. 536(2): p.158-63. 10.1016/j.abb.2013.03.010.

[13] Asrani, S.K., Devarbhavi, H., Eaton, J., Kamath, P.S. (2019). "Burden of liver diseases in the world." *J Hepatol*. 70(1): p.151-171. 10.1016/j.jhep.2018.09.014.

[14] Poordad, F.F. (2007). "Review article: the burden of hepatic encephalopathy." *Aliment Pharmacol Ther*. 25 Suppl 1: p.3-9. 10.1111/j.1746-6342.2006.03215.x.

[15] Koch, A., Herbers, U. (2016). "Erkrankungen der Leber." *E&M Ernährung und Medizin*. p.57– 61.

[16] Jablonowski, H. (2014). "Hepatische Enzephalopathie." *Thieme Praxis Report*. p.6(1): 1–16.

[17] Romero-Gómez, M., Boza, F., Garcia-Valdecasas, M.S., Garcia, E., Aguilar-Reina, J. (2001) "Subclinical hepatic encephalopathy predicts the development of overt hepatic encephalopathy." *Am J Gastroenterol*. p.96(9): 2718 –23. 10.1111/j.1572-0241.2001.04130.x.

[18] Das, A., Dhiman, R.K., Saraswat, V.A., Verma, M., Naik, S.R. (2001). "Prevalence and natural history of subclinical hepatic encephalopathy in cirrhosis." *J Gastroenterol Hepatol*. p.16(5): 531– 5. 10.1046/j.1440-1746.2001.02487.x.

[19] The Burden of Gastrointestinal Diseases. (2001). "Bethesda, Maryland." *American Gastroenterological Association*. p.41-2.

[20] Acharya, C. and Bajaj, J.S. (2018). "Current Management of Hepatic Encephalopathy." *Am J Gastroenterol*. 113(11): p.1600-1612. 10.1038/s41395-018-0179-4.

[21] Wang, F.S., Fan, J.G., Zhang, Z., Gao, B., Wang, H.Y. (2014). "The global burden of liver disease: the major impact of China." *Hepatology*. 60(6): p.2099-108. 10.1002/hep.27406.

[22] Lauridsen, M.M., Jepsen, P. and Vilstrup, H. (2011). "Critical flicker frequency and continuous reaction times for the diagnosis of minimal hepatic encephalopathy: a comparative study of 154 patients with liver disease." *Metab Brain Dis*. 26(2): p.135-9. 10.1007/s11011-011-9242-1.

[23] Kircheis, G., Knoche, A., Hilger, N., Manhart, F., Schnitzler, A., Schulze, H., Häussinger, D. (2009). "Hepatic encephalopathy and fitness to drive." *Gastroenterology*. 137(5):1706-15.e1-9. 10.1053/j.gastro.2009.08.003.

[24] Vilstrup, H., Amodio, P., Bajaj, J., Cordoba, J., Ferenci, P., Mullen, K.D., Weissenborn, K., Wong, P. (2014). "Hepatic encephalopathy in chronic liver disease: 2014 Practice Guideline by the American Association for the Study of Liver Diseases and the European Association for the Study of the Liver." *Hepatology*. 60(2): p.715-35. 10.1002/hep.27210.

[25] Bajaj, J.S., O'Leary, J.G., Tandon, P., Wong, F., Garcia-Tsao, G., Kamath, P.S., Maliakkal, B., Biggins S.W., Thuluvath, P.J., Fallon, M.B., Subramanian, R.M., Vargas, H.E., Lai, J., Thacker, L.R., Reddy, K.R. (2017). "Hepatic Encephalopathy Is Associated With Mortality in Patients With Cirrhosis Independent of Other Extrahepatic Organ Failures." *Clin Gastroenterol Hepatol*. 15(4): p.565-574 e4. 10.1016/j.cgh.2016.09.157.

[26] Lucidi, C., Corradini, S.G., Abraldes, J.G., Merli M., Tandon, P., Ferri, F., Parlati, L., Lattanzi, B., Poli, E., Gregorio, V.D., Farcomeni, A., Riggio, O. (2016). "Hepatic encephalopathy expands the predictivity of model for end-stage liver disease in liver transplant setting: Evidence by means of 2 independent cohorts." *Liver Transpl*. 22(10): p.1333-42. 10.1002/lt.24517.

[27] Prasad, S., Dhiman, R.K., Duseja, A., Chawla, Y.K., Sharma, A., Agarwal, R. (2007). "Lactulose improves cognitive functions and health-related quality of life in patients with cirrhosis who have minimal hepatic encephalopathy." *Hepatology*. 45(3): p.549-59. 10.1002/hep.21533.

[28] Weissenborn, K. (2015). "Diagnosis of minimal hepatic encephalopathy." *J Clin Exp Hepatol*. 5(Suppl 1): p.S54-9. 10.1016/j.jceh.2014.06.005.

[29] Bajaj, J.S., Heuman, D.M., Sterling, R.K., Sanyal, A.J., Siddiqui, M., Matherly, S., Luketic, V., Stravitz, R.T., Fuchs, M., Thacker, L.R., Gilles, H.C., White, M.B., Unser, A., Hovermale, J., Gavis, E., Noble, N.A., Wade, J.B. (2015). "Validation of EncephalApp, Smartphone-Based Stroop Test, for the Diagnosis of Covert Hepatic Encephalopathy." *Clin Gastroenterol Hepatol*. 13(10): p. 1828-1835 e1. 10.1016/j.cgh.2014.05.011.

[30] Amodio, P., Piccolo, F.D., Marchetti, P., Angeli, P., Lemmolo, R., Caregaro, L., Merkel, C., Gerunda, G., Gatta, A. (1999). "Clinical features and survivial of cirrhotic patients with subclinical cognitive alterations detected by the number connection test and computerized psychometric tests." *Hepatology*. 29(6): p.1662-7. 10.1002/hep.510290619.

[31] Lauridsen, M.M., Thiele, M., Kimer, N., Vilstrup, H. (2013). "The continuous reaction times method for diagnosing, grading, and monitoring minimal/covert hepatic encephalopathy." *Metab Brain Dis*. 28(2): p.231-4. 10.1007/s11011-012-9373-z.

[32] Bajaj, J.S., Saeian, K., Verber, M.D., Hischke, D., Hoffmann, R.G., Franco, J., Varma, R.R., Rao, S.M. (2007). "Inhibitory control test is a simple method to diagnose minimal hepatic encephalopathy and predict development of overt hepatic encephalopathy." *Am J Gastroenterol*. 102(4): p.754-60. 10.1111/j.1572-0241.2007.01048.x.

[33] Bandookwala, M. and Sengupta, P. (2020). "3-Nitrotyrosine: a versatile oxidative stress biomarker for major neurodegenerative diseases." *Int J Neurosci*. 130(10): p.1047-1062. 10.1080/00207454.2020.1713776.

[34] Kircheis, G., Wettstein, M., Timmermann, L., Schnitzler, A., Häussinger, D. (2002). "Critical flicker frequency for quantification of low-grade hepatic encephalopathy." *Hepatology*. 35(2): p.357-66. 10.1053/jhep.2002.30957.

[35] Weissenborn, K., Ennen, J.C., Schomerus, H., Rückert, N., Hecker, H. (2001). "Neuropsychological characterization of hepatic encephalopathy." *J Hepatol*. 34(5): p.768-73. 10.1016/s0168-8278(01)00026-5.

[36] Häussinger, D., Kircheis G. (2006). "Hepatic encephalopathy." *Praxis* (*Bern 1994*). 95(40): p. 1543-9.

[37] Christopher, C.F., Amodio, P., Bajaj, J.S., Dhiman, R.K., Montagnese, S., Taylor-Robinson, S.D., Vilstrup, H., Jalan, R. (2020). "Hepatic encephalopathy: Novel insights into classification, pathophysiology and therapy." *Journal of Hepatology*. 73(6): p.1526-1547. 10.1016/j.jhep.2020.07.013.

[38] Patwardhan, V.R., Jiang, Z.G., Risech-Neiman, Y., Piatkowski, G., Afdhal, N.H., Mukamal, K., Curry, M.P., Tapper, E.B. (2016). "Serum Ammonia is Associated With Transplant-free Survival in Hospitalized Patients With Acutely Decompensated Cirrhosis [corrected]." *J Clin Gastroenterol*. 50(4): p.345-50. 10.1097/mcg.0000000000000443.

[39] Vierling, J.M., Mokhtarani, M., Brown Jr, R.S., Mantry, P., Rockey, D.C., Ghabril, M., Rowell, R., Jurek, M., Coakley, D.F., Scharschmidt, B.F. (2016). "Fasting Blood Ammonia Predicts Risk and Frequency of Hepatic Encephalopathy Episodes in Patients With Cirrhosis." *Clin Gastroenterol Hepatol*. 14(6): p.903-906 e1. 10.1016/j.cgh.2015.11.018.

[40] Montoliu, C., Cauli, O., Urios, A., ElMlili, N., Serra, M.A., Giner-Duran, R. González-Lopez, O., Olmo, J.A.D., Wassel, A., Rodrigo, J.M., Felipoet, V. (2011). "3-nitro-tyrosine as a peripheral biomarker of minimal hepatic encephalopathy in patients with liver cirrhosis." *Am J Gastroenterol*. 106(9): p.1629-37. 10.1038/ajg.2011.123.

[41] Montoliu, C., Piedrafita, B., Serra, M.A., Olmo, J.A.D., Urios, A., Rodrigo, J.M., Felipo, V. (2009). "IL-6 and IL-18 in blood may discriminate cirrhotic patients with and without minimal hepatic encephalopathy." *J Clin Gastroenterol*. 43(3): p.272-9. 10.1097/mcg.0b013e31815e7f58.

[42] Häussinger, D. (1998). "Pathogenesis and treatment of chronic hepatic encephalopathy." *Digestion*. 59 Suppl 2: p.25-7. 10.1159/000051416.

[43] Cordoba, J., Ventura-Cots M., Simón-Talero, M., Amorós, À., Pavesi, M., Vilstrup, H., Angeli, P., Domenicali, M., Ginés, P., Bernardi, M., Arroyo, V. (2014). "Characteristics, risk factors, and mortality of cirrhotic patients hospitalized for hepatic encephalopathy with and without acute-on-chronic liver failure (ACLF)." *J Hepatol*. 60(2): p.275-81. 10.1016/j.jhep.2013.10.004.

[44] Amodio, P., Bemeur, C., Butterworth, R., Cordoba, J., Kato, A., Montagnese, S., Uribe, M., Vilstrup, H., Morgan, M.Y. (2013). "The nutritional management of hepatic encephalopathy in patients with cirrhosis: International society for hepatic encephalopathy and nitrogen metabolism consensus." *Hepatology*. 58(1): p.325-336. 10.1002/hep.26370.

[45] Shawcross, D.L., Sharifi, Y., Canavan, J.B, Yeoman, A.D., Abeles, R.D., Taylor, N.J., Auzinger, G., Bernal, W., Wendon, J.A. (2011). "Infection and systemic inflammation, not ammonia, are

associated with Grade 3/4 hepatic encephalopathy, but not mortality in cirrhosis." *Journal of Hepatology*. 54(4): p.640-649. 10.1016/j.jhep.2010.07.045.

[46] Riggio, O., Nardelli, S., Gioia, S., Lucidi, C., Merli, M. (2015). "Management of hepatic encephalopathy as an inpatient." *Clinical Liver Disease*. 5(3): p.79-82. 10.1002/cld.457.

[47] Jalan, R. and Kapoor, D. (2004). "Reversal of diuretic-induced hepatic encephalopathy with infusion of albumin but not colloid." *Clin Sci* (*Lond*). 106(5): p.467-74. 10.1042/cs20030357.

[48] Dam, G., Vilstrup, H., Watson, H., Jepsen, P. (2016). "Proton pump inhibitors as a risk factor for hepatic encephalopathy and spontaneous bacterial peritonitis in patients with cirrhosis with ascites." *Hepatology*. 64(4): p.1265-72. 10.1002/hep.28737.

[49] Nardelli, S., Gioia, S., Ridola, L., Farcomeni, A., Merli, M., Riggio, O. (2019). "Proton Pump Inhibitors Are Associated With Minimal and Overt Hepatic Encephalopathy and Increased Mortality in Patients With Cirrhosis." *Hepatology*. 70(2): p.640-649. 10.1002/hep.30304.

[50] Gupta, A., Dhiman, R.K., Kumari, S., Rana, S., Agarwal, R., Duseja, A., Chawla, Y. (2010). "Role of small intestinal bacterial overgrowth and delayed gastrointestinal transit time in cirrhotic patients with minimal hepatic encephalopathy." *J Hepatol*. 53(5): p.849-55. 10.1016/j.jhep.2010.05.017.

[51] Vom Dahl, S., Kircheis, G. and Häussinger, D. (2001). "Hepatic encephalopathy as a complication of liver disease." *World J Gastroenterol*. 7(2): p.152-6. 10.3748/wjg.v7.i2.152.

[52] Dhiman, R.K., Sawhney, M.S., Chawla, Y.K., Das, G., Ram, S., Dilawari, J.B. (2000). "Efficacy of lactulose in cirrhotic patients with subclinical hepatic encephalopathy." *Dig Dis Sci*. 45(8): p.1549-52. 10.1023/a:1005556826152.

[53] Strauss, E., Tramote, R., Silva, E.P., Caly, W.R., Honain, N.Z., Maffei, R.A., de Sá, M.F. (1992). "Double-blind randomized clinical trial comparing neomycin and placebo in the treatment of exogenous hepatic encephalopathy." *Hepatogastroenterology*. 39(6): p.542-5.

[54] Bass, N.M., Mullen, K.D., Sanyal, A., Poordad, F., Neff, G., Leevy, C.B., Sigal, S., Sheikh, M.Y., Beavers, K., Frederick, T., Teperman, L., Hillebrand, D., Huang, S., Merchant, K., Shaw, A. Bortey, E., Forbes, W.P., (2010). "Rifaximin treatment in hepatic encephalopathy." *N Engl J Med*. 362(12): p.1071-81. 10.1056/nejmoa0907893.

[55] Bianchi, G.P., Marchesini, G., Fabbri, A., Rondelli, A., Bugianesi, E., Zoli, M., Pisi, E. (1993). "Vegetable versus animal protein diet in cirrhotic patients with chronic encephalopathy. A randomized cross-over comparison." *J Intern Med*. 233(5): p.385-92. 10.1111/j.1365-2796.1993.tb00689.x.

[56] Reding, P., Duchateau, J., Bataille, C. (1984). "Oral zinc supplementation improves hepatic encephalopathy. Results of a randomised controlled trial." *Lancet*. 2(8401): p.493-5. 10.1016/s0140-6736(84)92567-4.

[57] Als-Nielsen, B., Gluud, L.L., Gluud, C. (2004). "Benzodiazepine receptor antagonists for hepatic encephalopathy." *Cochrane Database of Systematic Reviews*. (2):p.CD002798.10.1002/14651858.cd002798.pub2.

[58] Gluud, L.L., Dam, G., Borre, M., Les, I., Cordoba, J., Marchesini, G., Aagaard, N.K., Risum, N., Vilstrup, H. (2013). "Oral branched-chain amino acids have a beneficial effect on manifestations of hepatic encephalopathy in a systematic review with meta-analyses of randomized controlled trials." *J Nutr*. 143(8): p.1263-8. 10.3945/jn.113.174375.

[59] Bai, M., He, C., Yin, Z., Niu, J., Wang, Z., Qi, X., Liu, L., Yang, Z., Guo, W., Tie, J., Bai, W., Xia, J., Cai, H., Wang, J., Wu, K., Fan, D., Han, G. (2014). "Randomised clinical trial: L-ornithine-L-aspartate reduces significantly the increase of venous ammonia concentration after TIPSS." *Aliment Pharmacol Ther*. 40(1): p.63-71. 10.1111/apt.12795.

[60] Rahimi, R.S., Singal, A.G., Cuthbert, J.A., Rockey, D.C. (2014). "Lactulose vs polyethylene glycol 3350-electrolyte solution for treatment of overt hepatic encephalopathy: the HELP randomized clinical trial." *JAMA Intern Med*. 174(11): p.1727-33. 10.1001/jamainternmed.2014.4746.

[61] Bajaj, J.S., Kassam, Z., Fagan, A., Gavis, E.A., Liu, E., Cox, I.J., Kheradman, R., Heuman, D., Wang, J., Gurry, T., Williams, R., Sikaroodi, M, Fuchs, M., Alm, E., John, B., Thacker, L.R., Riva, A., Smith, M., Taylor-Robinson S.D., Gillevet, P.M. (2017). "Fecal microbiota transplant from a rational stool donor improves hepatic encephalopathy: A randomized clinical trial." *Hepatology*. 66(6): p.1727-1738. 10.1002/hep.29306.

[62] Bosoi, C.R., Parent-Robitaille, C., Anderson, K., Tremblay, M., Rose, C.F. (2011). "AST-120 (spherical carbon adsorbent) lowers ammonia levels and attenuates brain edema in bile duct-ligated rats." *Hepatology*. 53(6): p.1995-2002. 10.1002/hep.24273.

[63] Wiest, R., Albillos A., Trauner, M., Bajaj, J.S., Jalan, R. (2017). "Targeting the gut-liver axis in liver disease." *J Hepatol*. 67(5): p.1084-1103. 10.1016/j.jhep.2017.05.007.

[64] Safadi, R., Rahimi, R.S., Thabut, D., Bajaj, J.S., Bhamidimarri, K.R., Pyrsopoulos, N., Potthoff, A., Bukofzer, S., Wang, L., Jamil, K., Devarakonda, K.R. (2022). "Pharmacokinetics/ pharmacodynamics of L-ornithine phenylacetate in overt hepatic encephalopathy and the effect of plasma ammonia concentration reduction on clinical outcomes." *Clin Transl Sci*. 15(6): p.1449-1459. 10.1111/cts.13257.

[65] Maestri, N.E., Brusilow, S.W., Clissold, D.B., Bassett, S.S. (1996). "Long-term treatment of girls with ornithine transcarbamylase deficiency." *The New England Journal of Medicine*. 335(12): p.855-9. 10.1056/nejm199609193351204.

[66] Hassanein, T.I., Tofteng, F., Brown Jr, R.S., McGuire, B., Lynch, P., Mehta, R., Larsen, F.S., Gornbein, J., Stange, J., Blei, A.T. (2007). Randomized controlled study of extracorporeal albumin dialysis for hepatic encephalopathy in advanced cirrhosis. *Hepatology*. 46(6): p. 1853-62.

[67] Agarwal, B., Cañizares, R.B., Saliba, F., Ballester, M.P., Tomescu, D.R., Martin, D., Stadlbauer, V., Wright, G., Sheikh, M., Morgan, C., Alzola, C., Lavin, P., Green, D., Kumar, R., Sacleux, S.C., Schilcher, G., Koball, S., Tudor, A., Minten, J., Domenech, G., Aragones J.J., Oettl, K., Paar, M., Waterstradt, K., Bode-Boger, S.M., Ibáñez-Samaniego, L., Gander, A., Ramos, C., Chivu, A., Stange, J., Lamprecht, G., Sanchez, M., Mookerjee, R.P., Davenport, A., Davies, N., Pavesi, M., Andreola, F., Albillos, A., Cordingley, J., Schmidt, H., Carbonell-Asins, J.A., Arroyo, V., Fernandez, J., Mitzner, S., Jalan, R. (2023). "Randomized, controlled clinical trial of the DIALIVE liver dialysis device versus standard of care in patients with acute-on- chronic liver failure." *J Hepatol*. 79(1): p.79-92. 10.1016/j.jhep.2023.03.013.

[68] European Association for the Study of the Liver. (2016). "EASL clinical practice guidelines: liver transplantation." *J Hepatol*. 64: p.433-485.

[69] Görg, B., Karababa, A., Shafigullina, A., Bidmon, H.J., Häussinger, D. (2015). "Ammonia-induced senescence in cultured rat astrocytes and in human cerebral cortex in hepatic encephalopathy." *Glia*. 63(1): p.37-50. 10.1002/glia.22731.

[70] Häussinger, D. and Blei, A.T. (2007). "Hepatic encephalopathy." *The Oxford Textbook of Hepatology*, p.728-760.

[71] Schiodt, F.V., Bondesen, S., Tygstrup, N., Christensen, E. (1999). "Prediction of hepatic encephalopathy in paracetamol overdose: a prospective and validated study." *Scand J Gastroenterol*. 34(7): p.723-8. 10.1080/003655299750025949.

[72] Tapper, E.B., Henderson J.B., Parikh N.D., N Ioannou, G., Lok, A.S. (2019). "Incidence of and Risk Factors for Hepatic Encephalopathy in a Population-Based Cohort of Americans With Cirrhosis." *Hepatol Commun*. 3(11): p.1510-1519. 10.1002/hep4.1425.

[73] Moriwaki, H., Shiraki, M., Iwasa, J., Terakuraet, Y. (2010). "Hepatic encephalopathy as a complication liver cirrhosis: an Asian perspective." *J Gastroenterol Hepatol*. 25(5): p.858-63. 10.1111/j.1440-1746.2010.06242.x.

[74] Butterworth, R.F. (2015). "The concept of "the inflamed brain" in acute liver failure: mechanisms and new therapeutic opportunities." *Metabolic Brain Disease*. 31: p.1283-1287. 10.1007/s11011-015-9747-0.

[75] Azhari, H., Swain, M.G. (2018). "Role of peripheral inflammation in hepatic encephalopathy." *Journal of Clinical and Experimental Hepatology*. 8(3): p.281-285. 10.1016/j.jceh.2018.06.008.

[76] Häussinger, D., Butz M., Schnitzler, A., Görg, B. (2021). "Pathomechanisms in hepatic encephalopathy." *Biol Chem*. 402(9): p.1087-1102. 10.1515/hsz-2021-0168.

[77] Praktiknjo, M., Simón-Talero, M., Römer, J., Roccarina, D., Martínez, J., Lampichler, K., Baiges, A., Low, G., Llop, E., Maurer, M.H., Zipprich, A., Triolo, M., Maleux, G., Fialla, A.D., Dam, C., Vidal-González, J., Majumdar, A., Picón, C., Toth, D., Darnell, A., Abraldes, J.G., López, M., Jansen, C., Chang, J., Schierwagen, R., Uschner, F., Kukuk, G., Meyer, C., Thomas, D., Wolter, K., Strassburg, C.P., Laleman, W., Mura, V.L., Ripoll, C., Berzigotti, A., Calleja, J.L., Tandon, P., Hernandez-Gea, V., Reiberger, T., Albillos, A., Tsochatzis, E.A., Krag, A., Genescà, J., Trebicka, J. (2020). "Total area of spontaneous portosystemic shunts independently predicts hepatic encephalopathy and mortality in liver cirrhosis." *J Hepatol*. 72(6): p.1140-1150. 10.1016/j.jhep.2019.12.021.

[78] Qi, X., Tian, Y., Zhang, W., Yang, Z., Guo, X. (2017). "Covered versus bare stents for transjugular intrahepatic portosystemic shunt: an updated meta-analysis of randomized controlled trials." *Therap Adv Gastroenterol*. 10(1): p.32-41. 10.1177/1756283x16671286.

[79] Nicoara-Farcau, O., Han, G., Rudler, M., Angrisani, D., Monescillo, A., Torres, F., Casanovas, G., Bosch, J., Lv, Y., Dunne, P.D.J., Hayes, P.C., Thabut, D., Fan, D., Hernández-Gea, V., García-Pagán, J.C. (2023). "Pre-emptive TIPS in high-risk acute variceal bleeding. An updated and revised individual patient data meta-analysis." *Hepatology*. 1;79(3):624-635. 10.1097/hep.0000000000000613.

[80] Riggio, O., Amodio, P., Farcomeni, A., Merli, M., Nardelli, S., Pasquale, C., Pentassuglio, I., Gioia, S., Onori, E., Piazza, N., Rui, M.D., Schiff, S., Montagnese, S. (2015). "A Model for Predicting Development of Overt Hepatic Encephalopathy in Patients With Cirrhosis." *Clin Gastroenterol Hepatol*. 13(7): p.1346-52. 10.1016/j.cgh.2014.12.025.

[81] Guevara, M., Baccaro, M.E. Torre, A., Gómez-Ansón, B., Ríos, J., Torres, F., Rami, L., Monté-Rubio, G.C., Martín-Llahí, M., Arroyo, V., Ginès, P. (2009). "Hyponatremia is a risk factor of hepatic encephalopathy in patients with cirrhosis: a prospective study with time-dependent analysis." *Am J Gastroenterol*. 104(6): p.1382-9. 10.1038/ajg.2009.293.

[82] Yoo, H.Y., Edwin, D., Thuluvath, P.J. (2003). "Relationship of the model for end-stage liver disease (MELD) scale to hepatic encephalopathy, as defined by electroencephalography and neuropsychometric testing, and ascites." *Am J Gastroenterol*. 98(6): p.1395-9. 10.1111/j.1572-0241.2003.07466.x.

[83] Gil-Gomez, A., Ampuero, J., Rojas, Á., Gallego-Durán R., Muñoz-Hernández, R., Rico, M.C., Millán, R., García-Lozano, R., Francés, R., Soriano, G., Romero-Gómez, M. (2021). "Development and Validation of a Clinical-Genetic Risk Score to Predict Hepatic Encephalopathy in Patients With Liver Cirrhosis." *Am J Gastroenterol*. 116(6): p.1238-1247. 10.14309/ajg.0000000000001164.

[84] Romero-Gomez, M., Jover, M., Campo, J.A.D., Royo, J.L., Hoyas, E., Galán, J.J., Montoliu, C., Baccaro, E., Guevara, M., Córdoba, J., Soriano, G., Navarro, J.M., Martínez-Sierra, C., Grande, L., Galindo, A., Mira, E., Mañes, S., Ruiz, A. (2010). "Variations in the promoter region of the

glutaminase gene and the development of hepatic encephalopathy in patients with cirrhosis: a cohort study." *Ann Intern Med*. 153(5): p.281-8. 10.7326/0003-4819-153-5-201009070-00002.

[85] Goh, E.T., Way, M., Atkinson, S.R., McQuillin, A., Morgan, M.Y. (2016). "PWE-033 Promoter Region Variations in The Glutaminase Gene as A Risk Factor for The Development Hepatic Encephalopathy in Patients with Cirrhosis." *Gut*. 65(1). 10.1136/gutjnl-2016-312388.279.

[86] Rai, R., Saraswat, V.A., and Dhiman, R.K. (2015). "Gut microbiota: its role in hepatic encephalopathy." *J Clin Exp Hepatol*. 5(Suppl 1): p.S29-36. 10.1016/j.jceh.2014.12.003.

[87] Garcovich, M., Zocco, M.A., Roccarina, D., Ponziani, F.R., Gasbarrini, A. (2012). "Prevention and treatment of hepatic encephalopathy: focusing on gut microbiota." *World J Gastroenterol*. 18(46): p.6693-700. 10.3748/wjg.v18.i46.6693.

[88] Toris, G.T., Bikis, C.N., Tsouroufl is, G.S., Theocharis, S.E. (2011). "Hepatic encephalopathy: an updated approach from pathogenesis to treatment." *Med Sci Monit*. 17(2): p.RA53-63. 10.12659/msm.881387.

[89] Oster, J.R., Perez, G.O., Materson, B.J., Schiff, E.R., Vaamonde, C.A. (1978). "Exacerbation of hepatic encephalopathy by chronic renal failure: response to maintenance hemodialysis." *Clin Nephrol*. 9(6): p. 254-7.

[90] Jepsen, P., Watson, H., Andersen, P.K., Vilstrup, H. (2015). "Diabetes as a risk factor for hepatic encephalopathy in cirrhosis patients." *J Hepatol*. 63(5): p.1133-8. 10.1016/j.jhep.2015.07.007.

[91] Jepsen, P., Christensen, J., Weissenborn, K., Watson, H., Vilstrup, H. (2016). "Epilepsy as a risk factor for hepatic encephalopathy in patients with cirrhosis: a cohort study." *BMC Gastroenterol*. 16(1): p.77. 10.1186/s12876-016-0487-3.

[92] Verma, N., Dhiman R.K., Choudhury, A., Taneja, S., Duseja, A., Singh, V., Mahtab, M.A., Devarbhavi, H., Shukla, A., Ning, Q., Hamid, S.S., Butt, A.S., Jafri, W., Tan, S.S., Hu, J., Duan, Z., Treeprasertsuk, S., Lee, G.H., Ghazinyan, H., Lesmana, L.A., Sood, A., Midha, V., Goyal, O., Kim, D.J., Eapen, C.E., Goel, A., Tao, H., Shaojie, X., Yuemin, N., Dokmeci A.K., Sahu, M., Singh, A., Arora, A., Kumar, A., Kumar, R., Prasad, V.G.M., Shresta, A., Sollano, J., Payawal, D.A., Shah, S., Rao, P.N., Kulkarni, A., Lau, G.K., Sarin, S.K. (2021). "Dynamic assessments of hepatic encephalopathy and ammonia levels predict mortality in acute-on-chronic liver failure." *Hepatol Int*. 15(4): p.970-982. 10.1007/s12072-021-10221-7.

[93] Nardelli, S., Lattanzi B., Merli, M., Farcomeni, A., Gioia, S., Ridola, L., Riggio, O. (2019). "Muscle Alterations Are Associated With Minimal and Overt Hepatic Encephalopathy in Patients With Liver Cirrhosis." *Hepatology*. 70(5): p.1704-1713. 10.1002/hep.30692.

[94] Basile, A.S., Pannell, L., Jaouni, T., Gammal, S.H., Fales, H.M., Jones, E.A., Skolnick, P. (1990). "Brain concentrations of benzodiazepines are elevated in an animal model of hepatic encephalopathy." *Proc Natl Acad Sci USA*. 87(14): p.5263-7. 10.1073/pnas.87.14.5263.

[95] Moon, A.M., Jiang, Y., Rogal, S.S., Tapper, E.B., Lieber, S.R., Barritt, IV. A.S. (2020). "Opioid prescriptions are associated with hepatic encephalopathy in a national cohort of patients with compensated cirrhosis." *Aliment Pharmacol Ther*. 51(6): p.652-660. 10.1111/apt.15639.

[96] Häussinger, D., Laubenberger, J., Vom Dahl, S., Ernst, T., Bayer, S., Langer, M., Gerok, W., Hennig, J. (1994). "Proton magnetic resonance spectroscopy studies on human brain myo-inositol in hypo-osmolarity and hepatic encephalopathy." *Gastroenterology*. 107(5): p.1475-80. 10.1016/0016-5085(94)90552-5.

[97] Häussinger, D., Kircheis, G., Fischer, R., Schliess, F., Vom Dahl, S. (2000). "Hepatic encephalopathy in chronic liver disease a clinical manifestation of astrocyte swelling and low-

grade cerebral edema?" *Journal of Hepatology*. 32(6):1035-8. 10.1016/s0168-8278(00)80110-5

[98] Häussinger, D. and Görg, B. (2019). "Oxidative/nitrosative stress and hepatic encephalopathy." In: Sies, H. (Ed.). Oxidative stress: eustress and distress. *Elsevier, Cambridge*. p.669–686. 1 0.1016/B978-0-12-818606-0.00032-8.

[99] Damink, O., S.W., Dejong, C.H., Deutz, N.E., Van Berlo, C.L., Soeters, P.B. (1999). "Upper gastrointestinal bleeding: an ammoniagenic and catabolic event due to the total absence of isoleucine in the haemoglobin molecule." *Med Hypotheses*. 52(6): p.515-9. 10.1054/mehy.1998.0026

[100] Butterworth, R.F. (1996). "The neurobiology of hepatic encephalopathy." *Semin Liver Dis*. 16(3): p.235-44. 10.1055/s-2007-1007236.

[101] Blei, A.T. and Cordoba, J. (2001). "Practice Parameters Committee of the American College of, Hepatic Encephalopathy." *Am J Gastroenterol*. 96(7): p.1968-76. 10.1111/j.1572-0241.2001.03964.x.

[102] Cooper, A.J. and Lai, J.C. (1987). "Cerebral ammonia metabolism in normal and hyperammonemic rats." *Neurochem Pathol*. 6(1-2): p.67-95. 10.1007/bf02833601.

[103] Devasahayam, J., John, S., Assar, S.M., Bhat, Z., Kurup, A., Hosuru, S., Joseph, V., Pillai, U. (2014). "Hyperammonemia as an Adverse Effect in Parenteral Nutrition." *Living reference work entry*. p.1–15. 10.1007/978-1-4614-7836-2_159.

[104] Damink, S.W.O., Dejong, C.H., Deutz, N.E., Van Berlo, C.L., Soeters, P.B. (1999). "Upper gastrointestinal bleeding: an ammoniagenic and catabolic event due to the total absence of isoleucine in the haemoglobin molecule." *Med Hypotheses*. 52(6):515-9. 10.1054/mehy.1998.0026.

[105] Ott, P. and Larsen, F.S. (2004). "Blood-brain barrier permeability to ammonia in liver failure: a critical reappraisal." *Neurochem Int*. 44(4): p.185-98. 10.1016/s0197-0186(03)00153-0.

[106] Center, S.A. and Magne, M.L. (1990). "Historical, physical examination, and clinicopathologic features of portosystemic vascular anomalies in the dog and cat." *Semin Vet Med Surg Small Anim*. 5(2): p. 83-93.

[107] Aldridge, D.R., Tranah, E.J., Shawcross, D.L. (2015). "Pathogenesis of hepatic encephalopathy: role of ammonia and systemic inflammation." *J Clin Exp Hepatol*. 5(Suppl 1): p.S7-S20. DOI:10.1016/j.jceh.2014.06.004.

[108] Häussinger, D. (1990). "Nitrogen metabolism in liver: structural and functional organization and physiological relevance." *Biochem J*. 267(2): p.281-90. 10.1042/bj2670281.

[109] Ott, P. and Vilstrup, H. (2014). "Cerebral effects of ammonia in liver disease: current hypotheses." *Metab Brain Dis*. 29(4): p.901-11. 10.1007/s11011-014-9494-7.

[110] Häussinger, D. and Stehle, T. (1988). "Hepatocyte heterogeneity in response to icosanoids. The perivenous scavenger cell hypothesis." *Eur J Biochem*. 175(2): p.395-403. 10.1111/j.1432-1033.1988.tb14209.x

[111] Ali, E.Z., Khalid, M.K.N.M., Yunus, Z.M., Yakob, Y., Chin, C.B., Latif, K.A., Hock, N.L. (2016). "Carbamoylphosphate synthetase 1 (CPS1) deficiency: clinical, biochemical, and molecular characterization in Malaysian patients." *Eur J Pediatr*. 175(3): p.339-46. 10.1007/s00431-015-2644-z.

[112] Rose, C.F., Amodio, P., Bajaj, J.S., Dhiman, R.K., Montagnese, S., Taylor-Robinson, S.D., Vilstrup, H., Jalan, R. (2020). "Hepatic encephalopathy: Novel insights into classification, pathophysiology and therapy." *J Hepatol*. 73(6): p.1526-1547. 10.1016/j.jhep.2020.07.013.

[113] Häussinger, D. and Gerok, W. (1983). "Hepatocyte heterogeneity in glutamate uptake by isolated perfused rat liver." *European Journal of Biochemistry*. 136(2): p.421-5. 10.1111/j.1432-1033.1983.tb07759.x.

[114] Boon, L., Geerts, W.J., Jonker, A., Lamers, W.H., Van Noorden, C.J. (1999). "High protein diet induces pericentral glutamate dehydrogenase and ornithine aminotransferase to provide sufficient glutamate for pericentral detoxification of ammonia in rat liver lobules." *Histochem Cell Biol*. 111(6): p.445-52. 10.1007/s004180050380.

[115] Weiner, I.D., Miller, R.T., Verlander, J.W. (2003). "Localization of the ammonium transporters, Rh B glycoprotein and Rh C glycoprotein, in the mouse liver." *Gastroenterology*. 124(5): p.1432-40. 10.1016/s0016-5085(03)00277-4.

[116] Stoll, B. and Häussinger, D. (1991). "Hepatocyte heterogeneity in uptake and metabolism of malate and related dicarboxylates in perfused rat liver." *Eur J Biochem*. 195(1): p.121-9. 10.1111/j.1432-1033.1991.tb15684.x.

[117] Qvartskhava, N., Lang, P.A., Görg, B., Pozdeev, V.I., Ortiz, M.P., Lang, K.S., Bidmon, H.J., Lang, E., Leibrock, C.B., Herebian, D., Bode, J.G., Lang, F., Häussinger, D. (2015). "Hyperammonemia in gene-targeted mice lacking functional hepatic glutamine synthetase." *Proc Natl Acad Sci USA*. 112(17): p.5521-6. 10.1073/pnas.1423968112.

[118] Gebhardt, R. and Reichen, J. (1994). "Changes in distribution and activity of glutamine synthetase in carbon tetrachloride-induced cirrhosis in the rat: potential role in hyperammonemia." *Hepatology*. 20(3): p.684-91. 10.1002/hep.1840200320.

[119] Qvartskhava, N., Jin, C.J., Buschmann, T., Albrecht, U., Bode, J.G., Monhasery, N., Oenarto, J., Bidmon, H.J., Görg, B., Häussinger, D. (2019). "Taurine transporter (TauT) deficiency impairs ammonia detoxification in mouse liver." *Proc Natl Acad Sci USA*. 116(13): p.6313-6318. 10.1073/pnas.1813100116.

[120] Häberle, J., Görg, B., Rutsch, F., Schmidt, E., Toutain, A., Benoist, J., Gelot, A., Suc, A.L., Höhne, W., Schliess, F., Häussinger, D., Koch, H.G. (2005). "Congenital glutamine deficiency with glutamine synthetase mutations." *N Engl J Med*. 353(18): p.1926-33. 10.1056/nejmoa050456.

[121] Häussinger, D. (1983). "Hepatocyte heterogeneity in glutamine and ammonia metabolism and the role of an intercellular glutamine cycle during ureogenesis in perfused rat liver." *Eur J Biochem*. 133(2): p.269-75. 10.1111/j.1432-1033.1983.tb07458.x.

[122] Häussinger, D. and Gerok, W. (1984). "Hepatocyte heterogeneity in ammonia metabolism: impairment of glutamine synthesis in CCl4 induced liver cell necrosis with no effect on urea synthesis." *Chem Biol Interact*. 48(2): p.191-4. 10.1016/0009-2797(84)90120-0.

[123] Häussinger, D. (2006). "Low grade cerebral edema and the pathogenesis of hepatic encephalopathy in cirrhosis." *Hepatology*. 43(6): p.1187-90. 10.1002/hep.21235.

[124] Pascual, O., Achour, S.B., Rostaing, P., Triller, A., Bessis, A. (2012). "Microglia activation triggers astrocyte-mediated modulation of excitatory neurotransmission." *Proc Natl Acad Sci USA*. 109(4): p.E197-205. 10.1073/pnas.1111098109.

[125] Norenberg, M.D., Rama Rao, K.V., Jayakumar, A.R. (2005). "Mechanisms of ammonia-induced astrocyte swelling." *Metab Brain Dis*. 20(4): p.303-18. 10.1007/s11011-005-7911-7.

[126] Araque, A., Sanzgiri, R.P., Parpura, V., Haydon, P.G. (1999). "Astrocyte-induced modulation of synaptic transmission." *Can J Physiol Pharmacol*. 77(9): p.699-706.

[127] Norenberg, M.D. (1987). "The role of astrocytes in hepatic encephalopathy." *Neurochem Pathol*. 6(1-2): p.13-33. 10.1007/BF02833599.

[128] Brusilow, S.W. and Traystman, R. (1986). "Hepatic encephalopathy." *N Engl J Med*. 314(12): p. 786-7; author reply 787.

[129] Hyzinski-Garcia, M.C. (2011). "Hypo-osmotic swelling modifies glutamate-glutamine cycle in the cerebral cortex and in astrocyte cultures." *J Neurochem*. 118(1): p.140-52. 10.1111/j.1471-4159.2011.07289.x.

[130] Jayakumar, A.R., Rama Rao, K.V., Murthy, C.R.K., Norenberg, M.D. (2006). "Glutamine in the mechanism of ammonia-induced astrocyte swelling." *Neurochemistry international*. 48(6-7): p. 623-628. 10.1016/j.neuint.2005.11.017.

[131] Llansola, M., Rodrigo, R., Monfort, P., Montoliu, C., Kosenko, E., Cauli, O., Piedrafita, B., Mlili, N.E., Felipo, V. (2007). "NMDA receptors in hyperammonemia and hepatic encephalopathy." *Metabolic Brain Disease*. 22: p.321-335. 10.1007/s11011-007-9067-0.

[132] Jalan, R., Damink, S.W.M.O., Deutz, N.E.P., Davies, N.A., Garden, O.J., Madhavan, K.K., Hayes, P.C., Lee, A. (2003). "Moderate hypothermia prevents cerebral hyperemia and increase in intracranial pressure in patients undergoing liver transplantation for acute liver failure." *Transplantation*. 75(12): p.2034-9. 10.1097/01.tp.0000066240.42113.ff.

[133] Willard-Mack, C.L., Koehler, R.C., Hirata, T., Cork, L.C., Takahashi, H., Traystman, R.J., Brusilow, S.W. (1996). "Inhibition of glutamine synthetase reduces ammonia-induced astrocyte swelling in rat." *Neuroscience*. 71(2): p.589-99. 10.1016/0306-4522(95)00462-9.

[134] Lavoie, J., Layrargues, G.P., Butterworth, R.F. (1990). "Increased densities of peripheral-type benzodiazepine receptors in brain autopsy samples from cirrhotic patients with hepatic encephalopathy." *Hepatology*. 11(5): p.874-8. 10.1002/hep.1840110524.

[135] Bender, A.S. and Norenberg, M.D. (1998). "Effect of benzodiazepines and neurosteroids on ammonia-induced swelling in cultured astrocytes." *J Neurosci Res*. 54(5): p.673-80. 10.1002/(sici)1097-4547(19981201)54:5<673::aid-jnr12>3.0.co;2-p.

[136] Schliess, F., Görg, B., Fischer, R., Desjardins, P., Bidmon, H.J., Herrmann, A., Butterworth, R.F., Zilles, K., Häussinger, D. (2002). "Ammonia induces MK-801-sensitive nitration and phosphorylation of protein tyrosine residues in rat astrocytes." *FASEB J*. 16(7): p.739-41. 10.1096/fj.01-0862fje.

[137] Görg, B., Bidmon, H.J., Häussinger, D. (2013). "Gene expression profiling in the cerebral cortex of patients with cirrhosis with and without hepatic encephalopathy." *Hepatology*. 57(6): p. 2436-47. 10.1002/hep.26265.

[138] Rama Rao, R.K.V., Jayakumar, A.R., Tong, X.Y., Alvarez, V.M., Norenberg, M.D. (2010). "Marked potentiation of cell swelling by cytokines in ammonia-sensitized cultured astrocytes." *J Neuroinflammation*. 7: p.66. 10.1186/1742-2094-7-66.

[139] Pasantes-Morales, H., Franco, R., Ordaz, B., Ochoa, L.D. (2002). "Mechanisms counteracting swelling in brain cells during hyponatremia." *Arch Med Res*. 33(3): p.237-44. 10.1016/s0188-4409(02)00353-3.

[140] Schober, A.L. and Mongin, A.A. (2015). "Intracellular levels of glutamate in swollen astrocytes are preserved via neurotransmitter reuptake and de novo synthesis: implications for hyponatremia." *J Neurochem*. 135(1): p.176-85. 10.1111/jnc.13229.

[141] Görg, B., Qvartskhava, N., Keitel, V., Bidmon, H.J., Selbach, O., Schliess, F., Häussinger, D. (2008). "Ammonia induces RNA oxidation in cultured astrocytes and brain *in vivo*." *Hepatology*. 48(2): p.567-79. 10.1002/hep.22345.

[142] Görg, B., Karababa, A., Häussinger, D. (2018). "Hepatic Encephalopathy and Astrocyte Senescence." *J Clin Exp Hepatol*. 8(3): p. 294-300. 10.1016/j.jceh.2018.05.003.

[143] Görg, B., Qvartskhava, N., Bidmon, H.J., Palomero-Gallagher, N., Kircheis, G., Zilles, K., Häussinger, D. (2010). "Oxidative stress markers in the brain of patients with cirrhosis and hepatic encephalopathy." *Hepatology*. 52(1): p.256-65. 10.1002/hep.23656.

[144] Karababa, A., Görg, B, Schliess, F., Häussinger, D. (2014). "*O*-GlcNAcylation as a novel ammonia-induced posttranslational protein modification in cultured rat astrocytes." *Metab Brain Dis*. 29(4): p.975-82. 10.1007/s11011-013-9454-7.

[145] Jayakumar, A.R., Panickar, K.S., Murthy, Ch.R., Norenberg, M.D. (2006). "Oxidative stress and mitogen-activated protein kinase phosphorylation mediate ammonia-induced cell swelling and glutamate uptake inhibition in cultured astrocytes." *J Neurosci*. 26(18): p.4774-84. 10.1523/jneurosci.0120-06.2006.

[146] Swapna, I., Kumar, K.V.S.S., Murthy, Ch.R.K., Senthilkumaran, B. (2006). "Membrane alterations and fluidity changes in cerebral cortex during acute ammonia intoxication." *NeuroToxicology*. 27(3): p.402-408. 10.1016/j.neuro.2005.11.010.

[147] Zarkovic, N. (2020). "Roles and Functions of ROS and RNS in Cellular Physiology and Pathology." *Cells*. 9(3):767. 10.3390/cells9030767.

[148] Häussinger, D. and Görg, B. (2010). "Interaction of oxidative stress, astrocyte swelling and cerebral ammonia toxicity." *Curr Opin Clin Nutr Metab Care*. 13(1): p.87-92. 10.1097/mco.0b013e328333b829.

[149] Lachmann, V., Görg, B., Bidmon, H.J., Keitel, V., Häussinger, D. (2013). "Precipitants of hepatic encephalopathy induce rapid astrocyte swelling in an oxidative stress dependent manner." *Archives of Biochemistry and Biophysics*. 536(2):143-51. 10.1016/j.abb.2013.05.004.

[150] Görg, B., Foster, N., Reinehr, R., Bidmon, H.J., Höngen, A., Häussinger, D., Schliess, F. (2003). "Benzodiazepine-induced protein tyrosine nitration in rat astrocytes." *Hepatology*. 37(2): p. 334-42. 10.1053/jhep.2003.50061.

[151] Häussinger, D. and Schliess, F. (2008). "Pathogenetic mechanisms of hepatic encephalopathy." *Gut*. 57(8): p.1156-65. 10.1136/gut.2007.122176.

[152] Schliess, F., Görg, B., Häussinger, D. (2006). "Pathogenetic interplay between osmotic and oxidative stress: the hepatic encephalopathy paradigm." *Biol Chem*. 387(10-11): p.1363-70. 10.1515/bc.2006.171.

[153] Moriyama, M., Jayakumar, A.R., Tong, X.Y., Norenberg, M.D. (2010). "Role of mitogen-activated protein kinases in the mechanism of oxidant-induced cell swelling in cultured astrocytes." *J Neurosci Res*. 88(11): p.2450-8. 10.1002/jnr.22400.

[154] Schliess, F., Foster, N., Görg, B., Reinehr, R., Häussinger, D. (2004). "Hypoosmotic swelling increases protein tyrosine nitration in cultured rat astrocytes." *Glia*. 47(1): p.21-9. 10.1002/glia.20019.

[155] Oenarto, J., Görg, B., Moos, M., Bidmon, H.J., Häussinger, D. (2014). "Expression of organic osmolyte transporters in cultured rat astrocytes and rat and human cerebral cortex." *Arch Biochem Biophys*. 560: p.59-72. 10.1016/j.abb.2014.06.024.

[156] Fu, H., Li, B., Hertz, L., Peng, L. (2012). "Contributions in astrocytes of SMIT1/2 and HMIT to myo-inositol uptake at different concentrations and pH." *Neurochem Int*. 61(2): p.187-94. 10.1016/j.neuint.2012.04.010.

[157] Jayakumar, A.R., Rama Rao, K.V.R., Tong, XY., Norenberg, M.D. (2009). "Calcium in the mechanism of ammonia-induced astrocyte swelling." *J Neurochem*. 109 Suppl 1(0 1): p.252-7. 10.1111/j.1471-4159.2009.05842.x.

[158] Rama Rao, K.V., Chen, M., Simard, J.M., Norenberg, M.D. (2003). "Increased aquaporin-4 expression in ammonia-treated cultured astrocytes." *Neuroreport*. 14(18): p.2379-82. 10.1097/00001756-200312190-00018.

[159] Ismail, F.S., Faustmann, T.J., Corvace, F., Tsvetanova, A., Moinfar, Z., Faustmann, P.M. (2021). "Ammonia induced microglia activation was associated with limited effects on connexin 43 and

aquaporin 4 expression in an astrocyte-microglia co-culture model." *BMC Neurosci*. 22(1): p. 21. 10.1186/s12868-021-00628-1.

[160] Wright, G., Soper, R., Brooks, H.F., Stadlbauer, V., Vairappan, B., Davies, N.A., Andreola, F., Hodges, S., Moss, R.F., Davies, D.C., Jalan, R. (2010). "Role of aquaporin-4 in the development of brain oedema in liver failure." *J Hepatol*. 53(1): p.91-7. 10.1016/j.jhep.2010.02.020.

[161] Bobermin, L.D., K.M.W., Flores, M.P., Marina Concli Leite, André Quincozes-Santos, Carlos-Alberto Gonçalves, (2015). "Ammonia-induced oxidative damage in neurons is prevented by resveratrol and lipoic acid with participation of heme oxygenase 1." *NeuroToxicology*. 49: p.28-35. 10.1016/j.neuro.2015.05.005.

[162] Rama Rao, K.V., Brahmbhatt, M., Norenberg, M.D. (2013). "Microglia contribute to ammonia-induced astrocyte swelling in culture." *Metab Brain Dis*. 28(2): p.139-43. 10.1007/s11011-012-9339-1.

[163] Zemtsova, I., Görg, B., Keitel, V., Bidmon, H.J., Schrör, K., Häussinger, D. (2011). "Microglia activation in hepatic encephalopathy in rats and humans." *Hepatology*. 54(1): p.204-15.10.1002/hep.24326.

[164] Jayakumar, A.R., Tong, X.Y., Ospel, J., Norenberg, M.D. (2012). "Role of cerebral endothelial cells in the astrocyte swelling and brain edema associated with acute hepatic encephalopathy." *Neuroscience*. 218: p.305-16. 10.1016/j.neuroscience.2012.05.006.

[165] Bosoi, C.R., Yang, X.L., Huynh, J., Parent-Robitaille, C., Jiang, W.L., Tremblay, M., Rose, C.F., (2012). "Systemic oxidative stress is implicated in the pathogenesis of brain edema in rats with chronic liver failure." *Free Radical Biology and Medicine*. 52(7): p.1228-35. 10.1016/j.freeradbiomed.2012.01.006.

[166] Bosoi, C.R., Tremblay, M., Rose, C.F. (2014). "Induction of systemic oxidative stress leads to brain oedema in portacaval shunted rats." *Liver Int*. 34(9): p. 1322-9. 10.1111/liv.12414.

[167] Bandookwala, M. and Sengupta, P. (2020). "3-Nitrotyrosine: A versatile oxidative stress biomarker for major neurodegenerative diseases." *International Journal of Neuroscience*. 130(10): p. 1047-1062. 10.1080/00207454.2020.1713776.

[168] Felipo, V., Urios, A., Valero, P., Sánchez, M., Serra, M.A., Pareja, I., Rodríguez, F., Gimenez-Garzó, C.G., Sanmartín, J., Montoliu, C. (2013). "Serum nitrotyrosine and psychometric tests as indicators of impaired fitness to drive in cirrhotic patients with minimal hepatic encephalopathy." *Liver Int*. 33(10): p.1478-89. 10.1111/liv.12206.

[169] Görg, B., Bidmon, H.J., Keitel, V., Foster, N., Goerlich, R., Schliess, F., Häussinger, D. (2006). "Inflammatory cytokines induce protein tyrosine nitration in rat astrocytes." *Arch Biochem Biophys*. 449(1-2): p.104-14. 10.1016/j.abb.2006.02.012.

[170] Jayakumar, A.R., Rama Rao, K.V., Schousboe, A., Norenberg, M.D. (2004). "Glutamine-induced free radical production in cultured astrocytes." *Glia*. 46(3): p. 296-301.10.1002/glia.20003.

[171] Murthy, C.R., Rama Rao, K.V., Bai, G., Norenberg, M.D. (2001). "Ammonia-induced production of free radicals in primary cultures of rat astrocytes." *J Neurosci Res*. 66(2): p.282-8. 10.1002/jnr.1222.

[172] Dhanda, S., Sunkaria, A., Halder, A., Sandhir, R. (2017). "Mitochondrial dysfunctions contribute to energy deficits in rodent model of hepatic encephalopathy." *Metabolic Brain Disease*. 33: p. 209–223. 10.1007/s11011-017-0136-8.

[173] Mayer, M.L., Westbrook, G.L., Guthrie, P.B. (1984). "Voltage-dependent block by Mg^{2+} of NMDA responses in spinal cord neurones." *Nature*. 309(5965): p.261-3. 10.1038/309261a0.

[174] Nowak, L., Bregestovski, P., Ascher, P., Herbet, A., Prochiantz, A. (1984). "Magnesium gates glutamate-activated channels in mouse central neurones." *Nature*. 307(5950): p.462-5. 10.1038/307462a0.

[175] Görg, B., Morwinsky, A., Keitel, V., Qvartskhava, N., Schrör, K., Häussinger, D. (2010). "Ammonia triggers exocytotic release of L-glutamate from cultured rat astrocytes." *Glia*. 58(6): p.691-705. 10.1002/glia.20955.

[176] Reinehr, R., Görg, B., Becker, S., Qvartskhava, N., Bidmon, H.J., Selbach, O., Haas, H.L., Schliess, F., Häussinger, D. (2007). "Hypoosmotic swelling and ammonia increase oxidative stress by NADPH oxidase in cultured astrocytes and vital brain slices." *Glia*. 55(7): p.758-71. 10.1002/glia.20504.

[177] Sinke, A.P., Jayakumar, A.R., Panickar, K.S., Moriyama, M., Reddy, P.V., Norenberg, M.D. (2008). "NFkappaB in the mechanism of ammonia-induced astrocyte swelling in culture." *J Neurochem*. 106(6): p.2302-11. 10.1111/j.1471-4159.2008.05549.x.

[178] Pierzchala, K., Hadjihambi, A., Mosso, J., Jalan, R., Rose, C.F., Cudalbuet, C. (2023). "Lessons on brain edema in HE: from cellular to animal models and clinical studies." *Metab Brain Dis*. 39(3):403-437. 10.1007/s11011-023-01269-5.

[179] Kruczek, C., Görg, B., Keitel, V., Pirev, E., Kröncke, K.D., Schliess, F., Häussinger, D. (2009). "Hypoosmotic swelling affects zinc homeostasis in cultured rat astrocytes." *Glia*. 57(1): p.79-92. 10.1002/glia.20737.

[180] Radi, R. (2004). "Nitric oxide, oxidants, and protein tyrosine nitration." *Proc Natl Acad Sci USA*. 101(12): p.4003-8. 10.1073/pnas.0307446101.

[181] El-Mlili, N., Rodrigo, R., Naghizadeh, B., Cauli, O., Felipo, V. (2008). "Chronic hyperammonemia reduces the activity of neuronal nitric oxide synthase in cerebellum by altering its localization and increasing its phosphorylation by calcium-calmodulin kinase II." *J Neurochem*. 106(3): p. 1440-9.10.1111/j.1471-4159.2008.05495.x.

[182] Bai, G., Rama Rao, K.V., Murthy, C.R., Panickar, K.S., Jayakumar, A.R., Norenberg, M.D. (2001). "Ammonia induces the mitochondrial permeability transition in primary cultures of rat astrocytes." *J Neurosci Res*. 66(5): p.981-91. 10.1002/jnr.10056.

[183] Norenberg, M.D., Rama Rao, K.V.R., Jayakumar, A.R. (2008). "Signaling factors in the mechanism of ammonia neurotoxicity." *Metabolic Brain Disease*. 24: p.103–117. 10.1007/s11011-008-9113-6.

[184] Keitel, V., Görg, B., Bidmon, H.J., Zemtsova, I., Spomer, L., Zilles, K., Häussinger, D. (2010). "The bile acid receptor TGR5 (Gpbar-1) acts as a neurosteroid receptor in brain." *Glia*. 58(15): p. 1794-805. 10.1002/glia.21049.

[185] Sancho-Alonso, M., Garcia-Garcia, R., Teruel-Martí, V., Llansola, M., Felipo, V. (2022). "Hyperammonemia Enhances GABAergic Neurotransmission in Hippocampus: Underlying Mechanisms and Modulation by Extracellular cGMP." *Mol Neurobiol*. 59(6): p.3431-3448. 10.1007/s12035-022-02803-9.

[186] Ahboucha, S., Garcia-Garcia, R., Teruel-Martí, V., Llansola, M., Felipo, V. (2005). "Increased brain concentrations of a neuroinhibitory steroid in human hepatic encephalopathy." *Ann Neurol*. 58(1): p.169-70. 10.1002/ana.20534.

[187] Cagnin, A., Taylor-Robinson, S.D., Forton, D.M., Banati, R.B. (2006). "*In vivo* imaging of cerebral "peripheral benzodiazepine binding sites" in patients with hepatic encephalopathy." *Gut*. 55(4): p.547-53. 10.1136/gut.2005.075051.

[188] Warskulat, U., Kreuels, S., Müller, H.W., Häussinger, D. (2001). "Identification of osmosensitive and ammonia-regulated genes in rat astrocytes by Northern blotting and differential display

reverse transcriptase-polymerase chain reaction." *J Hepatol*. 35(3): p.358-66. 10.1016/s0168-8278(01)00149-0.

[189] Giatzakis, C. and Papadopoulos, V. (2004). "Differential utilization of the promoter of peripheral-type benzodiazepine receptor by steroidogenic versus nonsteroidogenic cell lines and the role of Sp1 and Sp3 in the regulation of basal activity." *Endocrinology*. 145(3): p.1113-23. 10.1210/en.2003-1330.

[190] Delerive, P., Fruchart, J.C., Staels, B. (2001). "Peroxisome proliferator-activated receptors in inflammation control." *J Endocrinol*. 169(3): p.453-9. 10.1677/joe.0.1690453.

[191] Dennis, C.V., Sheahan, P.J., Graeber, M.B., Sheedy, D.L., Kril, J.J., Sutherland, G.T. (2014). "Microglial proliferation in the brain of chronic alcoholics with hepatic encephalopathy." *Metab Brain Dis*. 29(4): p.1027-39. 10.1007/s11011-013-9469-0.

[192] Balan, I., Beattie, M.C., O'Buckley, T.K., Aurelian, L., Morrow, A.L. (2019). "Endogenous Neurosteroid (3alpha,5alpha)3-Hydroxypregnan-20-one Inhibits Toll-like-4 Receptor Activation and Pro-inflammatory Signaling in Macrophages and Brain." *Sci Rep*. 9(1): p.1220. 10.1038/s41598-018-37409-6.

[193] Jordens, M.S., Keitel, V., Karababa, A., Zemtsova, I., Bronger, H., Häussinger, D., Görg, B. (2015). "Multidrug resistance-associated protein 4 expression in ammonia-treated cultured rat astrocytes and cerebral cortex of cirrhotic patients with hepatic encephalopathy." *Glia*. 63(11): p.2092-2105. 10.1002/glia.22879.

[194] Decano, J.L., Singh, S.A., Bueno, C.G., Lee, L.H., Halu, A., Chelvanambi, S., Matamalas, J.T., Zhang, H., Mlynarchik, A.K., Qiao, J., Sharma, A., Mukai, S., Wang, J., Anderson, D.G., Ozaki, C.K., Libby, P., Aikawa, E., Aikawaet, M. (2021). "Systems Approach to Discovery of Therapeutic Targets for Vein Graft Disease: PPARalpha Pivotally Regulates Metabolism, Activation, and Heterogeneity of Macrophages and Lesion Development." *Circulation*. 143(25): p.2454-2470. 10.1161/circulationaha.119.043724.

[195] Escher, P. and Wahli, W. (2000). "Peroxisome proliferator-activated receptors: insight into multiple cellular functions." *Mutat Res*. 448(2): p.121-38. 10.1016/s0027-5107(99)00231-6.

[196] Devchand, P.R., Keller, H., Peters, J.M., Vazquez, M., Gonzalez, F.J., Wahli, W. (1996). "The PPARalpha-leukotriene B4 pathway to inflammation control." *Nature*. 384(6604): p.39-43. 10.1038/384039a0.

[197] Ricote, M., Li, A.C., Willson, T.M., Kelly, C.J., Glass, C.K. (1998). "The peroxisome proliferator-activated receptor-gamma is a negative regulator of macrophage activation." *Nature*. 391(6662): p.79-82. 10.1038/34178.

[198] Paumelle, R., Haas, J.T., Hennuyer, N., Baugé, E., Deleye, Y., Mesotten, D., Langouche, L., Vanhoutte, J., Cudejko, C., Wouters, K., Hannou, S.A., Legry, V., Lancel, S., Lalloyer, F., Polizzi, A., Smati, S., Gourdy, P., Vallez, E., Bouchaert, E., Derudas, B., Dehondt, H., Gheeraert, C., Fleury, S., Tailleux, A., Montagner, A., Wahli, W., Berghe, G.V.D., Guillou, H., Dombrowicz, D., Staels, B. (2019). "Hepatic PPARalpha is critical in the metabolic adaptation to sepsis." *J Hepatol*. 70(5): p.963-973. 10.1016/j.jhep.2018.12.037.

[199] Ren, Y., Sun, C., Sun, Y., Tan, H., Wu, Y., Cui, B., Wu, Z. (2009). "PPAR gamma protects cardiomyocytes against oxidative stress and apoptosis via Bcl-2 upregulation." *Vascul Pharmacol*. 51(2-3): p.169-74. 10.1016/j.vph.2009.06.004.

[200] Polvani, S., Tarocchi, M., Galli, A. (2012). "PPARgamma and Oxidative Stress: Con(beta) Catenating NRF2 and FOXO." *PPAR Res*. p.641087. 10.1155/2012/641087.

[201] Raso, G.M., Vitiello, E.E.S., Iacono, A., Santoro, A., D'Agostino, G. (2011). "Palmitoylethanolamide Stimulation Induces Allopregnanolone Synthesis in C6 Cells and

Primary Astrocytes: Involvement of Peroxisome-Proliferator Activated Receptor-α." *Journal of Neuroendocrinology*. 23(7):591-600. 10.1111/j.1365-2826.2011.02152.x.

[202] Locci, A. and Pinna, G. (2019). "Activation of PPAR-α by N-palmitoylethanolamine engages allopregnanolone biosynthesis to modulate emotional behavior." *Biological Psychiatry*. 85(12):1036-1045.

[203] Nagelhus, E.A. and Ottersen, O.P. (2013). "Physiological roles of aquaporin-4 in brain." *Physiol Rev*. 93(4): p.1543-62. 10.1152/physrev.00011.2013.

[204] Rama Rao, K.V. and Norenberg, M.D. (2007). "Aquaporin-4 in hepatic encephalopathy." *Metabolic Brain Disease*. 22: p.265–275. 10.1007/s11011-007-9063-4.

[206] Elsherbini, D.M.A., Ghoneim, F.M., El-Mancy, E.M., Ebrahim, H.A., El-Sherbiny, M., El-Shafey, M., Al-Serwi, R.H., Elsherbiny, N.M. (2022). "Astrocytes profiling in acute hepatic encephalopathy: Possible enrolling of glial fibrillary acidic protein, tumor necrosis factor-alpha, inwardly rectifying potassium channel (Kir 4.1) and aquaporin-4 in rat cerebral cortex." *Front Cell Neurosci*. 16: p.896172. 10.3389/fncel.2022.896172.

[207] Abo El Gheit, R.E., Atef, M.M., Badawi, G.A., Elwan, W.M., Alshenawy, H.A., Emam, M.N. (2020). "Role of serine protease inhibitor, ulinastatin, in rat model of hepatic encephalopathy: aquaporin 4 molecular targeting and therapeutic implication." *J Physiol Biochem*. 76(4): p.573-586. 10.1007/s13105-020-00762-0.

[208] Rama Rao, K.V., Verkman, A.S., Curtis, K.M., Norenberg, M.D. (2014). "Aquaporin-4 deletion in mice reduces encephalopathy and brain edema in experimental acute liver failure." *Neurobiol Dis*. 63: p.222-8. 10.1016/j.nbd.2013.11.018.

[209] Chen, J., Xia, Q., Lu, H. (2018). "Changes in AQP4 expression and the pathology of injured cultured astrocytes after AQP4 mRNA silencing." *Neuropsychiatry*. 7(4). 10.4172/neuropsychiatry.1000232.

[210] Geoffrey, T., Manley, M.F., Ma, T., Noshita, N., Filiz, F., Bollen, A.W., Chan, P., Verkman, A.S. (2000). "Aquaporin-4 deletion in mice reduces brain edema after acute water intoxication and ischemic stroke." *Nature Medicine*. 6(2):159-63. 10.1038/72256.

[211] Zhang, H., Zhang, W., Yu, G., Li, F., Hui, Y., Cha, S., Chen, M., Zhu, W., Zhang, J., Guo, G., Gong, X. (2022). "Comprehensive Analysis of lncRNAs, miRNAs and mRNAs in Mouse Hippocampus With Hepatic Encephalopathy." *Front Genet*. 13: p.868716. 10.3389/fgene.2022.868716.

[212] Oenarto, J., Karababa, A., Castoldi, M., Bidmon, H.J., Görg, B., Häussinger, D. (2016). "Ammonia-induced miRNA expression changes in cultured rat astrocytes." *Sci Rep*. 6: p.18493. 10.1038/srep18493.

[213] Lee, R.C., Feinbaum, R.L., Ambros, V. (1993). "The C. elegans heterochronic gene lin-4 encodes small RNAs with antisense complementarity to lin-14." *Cell*. 75(5): p.843-54. 10.1016/0092-8674(93)90529-y.

[214] Kumar, P. and Bhandari, N. (2022). "lncRNAs: Role in Regulation of Gene Expression." *Gene Expression*. 10.5772/intechopen.104900.

[215] Zhang, C., Ni, W., Zhu, Y., Lin, J., Li, H., Zhao, Z., Wang, K., Huo, H., Luo, M. (2022). "Construction and comprehensive analysis of a lncRNA-mRNA interactive network to reveal a potential lncRNA for hepatic encephalopathy development." *Hum Cell*. 35(4): p. 1060-1070.

[216] Zhang, H., Yu, G., Li, J., Tu, C., Hui, Y., Liu, D., Chen, M., Zhang, J., Gong, X., Guo, G. (2023). Overexpressing lnc240 Rescues Learning and Memory Dysfunction in Hepatic Encephalopathy Through miR-1264-5p/MEF2C Axis. *Mol Neurobiol*. 60(4): p.2277-2294. 10.1007/s13577-022-00714-4.

[217] Cheon, S.Y., Jo, D., Kim, Y., Song, J. (2022). "Long Noncoding RNAs Regulate Hyperammonemia-Induced Neuronal Damage in Hepatic Encephalopathy." *Oxid Med Cell Longev*. p.7628522. 10.1155/2022/7628522.

[218] Kobayashi, Y., Sakemura, R., Kumagai, A., Sumikawa, E., Fujii, M., Ayusawa, D. (2008). "Nuclear swelling occurs during premature senescence mediated by MAP kinases in normal human fibroblasts." *Bioscience, Biotechnology, and Biochemistry*. 72: p.1122–1125. 10.1271/bbb.70760

[219] Oberleithner, H., Reinhardt, J., Schillers, H., Pagel, P., Schneider, S.W. (2000). "Aldosterone and nuclear volume cycling." *Cell Physiol Biochem*. 10(5-6): p.429-34. 10.1159/000016379.

[220] Dahl, K.N., Engler, A.J., Pajerowski, J.D., Discher, D.E. (2005). "Power-law rheology of isolated nuclei with deformation mapping of nuclear substructures." *Biophys J*. 89(4): p.2855-64. 10.1529/biophysj.105.062554.

[221] Bruck, J., Görg, B., Bidmon, H.J., Zemtsova, I., Qvartskhava, N., Keitel, V., Kircheis, G., Häussinger, D. (2011). "Locomotor impairment and cerebrocortical oxidative stress in portal vein ligated rats *in vivo*." *J Hepatol*. 54(2): p.251-7. 10.1016/j.jhep.2010.06.035.

[222] Nunomura, A., Honda, K., Takeda, A., Hirai, K., Zhu, X., Smith, M.A., Perry, G. (2006). "Oxidative damage to RNA in neurodegenerative diseases." *J Biomed Biotechnol*. (3): p.82323. 10.1155/jbb/2006/82323.

[223] Schliess, F., Görg, B., Häussinger, D. (2009). "RNA oxidation and zinc in hepatic encephalopathy and hyperammonemia." *Metabolic Brain Disease*. 24: p.119–134. 10.1007/s11011-008-9125-2.

[224] Kruczek, C., Görg, B., Keitel, V., Bidmon, H.J., Schliess, F., Häussinger, D. (2011). "Ammonia increases nitric oxide, free Zn(2+), and metallothionein mRNA expression in cultured rat astrocytes." *Biol Chem*. 392(12): p.1155-65. 10.1515/bc.2011.199.

[225] Zhou, B.G. and Norenberg, M.D. (1999). "Ammonia downregulates GLAST mRNA glutamate transporter in rat astrocyte cultures." *Neurosci Lett*. 276(3): p.145-8. 10.1016/s0304-3940(99)00816-2.

[226] Chan, H., Hazell, A.S., Desjardins, P., Butterworth, R.F. (2000). "Effects of ammonia on glutamate transporter (GLAST) protein and mRNA in cultured rat cortical astrocytes." *Neurochem Int*. 37(2-3): p.243-8. 10.1016/s0197-0186(00)00026-7.

[227] Sobczyk, K., Jördens, M.S., Karababa, A., Görg, B., Häussinger, D. (2015). "Ephrin/Ephrin receptor expression in ammonia-treated rat astrocytes and in human cerebral cortex in hepatic encephalopathy." *Neurochem Res*. 40(2): p.274-83. 10.1007/s11064-014-1389-9.

[228] Schrimpf, A., Knappe, O., Qvartskhava, N., Poschmann, G., Stühler, K., Bidmon, H.J., Luedde, T., Häussinger, D., Görg, B. (2022). "Hyperammonemia-induced changes in the cerebral transcriptome and proteome." *Anal Biochem*. 641: p.114548. 10.1016/j.ab.2022.114548.

[229] Romero-Gómez, M., Montagnese, S., Jalan, R. (2015). "Hepatic encephalopathy in patients with acute decompensation of cirrhosis and acute-on-chronic liver failure." *J Hepatology*. pp.669–686. 10.1016/j.jhep.2014.09.005.

[230] Jia, G., Wang, R., Yue, Y., Dai, H. (2020). "Activation of Protein Kinase Cdelta Contributes to the Induction of Src/EGF Receptor/ERK Signaling in Ammonia-treated Astrocytes." *J Mol Neurosci*. 70(7): p.1110-1119. 10.1007/s12031-020-01517-8.

[231] Wagner, E.F. and Nebreda, A.R. (2009). "Signal integration by JNK and p38 MAPK pathways in cancer development." *Nat Rev Cancer*. 9(8): p.537-49. 10.1038/nrc2694.

[232] Taoro-Gonzalez, L., Arenas, Y.M., Cabrera-Pastor, A., Felipo, V. (2018). "Hyperammonemia alters membrane expression of GluA1 and GluA2 subunits of AMPA receptors in hippocampus by

enhancing activation of the IL-1 receptor: underlying mechanisms." *J Neuroinflammation*. 15(1): p.36. 10.1186/s12974-018-1082-z.

[233] Franca, M.E.R. and Peixoto, C.A. (2020). "cGMP signaling pathway in hepatic encephalopathy neuroinflammation and cognition." *International Immunopharmacology*. 79: p.106082. 10.1016/j.intimp.2019.106082.

[234] Montoliu, C., Rodrigo, R., Monfort, P., Llansola, M., Cauli, O., Boix, J., Elmlili, N., Agusti, A., Felipo, V. (2010). "Cyclic GMP pathways in hepatic encephalopathy. Neurological and therapeutic implications." *Metab Brain Dis*. 25(1): p.39-48. 10.1007/s11011-010-9184-z.

[235] Hermenegildo, C., Monfort, P., Felipo, V. (2000). "Activation of N-methyl-D-aspartate receptors in rat brain *in vivo* following acute ammonia intoxication: characterization by *in vivo* brain microdialysis." *Hepatology*. 31(3): p.709-15. 10.1002/hep.510310322.

[236] Corbalan, R., Chatauret, N., Behrends, S., Butterworth, R.F., Felipo, V. (2002). "Region selective alterations of soluble guanylate cyclase content and modulation in brain of cirrhotic patients." *Hepatology*. 36(5): p.1155-62. 10.1053/jhep.2002.36365.

[237] R Corbalán, C.M., Miñana, M.D., Del Olmo, J.A., Serra, M.A., Aparisi, L., Rodrigo, J.M., Felipo, V. (2002). "Altered modulation of soluble guanylate cyclase by nitric oxide in patients with liver disease." *Metabolic Brain Disease*. 17: p.295–301. 10.1023/a:1021953717331.

[238] Cauli, O., Rodrigo, R., Piedrafita, B., Boix, J., Felipo, V. (2007). "Inflammation and hepatic encephalopathy: ibuprofen restores learning ability in rats with portacaval shunts." *Hepatology*. 46(2): p.514-9. 10.1002/hep.21734.

[239] Matsumura, T., Zerrudo, Z., Hayflick, L. (1979). "Senescent human diploid cells in culture: survival, DNA synthesis and morphology." *J Gerontol*. 34(3): p.328-34. 10.1093/geronj/34.3.328.

[240] Hayflick, L. and Moorhead, P.S. (1961). "The serial cultivation of human diploid cell strains." *Exp Cell Res*. 25: p.585-621. 10.1016/0014-4827(61)90192-6.

[241] Toussaint, O., Remacle, J., Dierick, J., Pascal, T., Frippiat, C., Zdanov, S., Magalhaes, J.P., Royer, V., Chainiauxet, (2002). "From the Hayflick mosaic to the mosaics of ageing. Role of stress-induced premature senescence in human ageing." *Int J Biochem Cell Biol*. 34(11): p.1415-29. 10.1016/s1357-2725(02)00034-1.

[242] Debacq-Chainiaux, F., Ben Ameur, R., Bauwens, E., Dumortier, E., Toutfaire, M., Toussaint, O. (2016). "Stress-Induced (Premature) Senescence." *Cellular Ageing and Replicative Senescence*. p.243–262. 10.1007/978-3-319-26239-0_13.

[243] Kida, Y. and Goligorsky, M.S. (2016). "Sirtuins, Cell Senescence, and Vascular Aging." *Can J Cardiol*. 32(5): p.634-41. 10.1016/j.cjca.2015.11.022.

[244] Di Leonardo, A., Linke, S.P., Clarkin, K., Wahl, G.M. (1994). "DNA damage triggers a prolonged p53-dependent G1 arrest and long-term induction of Cip1 in normal human fibroblasts." *Genes Dev*. 8(21): p.2540-51. 10.1101/gad.8.21.2540.

[245] Di Micco, R., Fumagalli, M., Cicalese, A., Piccinin, S., Gasparini, P., Luise, C., Schurra, C., Garre, M., Nuciforo, P.G., Bensimon, A., Maestro, R., Pelicci, P.G., Fagagna, F. (2006). "Oncogene-induced senescence is a DNA damage response triggered by DNA hyper-replication." *Nature*. 444(7119): p.638-42. 10.1038/nature05327.

[246] Kuilman, T., Michaloglou, C., Mooi, W.J., Peeper, D.S. (2010). "The essence of senescence." *Genes Dev*. 24(22): p.2463-79. 10.1101/gad.1971610.

[247] Passos, J.F., Nelson, G., Wang, C., Richter, T., Simillion, C., Proctor, C.J., Miwa, S., Olijslagers, S., Hallinan, J., Wipat, A., Saretzki, G., Rudolph, K.L., Kirkwood, T.B., Von Zglinicki, T. (2010).

"Feedback between p21 and reactive oxygen production is necessary for cell senescence." *Mol Syst Biol*. 6: p.347. 10.1038/msb.2010.5.

[248] Pazolli, E., Alspach, E., Milczarek, A., Prior, J., Piwnica-Worms, D., Stewart, S.A. (2012). "Chromatin remodeling underlies the senescence-associated secretory phenotype of tumor stromal fibroblasts that supports cancer progression." *Cancer Res*. 72(9): p.2251-61. 10.1158/0008-5472.can-11-3386.

[249] Garcia-Prat, L., Martínez-Vicente, M., Perdiguero, E., Ortet, L., Rodríguez-Ubreva, J., Rebollo, E., Ruiz-Bonilla, V., Gutarra, S., Ballestar, E., Serrano, A.L., Sandri, M., Muñoz-Cánoves, P. (2016). "Autophagy maintains stemness by preventing senescence." *Nature*. 529(7584): p.37-42. 10.1038/nature19415.

[250] Engeland, K. (2022). "Cell cycle regulation: p53-p21-RB signaling." *Cell Death Differ*. 29(5): p. 946-960. 10.1038/s41418-022-00988-z.

[251] Kwon, S.M., Hong, S.M, Lee, Y.K., Min, S., Yoon, G. (2019). "Metabolic features and regulation in cell senescence." *BMB Rep*. 52(1): p.5-12. 10.5483/bmbrep.2019.52.1.291.

[252] Dimri, G.P., Lee, X., Basile, G., Acosta, M., Scott, G., Roskelley, C., Medrano, E.E., Linskens, M., Rubelj, I., Pereira-Smith, O. (1995). "A biomarker that identifies senescent human cells in culture and in aging skin *in vivo.*" *Proc Natl Acad Sci USA*. 92(20): p.9363-7. 10.1073/pnas.92.20.9363.

[253] Campisi, J. and d'Adda di Fagagna, F. (2007). "Cellular senescence: when bad things happen to good cells." *Nat Rev Mol Cell Biol*. 8(9): p.729-40. 10.1038/nrm2233.

[254] Di Malta, C., Fryer, J.D., Settembre, C., Ballabio, A. (2012). "Astrocyte dysfunction triggers neurodegeneration in a lysosomal storage disorder." *Proc Natl Acad Sci USA*. 109(35): p.E2334-42. 10.1073/pnas.1209577109.

[255] Kawano, H., Katsurabayashi, S., Kakazu, Y., Yamashita, Y., Kubo, N., Kubo, M., Okuda, H., Takasaki, K., Kubota, K., Mishima, K., Fujiwara, M., Harata, N.C., Iwasaki, K. (2012). "Long-term culture of astrocytes attenuates the readily releasable pool of synaptic vesicles." *PLoS One*. 7(10): p.e48034. 10.1371/journal.pone.0048034.

[256] Saez-Atienzar, S. and Masliah, E. (2020). "Cellular senescence and Alzheimer disease: the egg and the chicken scenario." *Nat Rev Neurosci*. 21(8): p.433-444. 10.1038/s41583-020-0325-z.

[257] Chinta, S.J., Lieu, C.A., Demaria, M., Laberge, R.M., Campisi, J., Andersen, J.K. (2013). "Environmental stress, ageing and glial cell senescence: a novel mechanistic link to Parkinson's disease?" *J Intern Med*. 273(5): p.429-36. 10.1111/joim.12029.

[258] Smith, M.L., Chen, I.T., Zhan, Q., Bae, I., Chen, C.Y., Gilmer, T.M., Kastan, M.B., O'Connor, P.M., Fornace Jr, A.J. (1994). "Interaction of the p53-regulated protein Gadd45 with proliferating cell nuclear antigen." *Science*. 266(5189): p.1376-80. 10.1126/science.7973727.

[259] Aparisi Rey, A., Karaulanov, E., Sharopov, S., Arab, K., Schäfer, A., Gierl, M., Guggenhuber, S., Brandes, C., Pennella, L., Gruhn, W.H., Jelinek, R., Maul, C., Conrad, A., Kilb, W., Luhmann, H.J., Niehrs, C., Lutz, B. (2019). "Gadd45alpha modulates aversive learning through post-transcriptional regulation of memory-related mRNAs." *EMBO Rep*. 20(6). 10.15252/embr.201846022.

[260] Mann, M. and Jensen, O.N. (2003). "Proteomic analysis of post-translational modifications." *Nat Biotechnol*. 21(3): p.255-61. 10.1038/nbt0303-255.

[261] Jensen, O.N. (2004). "Modification-specific proteomics: characterization of post-translational modifications by mass spectrometry." *Current Opinion in Chemical Biology*. 8(1):33-41 10.1016/j.cbpa.2003.12.009.

[262] Wrighton, K.H. (2015). "Protein folding. Phosphorylation regulates IDP folding." *Nat Rev Mol Cell Biol*. 16(2): p.66. 10.1038/nrm3942.

[263] Potel, C.M., Kurzawa, N., Becher, I., Typas, A., Mateus, A., Savitski, M.M. (2021). "Impact of phosphorylation on thermal stability of proteins." *Nature Methods*. 18(7):757-759.

[264] Schastnaya, E., Raguz Nakic, Z., Gruber, C.H., Doubleday, P.F., Krishnan, A., Johns, N.I., Park, J., Wang, H.H., Sauer, U. (2021). "Extensive regulation of enzyme activity by phosphorylation in *Escherichia coli.*" *Nat Commun*. 12(1): p.5650. 10.1038/s41467-021-25988-4.

[265] Chang, K.C., Hertz, J., Zhang, X., Jin, X.L., Shaw, P., Derosa, B.A., Li, J.Y., Venugopalan, P., Valenzuela, D.A., Patel, R.D., Russano, K.R., Alshamekh, S.A., Sun, C., Tenerelli, K., Li, C., Velmeshev, D., Cheng, Y., Boyce, T.M., Dreyfuss, A., Uddin, M.S., Muller, K.J., Dykxhoorn, D.M., Goldberg, J.L. (2017). "Novel Regulatory Mechanisms for the SoxC Transcriptional Network Required for Visual Pathway Development." *J Neurosci*. 37(19): p.4967-4981. 10.1523/jneurosci.3430-13.2017.

[266] Myers, S.A., Peddada, S., Chatterjee, N., Friedrich, T., Tomoda, K., Krings, G., Thomas, S., Maynard, J., Broeker, M., Thomson, M., Pollard, K., Yamanaka, S., Burlingame, A.L., Panning, B. (2016). "SOX2 *O*-GlcNAcylation alters its protein-protein interactions and genomic occupancy to modulate gene expression in pluripotent cells." *Elife*. 5: p.e10647. 10.7554/elife.10647.

[267] Kosenko, E.A., Tikhonova, L.A., Alilova, G.A., Montoliu, C., Barreto, G.E., Aliev, G., Kaminsky, Y.G. (2017). "Portacaval shunting causes differential mitochondrial superoxide production in brain regions." *Free Radic Biol Med*. 113: p.109-118. 10.1016/j.freeradbiomed.2017.09.023.

[268] Klose, J., Görg, B., Berndt, C., Häussinger, D., Aktas, O., Prozorovski, T. (2014). "Protein oxidative damage in the hippocampus in a mouse model of acute hyperammonemia." *European Journal of Medical Research*. 19(Suppl 1):S29. 10.1186/2047-783x-19-s1-s29.

[269] Widmer, R., Kaiser, B., Engels, M., Jung, T., Grune, T. (2007). "Hyperammonemia causes protein oxidation and enhanced proteasomal activity in response to mitochondria-mediated oxidative stress in rat primary astrocytes." *Arch Biochem Biophys*. 464(1): p.1-11. 10.1016/j.abb.2007.03.027.

[270] Yang, J., Yin, M., Hou, Y., Li, H., Guo, Y., Yu, H., Zhang, K., Zhang, C., Jia, L., Zhang, F., Li, X., Bian, H., Li, Z. (2022). "Role of ammonia for brain abnormal protein glycosylation during the development of hepatitis B virus-related liver diseases." *Cell Biosci*. 12(1): p.16. 10.1186/s13578-022-00751-4.

[271] Radi, R. (2013). "Protein tyrosine nitration: biochemical mechanisms and structural basis of functional effects." *Acc Chem Res*. 46(2): p.550-9. 10.1021/ar300234c.

[272] Suarez, I., Bodega, G., Arilla, E., Felipo, V., Fernández, B. (2006). "The expression of nNOS, iNOS and nitrotyrosine is increased in the rat cerebral cortex in experimental hepatic encephalopathy." *Neuropathol Appl Neurobiol*. 32(6): p.594-604. 10.1111/j.1365-2990.2006.00768.x.

[273] Schliess, F. and Häussinger, D. (2001). "Hepatic encephalopathy and nitric oxide." *J Hepatol*. 34(4): p.610-2. 10.1016/s0168-8278(01)00051-4.

[274] Jayakumar, A.R., Liu, M., Moriyama, M., Ramakrishnan, R., Forbush 3rd, B., Reddy, P.V.B., Norenberg, M.D. (2008). "Na-K-Cl Cotransporter-1 in the mechanism of ammonia-induced astrocyte swelling." *J Biol Chem*. 283(49): p.33874-82. 10.1074/jbc.m804016200.

[275] Görg, B., Qvartskhava, N., Voss, P., Grune, T., Häussinger, D., Schliess, F. (2007). "Reversible inhibition of mammalian glutamine synthetase by tyrosine nitration." *FEBS Lett*. 581(1): p.84-90. 10.1016/j.febslet.2006.11.081.

[276] Görg, B., Wettstein, M., Metzger, S., Schliess, F., Häussinger, D. (2005). "LPS-induced tyrosine nitration of hepatic glutamine synthetase." *Hepatology*. 42(2): p.499. 10.1002/hep.20820.

[277] Lockwood, A.H., McDonald, J.M., Reiman, R.E., Gelbard, A.S., Laughlin, J.S., Duffy, T.E., Plum, F. (1979). "The dynamics of ammonia metabolism in man. Effects of liver disease and hyperammonemia." *J Clin Invest*. 63(3): p.449-60. 10.1172/jci109322.

[278] Girard, G. and Butterworth, R.F. (1992). "Effect of portacaval anastomosis on glutamine synthetase activities in liver, brain, and skeletal muscle." *Dig Dis Sci*. 37(7): p.1121-6. 10.1007/bf01300297.

[279] Jayakumar, A.R. and Norenberg, M.D. (2010). "The Na-K-Cl Co-transporter in astrocyte swelling." *Metab Brain Dis*. 25(1): p.31-8. 10.1007/s11011-010-9180-3.

[280] Lam, P., Newland, J., Faull, R.L.M., Kwakowsky, A. (2023). "Cation-Chloride Cotransporters KCC2 and NKCC1 as Therapeutic Targets in Neurological and Neuropsychiatric Disorders." *Molecules*. 28(3), 1344. 10.3390/molecules28031344.

[281] Chen, H. and Sun, D. (2005). "The role of Na-K-Cl co-transporter in cerebral ischemia." *Neurol Res*. 27(3): p.280-6. 10.1179/016164105x25243.

[282] MacVicar, B.A. (2002). "Intrinsic optical signals in the rat optic nerve: role for K(+) uptake via NKCC1 and swelling of astrocytes." *Glia*. 37(2): p.114-23. 10.1002/glia.10023.

[283] Hochstrasser, M., (1996). "Ubiquitin-dependent protein degradation." *Annu Rev Genet*. 30: p. 405-39. 10.1146/annurev.genet.30.1.405.

[284] Deng, L., Meng, T., Chen, L., Wei, W., Wang, P. (2020). "The role of ubiquitination in tumorigenesis and targeted drug discovery." *Signal Transduct Target Ther*. 5(1): p.11. 10.1038/s41392-020-0107-0.

[285] Kulathu, Y. and Komander, D. (2012). "Atypical ubiquitylation - the unexplored world of polyubiquitin beyond Lys48 and Lys63 linkages." *Nat Rev Mol Cell Biol*. 13(8): p.508-23. 10.1038/nrm3394.

[286] French, M.E., Kretzmann, B.R., Hicke, L. (2009). "Regulation of the RSP5 ubiquitin ligase by an intrinsic ubiquitin-binding site." *J Biol Chem*, 284(18): p.12071-9. 10.1074/jbc.m901106200.

[287] Stadtman, E.R. (1990). "Metal ion-catalyzed oxidation of proteins: biochemical mechanism and biological consequences." *Free Radic Biol Med*. 9(4): p.315-25. 10.1016/0891-5849(90)90006-5.

[288] Bizzozero, O.A., DeJesus, G., Callahan, K., Pastuszyn, A. (2005). "Elevated protein carbonylation in the brain white matter and gray matter of patients with multiple sclerosis." *J Neurosci Res*. 81(5): p.687-95. 10.1002/jnr.20587.

[289] Sultana, R. and Butterfield, D.A. (2010). "Role of oxidative stress in the progression of Alzheimer's disease." *J Alzheimers Dis*, *Current Neuropharmacology*. 19(1): p.341-53. 10.2174/1570159x18666200122122512.

[290] Butterfield, D.A., Perluigi, M., Reed, T., Muharib, T., Hughes, C.P., Robinson, R.A.S., Sultana, R. (2012). "Redox proteomics in selected neurodegenerative disorders: from its infancy to future applications." *Antioxid Redox Signal*. 17(11): p.1610-55. 10.1089/ars.2011.4109.

[291] Hart, G.W. (1997). "Dynamic *O*-linked glycosylation of nuclear and cytoskeletal proteins." *Annu Rev Biochem*. 66: p.315-35. 10.1146/annurev.biochem.66.1.315.

[292] Hu, Y., Suarez, J., Fricovsky, E., Wang, H., Scott, B.T., Trauger, S.A., Han, W., Hu, Y., Oyeleye, M.O., Dillmann, W.H. (2009). "Increased enzymatic *O*-GlcNAcylation of mitochondrial proteins impairs mitochondrial function in cardiac myocytes exposed to high glucose." *J Biol Chem*. 284(1): p. 547-555. 10.1074/jbc.m808518200.

[293] Liu, F., K.I., Grundke-Iqbal, I., Hart, G.W., Gong, C.X. (2004). "*O*-GlcNAcylation regulates phosphorylation of tau: A mechanism involved in Alzheimer's disease." *Proceedings of the National Academy of Sciences of the United States of America*. 101: p.10804-10809. 10.1073/pnas.0400348101.

[294] Lee, B.E., Suh, P.G., Kim, J.I. (2021). "*O*-GlcNAcylation in health and neurodegenerative diseases." *Exp Mol Med*. 53(11): p.1674-1682. 10.1038/s12276-021-00709-5.

[295] Liu, Y., Yao, R.Z., Lian, S., Liu, P., Hu, Y.J., Shi, H.Z., Lv, H.M., Yang, Y.Y., Xu, B., Li, S.Z. (2021). "*O*-GlcNAcylation: the "stress and nutrition receptor" in cell stress response." *Cell Stress Chaperones*. 26(2): p.297-309. 10.1007/s12192-020-01177-y.

[296] Ma, J. and Hart, G.W. (2014). "*O*-GlcNAc profiling: from proteins to proteomes." *Clin Proteomics*. 11(1): p.8. 10.1186/1559-0275-11-8.

[297] Wulff-Fuentes, E., Berendt, R.R., Massman, L., Danner, L., Malard, F., Vora, J., Kahsay, R., Olivier-Van Stichelen, S. (2021). "The human *O*-GlcNAcome database and meta-analysis." *Sci Data*. 8(1): p.25. 10.1038/s41597-021-00810-4.

[298] Haltiwanger, R.S., Holt, G.D., Hart, G.W. (1990). "Enzymatic addition of *O*-GlcNAc to nuclear and cytoplasmic proteins. Identification of a uridine diphospho-N-acetylglucosamine:peptide beta-N-acetylglucosaminyltransferase." *J Biol Chem*. 265(5): p. 2563-8.

[299] Dong, D.L. and Hart, G.W. (1994). "Purification and characterization of an *O*-GlcNAc selective N-acetyl-beta-D-glucosaminidase from rat spleen cytosol." *J Biol Chem*. 269(30): p.19321-30.

[300] Butkinaree, C., Park, K., Hart, G.W. (2010). "*O*-linked beta-N-acetylglucosamine (*O*-GlcNAc): Extensive crosstalk with phosphorylation to regulate signaling and transcription in response to nutrients and stress." *Biochim Biophys Acta*. 1800(2): p.96-106. 10.1016/j.bbagen.2009.07.018.

[301] Hanover, J.A., Krause, M.W., Love, D.C. (2010). "The hexosamine signaling pathway: *O*-GlcNAc cycling in feast or famine." *Biochim Biophys Acta*. 1800(2): p.80-95. 10.1016/j.bbagen.2009.07.017.

[302] Yang, X. and Qian, K. (2017). "Protein *O*-GlcNAcylation: emerging mechanisms and functions." *Nat Rev Mol Cell Biol*. 18(7): p.452-465. 10.1038/nrm.2017.22.

[303] Gong, C.X., Liu, F., Iqbal, K. (2016). "*O*-GlcNAcylation: A regulator of tau pathology and neurodegeneration." *Alzheimers Dement*. 12(10): p.1078-1089. 10.1016/j.jalz.2016.02.011.

[304] Kreppel, L.K., Blomberg, M.A., Hart, G.W. (1997). "Dynamic glycosylation of nuclear and cytosolic proteins. Cloning and characterization of a unique *O*-GlcNAc transferase with multiple tetratricopeptide repeats." *J Biol Chem*. 272(14): p.9308-15. 10.1074/jbc.272.14.9308.

[305] Shafi, R., Iyer, S.P., Ellies, L.G., O'Donnell, N., Marek, K.W., Chui, D., Hart, G.W., Marth, J.D. (2000). "The *O*-GlcNAc transferase gene resides on the X chromosome and is essential for embryonic stem cell viability and mouse ontogeny." *Proc Natl Acad Sci USA*. 97(11): p.5735-9. 10.1073/pnas.100471497.

[306] Chen, J., Dong, X., Cheng, X., Zhu, Q., Zhang, J., Li, Q., Huang, X., Wang, M., Li, L., Guo, W., Sun, B., Shu, Q., Yi, W., Li, X. (2021). "Ogt controls neural stem/progenitor cell pool and adult neurogenesis through modulating Notch signaling." *Cell Rep*. 34(13): p.108905. 10.1016/j.celrep.2021.108905.

[307] Pravata, V.M., Muha, V., Gundogdu, M., Ferenbach, A.T., Kakade, P.S., Vandadi, V., Wilmes, A.C., Borodkin, V.S., Joss, S., Stavridis, M.P., Van Aalten, D.M.F. (2019). "Catalytic deficiency of *O*-GlcNAc transferase leads to X-linked intellectual disability." *Proc Natl Acad Sci USA*. 116(30): p. 14961-14970. 10.1073/pnas.1900065116.

[308] Deplus, R., Delatte, B., Schwinn, M.K., Defrance, M., Méndez, J., Murphy, N., Dawson, M.A., Volkmar, M., Putmans, P., Calonne, E., Shih, A.H., Levine, R.L., Bernard, O., Mercher, T., Solary,

E., Urh, M., Daniels, D.L., Fuks, F. (2013). "TET2 and TET3 regulate GlcNAcylation and H3K4 methylation through OGT and SET1/COMPASS." *EMBO J*. 32(5): p.645-55. 10.1038/emboj.2012.357.

[309] N. Iyer, S.P. and Hart, G.W. (2003). "Roles of the tetratricopeptide repeat domain in *O*-GlcNAc transferase targeting and protein substrate specificity." J Biol Chem. 278(27): p.24608-16. 10.1074/jbc.m300036200.

[310] Gloster, T. and Vocadlo, D.J. (2010). "Mechanism, Structure, and Inhibition of *O*-GlcNAc Processing Enzymes." *Curr Signal Transduct Ther*. 5(1): p.74-91. 10.2174/157436210790226537.

[311] Lazarus, B.D., Love, D.C., Hanover, J.A. (2006). "Recombinant *O*-GlcNAc transferase isoforms: identification of *O*-GlcNAcase, yes tyrosine kinase, and tau as isoform-specific substrates." *Glycobiology*. 16(5): p.415-21. 10.1093/glycob/cwj078.

[312] Gao, Y., Wells, L., Comer, F.I., Parker, G.J., Hart, G.W. (2001). "Dynamic *O*-glycosylation of nuclear and cytosolic proteins: cloning and characterization of a neutral, cytosolic beta-N-acetylglucosaminidase from human brain." *J Biol Chem*. 276(13): p.9838-45. 10.1074/jbc.m010420200.

[313] Alonso, J., Schimpl, M., Van Aalten, D.M. (2014). "*O*-GlcNAcase: promiscuous hexosaminidase or key regulator of *O*-GlcNAc signaling?" *J Biol Chem*. 289(50): p.34433-9. 10.1074/jbc.r114.609198.

[314] Comtesse, N., Maldener, E., Meese, E. (2001). "Identification of a nuclear variant of MGEA5, a cytoplasmic hyaluronidase and a beta-N-acetylglucosaminidase." *Biochemical and Biophysical Research Communications*. 283(3): p.634-640. 10.1006/bbrc.2001.4815.

[315] Schultz, J. and Pils, B. (2002). "Prediction of structure and functional residues for *O*-GlcNAcase, a divergent homologue of acetyltransferases." *FEBS Lett*. 529(2-3): p.179-82. 10.1016/s0014-5793(02)03322-7.

[316] Toleman, C., Paterson, A.J., Whisenhunt, T.R., Kudlow, J.E. (2004). "Characterization of the histone acetyltransferase (HAT) domain of a bifunctional protein with activable *O*-GlcNAcase and HAT activities." *J Biol Chem*. 279(51): p.53665-73. 10.1074/jbc.m410406200.

[317] Elbatrawy, A.A., Kim, E.J., Nam, G. (2020). *O*-GlcNAcase: "Emerging Mechanism, Substrate Recognition and Small-Molecule Inhibitors." *ChemMedChem*. 15(14): p.1244-1257. 10.1002/cmdc.202000077.

[318] Lu, S., Haskali, M.B., Ruley, K.M., Dreyfus, N.J., DuBois, S.L., Paul, S., Liow, J., Morse, C.L., Kowalski, A., Gladding, R.L., Gilmore, J., Mogg, A.J., Morin, S.M., Lindsay-Scott, P.J., Ruble, J.C., Kant, N.A., Shcherbinin, S., Barth, V.N., Johnson, M.P., Cuadrado, M., Jambrina, E., Mannes, A.J., Nuthall, H.N., Zoghbi, S.S., Jesudason, C.D., Innis, R.B., Pike, V.W. (2020). "PET ligands [$^{(18)}$F]LSN3316612 and [$^{(11)}$C]LSN3316612 quantify *O*-linked-beta-N-acetyl-glucosamine hydrolase in the brain." *Sci Transl Med*. 12(543). 10.1126/scitranslmed.aau2939.

[319] Yuzwa, S.A., Shan, X., Macauley, M.S., Clark, T., Skorobogatko, Y., Vosseller, K., Vocadlo, D.J. (2012). "Increasing *O*-GlcNAc slows neurodegeneration and stabilizes tau against aggregation." *Nat Chem Biol*. 8(4): p. 393-9. 10.1038/nchembio.797.

[320] Martinez, M., Renuse, S., Kreimer, S., O'Meally, R., Natov, P., Madugundu, A.K., Nirujogi, R.S., Tahir, R., Cole, R., Pandey, A., Zachara, E.N. (2021). "Quantitative Proteomics Reveals that the OGT Interactome Is Remodeled in Response to Oxidative Stress." *Mol Cell Proteomics*. 20: p. 100069. 10.1016/j.mcpro.2021.100069.

[321] Groves, J.A., Maduka, A.O., O'Meally, R.N., Cole, R.N., Zachara, N.E. (2017). "Fatty acid synthase inhibits the *O*-GlcNAcase during oxidative stress." *J Biol Chem*. 292(16): p.6493-6511. 10.1074/jbc.m116.760785.

[322] Cetinbas, N., Macauley, M.S., Stubbs, K.A., Drapala, R., Vocadlo, D.J. (2006). "Identification of Asp174 and Asp175 as the key catalytic residues of human *O*-GlcNAcase by functional analysis of site-directed mutants." *Biochemistry*. 45(11): p.3835-44. 10.1021/bi052370b.

[323] Hart, G.W., Housley, M.P., Slawson, C. (2007). "Cycling of *O*-linked beta-N-acetylglucosamine on nucleocytoplasmic proteins." *Nature*. 446(7139): p.1017-22. 10.1038/nature05815.

[324] Flores-Opazo, M., McGee, S.L., Hargreaves, M. (2020). "Exercise and GLUT4." *Exerc Sport Sci Rev*. 48(3): p.110-118. 10.1249/jes.0000000000000224.

[325] Marshall, S., Bacote, V., Traxinger, R.R. (1991). "Discovery of a metabolic pathway mediating glucose-induced desensitization of the glucose transport system. Role of hexosamine biosynthesis in the induction of insulin resistance." *J Biol Chem*. 266(8): p. 4706-12.

[326] Love, D.C. and Hanover, J.A. (2005). "The hexosamine signaling pathway: deciphering the "*O*-GlcNAc code". *Sci STKE*. (312): p.re13. 10.1126/stke.3122005re13.

[327] Wells, L., Vosseller, K., Hart, G.W. (2003). "A role for N-acetylglucosamine as a nutrient sensor and mediator of insulin resistance." *Cell Mol Life Sci*. 60(2): p.222-8. 10.1007/s000180300017.

[328] Paneque, A., Fortus, H., Zheng, J., Werlen, G., Jacinto, E. (2023). "The Hexosamine Biosynthesis Pathway: Regulation and Function." *Genes (Basel)*. 14(4):933. 10.3390/genes14040933.

[329] Coussement, P., Bauwens, D., Peters, G., Maertens, J., De Mey, M. (2020). "Mapping and refactoring pathway control through metabolic and protein engineering: The hexosamine biosynthesis pathway." *Biotechnol Adv*. 40: p.107512. 10.1016/j.biotechadv.2020.107512.

[330] Marshall, S. (2006). "Role of insulin, adipocyte hormones, and nutrient-sensing pathways in regulating fuel metabolism and energy homeostasis: a nutritional perspective of diabetes, obesity, and cancer." *Sci STKE*. (346): p.re7. 10.1126/stke.3462006re7.

[331] Zachara, N.E. and Hart, G.W. (2004). "*O*-GlcNAc modification: a nutritional sensor that modulates proteasome function." *Trends Cell Biol*. 14(5): p.218-21. 10.1016/j.tcb.2004.03.005.

[332] Zeidan, Q., Wang, Z., De Maio, A., Hart, G.W. (2010). *O*-GlcNAc cycling enzymes associate with the translational machinery and modify core ribosomal proteins. *Mol Biol Cell*. 21(12): p. 1922-36.

[333] Powers, E.T. (2015). "Translation: An *O*-GlcNAc stamp of approval." *Nat Chem Biol*. 11(5): p. 307-8. 10.1038/nchembio.1777.

[334] Hardiville, S. and Hart, G.W. (2014). "Nutrient regulation of signaling, transcription, and cell physiology by *O*-GlcNAcylation." *Cell Metab*. 20(2): p.208-13. 10.1016/j.cmet.2014.07.014.

[335] Ozcan, S., Andrali, S.S., Cantrell, J.E. (2010). "Modulation of transcription factor function by *O*-GlcNAc modification." *Biochim Biophys Acta*. 1799(5-6): p.353-64. 10.1016/j.bbagrm.2010.02.005.

[336] Slawson, C. and Hart, G.W. (2011). "*O*-GlcNAc signalling: implications for cancer cell biology." *Nat Rev Cancer*. 11(9): p. 678-84. 10.1038/nrc3114.

[337] Shi, W.W., Shi, C., Wang, T.Y., Li, Y.L., Zhou, Y.K., Zhang, X., Bierer, D., Zheng, J.S., Liu, L. (2022). "Total Chemical Synthesis of Correctly Folded Disulfide-Rich Proteins Using a Removable *O*-Linked beta-N-Acetylglucosamine Strategy." *J Am Chem Soc*. 144(1): p.349-357. 10.1021/jacs.1c10091.

[338] Guinez, C., Mir, A.M., Leroy, Y., Cacan, R., Michalski, J., Lefebvre, T. (2007). "Hsp70-GlcNAc-binding activity is released by stress, proteasome inhibition, and protein misfolding." *Biochem Biophys Res Commun*. 361(2): p.414-20. 10.1016/j.bbrc.2007.07.020.

[339] Wang, Z.V., Deng, Y., Gao, N., Pedrozo, Z., Li, D.L., Morales, C.R., Criollo, A., Luo, X., Tan, W., Jiang, N., Lehrman, M.A., Rothermel, B.A., Lee, A.H., Lavandero, S., Mammen, P.P.A., Ferdous, A., Gillette, T.G., Scherer, P.E., Hill, J.A. (2014). "Spliced X-box binding protein 1 couples the unfolded protein response to hexosamine biosynthetic pathway." *Cell*. 156(6): p.1179-1192. 10.1016/j.cell.2014.01.014.

[340] Ngoh, G.A., Hamid, T., Prabhu, S.D., Jones, S.P. (2009). "*O*-GlcNAc signaling attenuates ER stress-induced cardiomyocyte death." *Am J Physiol Heart Circ Physiol*. 297(5): p.H1711-9. 10.1152/ajpheart.00553.2009.

[341] Saha, A., Bello, D., Fernandez-Tejada, A. (2021). "Advances in chemical probing of protein *O*-GlcNAc glycosylation: structural role and molecular mechanisms." *Chem Soc Rev*. 50(18): p. 10451-10485. 10.1039/d0cs01275k.

[342] Roos, M.D., Su, K., Baker, J.R., Kudlow, J.E. (1997). "*O*-glycosylation of an Sp1-derived peptide blocks known Sp1 protein interactions." *The Journal of Molecular Cell Biology*. 17(11): p.6472-80. 10.1128/mcb.17.11.6472.

[343] Sayat, R., Leber, B., Grubac, V., Wiltshire, L., Persad, S. (2008). "*O*-GlcNAc-glycosylation of beta-catenin regulates its nuclear localization and transcriptional activity." *Exp Cell Res*. 314(15): p. 2774-87. 10.1016/j.yexcr.2008.05.017.

[344] Ruba, A. and Yang, W. (2016). "*O*-GlcNAc-ylation in the Nuclear Pore Complex." *Cell Mol Bioeng*. 9(2): p.227-233. 10.1007/s12195-016-0440-0.

[345] Dudognon, P., Maeder-Garavaglia, C., Carpentier, J.L., Paccaud, J.P. (2004). "Regulation of a COPII component by cytosolic *O*-glycosylation during mitosis." *FEBS Lett*. 561(1-3): p.44-50. 10.1016/s0014-5793(04)00109-7.

[346] Guinez, C., Morelle, W., Michalski, J.C., Lefebvre, T. (2005). "*O*-GlcNAc glycosylation: a signal for the nuclear transport of cytosolic proteins?" *Int J Biochem Cell Biol*. 37(4): p.765-74. 10.1016/j.biocel.2004.12.001.

[347] Wang, F., Chen, L., Zhang, B., Li, Z., Shen, M., Tang, L., Zhang, Z., Shao, J., Zhang, F., Zheng, S., Tan, S. (2022). "*O*-GlcNAcylation Coordinates Glutaminolysis by Regulating the Stability and Membrane Trafficking of ASCT2 in Hepatic Stellate Cells." *J Clin Transl Hepatol*. 10(6): p.1107-1116. 10.14218/jcth.2021.00413.

[348] Chu, C.S., Lo, P.W., Yeh, Y.H., Hsu, P.H., Peng, S.H., Teng, Y.C., Kang, M.L., Wong, C.H., Juan, L.J. (2014). "*O*-GlcNAcylation regulates EZH2 protein stability and function." *Proc Natl Acad Sci* USA. 111(4): p.1355-60. 10.1073/pnas.1323226111.

[349] Zhu, Y., Liu, T.W., Cecioni, S., Eskandari, R., Zandberg, W.F., Vocadlo, D.J. (2015). "*O*-GlcNAc occurs cotranslationally to stabilize nascent polypeptide chains." *Nat Chem Biol*. 11(5): p.319-25. 10.1038/nchembio.1774.

[350] Nagy, T., Champattanachai, V., Marchase, R.B., Chatham, J.C. (2006). "Glucosamine inhibits angiotensin II-induced cytoplasmic Ca^{2+} elevation in neonatal cardiomyocytes via protein-associated *O*-linked N-acetylglucosamine." *Am J Physiol Cell Physiol*. 290(1): p.C57-65. 10.1152/ajpcell.00263.2005.

[351] Liu, J., Pang, Y., Chang, T., Bounelis, P., Chatham, J.C., Marchase, R.B. (2006). "Increased hexosamine biosynthesis and protein *O*-GlcNAc levels associated with myocardial protection against calcium paradox and ischemia." *J Mol Cell Cardiol*. 40(2): p.303-12. 10.1016/j.yjmcc.2005.11.003.

[352] Yang, W.H., Kim, J.E., Nam, H.W., Ju, J.W., Kim, H.S., Kim, Y.S., Cho, J.W. (2006). "Modification of p53 with *O*-linked N-acetylglucosamine regulates p53 activity and stability." *Nat Cell Biol*. 8(10): p.1074-83. 10.1038/ncb1470.

[353] Shaw, P., Freeman, J., Bovey, R., Iggo, R. (1996). "Regulation of specific DNA binding by p53: evidence for a role for *O*-glycosylation and charged residues at the carboxy-terminus." *Oncogene*. 12(4): p. 921-30.

[354] Chou, T.Y. and Hart, G.W. (2001). "*O*-linked N-acetylglucosamine and cancer: messages from the glycosylation of c-Myc." *Adv Exp Med Biol*. 491: p.413-8. 10.1007/978-1-4615-1267-7_26.

[355] James, L.R., Tang, D., Ingram, A., Ly, H., Thai, K., Cai, L., Scholey, J.W. (2002). "Flux through the hexosamine pathway is a determinant of nuclear factor kappaB- dependent promoter activation." *Diabetes*. 51(4): p.1146-56. 10.2337/diabetes.51.4.1146.

[356] Golks, A., Tran, T.T., Goetschy, J.F., Guerini, D. (2007). "Requirement for *O*-linked N-acetylglucosaminyltransferase in lymphocytes activation." *EMBO J*. 26(20): p.4368-79. 10.1038/sj.emboj.7601845.

[357] Han, I. and Kudlow, J.E. (1997). "Reduced *O* glycosylation of Sp1 is associated with increased proteasome susceptibility." *Mol Cell Biol*. 17(5): p.2550-8. 10.1128/mcb.17.5.2550.

[358] Majumdar, G., Harmon, A., Candelaria, R., Martinez-Hernandez, A., Raghow, R., Solomon, S.S. (2003). "*O*-glycosylation of Sp1 and transcriptional regulation of the calmodulin gene by insulin and glucagon." *Am J Physiol Endocrinol Metab*. 285(3): p.E584-91. 10.1152/ajpendo.00140.2003.

[359] Ma, J. and Hart, G.W. (2013). "Protein *O*-GlcNAcylation in diabetes and diabetic complications." *Expert Rev Proteomics*. 10(4): p.365-80. 10.1586/14789450.2013.820536.

[360] Kadonaga, J.T., Courey, A.J., Ladika, J., Tjian, R. (1988). "Distinct regions of Sp1 modulate DNA binding and transcriptional activation." *Science*. 242(4885): p.1566-70. 10.1126/science.3059495.

[361] Weigert, C., Klopfer, K., Kausch, C., Brodbeck, K., Stumvoll, M., Häring, H.U., Schleicher, E.D. (2003). "Palmitate-induced activation of the hexosamine pathway in human myotubes: increased expression of glutamine:fructose-6-phosphate aminotransferase." *Diabetes*. 52(3): p.650-6. 10.2337/diabetes.52.3.650.

[362] Du, X.L., Edelstein, D., Rossetti, L., Fantus, I.G., Goldberg, H., Ziyadeh, F., Wu, J., Brownlee, M. (2000). "Hyperglycemia-induced mitochondrial superoxide overproduction activates the hexosamine pathway and induces plasminogen activator inhibitor-1 expression by increasing Sp1 glycosylation." *Proc Natl Acad Sci USA*. 97(22): p.12222-6. 10.1073/pnas.97.22.12222.

[363] Majumdar, G., right, J., Markowitz, P., Martinez-Hernandez, A., Raghow, R., Solomon, S.S. (2004). "Insulin stimulates and diabetes inhibits *O*-linked N-acetylglucosamine transferase and *O*-glycosylation of Sp1." *Diabetes*. 53(12): p.3184-92. 10.2337/diabetes.53.12.3184.

[364] Lim, K. and Chang, H.I. (2009). "*O*-GlcNAcylation of Sp1 interrupts Sp1 interaction with NF-Y." *Biochem Biophys Res Commun*. 382(3): p.593-7. 10.1016/j.bbrc.2009.03.075.

[365] Ha, C. and Lim, K. (2015). "*O*-GlcNAc modification of Sp3 and Sp4 transcription factors negatively regulates their transcriptional activities." *Biochem Biophys Res Commun*. 467(2): p. 341-7. 10.1016/j.bbrc.2015.09.155.

[366] Durgan, D.J., Pat, B.M., Laczy, B., Bradley, J.A., Tsai, J.Y., Grenett, M.H., Ratcliffe, W.F., Brewer, R.A., Nagendran, J., Villegas-Montoya, C., Zou, C., Zou, L., Johnson Jr, R.L., Dyck, J.R.B., Bray, M.S., Gamble, K.L., Chatham, J.C., Young, M.E. (2011). "*O*-GlcNAcylation, novel post-translational modification linking myocardial metabolism and cardiomyocyte circadian clock." *J Biol Chem*. 286(52): p.44606-19. 10.1074/jbc.m111.278903.

[367] Yang, A.Q., Li, D., Chi, L., Ye, X.S. (2017). "Validation, Identification, and Biological Consequences of the Site-specific *O*-GlcNAcylation Dynamics of Carbohydrate-responsive Element-binding Protein (ChREBP)." *Mol Cell Proteomics*. 16(7): p.1233-1243. 10.1074/mcp.M116.061416.

[368] Housley, M.P., Rodgers, J.T., Udeshi, N.D., Kelly, T.J., Shabanowitz, J., Hunt, D.F., Puigserver, P., Hart, G.W. (2008). "*O*-GlcNAc regulates FoxO activation in response to glucose." *J Biol Chem*. 283(24): p. 16283-92. 10.1074/jbc.m802240200.

[369] Fan, Q., Moen, A., Anonsen, J.H, Bindesbøll, C., Sæther, T., Carlson, C.R., Grønning-Wang, L.M. (2018). "*O*-GlcNAc site-mapping of liver X receptor-alpha and *O*-GlcNAc transferase." *Biochem Biophys Res Commun*. 499(2): p.354-360. 10.1016/j.bbrc.2018.03.164.

[370] Housley, M.P., Udeshi, N.D., Rodgers, J.T., Shabanowitz, J., Puigserver, P., Hunt, D.F., Hart, G.W. (2009). "A PGC-1alpha-*O*-GlcNAc transferase complex regulates FoxO transcription factor activity in response to glucose." *J Biol Chem*. 284(8): p.5148-57. 10.1074/jbc.m808890200.

[371] Ji, S., Park, S.Y., Roth, J., Kim, H.S., Cho, J.W. (2012). "*O*-GlcNAc modification of PPARgamma reduces its transcriptional activity." *Biochem Biophys Res Commun*. 417(4): p.1158-63. 10.1016/j.bbrc.2011.12.086.

[372] Barthel, A., Schmoll, D., Unterman, T.G. (2005). "FoxO proteins in insulin action and metabolism." *Trends Endocrinol Metab*. 16(4): p.183-9. 10.1016/j.tem.2005.03.010.

[373] Kuo, M., Zilberfarb, V., Gangneux, N., Christeff, N., Issad, T. (2008). "*O*-glycosylation of FoxO1 increases its transcriptional activity towards the glucose 6-phosphatase gene." *FEBS Lett*. 582(5): p.829-34. 10.1016/j.febslet.2008.02.010.

[374] Kuo, M., Zilberfarb, V., Gangneux, N., Christeff, N., Issad, T. (2008). "*O*-GlcNAc modification of FoxO1 increases its transcriptional activity: a role in the glucotoxicity phenomenon?" *Biochimie*. 90(5): p.679-85. 10.1016/j.biochi.2008.03.005.

[375] Li, Y.N., Chen, C.W., Trinh-Minh, T., Zhu, H., Matei, A., Györfi, A., Kuwert, F., Hubel, P., Ding, X., Manh, C.T., Xu, X., Liebel, C., Fedorchenko, V., Liang, R., Huang, K., Pfannstiel, J., Huang, M.C., Lin, N.Y., Ramming, A., Schett, G., Distler, J.H.W. (2022). "Dynamic changes in *O*-GlcNAcylation regulate osteoclast differentiation and bone loss via nucleoporin 153." *Bone Res*. 10(1): p.51. 10.1038/s41413-022-00218-9.

[376] Mizuguchi-Hata, C., Ogawa, Y., Oka, M., Yoneda, Y. (2013). "Quantitative regulation of nuclear pore complex proteins by *O*-GlcNAcylation." *Biochim Biophys Acta*. 1833(12): p.2682-2689. 10.1016/j.bbamcr.2013.06.008.

[377] Zhu, Y., Liu, T.W., Madden, Z., Yuzwa, S.A., Murray, K., Cecioni, S., Zachara, N., Vocadlo, D.J. (2016). "Post-translational *O*-GlcNAcylation is essential for nuclear pore integrity and maintenance of the pore selectivity filter." *J Mol Cell Biol*. 8(1): p.2-16. 10.1093/jmcb/mjv033.

[378] Guinez, C., Mir, A.M., Dehennaut, V., Cacan, R., Harduin-Lepers, A., Michalski, J.C., Lefebvre, T. (2008). "Protein ubiquitination is modulated by *O*-GlcNAc glycosylation." *FASEB J*. 22(8): p. 2901-11. 10.1096/fj.07-102509.

[379] Martinez, M.R., Dias, T.B., Natov, P.S., Zachara, N.E. (2017). "Stress-induced *O*-GlcNAcylation: an adaptive process of injured cells." *Biochem Soc Trans*. 45(1): p.237-249. 10.1042/bst20160153.

[380] Yuzwa, S.A. and Vocadlo, D.J. (2014). "*O*-GlcNAc and neurodegeneration: biochemical mechanisms and potential roles in Alzheimer's disease and beyond." *Chem Soc Rev*. 43(19): p. 6839-58. 10.1039/c4cs00038b.

[381] Chatham, J.C., Zhang, J., Wende, A.R. (2021). "Role of *O*-Linked N-Acetylglucosamine Protein Modification in Cellular (Patho)Physiology." *Physiol Rev*. 101(2): p.427-493. 10.1152/physrev.00043.2019.

[382] Lee, J.B., Pyo, K.H., Kim, H.R. (2021). "Role and Function of *O*-GlcNAcylation in Cancer." *Cancers* (*Basel*). 13(21). 10.3390/cancers13215365.

[383] Wani, W.Y., Chatham, J.C., Darley-Usmar, V., McMahon, L.L., Zhang, J. (2017). "*O*-GlcNAcylation and neurodegeneration." *Brain Res Bull*. 133: p.80-87. 10.1016/j.brainresbull.2016.08.002.

[384] Liu, Y., Chen, Q., Zhang, N., Zhang, K., Dou, T., Cao, Y., Liu, Y., Li, K., Hao, X., Xie, X., Li, W., Ren, Y., Zhang, J. (2020). "Proteomic profiling and genome-wide mapping of *O*-GlcNAc chromatin-associated proteins reveal an *O*-GlcNAc-regulated genotoxic stress response." *Nat Commun*. 11(1): p.5898. 10.1038/s41467-020-19579-y.

[385] Fahie, K.M.M., Papanicolaou, K.N., Zachara, N.E. (2022). "Integration of *O*-GlcNAc into Stress Response Pathways." *Cells*. 11(21), 3509. 10.3390/cells11213509.

[386] Lund, P.J., Elias, J.E., Davis, M.M. (2016). "Global Analysis of *O*-GlcNAc Glycoproteins in Activated Human T Cells." *J Immunol*. 197(8): p.3086-3098. 10.4049/jimmunol.1502031.

[387] Kaufman, R.J. (1999). "Stress signaling from the lumen of the endoplasmic reticulum: coordination of gene transcriptional and translational controls." *Genes Dev*. 13(10): p.1211-33. 10.1101/gad.13.10.1211.

[388] Soria, L.R., Makris, G., D'Alessio, A.M., Angelis, A.D., Boffa, I., Pravata, V.M., Rüfenacht, V., Attanasio, S., Nusco, E., Arena, P., Ferenbach, A.T., Paris, D., Cuomo, P., Motta, A., Nitzahn, M., Lipshutz, G.S., Martínez-Pizarro, A., Richard, E., Desviat, L.R., Häberle, J., Van Aalten, D.M.F., Brunetti-Pierri, N. (2022). "*O*-GlcNAcylation enhances CPS1 catalytic efficiency for ammonia and promotes ureagenesis." *Nat Commun*. 13(1): p.5212. 10.1038/s41467-022-32904-x.

[389] Wu, J., Liu, J., Lapenta, K., Desrouleaux, R., Li, M.D., Yang, X. (2022). "Regulation of the urea cycle by CPS1 *O*-GlcNAcylation in response to dietary restriction and aging." *J Mol Cell Biol*. 14(3). 10.1093/jmcb/mjac016.

[390] Comer, F.I., Giacomozzi, B., Joyce, J., Gray, A., Graham, D., Ousson, S., Neny, M., Beher, D., Carlson, G., O'Moore, J., Shearman, M., Hering, H. (2001). "Characterization of a mouse monoclonal antibody specific for *O*-linked N-acetylglucosamine." *Anal Biochem*. 293(2): p.169-77. 10.1006/abio.2001.5132.

[391] Snow, C.M., Senior, A., Gerace, L. (1987). "Monoclonal antibodies identify a group of nuclear pore complex glycoproteins." *J Cell Biol*. 104(5): p.1143-56. 10.1083/jcb.104.5.1143.

[392] Isono, T. (2011). "*O*-GlcNAc-specific antibody CTD110.6 cross-reacts with *N*-GlcNAc2-modified proteins induced under glucose deprivation." *PLoS One*. 6(4): p.e18959. 10.1371/journal.pone.0018959.

[393] Cameron, A., Giacomozzi, B., Joyce, J., Gray, A., Graham, D., Ousson, S., Neny, M., Beher, D., Carlson, G., O'Moore, J., Shearman, M., Hering, H. (2013). "Generation and characterization of a rabbit monoclonal antibody site-specific for tau *O*-GlcNAcylated at serine 400." *FEBS Lett*. 587(22): p.3722-8. 10.1016/j.febslet.2013.09.042.

[394] Fujiki, R., Hashiba, W., Sekine, H., Yokoyama, A., Chikanishi, T., Ito, S., Imai, Y., Kim, J., He, H.H., Igarashi, K., Kanno, J., Ohtake, F., Kitagawa, H., Roeder, R.G., Brown, M., Katoet, S. (2011). "GlcNAcylation of histone H2B facilitates its monoubiquitination." *Nature*. 480(7378): p.557-60. 10.1038/nature10656.

[395] Shan, H., Sun, J., Shi, M., Liu, X., Shi, Z., Yu, W., Gu, Y. (2018). "Generation and characterization of a site-specific antibody for SIRT1 *O*-GlcNAcylated at serine 549." *Glycobiology*. 28(7): p.482-487. 10.1093/glycob/cwy040.

[396] Ma, J. and Hart, G.W. (2017). "Analysis of protein *O*-GlcNAcylation by mass spectrometry." *Curr Protoc Protein Sci*. 87(1): p.24.10. 1-24.10. 16. 10.1002/cpps.24.

[397] Yin, R., Wang, X., Li, C., Gou, Y., Ma, X., Liu, Y., Peng, J., Wang, C., Zhang, Y. (2021). "Mass Spectrometry for *O*-GlcNAcylation." *Front Chem*. 9: p.737093. 10.3389/fchem.2021.737093.

[398] Vosseller, K., Trinidad, J.C., Chalkley, R.J., Specht, C.G., Thalhammer, A., Lynn, A.J., Snedecor, J.O., Guan, S., Medzihradszky, K.F., Maltby, D.A., Schoepfer, R., Burlingame, A.L. (2006). "*O*-linked N-acetylglucosamine proteomics of postsynaptic density preparations using lectin weak affinity chromatography and mass spectrometry." *Mol Cell Proteomics*. 5(5): p.923-34. 10.1074/mcp.t500040-mcp200.

[399] Ren, X.M., Li, D.F., Jiang, S., Lan, X.Q., Hu, Y., Sun, H., Wang, D.C. (2015). "Structural Basis of Specific Recognition of Non-Reducing Terminal *N*-Acetylglucosamine by an Agrocybe aegerita Lectin." *PLoS One*. 10(6): p.e0129608. 10.1371/journal.pone.0129608.

[400] Machon, O., Baldini, S.F., Ribeiro, J.P., Steenackers, A., Varrot, A., Lefebvre, T., Imberty, A. (2017). "Recombinant fungal lectin as a new tool to investigate *O*-GlcNAcylation processes." *Glycobiology*. 27(2): p.123-128. 10.1093/glycob/cww105.

[401] Zaro, B.W., Yang, Y.Y., Hang, H.C., Pratt, M.R. (2011). "Chemical reporters for fluorescent detection and identification of *O*-GlcNAc-modified proteins reveal glycosylation of the ubiquitin ligase NEDD4-1." *Proc Natl Acad Sci USA*. 108(20): p.8146-51. 10.1073/pnas.1102458108.

[402] Kolb, H.C., Finn, M.G., Sharpless, K.B. (2001). "Click Chemistry: Diverse Chemical Function from a Few Good Reactions." *Angewandte Chemie International Edition*. 40(11): p.2004-2021. 10.1002/1521-3773(20010601)40:11<2004::AID-ANIE2004>3.0.CO;2-5.

[403] Ramakrishnan, B. and Qasba, P.K. (2002). "Structure-based design of beta 1,4-galactosyltransferase I (beta 4Gal-T1) with equally efficient N-acetylgalactosaminyltransferase activity: point mutation broadens beta 4Gal-T1 donor specificity." *J Biol Chem*. 277(23): p. 20833-9. 10.1074/jbc.m111183200.

[404] Sprung, R., Nandi, A., Chen, Y., Kim, S.C., Barma, D., Falck, J.R., Zhao, Y. (2005). "Tagging-via-substrate strategy for probing *O*-GlcNAc modified proteins." *J Proteome Res*. 4(3): p.950-7. 10.1021/pr050033j.

[405] Li, J., Wang, J., Wen, L., Zhu, H., Li, S., Huang, K., Jiang, K., Li, X., Ma, C., Qu, J., Parameswaran, A., Song, J., Zhao, W., Wang, P.G. (2016). "An OGA-Resistant Probe Allows Specific Visualization and Accurate Identification of *O*-GlcNAc-Modified Proteins in Cells." *ACS Chem Biol*. 11(11): p. 3002-3006. 10.1021/acschembio.6b00678.

[406] Kim, E.J. (2018). "Chemical Reporters and Their Bioorthogonal Reactions for Labeling Protein *O*-GlcNAcylation." *Molecules*. 23(10), 2411. 10.3390/molecules23102411.

[407] Thirumurugan, P., Matosiuk, D., Jozwiak, K. (2013). "Click chemistry for drug development and diverse chemical-biology applications." *Chem Rev*. 113(7): p.4905-79. 10.1021/cr200409f.

[408] Tenhunen, R., Marver, H.S., Schmid, R., (1968). "The enzymatic conversion of heme to bilirubin by microsomal heme oxygenase." *Proc Natl Acad Sci USA*. 61(2): p.748-55. 10.1073/pnas.61.2.748.

[409] Maines, M.D. (1997). "The heme oxygenase system: a regulator of second messenger gases." *Annu Rev Pharmacol Toxicol*. 37: p.517-54. 10.1146/annurev.pharmtox.37.1.517.

[410] Maines, M.D. (2004). "The heme oxygenase system: past, present, and future." *Antioxid Redox Signal*. 6(5): p.797-801. 10.1089/ars.2004.6.797.

[411] Schipper, H.M., Song, W., Zukor, H., Hascalovici, J.R., Zeligman, D. (2009). "Heme oxygenase-1 and neurodegeneration: expanding frontiers of engagement." *J Neurochem*. 110(2): p.469-85. 10.1111/j.1471-4159.2009.06160.x.

[412] Sorrenti, V. (2019). "Editorial of Special Issue "Protective and Detrimental Role of Heme Oxygenase-1". *Int J Mol Sci*. 20(19),4744. 10.3390/ijms20194744.

[413] Stocker, R. (2004). "Antioxidant activities of bile pigments." *Antioxid Redox Signal*. 6(5): p.841-9. 10.1089/ars.2004.6.841.

[414] Ryter, S.W., Alam, J., Choi, A.M. (2006). "Heme oxygenase-1/carbon monoxide: from basic science to therapeutic applications." *Physiol Rev*. 86(2): p.583-650. 10.1152/physrev.00011.2005.

[415] Morikawa, T., Kajimura, M., Nakamura, T., Hishiki, T., Nakanishi, T., Yukutake, Y., Nagahata, Y., Ishikawa, M., Hattori, K., Takenouchi, T., Takahashi, T., Ishii, I., Matsubara, K., Kabe, Y., Uchiyama, S., Nagata, E., Gadalla, M.M., Snyder, S.H., Suematsu, M. (2012). "Hypoxic regulation of the cerebral microcirculation is mediated by a carbon monoxide-sensitive hydrogen sulfide pathway." *Proc Natl Acad Sci USA*. 109(4): p.1293-8. 10.1073/pnas.1119658109.

[416] Bellapadrona, G., Ardini, M., Ceci, P., Stefanini, S., Chiancone, E., (2010). "Dps proteins prevent Fenton-mediated oxidative damage by trapping hydroxyl radicals within the protein shell." *Free Radical Biology and Medicine*. 48(2): p.292-297. 10.1016/j.freeradbiomed.2009.10.053.

[417] Zhu, W., Fang, T., Zhang, W., Liang, A., Zhang, H., Zhang, Z.P., Zhang, X.E., Li, F. (2021). "A ROS scavenging protein nanocage for *in vitro* and *in vivo* antioxidant treatment." *Nanoscale*. 13(8): p.4634-4643. 10.1039/d0nr08878a.

[418] Choi, Y.K. and Kim, Y.M. (2022). "Beneficial and Detrimental Roles of Heme Oxygenase-1 in the Neurovascular System." *Int J Mol Sci*. 23(13):7041. 10.3390/ijms23137041.

[419] Barone, E., Domenico, F.D., Mancuso, C., Butterfield, D.A. (2014). "The Janus face of the heme oxygenase/biliverdin reductase system in Alzheimer disease: it's time for reconciliation." *Neurobiol Dis*. 62: p.144-59. 10.1016/j.nbd.2013.09.018.

[420] Sorrenti, V. (2019). "Editorial of Special Issue Protective and Detrimental Role of Heme Oxygenase-1." *International Journal of Molecular Sciences*. 20(19): p.220. 10.3390/ijms20194744.

[421] Harder, Y., Amon, M., Schramm, R., Georgi, M., Banic, A., Erni, D., Menger, M.D. (2005). "Heat shock preconditioning reduces ischemic tissue necrosis by heat shock protein (HSP)-32-mediated improvement of the microcirculation rather than induction of ischemic tolerance." *Ann Surg*. 242(6): p.869-78, discussion 878-9. 10.1097/01.sla.0000189671.06782.56.

[422] Gozzelino, R., Jeney, V., Soares, M.P. (2010). "Mechanisms of cell protection by heme oxygenase-1." *Annual Review of Pharmacology and Toxicology*. 50: p.323-54. 10.1146/annurev.pharmtox.010909.105600.

[423] Montellano, P.R. (2000). "The mechanism of heme oxygenase." *Curr Opin Chem Biol*. 4(2): p. 221-7. 10.1016/s1367-5931(99)00079-4.

[424] Chang, E.F., Claus, C.P., Vreman, H.J., Wong, R.J., Noble-Haeusslein, L.J. (2005). "Heme regulation in traumatic brain injury: relevance to the adult and developing brain." *J Cereb Blood Flow Metab*. 25(11): p.1401-17. 10.1038/sj.jcbfm.9600147.

[425] Muller, R.M., Taguchi, H., Shibahara, S., (1987). "Nucleotide sequence and organization of the rat heme oxygenase gene." *J Biol Chem*. 262(14): p.6795-802.

[426] Yoshida, T. and Sato, M. (1989). "Posttranslational and direct integration of heme oxygenase into microsomes." *Biochem Biophys Res Commun*. 163(2): p.1086-92. 10.1016/0006-291x(89)92332-2.

[427] Erez, E., Fass, D., Bibi, E. (2009). "How intramembrane proteases bury hydrolytic reactions in the membrane." *Nature*. 459(7245): p.371-8. 10.1038/nature08146.

[428] Hwang, H.W., Lee, J.R., Chou, K.Y., Suen, C.S., Hwang, M.J., Chen, C., Shieh, R.C., Chau, L.Y. (2009). "Oligomerization is crucial for the stability and function of heme oxygenase-1 in the endoplasmic reticulum." *J Biol Chem*. 284(34): p.22672-9. 10.1074/jbc.m109.028001.

[429] Dunn, L.L., Midwinter, R.G., Ni, J., Hamid, H.A., Parish, C.R., Stocker, R. (2014). "New insights into intracellular locations and functions of heme oxygenase-1." *Antioxid Redox Signal*. 20(11): p.1723-42. 10.1089/ars.2013.5675.

[430] Lin, Q., Weis, S., Yang, G., Weng, Y.H., Helston, R., Rish, K., Smith, A., Bordner, J., Polte, T., Gaunitz, F., Dennery, P.A. (2007). "Heme oxygenase-1 protein localizes to the nucleus and activates transcription factors important in oxidative stress." *J Biol Chem*. 282(28): p.20621-33. 10.1074/jbc.m607954200.

[431] Zheng, Y., Li, Z., Yin, M., Gong, X. (2021). "Heme oxygenase‐1 improves the survival of ischemic skin flaps (Review)." *Mol Med Rep*. 23(4). 10.3892/mmr.2021.11874.

[432] Yamada, N., Yamaya, M., Okinaga, S., Nakayama, K., Sekizawa, K., Shibahara, S., Sasaki, H. (2000). "Microsatellite polymorphism in the heme oxygenase-1 gene promoter is associated with susceptibility to emphysema." *Am J Hum Genet*. 66(1): p.187-95. 10.1086/302729.

[433] Matsunobu, T., Satoh, Y., Ogawa, K., Shiotani, A. (2009). "Heme oxygenase-1 expression in the guinea pig cochlea induced by intense noise stimulation." *Acta Otolaryngol Suppl*. (562): p.18-23. 10.1080/00016480902933056.

[434] Yi, L. and Ragsdale, S.W. (2007). "Evidence that the heme regulatory motifs in heme oxygenase-2 serve as a thiol/disulfide redox switch regulating heme binding." *J Biol Chem*. 282(29): p. 21056-67. 10.1074/jbc.m700664200.

[435] Fleischhacker, A.S., Carter, E.L., Ragsdale, S.W. (2018). "Redox Regulation of Heme Oxygenase-2 and the Transcription Factor, Rev-Erb, Through Heme Regulatory Motifs." *Antioxid Redox Signal*. 29(18): p.1841-1857. 10.1089/ars.2017.7368.

[436] Morse, D. and Choi, A.M. (2002). "Heme oxygenase-1: the "emerging molecule" has arrived." *Am J Respir Cell Mol Biol*. 27(1): p.8-16. 10.1165/ajrcmb.27.1.4862.

[437] Maines, M.D., (1988). "Heme oxygenase: function, multiplicity, regulatory mechanisms, and clinical applications." *FASEB J*. 2(10): p.2557-68. 10.1096/fasebj.2.10.3290025.

[438] Matz, P.G., Weinstein, P.R., Sharp, F.R. (1997). "Heme oxygenase-1 and heat shock protein 70 induction in glia and neurons throughout rat brain after experimental intracerebral hemorrhage." *Neurosurgery*. 40(1): p.152-60; discussion 160-2. 10.1097/00006123-199701000-00034.

[439] McCoubrey Jr, W.K., Huang, T.J., Maines, M.D. (1997). "Isolation and characterization of a cDNA from the rat brain that encodes hemoprotein heme oxygenase-3." *Eur J Biochem*. 247(2): p. 725-32. 10.1111/j.1432-1033.1997.00725.x.

[440] Scapagnini, G., D'Agata, V., Calabrese, V., Pascale, A., Colombrita, C., Alkon, D., Cavallaro, S. (2002). "Gene expression profiles of heme oxygenase isoforms in the rat brain." *Brain Res*. 954(1): p.51-9. 10.1016/s0006-8993(02)03338-3.

[441] Bian, C., Zhong, M., Nisar, M.F., Wu, Y., Ouyang, M., Bartsch, J.W., Zhong, J.L. (2018). "A novel heme oxygenase-1 splice variant, 14kDa HO-1, promotes cell proliferation and increases relative telomere length." *Biochem Biophys Res Commun*. 500(2): p.429-434. 10.1016/j.bbrc.2018.04.096.

[442] Immenschuh, S., V.H., A Ohlmann, V.H., Gifhorn-Katz, S., Katz, N., Jungermann, K., Kietzmann, T. (1998). "Transcriptional activation of the haem oxygenase-1 gene by cGMP via a cAMP response element/activator protein-1 element in primary cultures of rat hepatocytes." *Biochemical Journal*. 334(1): p.141-146. 10.1042/bj3340141.

[443] Alam, J., Killeen, E., Gong, P., Naquin, R., Hu, B., Stewart, D., Ingelfinger, J.R., Nath, K.A. (2003). "Heme activates the heme oxygenase-1 gene in renal epithelial cells by stabilizing Nrf2." *American Journal of Physiology-Renal Physiology*. 284(4): p.743-752. 10.1152/ajprenal.00376.2002.

[444] Bauer, M. and Bauer, I. (2002). "Heme Oxygenase-1: Redox Regulation and Role in the Hepatic Response to Oxidative Stress." *Antioxidants & Redox Signaling*. 10(4): p.749-758. 10.1089/152308602760598891.

[445] Sorrenti, V., Raffaele, M., Vanella, L., Acquaviva, R., Salerno, L., Pittalà, V., Intagliata, S., Giacomo, C.D. (2019). "Protective Effects of Caffeic Acid Phenethyl Ester (CAPE) and Novel Cape Analogue as Inducers of Heme Oxygenase-1 in Streptozotocin-Induced Type 1 Diabetic Rats." *Int J Mol Sci*. 20(10). 2441; 10.3390/ijms20102441.

[446] Durante, W., Kroll, M.H., Christodoulides, N., Peyton, K.J., Schafer, A.I. (1997). "Nitric oxide induces heme oxygenase-1 gene expression and carbon monoxide production in vascular smooth muscle cells." *Circ Res*. 80(4): p.557-64. 10.1161/01.res.80.4.557.

[447] Bouton, C. and Demple, B. (2000). "Nitric oxide-inducible expression of heme oxygenase-1 in human cells. Translation-independent stabilization of the mRNA and evidence for direct action of nitric oxide." *J Biol Chem*. 275(42): p.32688-93. 10.1074/jbc.275.42.32688.

[448] Wang, Y., Yang, C., Elsheikh, N.A.H., Li, C., Yang, F., Wang, G., Li, L. (2019). "HO-1 reduces heat stress-induced apoptosis in bovine granulosa cells by suppressing oxidative stress." *Aging (Albany NY)*. 11(15): p.5535-5547. 10.18632/aging.102136.

[449] Bauer, I., Rensing, H., Florax, A., Ulrich, C., Pistorius, G., Redl, H., Bauer, M. (2003). "Expression pattern and regulation of heme oxygenase-1/heat shock protein 32 in human liver cells." *Shock*. 20(2): p.116-122. 10.1097/01.shk.0000075568.93053.fa.

[450] Zhong, J.L., Edwards, G.P., Raval, C., Li, H., Tyrrell, R.M. (2010). "The role of Nrf2 in ultraviolet A mediated heme oxygenase 1 induction in human skin fibroblasts." *Photochem Photobiol Sci*. 9(1): p.18-24. 10.1039/b9pp00068b.

[451] Trekli, M.C., Riss, G., Goralczyk, R., Tyrrell, R.M. (2003). "Beta-carotene suppresses UVA-induced HO-1 gene expression in cultured FEK4." *Free Radic Biol Med*. 34(4): p.456-64. 10.1016/s0891-5849(02)01303-5.

[452] Koizumi, S., Gong, P., Suzuki, K., Murata, M. (2007). "Cadmium-responsive element of the human heme oxygenase-1 gene mediates heat shock factor 1-dependent transcriptional activation." *Journal of Biological Chemistry*. 282(12): p.8715–8723. 10.1074/jbc.m609427200.

[453] Alam, J. (1994). "Multiple elements within the 5' distal enhancer of the mouse heme oxygenase-1 gene mediate induction by heavy metals." *J Biol Chem*. 269(40): p.25049-56.

[454] Tracz, M.J., Juncos, J.P., Grande, J.P., Croatt, A.J., Ackerman, A.W., Rajagopalan, G., Knutson, K.L., Badley, A.D., Griffin, M.D., Alam, J., Nath, K.A. (2007). "Renal hemodynamic, inflammatory, and apoptotic responses to lipopolysaccharide in HO-1-/- mice." *Am J Pathol*. 170(6): p.1820-30. 10.2353/ajpath.2007.061093.

[455] Maeda, S., Nakatsuka, I., Hayashi, Y., Higuchi, H., Shimada, M., Miyawaki, T. (2008). "Heme oxygenase-1 induction in the brain during lipopolysaccharide-induced acute inflammation." *Neuropsychiatr Dis Treat*. 4(3): p.663-7. 10.2147/ndt.s3063.

[456] Li, C., Hossieny, P., Wu, B.J., Qawasmeh, A., Beck, K., Stocker, R. (2007). "Pharmacologic induction of heme oxygenase-1." *Antioxid Redox Signal*. 9(12): p.2227-39. 10.1089/ars.2007.1783.

[457] Shih, R.H. and Yang, C.M. (2010). "Induction of heme oxygenase-1 attenuates lipopolysaccharide-induced cyclooxygenase-2 expression in mouse brain endothelial cells." *J Neuroinflammation*. 7: p.86. 10.1186/1742-2094-7-86.

[458] Ryter, S.W., Otterbein, L.E., Morse, D., Choi, A.M. (2002). "Heme oxygenase/carbon monoxide signaling pathways: regulation and functional significance." *Mol Cell Biochem*. 234-235(1-2): p. 249-63. 10.1023/A:1015957026924.

[459] Ryter, S.W. and Tyrrell, R.M. (2000). "The heme synthesis and degradation pathways: role in oxidant sensitivity. Heme oxygenase has both pro- and antioxidant properties." *Free Radic Biol Med*. 28(2): p.289-309. 10.1016/s0891-5849(99)00223-3.

[460] Medina, M.V., Sapochnik, D., Solá, M.G., Coso, O. (2020). "Regulation of the Expression of Heme Oxygenase-1: Signal Transduction, Gene Promoter Activation, and Beyond." *Antioxid Redox Signal*. 32(14): p.1033-1044. 10.1089/ars.2019.7991.

[461] Alam, J., Killeen, E., Gong, P., Naquin, R., Hu, B., Stewart, D., Ingelfinger, J.R., Nath, K.A. (2003). "Heme activates the heme oxygenase-1 gene in renal epithelial cells by stabilizing Nrf2." *Am J Physiol Renal Physiol*. 284(4): p.F743-52. 10.1152/ajprenal.00376.2002.

[462] Itoh, K., Wakabayashi, N., Katoh, Y., Ishii, T., Igarashi, K., Engel, J.D., Yamamoto, M. (1999). "Keap1 represses nuclear activation of antioxidant responsive elements by Nrf2 through binding to the amino-terminal Neh2 domain." *Genes Dev*. 13(1): p.76-86. 10.1101/gad.13.1.76.

[463] Inouye, S., Kubo, T., Miyamoto, T., Iyoda, T., Okita, N., Akagi, R. (2022). "Heat shock-induced heme oxygenase-1 expression in a mouse hepatoma cell line is dependent on HSF1 and modified by NRF2 and BACH1." *Genes Cells*. 27(12): p.719-730. 10.1111/gtc.12986.

[464] Okinaga, S., Takahashi, K., Takeda, K., Yoshizawa, M., Fujita, H., Sasaki, H., Shibahara, S. (1996). "Regulation of human heme oxygenase-1 gene expression under thermal stress." *Blood*. 87(12): p. 5074-84.

[465] Martin, D., Rojo, A.I., Salinas, M., Diaz, R., Gallardo, G., Alam, J., Carlos, M., De Galarreta, R., Cuadrado, A. (2004). "Regulation of heme oxygenase-1 expression through the phosphatidylinositol 3-kinase/Akt pathway and the Nrf2 transcription factor in response to the antioxidant phytochemical carnosol." *Journal of Biological Chemistry*. 279(10): p.8919-8929. 10.1074/jbc.m309660200.

[466] Alam, J., Stewart, D., Touchard, C., Boinapally, S., Choi, A.M., Cook, J.L. (1999). "Nrf2, a Cap'n'Collar transcription factor, regulates induction of the heme oxygenase-1 gene." *J Biol Chem*. 274(37): p.26071-8. 10.1074/jbc.274.37.26071.

[467] Paine, A., Eiz-Vesper, B., Blasczyk, R., Immenschuh, S. (2010). "Signaling to heme oxygenase-1 and its anti-inflammatory therapeutic potential." *Biochem Pharmacol*. 80(12): p.1895-903. 10.1016/j.bcp.2010.07.014.

[468] Camhi, S.L., Alam, J., Otterbein, L., Sylvester, S.L., Choi, A.M. (1995). "Induction of heme oxygenase-1 gene expression by lipopolysaccharide is mediated by AP-1 activation." *Am J Respir Cell Mol Biol*. 13(4): p.387-98. 10.1165/ajrcmb.13.4.7546768.

[469] Alam, J. and Cook, J.L. (2007). "How many transcription factors does it take to turn on the heme oxygenase-1 gene?" *Am J Respir Cell Mol Biol*. 36(2): p.166-74. 10.1165/rcmb.2006-0340tr.

[470] Inouye, S., Hatori, Y., Kubo, T., Saito, S., Kitamura, H., Akagi, R. (2018). "NRF2 and HSF1 coordinately regulate heme oxygenase-1 expression." *Biochem Biophys Res Commun*. 506(1): p.7-11. 10.1016/j.bbrc.2018.10.030.

[471] Johnson, P.F. and McKnight, S.L. (1989). "Eukaryotic transcriptional regulatory proteins." *Annu Rev Biochem*. 58: p.799-839. 10.1146/annurev.bi.58.070189.004055.

[472] Ma, Q. (2013). "Role of nrf2 in oxidative stress and toxicity." *Annu Rev Pharmacol Toxicol*. 53: p.401-26. 10.1146/annurev-pharmtox-011112-140320.

[473] Johnson, J.A., Johnson, D.A., Kraft, A.D., Calkins, M.J., Jakel, R.J., Vargas, M.R., Chen, P.C., (2008). "The Nrf2-ARE pathway: an indicator and modulator of oxidative stress in neurodegeneration." *Ann N Y Acad Sci*. 1147: p.61-9. 10.1196/annals.1427.036.

[474] Kietzmann, T., Samoylenko, A., Immenschuh, S. (2003). "Transcriptional regulation of heme oxygenase-1 gene expression by MAP kinases of the JNK and p38 pathways in primary cultures of rat hepatocytes." *J Biol Chem*. 278(20): p.17927-36. 10.1074/jbc.m203929200.

[475] Sahana, T.G. and Zhang, K. (2021). "Mitogen-Activated Protein Kinase Pathway in Amyotrophic Lateral Sclerosis." *Biomedicines*. 9(8). 10.3390/biomedicines9080969.

[476] Chi, P.L., Lin, C.C., Chen, Y.W., Hsiao, L.D., Yang, C.M. (2015). "CO Induces Nrf2-Dependent Heme Oxygenase-1 Transcription by Cooperating with Sp1 and c-Jun in Rat Brain Astrocytes." *Mol Neurobiol*. 52(1): p.277-92. 10.1007/s12035-014-8869-4.

[477] Widmann, C., Gibson, S., Jarpe, M.B., Johnson, G.L. (1999). "Mitogen-activated protein kinase: conservation of a three-kinase module from yeast to human." *Physiol Rev*. 79(1): p.143-80. 10.1152/physrev.1999.79.1.143.

[478] Galicia-Moreno, M., Lucano-Landeros, S., Monroy-Ramirez, H.C., Silva-Gomez, J., Gutierrez-Cuevas, J., Santos, A., Armendariz-Borunda, J. (2020). "Roles of Nrf2 in Liver Diseases: Molecular, Pharmacological, and Epigenetic Aspects." *Antioxidants* (Basel). 9(10):980. 10.3390/antiox9100980.

[479] Win, S., Than, T.A., Zhang, J., Oo, C., Min, R.W.M., Kaplowitz, N. (2018). "New insights into the role and mechanism of c-Jun-N-terminal kinase signaling in the pathobiology of liver diseases." *Hepatology*. 67(5): p.2013-2024. 10.1002/hep.29689.

[480] Brenner, D.A. (2014). "Fra, Fra away: the complex role of activator protein 1 in liver injury." *Hepatology*. 59(1): p.19-20. 10.1002/hep.26637.

[481] Teramoto, H., Gutkind, J.S. (2013). "Mitogen-Activated Protein Kinase Family." *Encyclopedia of Biological Chemistry III*. p.58-62. 10.1016/b978-0-12-819460-7.00594-6.

[482] Zhao, W., Gasterich, N., Clarner, T., Voelz, C., Behrens, V., Beyer, C., Fragoulis, A., Zendedel, A. (2022). "Astrocytic Nrf2 expression protects spinal cord from oxidative stress following spinal cord injury in a male mouse model." *J Neuroinflammation*. 19(1): p.134. 10.1186/s12974-022-02491-1.

[483] Lu, T.H., Lambrecht, R.W., Pepe, J., Shan, Y., Kim, T., Bonkovsky, H.L. (1998). "Molecular cloning, characterization, and expression of the chicken heme oxygenase-1 gene in transfected primary cultures of chick embryo liver cells." *Gene*. 207(2): p.177-86. 10.1016/s0378-1119(97)00623-9.

[484] Elbirt, K.K. and Bonkovsky, H.L. (1999). "Heme oxygenase: recent advances in understanding its regulation and role." *Proc Assoc Am Physicians*. 111(5): p.438-47.

[485] Tenhunen, R., Marver, H.S., Schmid, R. (1969). "Microsomal heme oxygenase. Characterization of the enzyme." *J Biol Chem*. 244(23): p. 6388-94.

[486] Zhang, X., Shan, P., Otterbein, L.E., Alam, J., Flavell, R.A., Davis, R.J., Choi, A.M., Lee, P.J. (2003). "Carbon monoxide inhibition of apoptosis during ischemia-reperfusion lung injury is dependent on the p38 mitogen-activated protein kinase pathway and involves caspase 3." *J Biol Chem*. 278(2): p.1248-58. 10.1074/jbc.m208419200.

[487] Petrache, I., Otterbein, L.E., Alam, J., Wiegand, G.W., Choi, A.M. (2000). "Heme oxygenase-1 inhibits TNF-alpha-induced apoptosis in cultured fibroblasts." *Am J Physiol Lung Cell Mol Physiol*. 278(2): p.L312-9. 10.1152/ajplung.2000.278.2.l312.

[488] Sethi, J.M., Otterbein, L.E., Choi, A.M. (2002). "Differential modulation by exogenous carbon monoxide of TNF-alpha stimulated mitogen-activated protein kinases in rat pulmonary artery endothelial cells." *Antioxid Redox Signal*. 4(2): p.241-8. 10.1089/152308602753666299.

[489] Otterbein, L.E., Bach, F.H., Alam, J., Soares, M., Lu, T.H., Wysk, M., Davis, R.J., Flavell, R.A., Choi, A.M. (2000). "Carbon monoxide has anti-inflammatory effects involving the mitogen-activated protein kinase pathway." *Nat Med*. 6(4): p.422-8. 10.1038/74680.

[490] Alcaraz, M.J. and Ferrándiz, ML. (2020). "Relevance of Nrf2 and heme oxygenase-1 in articular diseases." *Free Radic Biol Med*. 157: p.83-93. 10.1016/j.freeradbiomed.2019.12.007.

[491] Zhang, Q., Liu, J., Duan, H., Li, R., Peng, W., Wu, C. (2021). "Activation of Nrf2/HO-1 signaling: An important molecular mechanism of herbal medicine in the treatment of atherosclerosis via the protection of vascular endothelial cells from oxidative stress." *J Adv Res*. 34: p.43-63. 10.1016/j.jare.2021.06.023.

[492] Biswas, C., Shah, N., Muthu, M., La, P., Fernando, A.P., Sengupta, S., Yang, G., Dennery, P.A. (2014). "Nuclear heme oxygenase-1 (HO-1) modulates subcellular distribution and activation of Nrf2, impacting metabolic and anti-oxidant defenses." *J Biol Chem*. 289(39): p.26882-26894. 10.1074/jbc.m114.567685.

[493] Turkseven, S., Kruger, A., Mingone, C.J., Kaminski, P., Inaba, M., Rodella, L.F., Ikehara, S., Wolin, M.S., Abraham, N.G. (2005). "Antioxidant mechanism of heme oxygenase-1 involves an increase in superoxide dismutase and catalase in experimental diabetes." *Am J Physiol Heart Circ Physiol*. 289(2): p.H701-7. 10.1152/ajpheart.00024.2005.

[494] Gottlieb, Y., Truman, M., Cohen, L.A., Leichtmann-Bardoogo, Y., Meyron-Holtz, E.G. (2012). "Endoplasmic reticulum anchored heme-oxygenase 1 faces the cytosol." *Haematologica*. 97(10): p.1489-93. 10.3324/haematol.2012.063651.

[495] Kim, H.P., Wang, X., Galbiati, F., Ryter, S.W., Choi, A.M. (2004). "Caveolae compartmentalization of heme oxygenase-1 in endothelial cells." *FASEB J*. 18(10): p.1080-9. 10.1096/fj.03-1391com.

[496] Mascaro, M., Alonso, E.N., Alonso, E.G., Lacunza, E., Curino, A.C., Facchinetti, M.M. (2021). "Nuclear Localization of Heme Oxygenase-1 in Pathophysiological Conditions: Does It Explain the Dual Role in Cancer?" *Antioxidants (Basel)*. 10(1):87. 10.3390/antiox10010087.

[497] Freeman, A. (1975). "Editorial: Medical attention isn't enough." *J Am Vet Med Assoc*. 167(2): p. 120-1.

[498] Srivastava, P. and Pandey, V.C. (1996). "Mitochondrial heme oxygenase of Mastomys coucha." *Int J Biochem Cell Biol*. 28(9): p.1071-7. 10.1016/1357-2725(96)00030-1.

[499] Suliman, H.B., Keenan, J.E., Piantadosi, C.A. (2017). "Mitochondrial quality-control dysregulation in conditional HO-1(-/-) mice." *JCI Insight*. 2(3): p.e89676. 10.1172/jci.insight.89676.

[500] Ishikawa, K., Sato, M., Yoshida, T. (1991). "Expression of rat heme oxygenase in Escherichia coli as a catalytically active, full-length form that binds to bacterial membranes." *Eur J Biochem*. 202(1): p.161-5. 10.1111/j.1432-1033.1991.tb16357.x.

[501] Hsu, F.F., Yeh, C.T., Sun, Y.J., Chiang, M.T., Lan, W.M., Li, F.A., Lee, W.H., Chau, L.Y. (2015). "Signal peptide peptidase-mediated nuclear localization of heme oxygenase-1 promotes cancer cell proliferation and invasion independent of its enzymatic activity." *Oncogene*. 34(18): p.2360-70. 10.1038/onc.2014.166.

[502] Murray, E.J., Grisanti, M.S., Bentley, G.V., Murray, S.S. (1997). "E64d, a membrane-permeable cysteine protease inhibitor, attenuates the effects of parathyroid hormone on osteoblasts *in vitro.*" *Metabolism*. 46(9): p.1090-4. 10.1016/s0026-0495(97)90284-5.

[503] Lin, Q.S., Weis, S., Yang, G., Zhuang, T., Abate, A., Dennery, P.A. (2008). "Catalytic inactive heme oxygenase-1 protein regulates its own expression in oxidative stress." *Free Radic Biol Med*. 44(5): p.847-55. 10.1016/j.freeradbiomed.2007.11.012.

[504] Gandini, N.A., Alonso, E.N., Fermento, M.E., Mascaró, M., Abba, M.C., Coló, G.P., Arévalo, J., Ferronato, M.J., Guevara, J.A., Núñez, M., Pichel, P., Curino, A.C., Facchinetti, M.M. (2019). "Heme Oxygenase-1 Has an Antitumor Role in Breast Cancer." *Antioxid Redox Signal*. 30(18): p. 2030-2049. 10.1089/ars.2018.7554.

[505] Chang, L.C., Chiang, S.K., Chen, S.E., Yu, Y.L., Chou, R.H., Chang, W.C. (2018). "Heme oxygenase-1 mediates BAY 11-7085 induced ferroptosis." *Cancer Lett*. 416: p.124-137. 10.1016/j.canlet.2017.12.025.

[506] Linnenbaum, M., Busker, M., Kraehling, J.R., Behrends, S. (2012). "Heme oxygenase isoforms differ in their subcellular trafficking during hypoxia and are differentially modulated by cytochrome P450 reductase." *PLoS One*. 7(4): p.e35483. 10.1371/journal.pone.0035483.

[507] Kochert, B.A., Fleischhacker, A.S., Wales, T.E., Becker, D.F., Engen, J.R., Ragsdale, S.W. (2019). "Dynamic and structural differences between heme oxygenase-1 and -2 are due to differences in their C-terminal regions." *J Biol Chem*. 294(20): p.8259-8272. 10.1074/jbc.ra119.008592.

[508] Huber, W.J., 3rd and Backes, W.L. (2007). "Expression and characterization of full-length human heme oxygenase-1: the presence of intact membrane-binding region leads to increased binding affinity for NADPH cytochrome P450 reductase." *Biochemistry*. 46(43): p.12212-9. 10.1021/bi701496z.

[509] Marohnic, C.C., Iii, W.J.H., Connick, J.P., Reed, J.R., McCammon, K., Panda, S.P., Martásek, P., Backes, W.L., Masters, B.S.S. (2011). "Mutations of human cytochrome P450 reductase differentially modulate heme oxygenase-1 activity and oligomerization." *Arch Biochem Biophys*. 513(1): p.42-50. 10.1016/j.abb.2011.06.008.

[510] Wu, J., Li, S., Li, C., Cui, L., Ma, J., Hui, Y. (2021). "The non-canonical effects of heme oxygenase-1, a classical fighter against oxidative stress." *Redox Biol*. 47: p.102170. 10.1016/j.redox.2021.102170.

[511] Malaguarnera, L., Madeddu, R., Palio, E., Arena, N., Malaguarnera, M. (2005). "Heme oxygenase-1 levels and oxidative stress-related parameters in non-alcoholic fatty liver disease patients." *J Hepatol*. 42(4): p.585-91. 10.1016/j.jhep.2004.11.040.

[512] Froh, M., Conzelmann, L., Walbrun, P., Netter, S., Wiest, R., Wheeler, M.D., Lehnert, M., Uesugi, T., Scholmerich, J., Thurman, R.G. (2007). "Heme oxygenase-1 overexpression increases liver injury after bile duct ligation in rats." *World J Gastroenterol*. 13(25): p.3478-86. 10.3748/wjg.v13.i25.3478.

[513] Wang, Q.M., Yin, X.Y., Duan, Z.J., Guo, S.B., Sun, X.Y. (2013). "Role of the heme oxygenase/carbon monoxide pathway in the pathogenesis and prevention of hepatic encephalopathy." *Mol Med Rep*. 8(1): p.67-74. 10.3892/mmr.2013.1472.

[514] Le, W.D., Xie, W.J., Appel, S.H. (1999). "Protective role of heme oxygenase-1 in oxidative stress-induced neuronal injury." *J Neurosci Res*. 56(6): p.652-8. 10.1002/(sici)1097-4547(19990615)56:6<652::aid-jnr11>3.0.co;2-5.

[515] Wu, Y.H. and Hsieh, H.L. (2022). "Roles of Heme Oxygenase-1 in Neuroinflammation and Brain Disorders." *Antioxidants (Basel)*. 11(5). 10.3390/antiox11050923.

[516] Chopra, V.S., Chalifour, L.E., Schipper, H.M. (1995). "Differential effects of cysteamine on heat shock protein induction and cytoplasmic granulation in astrocytes and glioma cells." *Brain Res Mol Brain Res*. 31(1-2): p.173-84. 10.1016/0169-328x(95)00049-x.

[517] Jiang, W., Desjardins, P., Butterworth, R.F. (2009). "Minocycline attenuates oxidative/nitrosative stress and cerebral complications of acute liver failure in rats." *Neurochem Int*. 55(7): p.601-5. 10.1016/j.neuint.2009.06.001.

[518] Wang, Q.M., Xue, Y.Y., Duan, Z.J., Guo, S.B., Sun, X.Y. (2013). "Role of the heme oxygenase/carbon monoxide pathway in the pathogenesis and prevention of hepatic encephalopathy." *Molecular Medicine Reports*. 8(1): p.67-74. 10.3892/mmr.2013.1472.

[519] Warskulat, U., Görg, B., Bidmon, H.J., Müller, H.W., Schliess, F., Häussinger, D. (2002). "Ammonia-induced heme oxygenase-1 expression in cultured rat astrocytes and rat brain *in vivo.*" *Glia*, 40(3): p.324-36. 10.1002/glia.10128.

[520] Liu, X.M., Peyton, K.J., Durante, W. (2017). "Ammonia promotes endothelial cell survival via the heme oxygenase-1-mediated release of carbon monoxide." *Free Radic Biol Med*, 102: p.37-46. 10.1016/j.freeradbiomed.2016.11.029.

[521] Schindelin, J., Arganda-Carreras, I., Frise, E., Kaynig, V., Longair, M., Pietzsch, T., Preibisch, S., Rueden, C., Saalfeld, S., Schmid, B., Tinevez, J.Y., White, D.J., Hartenstein, V., Eliceiri, K., Tomancak, P., Cardona, A. (2012). "Fiji: an open-source platform for biological-image analysis." *Nat Methods*. 9(7): p.676-82. 10.1038/nmeth.2019.

[522] Qiagen. (2016). *QuantiTect® Reverse Transcription Handbook.*

[523] Livak, K.J. and Schmittgen, T.D. (2001). "Analysis of relative gene expression data using real-time quantitative PCR and the 2(-Delta Delta C(T)) Method." *Methods*, 25(4): p.402-8. 10.1006/meth.2001.1262.

[524] Svingen, T., Letting, H., Hadrup, N., Hass, U., Vinggaard, A.M. (2015). "Selection of reference genes for quantitative RT-PCR (RT-qPCR) analysis of rat tissues under physiological and toxicological conditions." *PeerJ*. 3: p.e855. 10.7717/peerj.855.

[525] Huang da, W., Sherman, B.T., Lempicki, R.A. (2009). "Systematic and integrative analysis of large gene lists using DAVID bioinformatics resources." *Nat Protoc*. 4(1): p.44-57. 10.1038/nprot.2008.211.

[526] Benjamini, Y., and Hochberg, Y. (1995). "Controlling the False Discovery Rate: A Practical and Powerful Approach to Multiple Testing." *Journal of the Royal Statistical Society*: *Series B* (*Methodological*). 57(1): p.289-300. 10.1111/j.2517-6161.1995.tb02031.x.

[527] Castoldi, M., Kordes, C., Sawitza, I., Häussinger, D. (2016). "Isolation and characterization of vesicular and non-vesicular microRNAs circulating in sera of partially hepatectomized rats." *Sci Rep*. 6: p.31869. 10.1038/srep31869.

[528] Mehdiani, A., Maier, A., Pinto, A., Barth, M., Akhyari, P., Lichtenberg, A. (2015). "An innovative method for exosome quantification and size measurement." *J Vis Exp*. (95): p.50974. 10.3791/50974.

[529] Brenig, K., Grube, L., Schwarzländer, M., Köhrer, K., Stühler, K., Poschmann, G. (2020). "The Proteomic Landscape of Cysteine Oxidation That Underpins Retinoic Acid-Induced Neuronal Differentiation." *J Proteome Res*. 19(5): p.1923-1940. 10.1021/acs.jproteome.9b00752.

[530] Grube, L., Dellen, R., Kruse, F., Schwender, H., Stühler, K., Poschmann, G. (2018). "Mining the Secretome of C2C12 Muscle Cells: Data Dependent Experimental Approach To Analyze Protein Secretion Using Label-Free Quantification and Peptide Based Analysis." *J Proteome Res*. 17(2): p.879-890. 10.1021/acs.jproteome.7b00684.

[531] Tusher, V.G., Tibshirani, R., Chu, G. (2001). "Significance analysis of microarrays applied to the ionizing radiation response." *Proc Natl Acad Sci* USA. 98(9): p.5116-21. 10.1073/pnas.091062498.

[532] Zhao, L. Bonus, M., Poschmann, G., Gohlke, H., Stühler, K., Luedde, T., Häussinger, D., Görg, B. (2021). "Identification of ammonia-induced changes in the astrocyte *O*-GlcNAcome." *Z Gastroenterol*. 59(01): e32-e33. 10.1055/s-0040-1722033.

[533] Jayakumar, A.R., Rama Rao, K.V., Kalaiselvi, P., Norenberg, M.D. (2004). "Combined effects of ammonia and manganese on astrocytes in culture." *Neurochem Res*. 29(11): p.2051-6. 10.1007/s11064-004-6878-9.

[534] Swain, M., Butterworth, R.F., Blei, A.T. (1992). "Ammonia and related amino acids in the pathogenesis of brain edema in acute ischemic liver failure in rats." *Hepatology*. 15(3): p.449-53. 10.1002/hep.1840150316.

[535] Bélanger, M., Côté, J., Butterworth, R.F. (2006). "Neurobiological characterization of an azoxymethane mouse model of acute liver failure." *Neurochem Int*. 48(6-7): p.434-40. 10.1016/j.neuint.2005.11.022.

[536] Ma, J., Wang, W.H., Li, Z.X., Shabanowitz, J., Hunt, D.F., Hart, G.W. (2019). "*O*-GlcNAc Site Mapping by Using a Combination of Chemoenzymatic Labeling, Copper-Free Click Chemistry, Reductive Cleavage, and Electron-Transfer Dissociation Mass Spectrometry." *Anal Chem*. 91(4): p.2620-2625. 10.1021/acs.analchem.8b05688.

[537] Deracinois, B., Camoin, L., Lambert, M., Boyer, J.B., Dupont, E., Bastide, B., Cieniewski-Bernard, C. (2018). "*O*-GlcNAcylation site mapping by (azide-alkyne) click chemistry and mass spectrometry following intensive fractionation of skeletal muscle cells proteins." *J Proteomics*. 186: p.83-97. 10.1016/j.jprot.2018.07.005.

[538] Wei, R. and Zimmermann, W. (2017). "Microbial enzymes for the recycling of recalcitrant petroleum-based plastics: how far are we?" *Microb Biotechnol*. 10(6): p.1308-1322. 10.1111/1751-7915.12710.

[539] Szklarczyk, D., Gable, A.L., Nastou, K.C., Lyon, D., Kirsch, R., Pyysalo, S., Doncheva, N.T., Legeay, M., Fang, T., Bork, P., Jensen, L.J., Von Mering, C. (2021). "The STRING database in 2021: customizable protein-protein networks, and functional characterization of user-uploaded gene/measurement sets." *Nucleic Acids Res*. 49(D1): p.D605-D612. 10.1093/nar/gkaa1074.

[540] Tyanova, S. and Cox, J. (2018). "Perseus: A Bioinformatics Platform for Integrative Analysis of Proteomics Data in Cancer Research." *Methods Mol Biol*. 1711: p.133-148. 10.1007/978-1-4939-7493-1_7.

[541] Szklarczyk, D., Gable, A.L., Lyon, D., Junge, A., Wyder, S., Huerta-Cepas, J., Simonovic, M., Doncheva, N.T., Morris, J.H., Bork, P., Jensen, L.J., Von Mering, C. (2019). "STRING v11: protein-protein association networks with increased coverage, supporting functional discovery in genome-wide experimental datasets." *Nucleic Acids Res*. 47(D1): p.D607-d613. 10.1093/nar/gky1131.

[542] Gupta, R. and Brunak, S. (2002). "Prediction of glycosylation across the human proteome and the correlation to protein function." *Pac Symp Biocomput*. p.310-22.

[543] Jia, C., Zuo, Y., Zou, Q. (2018). "*O*-GlcNAcPRED-II: an integrated classification algorithm for identifying *O*-GlcNAcylation sites based on fuzzy undersampling and a K-means PCA oversampling technique." *Bioinformatics*. 34(12): p.2029-2036. 10.1093/bioinformatics/bty039.

[544] Konrad, R.J., Zhang, F.X., Hale, J.E., Knierman, M.D., Becker, G.W., Kudlow, J.E. (2002). "Alloxan is an inhibitor of the enzyme *O*-linked N-acetylglucosamine transferase." *Biochem Biophys Res Commun*. 293(1): p.207-12. 10.1016/s0006-291x(02)00200-0.

[545] Haltiwanger, R.S., Blomberg, M.A., Hart, G.W. (1992). "Glycosylation of nuclear and cytoplasmic proteins. Purification and characterization of a uridine diphospho-N-

acetylglucosamine:polypeptide beta-N-acetylglucosaminyltransferase." *J Biol Chem*. 267(13): p.9005-13.

[546] Converso, D.P., Taillé, C., Carreras, M.C., Jaitovich, A., Poderoso, J.J., Boczkowski, J. (2006). "HO-1 is located in liver mitochondria and modulates mitochondrial heme content and metabolism." *FASEB J*. 20(8): p.1236-8. 10.1096/fj.05-4204fje.

[547] Bansal, S., Biswas, G., Avadhani, N.G. (2014). "Mitochondria-targeted heme oxygenase-1 induces oxidative stress and mitochondrial dysfunction in macrophages, kidney fibroblasts and in chronic alcohol hepatotoxicity." *Redox Biol*. 2: p.273-83. 10.1016/j.redox.2013.07.004.

[548] Jayakumar, A.R., Valdes, V., Tong, X.Y., Shamaladevi, N., Gonzalez, W., Norenberg, M.D. (2014). "Sulfonylurea receptor 1 contributes to the astrocyte swelling and brain edema in acute liver failure." *Transl Stroke Res*. 5(1): p.28-37. 10.1007/s12975-014-0328-z.

[549] Cressatti, M., Galindez, J.M., Juwara, L., Orlovetskie, N., Velly, A.M., Eintracht, S., Liberman, A., Gornitsky, M., Schipper, H.M. (2021). "Characterization and heme oxygenase-1 content of extracellular vesicles in human biofluids." *J Neurochem*. 157(6): p.2195-2209. 10.1111/jnc.15167.

[550] Schaefer, B., Moriishi, K., Behrends, S. (2017). "Insights into the mechanism of isoenzyme-specific signal peptide peptidase-mediated translocation of heme oxygenase." *PLoS One*. 12(11): p.e0188344. 10.1371/journal.pone.0188344.

[551] Boname, J.M., Bloor, S., Wandel, M.P., Nathan, J.A., Antrobus, R., Dingwell, K.S., Thurston, T.L., Smith, D.L., Smith, J.C., Randow, F., Lehner, P.J. (2014). "Cleavage by signal peptide peptidase is required for the degradation of selected tail-anchored proteins." *J Cell Biol*. 205(6): p.847-62. 10.1083/jcb.201312009.

[552] Kim, K., Rhee, S.G., Stadtman, E.R. (1985). "Nonenzymatic cleavage of proteins by reactive oxygen species generated by dithiothreitol and iron." *J Biol Chem*. 260(29): p.15394-7.

[553] Zhang, S., Rodriguez, L.M.D.L., Li, F.F., Huang, R.J., Leung, I.K.H., Harris, P.W.R., Brimble, M.A. (2022). "A novel tyrosine hyperoxidation enables selective peptide cleavage." *Chem Sci*. 13(9): p.2753-2763. 10.1039/d1sc06216f.

[554] Hart, G.W. (2014). "Three Decades of Research on *O*-GlcNAcylation - A Major Nutrient Sensor That Regulates Signaling, Transcription and Cellular Metabolism." *Front Endocrinol* (*Lausanne*). 5: p.183. 10.3389/fendo.2014.00183.

[555] Rama Rao, K.V., Jayakumar, A.R., Norenberg, D.M. (2003). "Ammonia neurotoxicity: role of the mitochondrial permeability transition." *Metab Brain Dis*. 18(2): p.113-27. 10.1023/a:1023858902184.

[556] Drews, L., Zimmermann, M., Westhoff, P., Brilhaus, D., Poss, R.E., Bergmann, L., Wiek, C., Brenneisen, P., Piekorz, R.P., Mettler-Altmann, T., Weber, A.P.M., Reichert, A.S. (2020). "Ammonia inhibits energy metabolism in astrocytes in a rapid and glutamate dehydrogenase 2-dependent manner." *Dis Model Mech*. 13(10). 10.1242/dmm.047134.

[557] Niknahad, H., Jamshidzadeh, A., Heidari, R., Zarei, M., Ommatiet, M.M. (2017). "Ammonia-induced mitochondrial dysfunction and energy metabolism disturbances in isolated brain and liver mitochondria, and the effect of taurine administration: relevance to hepatic encephalopathy treatment." *Clin Exp Hepatol*. 3(3): p.141-151. 10.5114/ceh.2017.68833.

[558] Lai, J.C. and Cooper, A.J. (1991). "Neurotoxicity of ammonia and fatty acids: differential inhibition of mitochondrial dehydrogenases by ammonia and fatty acyl coenzyme A derivatives." *Neurochem Res*. 16(7): p.795-803. 10.1007/bf00965689.

[559] Kosenko, E., Kaminsky, Y., Kaminsky, A., Valencia, M., Lee, L., Hermenegildo, C., Felipo, V. (1997). "Superoxide production and antioxidant enzymes in ammonia intoxication in rats." *Free Radic Res*. 27(6): p.637-44. 10.3109/10715769709097867.

[560] Rama Rao, K.V. and Norenberg, M.D. (2014). "Glutamine in the pathogenesis of hepatic encephalopathy: the trojan horse hypothesis revisited." *Neurochem Res*. 39(3): p.593-8. 10.1007/s11064-012-0955-2.

[561] Rosso, L., Marques, A.C., Reichert, A.S., Kaessmann, H. (2008). "Mitochondrial targeting adaptation of the hominoid-specific glutamate dehydrogenase driven by positive Darwinian selection." *PLoS Genet*. 4(8): p.e1000150. 10.1371/journal.pgen.1000150.

[562] Moreadith, R.W. and Lehninger, A.L. (1984). "The pathways of glutamate and glutamine oxidation by tumor cell mitochondria. Role of mitochondrial NAD(P)+-dependent malic enzyme." *J Biol Chem*. 259(10): p. 6215-21.

[563] Rama Rao, K.V. and Norenberg, M.D. (2012). "Brain energy metabolism and mitochondrial dysfunction in acute and chronic hepatic encephalopathy." *Neurochem Int*. 60(7): p.697-706. 10.1016/j.neuint.2011.09.007.

[564] Hawkins, R.A. and Mans, A.M. (1990). "Cerebral function in hepatic encephalopathy." *Adv Exp Med Biol*. 272: p.1-22. 10.1007/978-1-4684-5826-8_1.

[565] Shorey, J., McCandless, D.W., Schenker, S. (1967). "Cerebral alpha-ketoglutarate in ammonia intoxication." *Gastroenterology*. 53(5): p. 706-11.

[566] Hindfelt, B. and Siesjö, B.K. (1971). "Cerebral effects of acute ammonia intoxication. II. The effect upon energy metabolism." *Scand J Clin Lab Invest*, 28(3): p.365-74. 10.3109/00365517109095711.

[567] Kim, K., Yoo, H.C., Kim, B.G., Kim, S., Sung, Y., Yoon, I., Yu, Y.C., Park, S.J., Kim, J.H., Myung, K., Hwang, K.Y., Kim, S., Han, J.M. (2022). "*O*-GlcNAc modification of leucyl-tRNA synthetase 1 integrates leucine and glucose availability to regulate mTORC1 and the metabolic fate of leucine." *Nat Commun*. 13(1): p.2904. 10.1038/s41467-022-30696-8.

[568] Rubio Gomez, M.A. and Ibba, M. (2020). "Aminoacyl-tRNA synthetases." *RNA*. 26(8): p. 910-936. 10.1261/rna.071720.119.

[569] Klose, J., Görg, B., Berndt, C., Häussinger, D., Aktas, O., Prozorovski, T. (2014). "Protein oxidative damage in the hippocampus in a mouse model of acute hyperammonemia." *Eur J Med Res*. 19(Suppl 1): p.S29. 10.1186/2047-783x-19-s1-s29.

[570] Lu, K., Zimmermann, M., Görg, B., Bidmon, H.J., Biermann, B., Klöcker, N., Häussinger, D., Reichert, A.S. (2019). "Hepatic encephalopathy is linked to alterations of autophagic flux in astrocytes." *EBioMedicine*. 48: p.539-553. 10.1016/j.ebiom.2019.09.058.

[571] Tanaka, R.D., Li, A.C., Fogelman, A.M., Edwards, P.A. (1986). "Inhibition of lysosomal protein degradation inhibits the basal degradation of 3-hydroxy-3-methylglutaryl coenzyme A reductase." *J Lipid Res*. 27(3): p.261-73.

[572] Seglen, P.O. and Reith, A. (1976). "Ammonia inhibition of protein degradation in isolated rat hepatocytes. Quantitative ultrastructural alterations in the lysosomal system." *Exp Cell Res*. 100(2): p. 276-80. 10.1016/0014-4827(76)90148-8.

[573] Abi Habib, J., Lesenfants, J., Vigneron, N., Van den Eynde, B.J. (2022). "Functional Differences between Proteasome Subtypes." *Cells*. 11(3). 10.3390/cells11030421.

[574] Muli, C.S., Tian, W., Trader, D.J. (2019). "Small-Molecule Inhibitors of the Proteasome's Regulatory Particle." *Chembiochem*. 20(14): p.1739-1753. 10.1002/cbic.201900017.

[575] Zhang, F.X., Su, K.H., Yang, X.Y., Bowe, D.B., Paterson, A.J., Kudlow, J.E. (2003). "*O*-GlcNAc modification is an endogenous inhibitor of the proteasome." *Cell*. 115(6): p.715-25. 10.1016/s0092-8674(03)00974-7.

[576] Shi, Q., Shen, Q.C., Liu, Y.F., Shi, Y., Huang, W.W., Wang, X., Li, Z.Q., Chai, Y.Y., Wang, H., Hu, X.J., Li, N., Zhang, Q., Cao, X.T. (2022). "Increased glucose metabolism in TAMs fuels *O*-GlcNAcylation of lysosomal Cathepsin B to promote cancer metastasis and chemoresistance." *Cancer Cell*. 40(10): p.1207-1222.e10. 10.1016/j.ccell.2022.08.012.

[577] Ni, J., Lan, F., Xu, Y., Nakanishi, H., Li, X. (2022). "Extralysosomal cathepsin B in central nervous system: Mechanisms and therapeutic implications." *Brain Pathol*. 32(5): p.e13071. 10.1111/bpa.13071.

[578] Aghdassi, A.A., John, D.S., Sendler, M., Weiss, F.U., Reinheckel, T., Mayerle, J., Lerch, M.M. (2018). "Cathepsin D regulates cathepsin B activation and disease severity predominantly in inflammatory cells during experimental pancreatitis." *J Biol Chem*. 293(3): p.1018-1029. 10.1074/jbc.m117.814772.

[579] Ma, Y. and Hendershot, L.M. (2004). "The role of the unfolded protein response in tumour development: friend or foe?" *Nat Rev Cancer*. 4(12): p.966-77. 10.1038/nrc1505.

[580] Chen, Y.M., Chen, W., Xu, Y., Lu, C.S., Zhu, M.M., Sun, R.Y., Wang, Y.H., Chen, Y., Shi, J., Wang, D. (2022). "Novel compound heterozygous SUCLG1 variants may contribute to mitochondria DNA depletion syndrome-9." *Mol Genet Genomic Med*. 10(9): p.e2010. 10.1002/mgg3.2010.

[581] Wulff-Fuentes, E., Boakye, J., Kroenke, K., Berendt, R.R., Martinez-Morant, C., Pereckas, M., Hanover, J.A., Stichelen, S.O.V. (2023). "*O*-GlcNAcylation regulates OTX2's proteostasis." *iScience*. 26(11): p.108184. 10.1016/j.isci.2023.108184.

[582] Wang, H., Sun, J., Sun, H., Wang, Y., Lin, B., Wu, L., Qin, W., Zhu, Q., Yi, W. (2024). "The OGT-c-Myc-PDK2 axis rewires the TCA cycle and promotes colorectal tumor growth." *Cell Death Differ*. 31(9): p.1157-1169. 10.1038/s41418-024-01315-4.

[583] Lim, K. and Chang, H.I. (2009). "*O*-GlcNAc inhibits interaction between Sp1 and Elf-1 transcription factors." *Biochem Biophys Res Commun*. 380(3): p.569-74. 10.1016/j.bbrc.2009.01.121.

[584] Chou, T.Y., Hart, G.W., Dang, C.V. (1995). "c-Myc is glycosylated at threonine 58, a known phosphorylation site and a mutational hot spot in lymphomas." *J Biol Chem*. 270(32): p.18961-5. 10.1074/jbc.270.32.18961.

[585] Chou, T.Y., Dang, C.V., Hart, G.W. (1995). "Glycosylation of the c-Myc transactivation domain." *Proc Natl Acad Sci USA*. 92(10): p.4417-21. 10.1073/pnas.92.10.4417.

[586] Mitchell, C.W., Czajewski, I., Van Aalten, D.M.F. (2022). "Bioinformatic prediction of putative conveyers of *O*-GlcNAc transferase intellectual disability." *J Biol Chem*. 298(9): p.102276. 10.1016/j.jbc.2022.102276.

[587] Gu, W. and Roeder, R.G. (1997). "Activation of p53 sequence-specific DNA binding by acetylation of the p53 C-terminal domain." *Cell*. 90(4): p.595-606. 10.1016/s0092-8674(00)80521-8.

[588] Yang, X., Zhang, F., Kudlow, J.E. (2002). "Recruitment of *O*-GlcNAc transferase to promoters by corepressor mSin3A: coupling protein *O*-GlcNAcylation to transcriptional repression." *Cell*. 110(1): p.69-80. 10.1016/s0092-8674(02)00810-3.

[589] Liu, F., Iqbal, K., Grundke-Iqbal, I., Hart, G.W., Gong, C.X. (2004). "*O*-GlcNAcylation regulates phosphorylation of tau: a mechanism involved in Alzheimer's disease." *Proc Natl Acad Sci USA*. 101(29): p. 10804-9. 10.1073/pnas.0400348101.

[590] Rexach, J.E., Clark, P.M., Mason, D.E., Neve, R.L., Peters, E.C., Hsieh-Wilson, L.C. (2012). "Dynamic *O*-GlcNAc modification regulates CREB-mediated gene expression and memory formation." *Nat Chem Biol*. 8(3): p.253-61. 10.1038/nchembio.770.

[591] Liu, A.R. and Ramakrishnan, P. (2021). "Regulation of Nuclear Factor-kappaB Function by *O*-GlcNAcylation in Inflammation and Cancer." *Front Cell Dev Biol*. 9: p.751761. 10.3389/fcell.2021.751761.

[592] Gassama, Y. and Favereaux, A. (2021). "Emerging Roles of Extracellular Vesicles in the Central Nervous System: Physiology, Pathology, and Therapeutic Perspectives." *Front Cell Neurosci*. 15: p.626043. 10.3389/fncel.2021.626043.

[593] Mueller, C., Zhou, W., Vanmeter, A., Heiby, M., Magaki, S., Ross, M.M., Espina, V., Schrag, M., Dickson, C., Liotta, L.A., Kirsch, W.M. (2010). "The heme degradation pathway is a promising serum biomarker source for the early detection of Alzheimer's disease." *J Alzheimers Dis*. 19(3): p.1081-91. 10.3233/jad-2010-1303.

[594] Lin, P.H., Chiang, M.T., Chau, L.Y. (2008). "Ubiquitin-proteasome system mediates heme oxygenase-1 degradation through endoplasmic reticulum-associated degradation pathway." *Biochim Biophys Acta*. 1783(10): p.1826-34. 10.1016/j.bbamcr.2008.05.008.

[595] Wang, Q., Li, L., Ye, Y. (2008). "Inhibition of p97-dependent protein degradation by Eeyarestatin I." *J Biol Chem*. 283(12): p.7445-54. 10.1074/jbc.m708347200.

[596] Guptasarma, P., Balasubramanian, D., Matsugo, S., Saito, I. (1992). "Hydroxyl radical mediated damage to proteins, with special reference to the crystallins." *Biochemistry*. 31(17): p.4296-303. 10.1021/bi00132a021.

[597] Yoshida, T., Ishikawa, K., Sato, M. (1991). "Degradation of heme by a soluble peptide of heme oxygenase obtained from rat liver microsomes by mild trypsinization." *Eur J Biochem*. 199(3): p.729-33. 10.1111/j.1432-1033.1991.tb16177.x.

[598] Zhang, J., Wei, K.Y., Qu, W.Z., Wang, M., Zhu, Q., Dong, X., Huang, X., Yi, W., Xu, S.L., Li, X.K. (2023). "Ogt Deficiency Induces Abnormal Cerebellar Function and Behavioral Deficits of Adult Mice through Modulating RhoA/ROCK Signaling." *J Neurosci*. 43(25): p.4559-4579. 10.1523/jneurosci.1962-22.2023.

[599] Liu, F., Li, S., Zhao, X., Xue, S.S., Li, H., Yang G.C., Li, Y., Wu, Y., Zhu, L.L, Chen, L., Wu, H. (2023). "*O*-GlcNAcylation Is Required for the Survival of Cerebellar Purkinje Cells by Inhibiting ROS Generation." *Antioxidants* (*Basel*). 12(4). 10.3390/antiox12040806.

6. Appendix

Supplemental Table 1: Top GO enrichment categories for *O*-GlcNAcylated protein species. This table summarizes the top ten enriched Gene Ontology (GO) categories for biological processes (BP), cellular components (CC) and molecular functions (MF) associated with the *O*-GlcNAcylated proteins listed in table 3.1 (significantly enriched in samples from astrocytes incubated with NH_4Cl compared to the NH_4Cl-background control). FDR: false discovery rate (method of Benjamini-Hochberg [*526*]).

Term Description (Term ID)	Category	p-value	FDR	Matching Proteins
Protein stabilization (0050821)	Biological process	2.04E-13	1.10E-10	Hsp90aa1, Gapdh, Cct4, Cct6a, Cct8, Cct7, Cct2, Cct3, Cct5, Epha4, Pfn2, Ipo9, Rab21, Usp9x, Hspa1a, Ank2, Lamp2, Rpl5, Rpl5l1, Lamp1, Rpl23, Ctnnd1, Ptges3;Ptges3l1,
Positive regulation of establishment of protein localization to telomere (1904851)	Biological process	2.14E-11	5.25E-09	Cct4, Cct6a, Cct8, Cct7, Cct2, Cct3, Cct5
Positive regulation of telomere maintenance via telomerase (0032212)	Biological process	4.19E-11	9.43E-09	Mapk3, Mapk1, Cct4, Cct6a, Cct8, Cct7, Cct2, Cct3, Cct5, Ctnnb1
Protein folding (0006457)	Biological process	2.30E-10	4.44E-08	Hsp90aa1, Hspa4, Cct4, Cct6a, Cct8, Cct7, Cct2, Cct3, Cct5, Uggt1, Ppid;Ppidl1, Hspa1a, Ptges3;Ptges3l1
Chaperone-mediated protein folding (0061077)	Biological process	7.57E-10	1.23E-07	Cct4, Cct6a, Cct8, Cct7, Cct2, Cct3, Cct5, Ppid;Ppidl1, Fkbp2
Response to xenobiotic stimulus (0009410)	Biological process	1.75E-08	2.02E-06	Anxa1, Hsd17b4, Eno2, Hsp90aa1, Aldh1a1, Hadha, Ldha, Atp1a1, Gnas, Maob, Eef2, Txnrd1, Abat, Pdxk;RGD1566085, Acot2, Hadh, Ctnnb1, Dbn1, Uqcrc2, Cpt1a, Fn1, Xpo1, Rpn2, Myo6, Stat3, S100a10
Chaperone-mediated protein complex assembly (0051131)	Biological process	1.79E-08	2.02E-06	Hsp90aa1, Hspa4, Cct2, Lonp1, Hspa1a, Ptges3;Ptges3l1
One-carbon metabolic process (0006730)	Biological process	2.12E-08	2.29E-06	Ahcy, Sfxn1, Mthfd1, Aldh1l1, Sfxn3, Shmt2, Ahcyl1;Ahcyl2
Positive regulation of telomerase activity (0051973)	Biological process	4.56E-08	4.25E-06	Mapk3, Mapk1, Hsp90aa1, Cct4, Cct2, Ctnnb1, Ptges3;Ptges3l1
Fatty acid beta-oxidation (0006635)	Biological process	8.56E-08	7.71E-06	Hsd17b4, Hsd17b10, Hadha, Decr1, Hadh, Acaa2, Cpt2, Cpt1a, Echs1

Supplemental Table 1 (continued)

Term Description (Term ID)	Category	p-value	FDR	Matching Proteins
Cytosol (0005829)	Cellular component	1.61E-22	4.35E-19	Xpnpep1, Actn1, Ldhb,Fscn1, Mapk3, Mapk1, Hsp90aa1, Gapdh, Aldh1a1, Tubb4a, Hspa4, Ldha, Pdlim5, Myh9, Ddx5, Idh2, Rac1, Rac3, Tuba1b, Cct6a, Cltc, Gnas, Cct8, Sptbn1, Ahcy, Cpne1, Esd, Cand1, Myh10, Man2c1, Acss2, Hk1, Ddx1, Pgd, Dnpep, Eef2, Pkm, Txnrd1, Pgm1, Nisch, Snx27, Rangap1, Itgav, Map1a, Dnaja1, Copb1, Ehd2, Ephb2, Ephb1, Mthfd1, Aldh1l1, Pfkl, Pfkm, Ipo9, Cryz, Aox1, Me1, Gbe1, Ppp6c, Gart, Plcd1, Sbds, Kpna4, Sec24c, Pfkp, Dhx9, Ogt, Coro7, Aimp1, Dpp7, Vps35, Dbnl, Usp9x, Ampd3, Jup, Lonp1, Ppm1f, Ctnnb1, Ufl1, Etf1, Csad, Asns, Cops3, Synpo, Gsto1, Fasn, Nsf, Snd1, Dnm2, Cndp2, Ppp1r12a, Psmd13, Dctn1, Arpc2, Psma4, Vta1, Shmt2, Ahcyl1, Ahcyl2, Ube2d3, Ubr4, Hnrnpf, Prmt1, Ndufv1, Hspa1a, Acly, Ppp2r2d, Ppp2r2a, Cotl1, Gna13, Copg1, Prkar2a, Lta4h, Hras, Sri, Rtcb, Myo6, Stat3, Sec23a, Stat1, Ptges3;Ptges3l1, Aco1, Prps2, Adh4;Adh5, Dpp3, Lamp1, Gstt2, Ctnnd1, Tnik, Cse1l, Ipo7, Pdxk;RGD1566085, Paics;LOC100359876
Cytoplasm (0005737)	Cellular component	9.04E-12	2.71E-09	Gdi2, Xpnpep1, Actn1, Fscn1, Mapk3, Tubb5, Mapk1, Anxa1, Arpc1b, Eno2, Hsp90aa1, Gapdh, Aldh1a1, Tubb4b;Tubb4a, Hspa4, Tln1, Myh9, Oat, Iqgap1, Tuba1b, Acadl, Myh14, Tubb6, Gnas, Cct8, Sptbn1, Cpne1, Cand1, Myh10, Acss2, Ddx1, Eef2, Pkm, Txnrd1, Pgm1, Dync1li2, Nisch, Rangap1, Map1a, Tnpo1, Tnpo2, Dnaja1, Gla, Dync1h1, Epha4, Ephb1, Mthfd1, Pfn2, Ipo9, Myo1c, Mprip, Me1, Gbe1, Ppp6c, Plcd1, Sbds, Tpm4, Pfkp, Ppid, Ppidl1, Impa1, Eif2s3, Dhx9, Huwe1, Ogt, Psme2, Vps35, Dbnl, Usp9x, Psmb5, Ptpn9, Alg2, Isyna1, Jup, Itga7, Acsbg1, Ctnnb1, Copa, Ufl1, Arvcf, Etf1, Csad, Ctbp1, Sorbs3, Tuba1c, Sntb1, Gbp2, Ipo5, Cops3, Llgl1, Gsto1, Fasn, Sec31a, Snd1, Dnm2, Dbn1, Lancl1, Itgb1, Parp3, Ppp1r12a, Matr3, Dctn1, Psma4, Api5, Vta1, Shmt2, Ahcyl1, Ddb1, Prmt1, Hspa1a, Gna13, Prkar2a, Ank2, Xpo1, Lta4h, Ttll12, Kras, Hras, Rtcb, Tln2, Itpa, Myo6, Stat3, Stat1, Aco1, Prps1, Prps2, Prps1l1, S100a10, Iqgap2, Rpl5, Rpl5l1, Adh5, Rps4x, Rps4y2, Dpysl5, Myo1d, Dpp3, Lamp1, Gstt2, Psma3, Ctnnd1, Cyfip1, Map4k4, Mink1, Tnik, Paics;LOC100359876, Actg2;Acta2

Supplemental Table 1 (continued)

Term Description (Term ID)	Category	p-value	FDR	Matching Proteins
Mitochondrion (0005739)	Cellular component	7.90E-13	3.56E-10	Ivd, Mapk3, Mapk1, Idh3a, Hsp90aa1, Hsd17b10, Hspa4, Hadha, Myh9, Oat, Idh2, Aldh6a1, Nnt, Acadl, Cltc, Cyc1, Cct7, Maob, Sfxn1, Ctsa, Decr1, Hk1, Ddx1, Txnrd1, Abat, Slc44a2, Dnaja1, Gcdh, Acot2, Hadh, Sfxn3, Me1, Ppp6c, Dlst, Ogdh, Me2, Ppid, Ppidl1, Acaa2, Huwe1, Ogt, Vps35, Dhrs1, Slc25a12, Lonp1, Cpt2, Ppp1cc, Uqcrc2, Cpt1a, Shmt2, Acad9, Aadat, Slc27a1, Ndufv1, Hspa1a, Echs1, Aldh18a1, Ank2, Kras, Sri, Suclg1, Stat3, Aco1, Adh5
Chaperonin-containing T-complex (0005832)	Cellular component	2.14E-11	5.25E-09	Cct4, Cct6a, Cct8, Cct7, Cct2, Cct3, Cct5
Neuron projection (0043005)	Cellular component	2.14E-10	4.44E-08	Eno2, Hsp90aa1, Iqgap1, Rac3, Ahcy, Myh10, Abat, Map1a, Map4, Ogt, Rab21, Vps35, Ctnnb1, Ufl1, Ctbp1, Dctn1, Arpc2, Ahcyl2, Rnpep, Ank2, Ptges3;Ptges3l1, Pafah1b1, Myo1d, Cyfip1, Ephb2;Epha6;Epha4;Ephb4, Ephb3;Ephb1;Epha7,
Protein-containing complex (0032991)	Cellular component	1.70E-09	2.47E-07	Mapk3, Mapk1, Anxa1, Hsp90aa1, Myh9, Iqgap1, Atp1a1, Sptbn1, Hk1, Ap2a1, Atp2a2, Aldh1l1, Uggt1, Stip1, Rbm39, Dhx9, Ogt, Ppm1f, Ctnnb1, Ufl1, Rpl3, Sntb1, Dnm2, Dctn1, Ddb1, Prmt1, Hspa1a, Prkar2a, Xpo1, Suclg1, Myo6, Stat1, Ptges3;Ptges3l1, Prps2, Rpl5, Rpl5l1, Dpysl5, B4galt1
Melanosome (0042470)	Cellular component	6.23E-09	8.02E-07	Hsp90aa1, Ganab, Atp1a1, Cct4, Rac1, Cltc, Ahcy, Fasn, Snd1, Sec22b, Itgb1, Gna13, Lamp1
Microtubule (0005874)	Cellular component	1.51E-08	1.86E-06	Tubb5, Iqgap1, Cct4, Tuba1b, Cct6a, Tubb6, Cct8, Cct7, Cct2, Cct3, Dync1li2, Cct5, Map1a, Dync1h1, Map4, Tuba1c, Dnm2, Dctn1, Iqgap2, Tubb4b;Tubb4a
Glutamatergic synapse (0098978)	Cellular component	2.66E-08	2.77E-06	Actn1, Mapk3, Gapdh, Rac3, Sptbn1, Myh10, Eef2, Snx27, Pfn2, Ogt, Vps35, Dbnl, Ctnnb1, Ctbp1, Synpo, Sacm1l, Dnm2, Dbn1, Itgb1, Arpc2, Prkar2a, Hras, Myo6, Stat3, Pafah1b1, Lama5, Ctnnd1, Ephb2;Epha4;Ephb1;Epha7, Tnik,
Stress fiber (0001725)	Cellular component	9.45E-08	8.23E-06	Actn1, Fscn1, Pdlim5, Myh9, Myh14, Myh10, Mprip, Tpm4, Synpo, Actg2;Acta2

Supplemental Table 1 (continued)

Term Description (Term ID)	Category	p-value	FDR	Matching Proteins
Identical protein binding (0042802)	Molecular function	1.34E-15	1.82E-12	Ivd, Ldhb, Mapk3, Mapk1, Anxa1, Hsd17b4, Eno2, Hsp90aa1, Gapdh, Aldh1a1, Hsd17b10, Ldha, Myh9, Oat, Paics;LOC100359876, Acadl, Cltc, Ahcy, Cpne1, Esd, Maob, Myh10, Decr1, Hk1, Dnpep, Pkm, Txnrd1, Abat, Dync1li2, Nisch, Ehd2, Ephb2;Epha4, Hadh, Atl3, Pfkl, Pfkm, Cryz, Aox1, Me1, Tpm4, Pfkp, Impa1, Ogt, Slc16a1, Psme2, Slc25a12, Lonp1, Ctbp1, Esyt1, Asns, Gbp2, Fasn, Matr3, Cpt1a, Dctn1, Fn1, Shmt2, Ahcyl1, Slc27a1, Prmt1, Oplah, Aldh18a1, Prkar2a, Snrnp200, Kras, Hexb, Sri, Itpa, Myo6, Stat3, Stat1, Prps2, Adh5, Pafah1b1, B4galt1
NAD binding (0051287)	Molecular function	2.48E-15	2.24E-12	Ldhb, Cyb5r3, Idh3a, Gapdh, Aldh1a1, Hsd17b10, Hadha, Ldha, Idh2, Nnt, Ahcy, Aox1, Me1, Me2, Ctbp1, Ndufv1, Adh4;Adh5
ATP binding (0005524)	Molecular function	7.46E-15	5.04E-12	Mapk3, Mapk1, Hsp90aa1, Hspa4, Myh9, Ddx5, Paics, LOC100359876, Atp1a1, Cct4, Cct6a, Myh14, Cct8, Cct7, Myh10, Cct2, Acss2, Hk1, Ddx1, Pkm, Cct3, Dync1li2, Cct5, Pdxk;RGD1566085, Dnaja1, Ehd2, Dync1h1, Ephb2, Epha6, Epha4, Ephb4, Ephb3, Ephb1, Epha7, Atp2a2, Mthfd1, Pfkl, Pfkm, Myo1c, Farsb, Gart, Pfkp, Dhx9, Lonp1, Acsbg1, Asns, Nsf, Ube2d2, Ube2d3, Hspa1a, Acly, Oplah, Actg2, Acta2, Aldh18a1, Snrnp200, Ttll12, Myo6, Hyou1, Prps1, Prps2, Prps1l1, Myo1d, Map4k4, Mink1, Tnik
ATP-dependent protein folding chaperone (0140662)	Molecular function	1.92E-12	7.40E-10	Hsp90aa1, Hspa4, Cct4, Cct6a, Cct8, Cct7, Cct2, Cct3, Cct5, Hspa1a, Hyou1
Actin filament binding (0051015)	Molecular function	3.51E-12	1.18E-09	Actn1, Fscn1, Arpc1b, Tln1, Myh9, Iqgap1, Myh14, Sptbn1, Myh10, Eef2, Myo1c, Mprip, Tpm4, Coro7, Dbnl, Dbn1, Cotl1, Tln2, Myo6, Iqgap2, Myo1d, Cyfip1
Transmembrane-ephrin receptor activity (0005005)	Molecular function	5.80E-10	1.04E-07	Ephb2;Epha6;Epha4;Ephb4;Ephb3;Ephb1;Epha7
Structural constituent of cytoskeleton (0005200)	Molecular function	7.75E-10	1.23E-07	Tubb5, Arpc1b, Tln1, Tuba1b, Tubb6, Sptbn1, Tuba1c, Arpc2, Ank2, Tln2, Tubb4b;Tubb4a
Unfolded protein binding (0051082)	Molecular function	1.73E-09	2.47E-07	Hsp90aa1, Cct4, Cct6a, Cct8, Cct7, Cct2, Cct3, Cct5, Dnaja1, Uggt1, Hspa1a, Ptges3;Ptges3l1
GTP binding (0005525)	Molecular function	5.48E-09	7.40E-07	Tubb5, Hsp90aa1, Rac1;Rac3, Tuba1b, Tubb6, Gnas, Eef2, Rab18, Ehd2, Atl3, Rab21, Tuba1c, Gbp2, Dnm2, Gna13, Kras;Nras;Hras, Rtcb, Tubb4b;Tubb4a, Eif2s3;Eif2s3y

Supplemental Table 1 (continued)

Term Description (Term ID)	Category	p-value	FDR	Matching Proteins
GTPase activity (0003924)	Molecular function	3.71E-08	3.71E-06	Tubb5, Rac1;Rac3, Tuba1b, Tubb6, Gnas, Eef2, Rab18, Atl3, Rab21, Gbp2, Dnm2, Gna13, Eif2s3;Eif2s3y; Tubb4b;Tubb4a, Kras;Nras;Hras

Supplemental Table 2: Top KEGG pathway enrichment of *O*-GlcNAcylated protein species. This table summarizes the top ten enriched KEGG pathways associated with the *O*-GlcNAcylated protein species listed identified in table 3.1. The abundance of these protein species was significantly increased in NH_4Cl-treated astrocytes compared to NH_4Cl-background controls. The enrichment analysis was performed using Database for Annotation, Visualization and Integrated Discovery (DAVID) (https://david.ncifcrf.gov/home.jsp) with a focus on proteins with a q-value less than 0.05. FDR: false discovery rate (method of Benjamini-Hochberg [526]).

Term Description (Term ID)	Classification	p-value	FDR	Matching Proteins
Glycolysis / Gluconeogenesis (rno00010)	Metabolism	1.89E-08	1.69E-06	Ldhb, Eno2, Gapdh, Ldha, Acss2, Hk1, Pkm, Pgm1, Pfkl, Pfkm, Pfkp, Adh4;Adh5
Fatty acid degradation (rno00071)	Metabolism	4.16E-08	2.42E-06	Cct4, Cct6a, Cct8, Cct7, Cct2, Cct3, Cct5
Valine, leucine and isoleucine degradation (rno00280)	Metabolism	1.38E-05	0.00027	Ivd, Hsd17b10, Hadha, Aldh6a1, Abat, Hadh, Aox1, Acaa2, Echs1
Purine metabolism (rno00230)	Metabolism	0.022570	0.06848	Paics, Pgm1, Gart, Ampd3, Itpa, Prps1;Prps2;Prps1l1
Pentose phosphate pathway (rno00030)	Metabolism	7.45E-07	3.32E-05	Pgd, Pgm1, Pfkl, Pfkm, Pfkp, Prps1;Prps2;Prps1l1
Galactose metabolism (rno00052)	Metabolism	1.57E-05	0.00028	Hk1, Pgm1, Gla, Pfkl, Pfkm, Pfkp, B4galt1
Citrate cycle (TCA cycle) (rno00020)	Metabolism	1.57E-05	0.00028	Idh3a, Idh2, Dlst, Ogdh, Acly, Suclg1, Aco1
Fatty acid elongation (rno00062)	Metabolism	0.000870	0.00704	Hadha, Acot2, Hadh, Acaa2, Echs1
Cysteine and methionine metabolism (rno00270)	Metabolism	0.010769	0.04358	Ldhb, Ldha, Ahcy, Ahcyl1;Ahcyl2
Fructose and mannose metabolism (rno00051)	Metabolism	0.014402	0.05127	Hk1, Pfkl, Pfkm, Pfkp

7. Acknowledgements

I am deeply grateful to Prof. Dr. Dieter Häussinger, my PhD Supervisor, whose unwavering support has been pivotal in shaping my academic and personal journey. His belief in my potential not only granted me the opportunity to pursue my PhD but also extended to providing invaluable medical assistance to my family. During the challenging times of the coronavirus epidemic, Prof. Dr. Dieter Häussinger's compassion and assistance were invaluable, offering support not only to me but also to my family. Without his generosity, guidance, and kindness, I would not be where I am today, and for that, I am immensely grateful.

I am also deeply grateful to Dr. Boris Görg, who co-supervised my PhD studies. His guidance, encouragement, and unwavering support throughout my research journey were invaluable. His expertise in molecular biology and fluorescence microscopy, which were particularly instructive, further contributed to the quality of my research.

I would also like to express my gratitude to Prof. Dr. Holger Gohlke for his invaluable support as my co-supervisor. I particularly appreciate his dedication in meticulously reviewing my PhD thesis.

I would also like to thank Dr. Mirco Castoldi for his invaluable technical support in particle measurement and analysis. His expertise and assistance have been instrumental in advancing my research efforts.

My sincere gratitude extends to our collaborators, Prof. Dr. Tom Lüdde, Prof. Dr. Gereon Poschmann, Prof. Dr. Kai Stühler, Dr. Mihael Vucur, Dr. Mohanraj Gopalswamy, Dr. Michele Bonus and Dr. Hans Jürgen Bidmon. Their continuous support, valuable suggestions, and provision of essential materials have significantly contributed to the success of this project.

I am also grateful to our laboratory technical assistants, Michaela Fastrich, Vanessa Herbertz, Nicole Eichhorst and Torsten Janssen, for their invaluable technical assistance and engaging insights.

I would also like to express my appreciation to my colleagues Marijana Suzanj, Dr. Alina Schrimpf, Dr. Chengjun Jin, Dr. Kathleen Deutschmann, Dr. Martha Paluschinski, Dr. Maria Reich,

Dr. Natalia Qvartskhava, Dr. Christian Ehlting, Dr. Stephanie Wolf and Dr. Jan Stindt. Working with these talented researchers in a supportive and friendly environment has been a privilege.

I would like to express my sincere gratitude to Dr. Ute Albrecht from the Centre for Scientific Management of Liver Research and Dr. Yasmin Wittgenstein from the Centre for Coordinating Clinician-Scientist Programs for their invaluable assistance and support during my doctorate. Their guidance, expertise, and unwavering encouragement have been instrumental in shaping my research endeavors and personal growth. I am truly grateful for their dedication and assistance.

I would like to express my gratitude to my PhD program managers Dr. Jessica Gätjens and Ms. Olympia Grazia Glomb, for the support and guidance they provided throughout my doctorate, especially through the well-organized training courses and seminars offered by the Graduate Center.

Last but certainly not least, I express my deepest gratitude to my parents for their unwavering support, understanding and patience throughout this journey. Without their endless encouragement and belief in me, none of this would have been possible. Their kind support has been my rock, and their profound influence on my life is immeasurable. I am forever grateful for their love, guidance and unwavering presence.